Resummation of Jet Observables

Dissertation

zur
Erlangung der naturwissenschaftlichen Doktorwürde
(Dr. sc. nat.)
vorgelegt der
Mathematisch-naturwissenschaftliche Fakultät
der
Universität Zürich
von

Pier Francesco Monni

aus
Italien

Promotionskomitee

Prof. Dr. Thomas Gehrmann
Prof. Dr. Aude Gehrmann-De Ridder
Prof. Dr. Ulrich Straumann
Prof. Dr. Daniel Wyler

Zürich, 2013

Acknowledgements

I wish to thank my PhD supervisor Prof. Thomas Gehrmann for giving me the great opportunity to work in his research group. His valuable support has been of primary importance to me to understand several aspects of particle physics as well as to learn how to deal with professional issues in the academic world. I would also like to thank Andrea Banfi, Gionata Luisoni, Massimiliano Grazzini, Gavin Salam and Giulia Zanderighi for the countless discussions about technical aspects of QCD and fruitful research collaborations during the last years.

Zusammenfassung

Die genaue Beschreibung experimenteller Daten, die mit Hochenergie-Beschleunigern gemessen wurden, ist der Schlüssel, um die Physik der mikroskopischen Welt im hochenergetischen Bereich zu verstehen. Physikalische Observablen werden experimentell mit Hilfe der *Spuren* gemessen, welche energiereiche Teilchen (*z.B.* Hadronen, Leptonen, Photonen) in den Detektoren hinterlassen, während theoretische Vorhersagen im Rahmen des Standardmodells der Teilchenphysik näherungsweise berechnet werden. Insbesondere wird die Dynamik der stark wechselwirkenden Teilchen (*d.h.* Hadronen) durch die Wechselwirkungen zwischen den elementaren Bausteinen simuliert, aus denen diese Teilchen bestehen und deren Physik durch die Quantenchromodynamik (QCD) beschrieben wird. Korrekturen zum partonischen Modell (*z.B.* Hadronisierung, Underlying Events, ...) können mit phänomenologischen Modellen berechnet werden, deren Parameter an experimentellen Daten gefittet werden müssen. Auf der partonischen Ebene werden Prognosen durch Verwendung einer perturbativen Entwicklung in der starken Kopplungskonstanten berechnet. In der Praxis beeinträchtigen oft die kinematischen Restriktionen (aufgrund der Definition einiger Observablen) auf dem Phasenraum des Endzustandes die Genauigkeit dieser Entwicklung. Eine Möglichkeit, die theoretischen Vorhersagen zu retten, wird mittels eines mathematischen Verfahrens gegeben, welches *Resummation* genannt wird.

In der vorliegenden Dissertation untersuchen wir die Ursache des Problems und diskutieren zwei unterschiedliche Methoden zur QCD-Resummation im Rahmen von zwei phänomenologischen Anwendungen. Einerseits wird die Verteilung der Thrust-Variablen in e^+e^- Kollisionen mittels RG-Evolutionsgleichungen im Laplace-Raum-Formalismus zur NNLL-Genauigkeit resummiert. Andererseits präsentieren wir eine allgemeinere Methode, welche auf eine grosse Klasse von Observablen angewendet werden kann. Darüber hinaus schlagen wir eine neue Erweiterung des Algorithmus vor um NNLL-Genauigkeit zu erreichen. Als phänomenologische Anwendung untersuchen wir die Resummation der Transversalimpuls-Verteilung des führenden Jets im Rahmen der Farb-Singulett-Produktion (*z.B.* Higgs-Boson) in hadronischen Beschleunigern.

Abstract

The precise description of experimental data measured at high energy colliders is the key to understand the physics of the microscopic world in this energy regime. Physical observables are measured experimentally by using the *traces* that energetic particles (*e.g.* hadrons, leptons, photons) leave in the detectors, whilst theoretical calculations are carried out using approximate solutions to the quantum theory of fundamental forces. In particular, the dynamics of strongly interacting particles (*i.e.* hadrons) is simulated through the interactions among the elementary building blocks they are made of, whose physics is described by Quantum Chromodynamics (QCD). Corrections to the partonic picture (*e.g.* hadronisation, underlying events, ...) can be subsequently computed using phenomenological models whose parameters have to be tuned on existing experimental data. At the partonic level, predictions are obtained using a perturbative expansion in the strong coupling constant. Often in practice the kinematical constraints (due to the definition of some observables) on the final state particles spoil the accuracy of the latter expansion. One way to rescue the theoretical prediction is through a mathematical procedure called *resummation*.

In the present thesis we examine the origin of the problem and discuss two different approaches to QCD resummation in the context of two phenomenological applications. On the one hand, the thrust distribution in e^+e^- collisions is resummed to NNLL accuracy using RG evolution equations in the Laplace space formalism. On the other hand, we present a more general method which can be applied to a wide class of observables and furthermore we propose a novel extension of the algorithm to achieve NNLL accuracy. As a phenomenological application, we consider the resummation of the leading jet's transverse momentum distribution in the context of colour-singlet production (*e.g.* Higgs boson) at hadron colliders.

Contents

List of Figures

LIST OF FIGURES

List of Tables

LIST OF TABLES

1

Introduction to the Standard Model of particle physics

The current status of elementary particle physics underlines the remarkable success of the theoretical efforts made in the last decades to model the microscopic behaviour of nature. The most impressive achievement of such efforts is a quantum theory which nowadays can describe three of the four fundamental forces present in nature. The Standard Model (SM) of particle physics is a quantum-field-theory (QFT) which explains the interaction between elementary matter's building blocks in terms of the exchange of quantum fields. It succesfully describes the electro-magnetic force and the two nuclear forces (weak and strong) and it has been succesfully tested in minute detail throughout the years in many collider experiments such as SPS, LEP, HERA, Tevatron and the LHC. Gravitation, although being the most evident force for people in everyday's life, is the weakest of the four forces and its strength can be safely neglected at normal collider energy scales. At macroscopic scales it is very well described by General Relativity [1], but a proper quantum description at the microscopic level is still an open issue.
The SM is a gauge theory with local gauge symmetry $\mathrm{SU}(3)_C \otimes \mathrm{SU}(2)_L \otimes \mathrm{U}(1)_Y$. It consists of two different quantum field theories describing two different interactions. The electro-weak sector is described by the symmetry group $\mathrm{SU}(2)_L \otimes \mathrm{U}(1)_Y$ which is spontaneously broken at the electro-weak scale ($\sim$ 100 GeV) according to the Higgs-Brout-Englert [1–5] mechanism. At low energy it is well approximated by the two effective thories of Quantum-Electrodynamics (QED) -responsible for the electro-magnetic interaction- and Fermi's theory which describes the weak nuclear interaction. The symmetry-breaking mechanism gives mass to all particles in the SM and it is being tested with very high precision at the CERN's Large Hadron Collider (LHC). The strong sector has gauge symmetry $SU(3)_C$ and it describes the strong nuclear interaction between the elementary constituents of hadrons (*e.g.* nucleons). This sector is

[1] Though important discrepancies show up at cosmological scales

called Quantum-Chromodynamics and we will focus on it in the next chapters of this thesis. The reader may refer to Refs. [8–10] for an exhaustive discussion of the SM. The particle content of the SM consists of six types of leptons (*e.g.* electron, muon, neutrinos,...) grouped into three families (*generations*) according to the lepton flavour quantum number. They interact among themselves through electro-weak (EW) interaction, carried by the three weak bosons $W^{\pm}$, Z^0 (massive) and the photon γ (massless). Additionally, the strong sector contains six types of quarks which are classified into three families according to their *flavour*. They interact with each other both through EW force and through the exchange of gluons, *i.e.* vector bosons which mediate the strong nuclear (*colour*) force. Moreover they interact with leptons through the electro-weak sector. Finally, the currently most popular SM particle is a scalar boson which embodies the remnants of the symmetry breaking process: the Higgs boson. The hunt for the Higgs boson went on for almost four decades until the two main experiments at the LHC (ATLAS and CMS) announced the discovery of a particle with very similar features in July 2012 [6, 7]. This discovery is a further confirmation of the extraordinary success of the SM and brings many new questions concerning the structure of nature at higher energy scales. Despite it being a remarkable theory, the SM is not able to answer many open questions in particle physics (*e.g.* CP violation for baryonic asymmetry, Dark matter, ...) and furthermore it suffers from some theoretical pathologies (*e.g.* fine tuning). The SM is further challenged by some small discrepancies (*e.g.* quark mixing parameters) between the theory and experimental data. Such problems may be an initial hint of the presence of a wider and more general theory of which the SM is just an effective model. A lot of work is being carried out by the theorists in order to understand such problems and many extensions to the SM have been formulated in the literature throughout the years.

Precise predictions for the SM processes are required in order to address these issues and to measure the SM parameters with high enough precision so as to unveil the discrepancies with the data. To this end many new computational methods have been proposed in the last decades which allow us to perform precise calculations of the relevant SM processes. The recent discovery of the Higgs-like boson at the LHC would not have been possible without the theoretical simulations obtained with such methods. In the present thesis we will analyse some of these tools, which are relevant to understand the QCD radiation in high energy collisions and allow us to obtain reliable predictions for the relevant physical quantities when the standard perturbative approach fails. Chapter 2 contains an introduction to QCD and a discussion of the main properties that will be needed throughout the thesis. In Chapter 3 we discuss some issues of the perturbative approach and present a way to heal them, introducing the concept of resummation. In Chapters 4, 5 and 6 we present some detailed phenomenological applications to e^+e^- annihilations and to hadron colliders in the context

of Higgs-boson production, respectively. Finally, Chapter 7 contains the conclusions and perspectives for future research work in this area.

1. INTRODUCTION TO THE STANDARD MODEL OF PARTICLE PHYSICS

2

Quantum Chromodynamics

This chapter contains an introduction to perturbative Quantum Chromodynamics introducing the main concepts that will be used in the rest of the thesis. For an exhaustive description of the theory model and its properties, the reader may refer to the following text books [11–13].

2.1 Origin of QCD and SU(3)

Quantum Chromodynamics (QCD) is the Standard Model sector which describes the strong nuclear interaction among hadrons (*e.g.* protons, neutrons,...). In the context of the quark model, hadrons are made of elementary building blocks called quarks. Nowadays we can describe the whole observed hadronic spectrum by combining six quark types (and respective antiparticles) which differ in mass and additional quantum numbers as reported in Tab. **??**. A new quantum number, the *flavour*, is associated

Quark	Charge	Mass	Baryon Number	Isospin
u	$+\frac{2}{3}$	$\sim 4\,\mathrm{MeV}$	$\frac{1}{3}$	$+\frac{1}{2}$
d	$-\frac{1}{3}$	$\sim 7\,\mathrm{MeV}$	$\frac{1}{3}$	$-\frac{1}{2}$
s	$-\frac{1}{3}$	$\sim 135\,\mathrm{MeV}$	$\frac{1}{3}$	0
c	$+\frac{2}{3}$	$\sim 1.5\,\mathrm{GeV}$	$\frac{1}{3}$	0
b	$-\frac{1}{3}$	$\sim 5\,\mathrm{GeV}$	$\frac{1}{3}$	0
t	$+\frac{2}{3}$	$\sim 175\,\mathrm{GeV}$	$\frac{1}{3}$	0

Table 2.1: The six quark types ordered by their masses. Baryon number and Isospin as well as their electric charges are also reported.

to each quark type (*e.g.* *u, d, s,...*). The first three quarks are light enough with

respect to the typical hadronic scale ($\sim 1\,\mathrm{GeV}$) and their masses can be neglected at high energies. One can thus consider the first three quark types as different states of the same particle. As a consequence, the *light* hadronic spectrum can be organized according to the irreducible representations of the symmetry group $\mathrm{SU(3)_{Flavour}}$, which can be seen as an extension of the $\mathrm{SU(2)_{Isospin}}$ symmetry between the quarks up (u) and down (d). This assumption led to the static quark model proposed by M. Gell-Mann, Y. Dothan and Y. Ne'eman [14]. Such a model fails once we take into account the heavier quark types since flavour symmetry is broken by mass effects. Nevertheless, it provides a remarkably good description of the spectrum of (light) hadrons that can be obtained as a combination of the three light quarks. Such hadrons can be classified into two categories. They can be bound states made of either three quarks plus any number of quark-antiquark pairs (*baryons* with baryon number 1) or quark-antiquark pairs (*mesons* with baryon number 0). So far only the *plain* qqq and $q\bar{q}$ states have been observed in nature. The success of this model is mainly due to the discovery of the Ω^- hadron, as it was previously predicted by the theory.
The flavour quantum number alone does not always provide a reliable description of the hadronic spectrum. The canonical example is the baryonic resonance Δ^{++} which is a composite state of three valence up quarks and has spin $J_z = +3/2$:

$$\left|\Delta^{++}; +3/2\right\rangle \;=\; |u\uparrow\rangle\,|u\uparrow\rangle\,|u\uparrow\rangle\;. \tag{2.1}$$

This situation would imply a violation of Pauli's spin-statistic theorem. The Pauli-principle can be restored by introducing a new degree of freedom called *colour* [15] and assuming that the resonance's colour wave function is completely antisymmetric:

$$\left|\Delta^{++}; +3/2\right\rangle \;=\; \frac{1}{\sqrt{6}}\sum_{i,j,k=1}^{N} \varepsilon_{ijk}\,|u_i\uparrow\rangle\,|u_j\uparrow\rangle\,|u_k\uparrow\rangle\;, \tag{2.2}$$

where ε_{ijk} is the Levi-Civita tensor. So each quark state must be invariant under the rotations of some symmetry group. A good candidate is the special unitary group $\mathrm{SU(N)_{Colour}}$. This choice provides an excellent description of experimental data, which allows one to set the number of colours to three ($N = 3$). The choice of the $\mathrm{SU(3)_{Colour}}$ symmetry stems from the fact that coloured hadronic states were never observed at collider experiments. This leads to the assumption that all hadrons must be in a colour-singlet state. If we assume that the quarks (antiquarks) live in the fundamental (antifundamental) representations of $\mathrm{SU(3)_{Colour}}$, we see that the only way to produce colour-singlets is through a composition of either a quark-antiquark pair or three quarks (Eq. 2.3)

$$\begin{aligned} \mathbf{3}\otimes\bar{\mathbf{3}} &= \mathbf{8}\oplus\mathbf{1}, \\ \mathbf{3}\otimes\mathbf{3}\otimes\mathbf{3} &= \mathbf{10}\oplus\mathbf{8}\oplus\mathbf{8}\oplus\mathbf{1}, \end{aligned} \tag{2.3}$$

in agreement with the static quark model and experimental observations. The symmetry group is unitary for the same reason. If one assumed the existence of an $SO(3)_{\text{Colour}}$ symmetry instead, then the composition of two quarks would lead to a colour singlet, in contrast with the experimental data. The success of the colour symmetry suggests that the strong nuclear interactions can be described by a gauge theory with gauge group $SU(3)_{\text{Colour}}$. In this model, fermions (quarks) transform according to the fundamental (three-dimensional) representation while the massless gauge bosons (gluons) transform according to the (eight-dimensional) adjoint representation. Note that this is in close analogy with Quantum Electrodynamics (QED). However, unlike the photon (electrically neutral), QCD contains eight gluons which carry colour charge.

2.2 The QCD Lagrangian

QCD is a non-abelian and renormalizable Yang-Mills theory [16] whose dynamics is described by the following Lagrangian

$$\mathcal{L}_{QCD} = \mathcal{L}_{\text{YM}} + \mathcal{L}_{\text{gauge-fixing}} + \mathcal{L}_{\text{ghost}} \,. \tag{2.4}$$

The term $\mathcal{L}_{\text{YM}}$ in Eq. 2.4 is invariant under local $SU(3)_{\text{Colour}}$ gauge transformations. It can be constructed starting from the Dirac Lagrangian by demanding local $SU(3)_{\text{Colour}}$ gauge invariance and it contains the kinetic terms of quark and gluon fields and all the quark-gluon and gluon-gluon interaction vertices. Adopting Einstein's summation convention we can write it as

$$\mathcal{L}_{\text{YM}} = \sum_f \bar{q}_{f_i} \left(i \not{D} - m_q \right)_{ij} q_{f_j} - \frac{1}{4} F^{\mu\nu,\,a} F^a_{\mu\nu} \,, \tag{2.5}$$

where the sum runs over all quark flavours f. The field strength tensor $F^a_{\mu\nu}$ and the covariant derivative $\not{D}$ can be written in terms of the gluon field A^a_μ as

$$F^a_{\mu\nu} = \partial_\mu A^a_\nu - \partial_\nu A^a_\mu - g_s \, f^{abc} \, A^b_\mu \, A^c_\nu \,, \tag{2.6}$$

$$\not{D}_{ij} = (\gamma^\mu D_\mu)_{ij} = \gamma^\mu \left(\delta_{ij} \partial_\mu + i \, g_s \, T^a_{ij} \, A^a_\mu \right) \,, \tag{2.7}$$

$$(m_q)_{ij} = m_q \delta_{ij} \,. \tag{2.8}$$

In the above equations g_s is the bare gauge coupling, T^a_{ij} the generators of the SU(3) gauge group in the fundamental representation and f^{abc} are its structure constants.

The gauge-fixing term $\mathcal{L}_{\text{gauge-fixing}}$ specifies the gauge choice and breaks gauge invariance. It allows one to define the gluon propagator unambiguously. Finally, the ghost sector $\mathcal{L}_{\text{ghost}}$ describes the dynamics of auxiliary, bosonic (ghost) fields η^a which obey Fermi-Dirac statistics. Such unphysical fields are introduced to compensate for

unphysical polarizations in 3-boson vertices and external gauge boson states. The popular covariant gauge leads to the gauge fixing term

$$\mathcal{L}_{\text{gauge-fixing}} = \frac{1}{2\xi}\left(\partial^\mu A^a_\mu\right)^2, \tag{2.9}$$

where ξ is a parameter contributing only to the overall normalisation. The Lagrangian of the ghost fields is given by

$$\mathcal{L}_{\text{ghost}} = \partial_\mu \bar{\eta}^a \left(\partial^\mu \delta^{ab} + g_S\, f_{abc}\, A^{c,\mu}\right) \eta^b . \tag{2.10}$$

As mentioned, the two terms $\mathcal{L}_{\text{gauge-fixing}}$ and $\mathcal{L}_{\text{ghost}}$ break gauge symmetry by imposing a particular gauge choice. However, a more general symmetry is still intact and was first derived by C. Becchi, A. Rouet and R. Stora [17]. From $\mathcal{L}_{QCD}$ it is possible to derive the Feynman rules given in Figure 2.1.

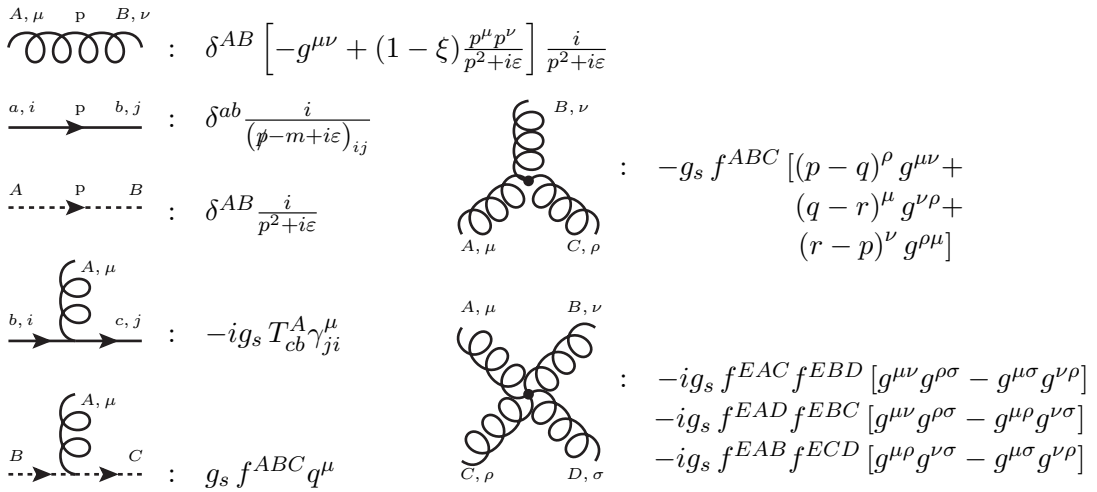

Figure 2.1: QCD Feynman rules in the covariant gauge.

2.2.1 Renormalisation and asymptotic freedom

To compute physical quantities in collider experiments, we rely on a perturbative approach and we expand any observable in a power series in the strong coupling constant

$$\alpha_s = \frac{g^2}{4\pi}. \tag{2.11}$$

Such an approximation is justified as long as the expansion parameter α_s is much smaller than one. In the present section we will go through the properties of the running coupling constant and show that the perturbative treatment is well motivated.

The Lagrangian 2.4 by itself does not allow one to compute precise predictions of physical observables. The main issue shows up when one computes radiative corrections to any QCD process. In computing the virtual (loop) corrections one encounters divergences when the particle running in the loop has very large momentum

$$\int \mathrm{d}^4k \frac{1}{(k+p)^2\,k^2} \sim \lim_{\Lambda\to\infty} \int \mathrm{d}\Omega_3 \int_0^\Lambda \mathrm{d}k\, k^3 \frac{1}{(k^2)^2} \sim \lim_{\Lambda\to\infty} \int_0^\Lambda \frac{\mathrm{d}k}{k} \sim \lim_{\Lambda\to\infty} \ln\Lambda\,. \quad (2.12)$$

In the quantum field theory formulation, such a particle is virtual and its momentum can take any value. This clearly allows the virtual particle to probe an unphysical region and such an approximation gives rise to the divergences mentioned above. Singularities of this type are called Ultra-Violet (UV) divergences and in renormalisable theories they can be completely subtracted through a redefinition of the free parameters in the Lagrangian (*i.e.* strong coupling constant and quark masses). The redefined parameters are set to their physical values and can be determined directly by comparing the theory prediction to experimental data. The mathematical machinery of UV-divergences subtraction is called *renormalisation* and it is one of the most important ingredients for a perturbative treatment of quantum field theories. As a first step one needs to single out all the possible UV divergences. To do so, we need to introduce a regulator which allows us to compute the divergent integrals. Several choices are possible, but the most commonly used is Dimensional Regularisation (DR) [18] which preserves gauge and Lorentz invariance. Throughout this thesis we make use of DR in $4-2\epsilon$ dimensions. In the context of DR the divergences show up as poles in the parameter ϵ. Once they have been isolated, we subtract them by absorbing them into the Lagrangian parameters. This procedure gives the Lagrangian parameters an anomalous dimension which is responsible for their running as a function of the scale at which they are evaluated. The running is described by Renormalisation Group Equations (RGE) and it leads to the two main properties that allow for a perturbative treatment of QCD. The RGE for the strong coupling constant reads

$$\frac{\partial\alpha_s(\mu)}{\partial\ln\mu^2} = -\alpha_s(\mu)\left(\frac{\alpha_s(\mu)}{\pi}\beta_0 + \frac{\alpha_s^2(\mu)}{\pi^2}\beta_1 + \left(\frac{\alpha_s^2(\mu)}{\pi^2}\right)^2\beta_2 + \left(\frac{\alpha_s^2(\mu)}{\pi^2}\right)^3\beta_3 + \dots\right). \quad (2.13)$$

The perturbative series in the r.h.s. of the previous equation is called β-function. Its coefficients can be computed in perturbation theory and are reported in Appendix A.1. Solving such an equation for the running coupling $\alpha_s(\mu)$ at lowest order yields the following expression

$$\bar{\alpha}_s(\mu) = \frac{\bar{\alpha}_s(\mu_0)}{1 + 2\bar{\alpha}_s(\mu_0)\,\beta_0 \ln\left(\frac{\mu^2}{\mu_0^2}\right)}, \quad (2.14)$$

where μ_0 is some initial scale at which the coupling is known and $\bar{\alpha}_s = \alpha_s/(2\pi)$. The scale μ is known as renormalisation scale and it defines the scale at which the subtraction of divergences occurs. From Eq. 2.14 it follows that $\alpha_s \to 0$ when $\mu \to \infty$. This property is known as *asymptotic freedom* and it is due to the sign of the first coefficient (β_0) of the β-function. Unlike QED, QCD's β_0 coefficient is positive if the number of flavours is less than 33/2. In this case, we can perform the perturbative expansion in α_s at high energies since the strong coupling gets small in this regime and the perturbative approach is justified. Physically, this means that in processes at large momentum transfer, hadrons behave as collections of free (*i.e.* weakly interacting) partons and perturbation theory offers an excellent approximation of the exact theoretical description. At low scales, the strong coupling gets large and, in general, perturbation theory fails in describing the experimental data. We can parametrise such a behaviour assuming that at some scale Λ_{QCD} the coupling diverges

$$\frac{1}{\alpha_s(\Lambda_{\mathrm{QCD}})} = 0. \tag{2.15}$$

Using Eq. 2.15 as initial condition for the coupling's RGE, we find the following solution at leading order

$$\bar{\alpha}_s(\mu) = \frac{1}{2\beta_0 \ln \frac{\mu^2}{\Lambda^2_{\mathrm{QCD}}}} \left(1 + \mathcal{O}(\frac{1}{\ln \frac{\mu^2}{\Lambda^2_{\mathrm{QCD}}}}) \right). \tag{2.16}$$

The scale Λ_{QCD} marks the boundary between the perturbative and non-perturbative regimes and it can be determined through a fit of experimental data. Its value is of the order of $\sim 200\,\mathrm{MeV}$. Below such a scale the strong coupling constant gets very large, consistently with the hypothesis of *confinement* and a non-perturbative analysis is required.

The second relevant property follows from the RGE for the quark masses (which are free parameters of the theory), which obeys the same asymptotic behaviour as the running coupling does

$$\lim_{\mu \to \infty} m(\mu) = 0, \tag{2.17}$$

meaning that we can neglect the quark masses if the scale of the process (normally of the order of the renormalisation scale) is much higher than the masses themselves. In practice, at normal collider energies, this allows us to neglect all quark masses but the top (t) and bottom (b) ones.

2.3 Infrared structure of pQCD cross sections

2.3.1 Parton model and factorisation

Asymptotic freedom of QCD ensures that at high energies hadrons behave like bunches of (almost) free partons (quarks and gluons). At such scales we can then factorise the short-distance physics from the long-distance one. This assumption is formulated in the parton model according to which one can compute hadronic cross sections in terms of partonic cross sections. The main idea behind the parton model is that when two highly energetic hadrons collide, the internal interactions are time dilated because of the Lorentz boost, so the partons will be well separated in the transverse directions. It follows that each parton in the colliding hadrons interacts incoherently since interactions among partons within a hadron cannot interfere with the hard scattering because they happen on longer time scales. Thus, an inclusive hadronic cross section σ_{AB} for the process $A + B \to X$ with two hadrons in the initial state can be expressed as

$$\sigma_{AB} = \sum_{a,b} f_{a/A}(\mu) \otimes f_{b/B}(\mu) \otimes \hat{\sigma}_{ab}(\mu), \tag{2.18}$$

where the parton distribution functions (PDFs) $f_{h/H}(\mu)$ describe the distribution of a parton h in the hadron H. Long-distance effects are separated from the short-distance scattering by the factorisation scale μ. The PDFs are hadron-dependent and do not depend on the process. They cannot be computed using perturbative QCD and they are extracted from experimental data assuming some phenomenological model. If specific hadrons are produced in the final state, then Eq. 2.18 must be convoluted with some parton fragmentation function describing the distribution of partons in the hadron X. The factorisation of the hadronic cross section neglects power-suppressed terms ($\sim 1/Q^m$) which arise from hadronisation corrections and multiple (coherent) collisions within a hadron (*higher twist corrections*). Its validity can be demonstrated for inclusive enough quantities (*i.e.* Deeply Inelastic Scattering) but in the general case no rigorous (field theoretical) proof is available yet. In most cases of phenomenological interest we want to analyse non-inclusive processes with some arbitrarily complicated physical observable. In such cases the factorisation theorem is simply assumed to hold true. The hard parton scattering cross section $\hat{\sigma}_{ab}(\mu)$ can be computed with the perturbative approach using the QCD Feynman rules. Its general form is

$$\hat{\sigma}_{ab} = \sum_{a',b'} c_{a'/a}(\mu) \otimes c_{b'/b}(\mu) \otimes \hat{\sigma}_{a'b'}, \tag{2.19}$$

where now the $c_{p'/p}(\mu)$ terms are coefficient functions describing the parton-in-parton distribution due to the higher order corrections to the parton p and the evolution with the factorisation scale μ. Both the $c_{p'/p}(\mu)$ and the $\hat{\sigma}_{a'b'}$ functions are well defined

objects in perturbation theory and they are finite if the observable we are computing is Infrared and Collinear (IRC) Safe. We will come back to this concept later on.

2.3.2 Infrared divergences

In the perturbative approach, a generic physical cross section $\sigma(\bar{\alpha}_s)$ can be expressed as a power series in the strong coupling constant $\bar{\alpha}_s$

$$\sigma(\bar{\alpha}_s) = \sigma^{\mathrm{LO}} + \sigma^{\mathrm{NLO}} + \ldots, \tag{2.20}$$

where we omitted the dependence on the relevant scales in the process (*e.g.* renormalisation and factorisation scales, phase space cuts, masses, etc). Assuming that the process involves m final state particles, the leading order cross section can be expressed as

$$\sigma^{\mathrm{LO}} = \int_m d\sigma^{\mathrm{LO}}. \tag{2.21}$$

The cross section element reads

$$d\sigma^{\mathrm{LO}} = d\phi^{(m)} |M_m^{(\mathrm{tree})}(\{p_i\})|^2 J^{(m)}(\{p_i\}), \tag{2.22}$$

where $d\phi^{(m)}$ is the m-particle phase space

$$d\phi^{(m)} = \prod_{i=1}^{m} \frac{d^4 p_i}{(2\pi)^3} \delta^{(+)}(p_i^2) \delta^{(4)}(p_{in} - \sum_i p_i), \tag{2.23}$$

and $J^{(m)}(\{p_i\})$ is a phase space function defining the physical observable we want to compute, and specifying all the necessary phase space cuts.

Beyond leading order, the process receives quantum radiative corrections that can be computed in perturbation theory. At next-to-leading-order (NLO) the corrections are of two types. Real corrections involving the emission of an additional final state particle, and virtual corrections in which the additional particle is emitted and subsequently reabsorbed by one of the particles taking part in the hard process. The final state phase spaces for the two corrections will therefore be different since the real corrections involve $m+1$ particles, while the virtual corrections only m. Simbolically we can express it as

$$\sigma^{\mathrm{NLO}} = \int_m d\sigma^{(V)} + \int_{m+1} d\sigma^{(R)}. \tag{2.24}$$

When we compute each of the contributions in Eq. 2.24 we find a new class of divergences. These singularities are different from the UV ones we discussed previously and they cannot be renormalised away. They actually arise from the opposite region

of the phase space and show up when the extra particle either gets *collinear* to the emitting leg or is emitted with very low energy (*soft*). For these reasons they are called Infrared and Collinear (IRC) divergences. In the real corrections they show up when we integrate the $m+1$ tree-level matrix element over its phase space, while in virtual corrections they arise from the loop integrals, when the loop momentum probes the IRC region.

We can see them explicitly by considering a generic $2 \to 2$ process with an outgoing quark-antiquark pair and by assuming that an additional gluon is emitted off the outgoing quark:

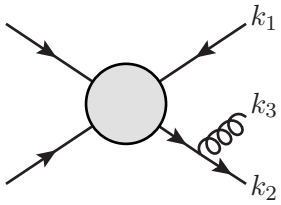

We shall assume that all the three momenta k_1, k_2, k_3 are outgoing. The internal fermion propagator of the quark goes on-shell, if either the energy of the gluon or the angle between the quark and the gluon (or both) gets very small

$$\frac{1}{(k_2 + k_3)^2} = \frac{1}{2E_1E_3\,(1 - \cos\theta_{13})} \longrightarrow \infty \quad \text{if} \quad E_3 \to 0 \quad \text{or} \quad \theta_{13} \to 0.$$

In the collinear case ($\theta_{13} \to 0$) the propagator becomes strictly singular only in the limit of massless quarks. Quark masses regularise the collinear singularities but they lead to further complications in the calculation. Taking into account the spinors of the outgoing quark (antiquark) it is easy to see that the limit $E_1 \to 0$ leads to an integrable singularity. The internal fermion propagator is off-shell by an amount $p_{g_\perp}^2 = 2p_q \cdot p_g$, where $p_{g_\perp}$ is the transverse momentum of the gluon relative to the quark-antiquark system. The virtual quark (antiquark) survives for a time $1/p_{g_\perp}$ before the gluon is radiated and can therefore travel an indefinite distance if the radiated gluon is soft, collinear or both. We therefore see that the IRC singularities carry information about long distance physics, that cannot be described with the standard perturbative approach.

In fact, divergences due to soft bremsstrahlung are already known from QED, where the emission of a soft photon off a scattered electron is enhanced by a factor $\ln\left(\frac{q^2}{m_e^2}\right)$ for collinear radiation[1]. The parameter m_e here is the mass of the electron and q is the 4-momentum transferred to the electron in the scattering process. The same holds for quarks emitting soft and collinear gluons. The origin of these singularities is a fundamental assumption made in contructing the quantum field theory. We indeed assume

[1] A detailed discussion of IRC-divergences in QED can be found for example in [19].

that the asymptotic states are free of any interaction, which is not true if a particle can propagate indefinitely before radiating soft partons. The real asymptotic states can be perturbatively approximated by constructing coherent states [21]. However, both in QCD and in QED there is an experimental limit in the sensitivity to soft and collinear radiation [1].

However, quantum mechanics teaches us that we have to sum over all possible and undistinguishable reactions that lead to the same final state configuration. This idea was formalized in a theorem by F. Bloch and A. Nordsieck [22] and by T. Kinoshita [23], T. Lee and M. Nauenberg [24] (the so-called KLN theorem), which states that observable transition probabilities are free of IRC singularities. After summing over all possible configurations, the IRC singularities from the virtual corrections exactly cancel againts those from the real contribution leading to a finite prediction. Several algorithms to implement the *IRC cancellation* have been proposed during the years [25–37] and allow one to obtain precise predictions for physical observables.

2.3.3 Matrix element factorisation in the soft and collinear limits

The IRC properties of a cross section can be studied in detail by analysing the matrix elements describing the process at the corners of the phase space where the singularities arise from. One finds that in both limits the matrix elements factorise in a product of a singular universal factor and a matrix element where the collinear particles have been replaced by a single *parent* particle and the soft particles have been removed. In the present thesis we will make often use of such factorisation properties so it is worth recalling them separately for the soft and the collinear case.

2.3.3.1 Factorisation in the soft limit

We consider the process depicted in Fig. 2.2 where the index i of the colour matrix T_i^a represents the parton which the gluon was emitted off, *i.e.* it can be in the fundamental or adjoint representation.
The m-parton matrix element has a tilde since it is a vector in Dirac space.

The soft limit is defined by setting $k_j^\mu = \lambda q^\mu$ with $\lambda > 0$ and by sending $\lambda \to 0$ keeping q^μ fixed. In this limit the emission of the soft gluon off internal propagators is

[1] There is nevertheless a big difference between QED and QCD in how collinear and soft radiation is measured experimentally. In QED there is no confinement and the final state, including soft bremsstrahlung, can in principle be measured. The bremsstrahlung detected in an experiment only depends on the sensitivity and the energy resolution of the detector. A soft photon is only measurable if the finite resolution of the detector allows for it. In QCD however, there are also physical restrictions in addition to the technical ones. Whether a soft or collinear gluon is radiated or not, the quarks will undergo some soft interaction in the hadronisation process, until all coloured particles are collected into colour-singlet hadrons. In a final state the particles produced during the hadronisation and the result of the hadronisation of a soft gluon are not distinguishable if the gluon has a transverse momentum smaller than the typical hadronic scale: roughly 1 GeV.

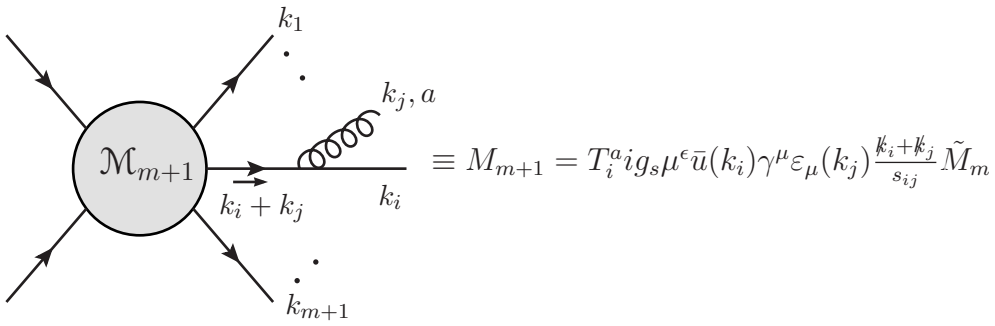

Figure 2.2: Soft or collinear emission off one external leg.

IR finite. If we consider the emission of a soft gluon off an external quark (Figure 2.2), the amplitude M_{m+1} reduces to

$$\begin{aligned} M_{m+1} &= T_i^a \, i g_s \mu^\epsilon \bar{u}(k_i)\gamma^\mu \varepsilon_\mu(k_j) \frac{\not{k}_i + \not{k}_j}{s_{ij}} \tilde{M}_m \\ &\overset{k_j \to 0}{=} T_i^a \, i g_s \mu^\epsilon \frac{1}{s_{ij}} \bar{u}(k_i)\gamma^\mu \varepsilon_\mu(k_j) \not{k}_i \tilde{M}_m \\ &= T_i^a \, i g_s \mu^\epsilon \frac{k_i^\mu}{k_i \cdot k_j} \varepsilon_\mu(k_j) M_m \,. \end{aligned} \tag{2.25}$$

In the last line we used the anticommutation relation between γ-matrices and the Dirac equation. The Dirac spinor was absorbed in the m-parton matrix element M_m and therefore we can drop the tilde on top of it. A similar result can be obtained also in case a gluon emits another gluon, while the emission of soft quarks leads to a integrable singularity because the fermion propagator is less singular than the gluon one. Since in general we do not know which leg the soft gluon is emitted off, we have to sum over all external partons. We find that in the soft limit the $m+1$ matrix element reduces to

$$\left| M_{m+1}^0 \right\rangle \overset{k_j \to 0}{\to} i g_s \mu^\epsilon \varepsilon_\mu(k_j) J^\mu(k_j) \left| M_m^0 \right\rangle \,, \tag{2.26}$$

where

$$J^\mu(k_j) = \sum_{n=1}^{m} T_n^a \frac{k_n^\mu}{k_n \cdot k_j} \tag{2.27}$$

is called *eikonal* current. We observe that the $(m+1)$-parton matrix element factorises into a m-parton matrix element (which is clearly process dependent) and a universal eikonal factor.

2.3.3.2 Factorisation in the collinear limit

To study the collinear limit of a $(m+1)$-parton matrix element we work in a physical gauge and consider directly a squared amplitude. There are different possible splittings summarised in Table 2.2. We look again at the case considered before, of a quark splitting into a collinear gluon and a quark. Focusing only on the splitting part of the squared amplitude we have

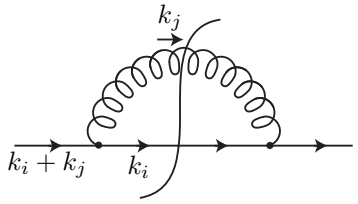

$$\equiv \mathcal{A} = C_F g_s^2 \mu^{2\epsilon} \frac{\not{k}_i + \not{k}_j}{s_{ij}} \gamma^\mu \not{k}_i \gamma^\nu d_{\mu\nu}(k_j, n) \frac{\not{k}_i + \not{k}_j}{s_{ij}},$$

where $d_{\mu\nu}(k_j, n)$ is the propagator in the physical gauge

$$d_{\mu\nu}(p, n) = -g_{\mu\nu} + \frac{p_\mu n_\nu + n_\mu p_\nu}{p \cdot n},$$

and n^μ is an arbitrary light-like vector. Inserting this in $\mathcal{A}$ we find

$$\mathcal{A} = C_F \, 4\pi\alpha_s \mu^{2\epsilon} \frac{\not{k}_i + \not{k}_j}{s_{ij}} \left(-\gamma^\mu \not{k}_i \gamma_\mu + \frac{\not{k}_j \not{k}_i \not{n} + \not{n} \not{k}_i \not{k}_j}{k_j \cdot n} \right) \frac{\not{k}_i + \not{k}_j}{s_{ij}}, \tag{2.28}$$

and after some Dirac algebra this becomes

$$\mathcal{A} = C_F \, 4\pi\alpha_s \mu^{2\epsilon} \frac{1}{s_{ij}} \left[(d-2)\not{k}_j + \frac{1}{k_j \cdot n} \left(4k_i \cdot n \not{k}_i + 2k_i \cdot n \not{k}_j + 2k_j \cdot n \not{k}_i - s_{ij} \not{n} \right) \right]. \tag{2.29}$$

The collinear limit of momenta k_i and k_j is defined by the Sudakov parametrisation:

$$\begin{aligned} k_i^\mu &= z k^\mu + k_{i\perp}^\mu - \frac{k_{i\perp}^2}{z} \frac{n^\mu}{2\, k \cdot n}, \\ k_j^\mu &= (1-z) k^\mu + k_{j\perp}^\mu - \frac{k_{j\perp}^2}{(1-z)} \frac{n^\mu}{2\, k \cdot n}, \end{aligned}$$

where $k_{i\perp}^\mu + k_{j\perp}^\mu = 0$. The vector k^μ gives the collinear direction and

$$k^2 = 0 \quad , \quad n^2 = 0 \quad , \quad k_{i\perp} \cdot k = k_{j\perp} \cdot k = k_{i\perp} \cdot n = k_{j\perp} \cdot n = 0 .$$

In the collinear limit $k_{i\perp}^\mu, \, k_{j\perp}^\mu \to 0$ and $s_{ij} \to -\frac{k_{j\perp}^2}{z(1-z)}$.

Using the Sudakov parametrisation in Eq. 2.29 and keeping only the most divergent term in the limit $k_{i\perp} = -k_{j\perp} \to 0$ we obtain

$$\begin{aligned} \mathcal{A} &\overset{k_{i\perp} \to 0}{\to} 4\pi\alpha_s \mu^{2\epsilon} \frac{2C_F}{s_{ij}} \left[\frac{1+z^2}{1-z} - \epsilon (1-z) \right] \not{k} + \mathcal{O}\left(k_{i\perp}^\mu\right) \\ &= 4\pi\alpha_s \mu^{2\epsilon} \frac{1}{s_{ij}} \tilde{P}^0_{q \to qg}(z) \not{k} + \mathcal{O}\left(k_{i\perp}^\mu\right), \end{aligned} \tag{2.30}$$

where

$$\tilde{P}^0_{q\to qg}(z) = 2C_F\left[\frac{1+z^2}{1-z} - \epsilon\,(1-z)\right].$$

Therefore the collinear limit for the whole matrix element squared is given by

$$\left\langle M^0_{m+1}|M^0_{m+1}\right\rangle \overset{k_j||k_i}{\to} 4\pi\alpha_s\mu^{2\epsilon}\frac{\tilde{P}^0_{q\to qg}}{s_{ij}}\left\langle M^0_m|M^0_m\right\rangle + \mathcal{O}\left(k^\mu_{i\perp}\right). \tag{2.31}$$

The function $\tilde{P}^0_{q\to qg}(z)$ is one of the so-called Altarelli-Parisi [38] splitting functions and is associated with the branching $q \to qg$. There are four different splitting functions associated with the different possible splittings and they can be expanded in powers of α_s. Furthermore there are two families of splitting functions associated with timelike or spacelike splitting. The two families are identical at leading order and differ at higher orders.

The result we derived for $\tilde{P}^0_{q\to qg}(z)$ is divergent for $z \to 1$. This behaviour encapsulates the soft singularity, since for $z \to 0$ the gluon becomes not only collinear but also soft. In order to remove this singularity we have to add the virtual contribution

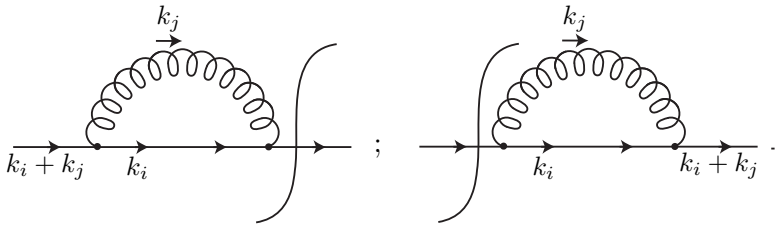

However, instead of computing these contribution explicitly we can make use of fermion number conservation, from which it follows directly that[1]

$$\int_0^1 \mathrm{d}z\, P^0_{q\to qg}(z) = 0\,. \tag{2.32}$$

Since the virtual contributions can only have influence on terms proportional to $\delta(1-z)$, we make the ansatz

$$P^0_{q\to qg}(z) = 2C_F\left[\frac{1+z^2}{1-z} + C\,\delta(1-z)\right] + \mathcal{O}(\epsilon)\,.$$

From the condition 2.32 it follows that

$$C = -\delta(1-z)\int_0^1 \mathrm{d}z\, P^0_{q\to qg}(z)\,.$$

[1] The spacelike $P^0_{q\to qg}(z)$ splitting function appears in the $\mathcal{O}(\alpha_s)$ corrections to the quark PDF, where z is the Bjorken variable of the quark. From $\int \mathrm{d}z\, q(z,Q^2) = 0$ it follows that the integral over z of the splitting function must vanish.

However, if we perform the integral naïvely, it diverges at the upper bound. We can then express the resulting splitting function in terms of (+)-distributions. By splitting up the singular part we obtain

$$\begin{aligned} P^0_{q\to qg}(z) =& 2C_F\left[\frac{2}{1-z} - (1+z) - \delta(1-z)\int_0^1 \mathrm{d}z'\left(-(1+z') + \frac{2}{1-z'}\right)\right] \\ =& 2C_F\left[\frac{2}{1-z} - (1+z) + \frac{3}{2}\delta(1-z) - \delta(1-z)\int_0^1 \mathrm{d}z'\frac{2}{1-z'}\right] \\ =& 2C_F\left[\frac{2}{(1-z)_+} - (1+z) + \frac{3}{2}\delta(1-z)\right] \\ =& 2C_F\left[\frac{1+z^2}{(1-z)_+} + \frac{3}{2}\delta(1-z)\right], \end{aligned} \tag{2.33}$$

with the (+)-distribution being defined as

$$\begin{aligned} \int_0^1 \mathrm{d}z\,[f(z)]_+\,g(z) &= \int_0^1 \mathrm{d}z f(z)\,[g(z)-g(1)] \\ &= \int_0^1 \mathrm{d}z\left[f(z)g(z) - \delta(1-z)g(z)\int_0^1 \mathrm{d}z' f(z)\right], \end{aligned} \tag{2.34}$$

where $g(z)$ is a smooth and divergence-free function in the interval $z \in [0,1]$.

The other splitting functions can be derived in a similar way. The leading order results, labeled by a 0, are summarised in Table 2.2, where we shortened a bit the notation by labeling a splitting of the type $a \to bX$ as $P^0_{ba}(z)$. This is the customary notation for splitting functions used in many textbooks. Nowadays splitting functions are known up to NNLO [139, 140] accuracy.

Splitting process	Altarelli-Parisi splitting function
$q \to qg$	$P^0_{qq} = C_F\left[\frac{1+z^2}{(1-z)_+} + \frac{3}{2}\delta(1-z)\right]$
$q \to gq$	$P^0_{gq} = C_F\left[\frac{1+(1-z)^2}{z}\right]$
$g \to q\bar{q}$	$P^0_{qg} = \left[z^2 + (1-z^2)\right]$
$g \to gg$	$P^0_{gg} = 2C_A\left[\frac{z}{(1-z)_+} + \frac{(1-z)}{z} + z(1-z)\right] + \frac{1}{2}\delta(1-z)\frac{(11C_A - 2N_F)}{3}$

Table 2.2: Leading order splitting functions normalised according to the thesis notation.

Knowing the way matrix elements behave in the singular regions of phase space, we can compute exactly the IRC divergent terms of a cross section. This allows one to perform the cancellation of IRC singularities leading to a finite result.

2.3.4 Infrared and Collinear Safety

For inclusive cross sections, the KLN theorem ensures that higher order radiative corrections are well defined and finite. In real life, we often want to compute non-inclusive observables defined in order to measure specific properties of the event. In the general case IRC singularities do not cancel completely when we sum real and virtual contributions. For this reason we need to define more precisely which requirements a physical observable must fulfil in order to be actually computable. A first criterion to build proper physical observables was first proposed by Sterman and Weinberg [39] and it is called Infrared and Collinear Safety. This criterion can be summarized in the following two requirements:

1. If, in a final state consisting of m particles, two emissions have collinear momenta, the observable computed with all m emissions must equal the observable with the two collinear particles replaced by a pseudo-particle whose momentum equals the sum of the two collinear momenta. This first requirement is known as *collinear safety*

2. If, in a final state consisting of m particles, one emission is soft, then the observable computed with all m emissions must equal the observable obtained by neglecting the soft emission. This part of the criterion is known as *infrared safety.*

We can write these two criteria more formally as

$$\begin{aligned} v_m\left(p_1, p_2, \ldots, p_m\right) &\overset{p_1 \| p_2}{\longrightarrow} v_{m-1}\left(p_1 + p_2, p_3, \ldots, p_m\right) , \\ v_m\left(p_1, p_2, \ldots, p_m\right) &\overset{E_1 \to 0}{\longrightarrow} v_{m-1}\left(p_2, p_3, \ldots, p_m\right) . \end{aligned} \tag{2.35}$$

All the perturbative observables should fulfil this two requirements in order for the radiative corrections to be finite and well defined. The IRC safety implies that computable quantities cannot resolve the long-distance phenomena for which the perturbative description is not accurate.
IRC safety suggests us the way physical observables should be defined in a proper way. Nevertheless we still need a description of the connection between the perturbative treatment (in terms of partons) and what experiments observe (hadrons). Unlike QED, where the soft radiation can be resolved up to the detector resolution, in QCD things are way more complicated since the confinement ensures that we never observe free partons. For a proper simulation of the real event we need to model the transition from parton level to hadron level reproducing the particles that are observed in the detector. Such a transition is called *hadronisation* and it can be simulated through phenomenological models. So far, no rigorous field theoretical description of this phenomenon is available. We will analyse one particular model in Chapter 5 in the context

of electron-positron collisions. In general, such corrections are usually (fortunately) suppressed by some negative power of the centre-of-mass energy so they can be neglected at very high energies. The observables can thus be defined at parton level rather than at hadron level and the agreement between the perturbative prediction and real data will improve as we move to higher energies. Though at current collider energies non-perturbative corrections are still quite sizeable and we need to account for them.

Often, rather than computing the collider observables using the plain partons, the elementary final state particles in an event are clustered in collimated bunches of particles called *jets*. The physical observables are then computed using these new objects. Jets are defined through a routine called *jet algorithm* that describes how to build the clusters out of the final state partons. Experimentally it is not obvious how final state particles should be grouped into jets. The definition of *jet algorithms* permits a suitable procedure for the classification of a final state consisting of hadrons (experimentally) or quarks and gluons (perturbatively) according to the number of jets. In practice a jet algorithm consists of two important parts. The algorithm itself is a set of rules for grouping the particles into jets and usually involves a set of parameters that specify how close two particles must be to get clustered into the same jet. The two particles get eventually combined to form a jet according to some *recombination scheme* that specifies how the two momenta should be combined. The Snowmass accord of 1990 [40] collects all the main features a jet algorithm should have in order to be successfully used both in theory and in experiments. There are two broad categories of jet algorithms: the cone algorithms and the sequential recombination algorithms (for a review see [41]). Recently, in view of the large jet activity at the LHC, a lot of progress was made in the development of fast and theoretically well defined jet algorithms.

3

Perturbation theory beyond fixed-order

In the previous section we showed that QCD properties allow us to compute physical observables through a perturbative approach. The detailed study of hadronic final state properties requires to perform higher order perturbative calculations which are well defined only in the case of IRC safe observables. In such cases the IRC singularities cancel between real and virtual corrections giving rise to a finite result. Often in practice we are interested in computing non-inclusive observables that implicitly apply phase space cuts constraining the energy or the rapidity of the real radiation. If real and virtual corrections are unbalanced, the cancellation of IRC singularities is no longer complete and the residual (unbalanced) divergences manifest themselves in form of logarithms of the constraining phase space cuts (or ratios of them if they are not dimensionless). When the real radiation is heavily constrained (often this is required to increase the experimental sensitivity of the process and reduce the background noise) the logarithmically-enhanced contributions are large and persist at any order in perturbation theory. To show this phenomenon with a simple example, we consider a quark-antiquark dipole with centre-of-mass energy Q which emits a soft and collinear gluon with momentum $k^\mu = (k^+, k^-, k_\perp)$ (k^+ and k^- are the light cone components along the directions of the quark and antiquark, respectively) of which we want to measure the transverse momentum. For the sake of simplicity we limit ourselves to the case of soft-collinear emission, but the same conclusions hold for the hard-collinear case. The matrix element squared of a single soft emission off a quark-antiquark dipole is given by the eikonal factor (Eq. 2.27). The real contribution reads

$$dW_{\text{real}} = 2\frac{\alpha_s}{\pi} C_F \frac{dk_\perp}{k_\perp} \frac{d\phi}{2\pi} d\eta |M_0^{\text{tree}}|^2 \Theta(p_t - k_\perp), \tag{3.1}$$

where η is the rapidity of the emission with respect to the emitting leg and the factor of 2 stems from the fact that the soft gluon can be emitted off each of the two legs.

The rapidity of the emission is constrained by

$$|\eta| \leq |\eta_{max}| = \ln \frac{Q}{k_\perp} + \mathcal{O}(1), \tag{3.2}$$

where we neglected the second term in the r.h.s. since it gives rise to non-singular contributions which are not relevant in this context. The cross section for this simple process reads

$$\sigma^{\mathrm{LO}} + \sigma^{\mathrm{NLO}} = \sigma^{\mathrm{LO}} \left(1 + 2C_F \frac{\alpha_s}{\pi} \int \frac{dk_\perp}{k_\perp} \int_{-\ln Q/k_\perp}^{\ln Q/k_\perp} d\eta \left(\Theta(p_t - k_\perp) - 1 \right) \right), \tag{3.3}$$

where the -1 term encodes the virtual contribution. Eq. 3.3 leads to

$$\sigma^{\mathrm{LO}} + \sigma^{\mathrm{NLO}} = \sigma^{\mathrm{LO}} \left(1 - 2C_F \frac{\alpha_s}{\pi} L^2 \right), \tag{3.4}$$

where $L = \ln \frac{Q}{p_t}$. The double logarithm is the remnant of the soft and collinear singularity, each of which contributes with a single logarithm. The hard-collinear (non-soft) case would contribute with an additional single-logarithmic term. In the phase space region where $p_t \ll Q$ the logarithmically enhanced terms get dramatically large and the cross section becomes negative (!). Moreover, if $\alpha_s L \sim 1$ then the NLO and higher order terms are not suppressed with respect to the leading order contribution (they are actually enhanced), meaning that the perturbative series gets poorly convergent and the prediction is completely spoiled. This type of logarithms are called *Sudakov* logarithms and they originate from the infrared and collinear regions of the phase space whenever we constrain either the angle or the energy of the real radiation. The previous example shows that in spite of the KLN theorem, soft gluon effects can be large if real and virtual terms are kinematically highly unbalanced. In this cases we cannot truncate the perturbative series at some order in the strong coupling, but we need to calculate the perturbative solution to all-orders. Since an exact treatment is technically impossible, one possible solution is to reorganize the perturbative expansion by summing classes of logarithms (*resummation*). The main idea can be illustrated with the help of Table 3.1.

Each line in the table reports the logarithmic contributions at each order in the standard perturbative expansion. This is what is known as *fixed-order* approach. If we instead look at the columns, we see that each column is suppressed by a factor of $1/L$ with respect to the one to its left. This suppression is effective if the logarithms are large. To rescue the perturbative approach we then sum the terms in each column to all orders in α_s. The first column contains the dominant class of logarithms, and the corresponding accuracy is referred to as leading-logarithmic (LL) accuracy. A LL-accurate result sums *all* the terms in the first column, the next-to-leading-logarithmic (NLL) result also contains the elements in the second column and so forth. Many

$\alpha_s L^2$	$\alpha_s L$				$\mathcal{O}(\alpha_s)$
$\alpha_s^2 L^4$	$\alpha_s^2 L^3$	$\alpha_s^2 L^2$	$\alpha_s^2 L$		$\mathcal{O}(\alpha_s^2)$
...	...	...	...	...	
$\alpha_s^n L^{2n}$	$\alpha_s^n L^{2n-1}$	$\alpha_s^n L^{2n-2}$	$\alpha_s^n L^{2n-3}$	...	$\mathcal{O}(\alpha_s^n)$

Table 3.1: Resummation is a reorganization of the perturbative expansion in terms of classes of logarithms.

observables have an additional interesting property, *i.e.* the lowest class of logarithms exponentiate (*exponentiation*). This allows us to define a more accurate logarithmic ordering in the resummed perturbative series. At the *exponent level*, we usually define as leading logarithms the terms of order $\alpha_s^n L^{n+1}$, NLL as $\alpha_s^n L^n$ and so on. It is easy to see that this new ordering is more accurate than the previous one already at $\mathcal{O}(\alpha_s^2)$ since a NLL result provides us with the terms of order $\mathcal{O}(\alpha_s^2 L^2)$. Throughout this thesis we will always use this ordering. For *non-exponentiating* observables (*e.g.* the JADE jet algorithm) the first convention applies.
Another useful example of resummation of logarithmic terms is given by the running coupling. Looking at the solution to the RGE equation for α_s (Eq. 2.14) we see that it resums all terms of the form $\bar{\alpha}_s^n L^n$. These logarithms have an UV origin rather than an IRC one, but they offer a perfect example of resummation in a simple form.

3.1 Colour coherence and independent emission picture

The resummation of Sudakov logarithms requires the simulation of QCD radiation to all orders in the strong coupling constant. There are different available techniques to perform this analysis, and in this thesis we discuss two of them. We start by recalling some important properties of all-order soft and collinear radiation that will be useful to understand the following chapters.

3.1.1 The eikonal identity

The first result we recall is the *eikonal identity* and allows us to express in a compact form the emission probability of any number of soft gluons. We prove the identity for two emissions. Consider a given hard leg (quark) with momentum $p + k_1 + k_2$ which emits two subsequent independent (uncorrelated) soft gluons with momenta k_1, $k_2 \ll p$. The double soft current in this case reads (we omit colour factors for the sake

of simplicity)

$$M^{\mu,\nu}(p,k_1,k_2) = \frac{2p^\mu}{(p+k_1+k_2)^2}\frac{2p^\nu}{(p+k_2)^2} + \frac{2p^\mu}{(p+k_1+k_2)^2}\frac{2p^\nu}{(p+k_1)^2}, \tag{3.5}$$

where we summed over the two possible permutations. With some algebra we can recast the previous expression as

$$M^{\mu,\nu}(p,k_1,k_2) = p^\mu p^\nu \frac{1}{p\cdot k_1 + p\cdot k_2 + k_1\cdot k_2}\left(\frac{1}{p\cdot k_1} + \frac{1}{p\cdot k_2}\right). \tag{3.6}$$

We neglect the term $k_1 \cdot k_2$ since it is suppressed by the low gluon energies and we eventually get

$$M^{\mu,\nu}(p,k_1,k_2) = \frac{p^\mu}{p\cdot k_1}\frac{p^\nu}{p\cdot k_2}, \tag{3.7}$$

which shows that the emission of two independent soft gluons can be expressed as the product of two independent eikonal factors. The extension to the case with an arbitrary number of emissions is straightforward and can be done by induction assuming the validity of the identity for n gluons and proving it for $n+1$ gluons. This, together with the two gluon case shown above gives a general proof for the eikonal identity.

3.1.2 Colour coherence

Consider a hard process with n external legs having four-momenta $\{p_i\}$. One of them emits a soft gluon with momentum k. The emission of a soft gluon can be expressed according to the eikonal formula

$$|M^\mu(\{p_i\},k)\rangle = \sum_{l=1}^{n} igT_l^a \frac{p_l^\mu}{p_l\cdot k}|M(\{p_i\})\rangle, \tag{3.8}$$

where μ is Lorentz index of the gluon and $|M(\{p_i\})\rangle$ is a vector in colour space. The matrix element squared reads

$$\langle M(\{p_i\})| - g^2 \sum_{l,m=1}^{n} T_l^a \cdot T_m^a \frac{p_l\cdot p_m}{p_l\cdot k\, p_m\cdot k}|M(\{p_i\})\rangle. \tag{3.9}$$

The previous formula shows that we cannot factorise the soft gluon probability beacuse of the correlation between the different colour matrices which act on the Born matrix element. The soft gluon pattern depends on the detailed colour flow (interference) in the hard scattering process and it is usually quite involved. However, such a structure can be simplified if we assume that the gluon is emitted almost collinearly to one of the legs. This approximation allows us to compute only the most singular (soft and collinear) contribution. Subleading single-logarithmic effects due to the emission of a

either a hard-collinear gluon or a wide-angle soft gluon can be included as subsequent corrections. Assuming that the gluon is emitted collinearly to the leg p_j (*i.e.* $\theta_{jk} \ll \min \theta_{lm}$), we can rewrite the eikonal factor as

$$\begin{aligned} -4\pi\alpha_s \sum_{l,m=1}^{n} T_l^a \cdot T_m^a \frac{p_l \cdot p_m}{p_l \cdot k \, p_m \cdot k} &= -8\pi\alpha_s \sum_{l<m} T_l^a \cdot T_m^a \frac{1}{\omega^2} \frac{1-\cos\theta_{lm}}{(1-\cos\theta_{lk})(1-\cos\theta_{mk})} \\ &= -\frac{8\pi\alpha_s}{\omega^2} \frac{1}{1-\cos\theta_{jk}} T_j^a \cdot \sum_{l\neq j} T_l^a \frac{1-\cos\theta_{lj}}{1-\cos\theta_{lk}} + \dots \\ &= -\frac{16\pi\alpha_s}{\omega^2\theta_{jk}^2} T_j^a \cdot \sum_{l\neq j} T_l^a + \dots, \end{aligned} \tag{3.10}$$

where ω is the soft gluon energy and in the last two lines we neglected terms which are regular as $\theta_{jk} \to 0$. Using colour conservation $\sum_{l\neq j} T_l^a = -T_j^a$ we obtain

$$-\frac{16\pi\alpha_s}{\omega^2\theta_{jk}^2} T_j^a \cdot \sum_{l\neq j} T_l^a = \frac{16\pi\alpha_s}{\omega^2\theta_{jk}^2} T_j^a \cdot T_j^a. \tag{3.11}$$

Including the phase space factor we reproduce the single soft gluon emission probability

$$dW_1 = \frac{\alpha_s}{\pi} (T_j^a \cdot T_j^a) \frac{d\phi}{2\pi} \frac{d\theta^2}{\theta^2} \frac{d\omega}{\omega} = \frac{\alpha_s}{\pi} (T_j^a \cdot T_j^a) \frac{dz}{z} \frac{d\phi}{2\pi} \frac{dk_\perp^2}{k_\perp^2}. \tag{3.12}$$

The previous expression does not contain any traces of interference, meaning that the soft radiation (at leading logarithmic accuracy) can be seen as the sum of radiation off *independent* emitters. In other words the destructive interference between different emissions cancels the radiation at large angles (*i.e.* for $\theta_{kj} > \min \theta_{lm}$) and its effect can be approximated by angular ordering, *i.e.* subsequent radiation is emitted with an angle smaller than the one of previous emissions. This important property is known as *colour coherence* and it tells us that soft gluons only see the effective colour charge of the emitter and cannot resolve the details of the interaction at shorter distances. The previous result is of primary relevance for all Monte Carlo parton shower programmes which simulate QCD radiation at all orders. It can be easily proved that the same result holds without taking the collinear limit if we perform the azimuth average of the eikonal factor. In general, we are not allowed to integrate inclusively over the azimuth angle, since a generic observable will have a non-trivial azimuth dependence. While the previous derivation holds in general for any physical observable.

The previous property can be seen as a QED-like approximation to QCD. Actually an additional complication comes from the non-abelian nature of QCD. Unlike in QED, the emitted gluon can split into a gg pair whose colour structure is related to the one of the parent gluon. In the following section we will show that such an effect can be accounted for through a physical redefinition of the running coupling. Thanks to colour coherence

and to the eikonal identity we can express the emission probability for n gluons as the product of n single independent gluon emissions. We will refer to this approximation as the *independent emission picture*. So far we only considered soft and collinear gluons, but we can actually repeat the full exercise by taking into account the hard-collinear limit that is, replacing the eikonal probability with the whole Altarelli-Parisi splitting function

$$dW_1 = \frac{\alpha_s}{2\pi}(T_j^a \cdot T_j^a)\frac{zP_{ab}(z)}{z}dz\frac{d\phi}{2\pi}\frac{dk_\perp^2}{k_\perp^2}, \tag{3.13}$$

this is the form that we will use throughout this thesis. For the class of observables that will be introduced in the next section, this approximation is enough to achieve a NLL accuracy for processes with two hard emitters at the Born level. Cases with three or more Born partons will receive NLL contributions also from soft radiation emitted with a wide angle that we neglected in obtaining the independent emission formula. Such contributions can be included as subsequent corrections.

3.2 A condition for exponentiation: *recursive* Infrared and Collinear safety

In the beginning of this chapter we mentioned that there are collider observables which have an additional property called exponentiation. For such observables the leading logarithms sum up to an exponential function. In the present section we formulate this property in a more formal way, defining the requirements that observables must fulfil in order to have it. To do so, we need to revisit the definition of IRC safe observable, adding some requirement concerning the behaviour of the latter under multiple emissions.

In the following we limit ourselves to the analysis of *continuous global* observables, namely observables which do not have any discontinuity in some regions of the phase space. Parametrising the generic observable for a single emission $v(k)$ as a function of rapidity with respect to the emitting leg η_l, the azimuth ϕ and the transverse momentum $k_\perp$, we can reformulate the previous requirement stating that the $k_\perp$ dependence of the observable for a single emission does not depend on neither the rapidity nor the azimuthal angle of the emission itself. This requirement ensures (at any order) the absence of the so called *non-global* logarithms [43, 44] which are not discussed in this thesis.

To perform the resummation we need to know the exact behaviour of the observables in presence of any number of soft and/or collinear emissions. To formulate our condition in a formal way we define a momentum mapping $\kappa_i(\zeta)$ such that the value of the observable for the corresponding emission is $v(\kappa_i(\zeta)) = \zeta$. We do not need to introduce an explicit form for this mapping for the purpose of this chapter, however a

useful representation can be found in [42]. We require that in the presence of multiple emissions the observable scales in the same fashion as it would do for a single emission. In formulae, we require that for an arbitrary number of emissions m the following limit

$$\lim_{\bar{v}\to 0}\frac{1}{\bar{v}}v(\kappa_1(\bar{v}\zeta_1),\kappa_2(\bar{v}\zeta_2),...,\kappa_m(\bar{v}\zeta_m)) \tag{3.14}$$

is well-defined and non-zero, for any choice of (non-zero) values for ζ_i. Here $\bar{v}$ is a parameter that we vary to probe the observable's properties. The above condition guarantees that in the limit of small $\bar{v}$, any set of emissions close to the boundary $v(k) = \bar{v}$ will give a value of the observable of order $\bar{v}$. In a process with hard scale Q and infrared/collinear scale set by the observable $v(k) = v$, the standard formulation of IRC safety requires that additional soft and/or collinear splittings do not change the observable value by more than a positive power of the softness/collinearity of the splitting, normalised to the hard scale Q. We additionally require that, for sufficiently small values of v, there exists some $\epsilon \ll 1$, *independent of* v, such that splittings at scales smaller than ϵv will change the observable by an amount $\epsilon^p v$, where p is some positive power. The crucial property is that ϵ can be chosen independently of v. The standard formulation of IRC safety can be expressed as

$$\lim_{\zeta_{m+1}\to 0} v(\kappa_1(\bar{v}\zeta_1),\kappa_2(\bar{v}\zeta_2),...,\kappa_m(\bar{v}\zeta_m),\kappa_{m+1}(\bar{v}\zeta_{m+1})) = v(\kappa_1(\bar{v}\zeta_1),\kappa_2(\bar{v}\zeta_2),...,\kappa_m(\bar{v}\zeta_m)), \tag{3.15}$$

while the analogous condition for *recursive* Infrared and Collinear (rIRC) safety is given by the double limit

$$\lim_{\zeta_{m+1}\to 0}\lim_{\bar{v}\to 0}\frac{1}{\bar{v}}v(\kappa_1(\bar{v}\zeta_1),\kappa_2(\bar{v}\zeta_2),...,\kappa_m(\bar{v}\zeta_m),\kappa_{m+1}(\bar{v}\zeta_{m+1})) = \lim_{\bar{v}\to 0}\frac{1}{\bar{v}}v(\kappa_1(\bar{v}\zeta_1),\kappa_2(\bar{v}\zeta_2),...,\kappa_m(\bar{v}\zeta_m)), \tag{3.16}$$

where the last limit is well-defined and non-zero. The order of the limits in Eq. 3.16 is important and expresses the condition we discussed above: if the softness/collinearity ζ_{m+1} at which the $(m+1)$-th emission becomes irrelevant depends on $\bar{v}$ (*i.e.* it scales as a power of $\bar{v}$) , then even for very small values of $\bar{v}$ the $(m+1)$-th emission will never become irrelevant and the condition 3.16 will not be fulfilled. For a complete formulation we need to include the situation where one or more emissions split softly and/or collinearly. If we consider a splitting $\kappa_i(\zeta) \to \{\kappa_{ia},\kappa_{ib}\}(\zeta,\mu)$ with $\mu^2 = (\kappa_{ia}+\kappa_{ib})^2/\kappa_i^2$ and $\lim_{\mu\to 0}(\kappa_{ia}+\kappa_{ib}) = \kappa_i$, we then require

$$\lim_{\mu\to 0}\lim_{\bar{v}\to 0}\frac{1}{\bar{v}}v(\kappa_1(\bar{v}\zeta_1),\kappa_2(\bar{v}\zeta_2),...,\{\kappa_{ia},\kappa_{ib}\}(\zeta,\mu),...,\kappa_m(\bar{v}\zeta_m)) = \lim_{\bar{v}\to 0}\frac{1}{\bar{v}}v(\kappa_1(\bar{v}\zeta_1),\kappa_2(\bar{v}\zeta_2),...,\kappa_i(\bar{v}\zeta_i),...,\kappa_m(\bar{v}\zeta_m)), \tag{3.17}$$

regardless of how the $\mu \to 0$ limit is taken.
Equations 3.16, 3.17 summarise the rIRC safety requirement that we are going to use in the following section to resum the Sudakov logarithms for this class of observables. Nowadays, most of the collider observables (*e.g* event-shapes, jet observables, jet masses,...) fulfil such a requirement and can be treated following the method outlined in this thesis. Nevertheless there are some particular observables used in the past (LEP era) which are not rIRC safe despite them being IRC safe (*e.g.* JADE and Geneva jet algorithms). A general resummation algorithm for such observables has not yet been found.

3.3 Resummation for rIRC safe observables

In the present section we use our knowledge about QCD radiation together with rIRC safety to obtain a general resummation formula which allows one to resum Sudakov logarithms up to NLL accuracy. For the sake of simplicity we only consider the case of two hard emitters at the Born level since this will be the class of processes discussed in the following sections. Such processes include e^+e^- annihilation, DIS and Drell-Yan like processes (*e.g.* Higgs-boson production). The extension of the algorithm to NNLL accuracy is not straightforward since it requires to consider effects which go beyond colour coherence and the independent emission picture. A general NNLL algorithm is not yet available, and its development is still work in progress at the time of this thesis. A particular example, concerning the production of a colour singlet, will be discussed in Section 6. In the following we briefly discuss the NLL approach. The reader can refer to [42] for further technical details.
For observables v of the type discussed above, the resummed cross section has the general form

$$\Sigma(v) = \exp\left(-\int [dk]|M(k)|^2\right) \sum_{m=1}^{\infty} \frac{1}{m!} \prod_{i=1}^{m} \int [dk_i]|M(k_i)|^2 \Theta(v - v(k_1, ..., k_m)), \quad (3.18)$$

where the exponential factor resums all the virtual corrections, while the remaining sum accounts for an arbitrary number of real emissions. Both real and virtual contributions are regularised and the coupling is always evaluated in the CMW scheme [45] to account for running coupling effects. In this scheme the coupling is defined as the physical strength of soft gluon radiation. For a NLL resummation it is enough to express the coupling through this scheme up to and including corrections of order $\mathcal{O}(\alpha_s^2)$, which encode the inclusive contribution of a correlated soft gluon splitting (for a discussion of this approximation and its physical interpretation the reader may refer to Section 2.2.2 of [42]). It can be shown that for rIRC safe observables, the non-inclusive contribution of the correlated emission gives rise to NNLL corrections [42]. This approximation is

not accurate in the hard-collinear region, but the corrections are subleading (NNLL). For a NNLL algorithm this scheme must be extended accordingly to account for all the wide angle soft and hard collinear contributions. The previous formula allows us to simulate an ensamble of any number of emissions as an uncorrelated product of many single emissions, in agreement with colour coherence and the independent emission picture. In this context, we can express the integrand using Eq. 3.13 as

$$[dk]|M(k)|^2 = dW_1 = \frac{\alpha_s}{2\pi}(T_j^a \cdot T_j^a)\frac{zP_{ab}(z)}{z}dz\frac{d\phi}{2\pi}\frac{dk_\perp^2}{k_\perp^2}. \tag{3.19}$$

It is useful to split the sum in Eq. 3.18 into two contributions. The first involving emissions with $v(k_i) > \epsilon v$ and the second with $v(k_i) < \epsilon v$, respectively. Here $\epsilon \ll 1$ is an arbitrary parameter that can be chosen independently of v and with $\ln 1/\epsilon \ll \ln 1/v$. We can write

$$\begin{aligned}\sum_{m=1}^{\infty}\frac{1}{m!}\prod_{i=1}^{m}\int[dk_i]|M(k_i)|^2 = \sum_{n=1}^{\infty}\frac{1}{n!}\prod_{i=1}^{n}\int_{\epsilon v}[dk_i]|M(k_i)|^2 \\ \times\sum_{k=0}^{\infty}\frac{1}{k!}\prod_{i=n+1}^{n+k}\int^{\epsilon v}[dk_i]|M(k_i)|^2,\end{aligned} \tag{3.20}$$

where we used a shorthand notation for the integration limits that apply directly to $v_i = v(k_i)$. We can now make use of the rIRC properties to observe that for sufficiently small ϵ all emissions below ϵv are irrelevant for the final observable value

$$v(k_1, k_2, ..., k_n, k_{n+1}, ..., k_{n+k}) = v(k_1, k_2, ..., k_n) + \mathcal{O}(\epsilon^p v). \tag{3.21}$$

We can therefore exponentiate their contribution to the cross section getting

$$\Sigma(v) = e^{-\int[dk]|M(k)|^2(1-\Theta(\epsilon v - v(k)))}\sum_{n=1}^{\infty}\frac{1}{n!}\prod_{i=1}^{n}\int_{\epsilon v}[dk_i]|M(k_i)|^2\Theta(v - v(k_1, ..., k_n)). \tag{3.22}$$

The term in the exponent contains the Sudakov radiator that expresses the no-emission probability. It encodes virtual and real unresolved ($< \epsilon v$) contributions. Its NLL expression reads

$$R(v) = \int\frac{\alpha_s^{\mathrm{CMW}}(k_\perp)}{2\pi}C\frac{zP_{ab}(z)}{z}dz\frac{d\phi}{2\pi}\frac{dk_\perp^2}{k_\perp^2}(1 - \Theta(v - v(k))), \tag{3.23}$$

where the strong coupling is evaluated at $k_\perp$ and in the CMW physical scheme [42, 45], namely

$$\alpha_s^{\mathrm{CMW}}(k_\perp) = \alpha_s(k_\perp)\left(1 + \frac{\alpha_s}{2\pi}\left(C_A\left(\frac{67}{18} - \frac{\pi^2}{6}\right) - \frac{5}{9}n_f\right)\right), \tag{3.24}$$

and the α_s in the r.h.s. is meant to be defined in the usual $\overline{\text{MS}}$ scheme. The constant C is the Casimir operator of the emitting leg ($C = C_A = 3$ for gluons and $C = C_F = 4/3$ for quarks). We can then expand in ϵ the exponent of Eq. 3.22 getting

$$\Sigma(v) = e^{-R(v)-R' \ln \frac{1}{\epsilon}+\dots} \sum_{n=1}^{\infty} \frac{1}{n!} \prod_{i=1}^{n} \int_{\epsilon v} [dk_i] |M(k_i)|^2 \Theta(v - v(k_1, ..., k_n)), \tag{3.25}$$

where we neglected subleading (NNLL) terms. They should be considered to achieve a complete NNLL accuracy. R' is the logarithmic derivative of the Sudakov radiator

$$R' = \frac{dR}{d \ln 1/v}. \tag{3.26}$$

We now focus on the real (resolved) emission contribution. Since the integrals in the sum are bounded both from below (ϵv) and from above (v), it is straightforward to see that to achieve a single logarithmic (NLL) accuracy it is enough to consider soft *and* collinear emissions (*i.e.* the hard collinear region in the real contribution gives rise to subleading NNLL terms). So we replace the squared matrix elements in the sum with their soft-collinear limit

$$[dk_i] |M_{sc}(k_i)|^2 = \frac{\alpha_s(k_\perp)}{\pi} C d\eta \frac{d\phi}{2\pi} \frac{dk_\perp^2}{k_\perp^2}, \tag{3.27}$$

moreover the coupling is now evaluated in the $\overline{\text{MS}}$ scheme, since the corrections due to the CMW scheme give rise to subleading contributions. The NLL-resummed cross section for a rIRC safe observable has the simple form

$$\Sigma(v) = e^{-R(v)} \mathcal{F}, \tag{3.28}$$

where $\mathcal{F}$ is called multiple emission function and its expression reads

$$\mathcal{F} = e^{-R' \ln \frac{1}{\epsilon}} \sum_{n=1}^{\infty} \frac{1}{n!} \prod_{i=1}^{n} \int_{\epsilon v} [dk_i] |M_{sc}(k_i)|^2 \Theta(v - v(k_1, ..., k_n)). \tag{3.29}$$

The previous equation contains all the physics we discussed so far and gives a clear physical picture of the all order behaviour of the QCD radiation at next-to-leading-logarithmic accuracy. The picture we obtained makes use of the colour coherence property of the matrix elements which guarantees that emissions widely separated in rapidity are effectively independent. This happens because emissions at some given angular scale are emitted coherently from the ensamble of emissions at much smaller angles. Moreover, we used a property of the rIRC safe observables which ensures that the details of the correlation of two emissions close in rapidity affect the prediction only at NNLL [42] (exept for its inclusive contribution that enters the running coupling

in the Sudakov radiator through the CMW scheme). Eq. 3.29 can be implemented in a Monte Carlo programme after some manipulations useful to make the numerical evaluation efficient. This was done in the computer code `CAESAR` [42], where the Monte Carlo implementation is discussed in detail. This method was succesfully applied to the resummation of a wide class of collider observables. For processes with three or more hard emitters at the Born level, one has to take into account also additional effects due to wide angle soft radiation that contributes at NLL level. This can be easily done by including an additional analytically known term in the Sudakov radiator, without modifying the multiple emission fuction [42].

3.4 Different approaches to Sudakov resummation

As already mentioned in the introduction to the present section, there is no standard way to resum a generic collider observable. Some observables may not even admit a resummed structure. Different approaches to Sudakov resummation have been proposed during the years. They rely on different theoretical backgrounds and we can divide them into two categories that we discuss qualitatively below.

3.4.1 Algorithms based on coherent branching

The first family of algorithms uses the properties of QCD radiation (coherence and angular ordering) to simulate the effect of any number of emissions to the desired logarithmic accuracy. We will refer to them as *coherent algorithms*. The first of such algorithms was first introduced by Catani, Marchesini and Webber [45] in the context of DIS and Drell-Yan processes. It was succesfully applied to some event-shape observables measured at the LEP collider, (*i.e.* thrust, heavy jet mass [47], C parameter [46], broadenings [48], energy-energy correlation [49]) to compute the average jet multiplicity in e^+e^- collisions [50, 51] and to obtain the resummed transverse momentum and threshold spectrum for Higgs boson production at hadron colliders [52–54]. The resummation of large logarithms is achieved by obtaining evolution equations for each of the hard jets (by hard jet here we mean a collimated bunch of soft and/or collinear partons, not necessarily involving any jet algorithm) which are assumed to emit coherently and to evolve independently of each other. The evolution equations can be solved analytically only in proper conjugate spaces (*e.g.* Laplace, Fourier, Mellin) where the observable factorises and eventually the resummed cross section is obtained by the inverse integral transform. Except for sufficiently inclusive quantities such as the energy-energy correlation, transverse momentum and threshold for which a NNLL result is available, this method achieves NLL accuracy and a systematic extension to NNLL is currently not available. Beyond NLL accuracy one should account for the cross-talk between different jets due to the exchange of soft radiation emitted with

large angle. The inclusion of such a contribution is not trivial in this context.
A similar algorithm called CAESAR, based on the same theoretical background but with a different implementation was proposed in [55] in the context of event-shape resummation in e^+e^- collisions. In the same paper they present results for new event shapes such as Thrust minor and major, oblateness and the three jet resolution in the Durham k_t-algorithm. Moreover, it was also applied to the resummation of jet observables at hadron colliders in [56] and the leading jet transverse momentum spectrum in Higgs and Z-boson production [**?**]. All these results are NLL accurate and currently work on an extension of the algorithm to include all the non-trivial NNLL corrections is ongoing. As a first result, the leading jet transverse momentum spectrum in Higgs and Z-boson production to NNLL accuracy was obtained in [58]. In this case resummation is achieved by simulating numerically the radiation to all orders in the strong coupling constant through the implementation of a dedicated Monte Carlo method. Nevertheless, in the case of factorisation of the observable in a proper conjugate space, analytical results can be obtained and they reproduce those of the coherent branching algorithm discussed above. The big advantage of this algorithm is that it allows one to treat observables that do not have any factorisation properties (*e.g.* jet algorithms) and thus cannot be resummed with any other approach.
The latter method is similar to the so called *parton showers*, *i.e* Monte Carlo programmes to simulate the subsequent coherent branchings of the final state partons down to infrared non-perturbative scales at which the hadronisation process takes place. In this programmes colour coherence is implemented through either angular ordering or ordering in some other kinematical variable (*e.g.* $k_\perp$, energy,...). Such splittings are implemented in a Markov chain and the implementation differs substantially from the CAESAR algorithm. Due to technical limitations of the algorithm, Parton Shower simulations nowadays are limited to LL accuracy, while NLL results can be obtained for a few *inclusive-enough* observables. On the other hand the algorithm is completely general and it can be applied to any collider observable.

3.4.2 Algorithms based on factorisation and RGE evolution

The second class of methods we are going to discuss is based on the factorisation properties of the cross section in the singular regions of the phase space. The first of such methods was initially proposed by Sterman et al. [59] for DIS and Drell-Yan processes and applied to the resummation of factorising event-shapes as well as to inclusive heavy quark decays and threshold resummation in $t\bar{t}$ pair production. The main idea relies on the all-order analysis of the factorisation properties of jet cross sections [60]. From this analysis it turns out that we can factorise a generic cross section in a convolution of leading kinematical subprocesses, each of them accounting for the soft, collinear and

hard-virtual modes, respectively. For a generic jet observable, the complete factorisation of the cross section is achieved provided the observable factorises. To this end, an integral transform is often needed in order to work in a conjugate space in which the observable can be split into a product of contributions due to the different leading kinematical regions. Once this is done, resummation is achieved by solving the renormalisation group equations for each of the subprocesses whose solutions encode all the Sudakov logarithms. Once the factorisation is obtained, this method provides us with a systematic way to perform Sudakov resummation to any logarithmic order. Notably the calculations needed to go beyond NLL are quite cumbersome due to the particular regulators used to disentangle the collinear singularities from the soft ones. For a good review of the method, the reader may refer to [61].

A similar and more recent approach relies on Soft-Collinear-Effective-Theory (SCET) [96], an effective theory of QCD that integrates out the non-singular modes of the QCD fields (quarks and gluons), describing in detail the soft and collinear dynamics. SCET offers a powerful tool to obtain factorisation theorems for a wide class of (factorising) observables. As in Sterman's approach, the cross section is factorised in terms of convolutions and products of different kinematical subprocesses and the resummation is carried out by means of RGE for each subprocess. The main difference from the other RGE approach discussed above is that the singular degrees of freedom are factorised at the Lagrangian level, rather than at the cross section level. This requires a complete specification of the scaling of all possible singular modes involved in the process which are observable-dependent. Each field in the Lagrangian is expanded in modes and only the singular ones (*e.g.* soft, collinear, Glauber modes,...) are kept. In doing so, one ends up with a new set of Feynman rules for the singular modes, that are used to achieve the desired factorisation. As above the full factorisation is obtained in conjugate spaces where the observable factorises in terms of contributions due to the different kinematical subregions, it thus cannot be applied to non-factorising observables. The RGE are then solved in this space before performing the inverse transform. Once the full factorisation is achieved, it can be used to perform the resummation to any logarithmic order. The effective theory approach was used to obtain predictions beyond NLL for some event-shape observables (thrust [99], heavy-jet mass [103],broadenings [106]) as well as for other jet observables such as N-jettiness [108] and beam-thrust [107]. It was recently also applied to the resummation of the jet-mass *global-logarithms* in hadronic collisions (note that the result lacks a complete treatment of non-global logarithms) and Higgs-boson and leading jet $k_\perp$ spectra in Higgs-boson production [109, 110] as well as threshold resummation for Drell-Yan-like processes [111].

In the following chapters we give two examples of resummation using different techniques. In Chapter 4 we resum the thrust distribution in e^+e^- annihilation to NNLL using an approach based on a factorisation theorem and RGE evolution. In Chapter 5 we apply the obtained results to perform a fit of the strong coupling constant using experimental data taken over a broad spectrum of energies. In Chapter 6 we resum the Higgs and Z production cross section with a cut on jets transverse momentum using an extension of the `CAESAR` algorithm to NNLL accuracy.

4

Factorisation and RGE resummation: analysis of thrust

4.1 Event-shape observables

Event-shape distributions in e^+e^- annihilation are observables which measure the geometrical properties of energy-momentum flow in a hadronic final state. They have been measured over a broad range in energies at LEP [62–65] as well as at earlier electron-positron colliders [66, 67]. The event-shape distributions allow for a detailed probe of the dynamics of QCD and especially for a precise determination of the strong coupling constant α_s. Owing to their infrared and collinear safety, they can be computed systematically in perturbation theory. They usually span the range between the kinematical situation of two collimated back-to-back jets (dijet limit) and a perfectly spherical final state.

The fixed-order description, which expands the distribution in powers of the strong coupling constant to leading order (LO), next-to-leading order (NLO), next-to-next-to-leading order (NNLO) and so on, is reliable and convergent over most of the kinematical range of the event-shape. In the dijet limit, which is attained for the thrust variable [69] as $T \to 1$, the convergence of the fixed-order expansion is spoilt by large logarithmic terms $\ln(1-T)$ at each order in the strong coupling constant, which necessitates a resummed description. Resummation of the event-shape distribution accounts for the logarithmically enhanced terms to all orders in perturbation theory, and ensures a reliable prediction in the dijet region. The resummed cross section is organized in terms of leading logarithms (LL), next-to-leading logarithms (NLL) and so on. During LEP times, precision studies of a standard set of six event-shapes were based on the combination of fixed-order NLO calculations [70–77] with NLL resummation [47, 48, 55]. To avoid the double counting of terms, both expansions need to be matched onto each other and different matching procedures are available [78].

4. FACTORISATION AND RGE RESUMMATION: ANALYSIS OF THRUST

In the recent past, substantial progress was made both on the fixed-order and the resummed description of event-shapes. Following the development of new methods for calculations of QCD jet observables at NNLO [37], the NNLO corrections to $e^+e^- \to 3$ jets and related event-shape observables were computed [80–85]. These calculations are based on a numerical integration of the relevant three-parton, four-parton and five-parton matrix elements, which are combined into a parton-level event generator. Next-to-leading order electroweak corrections were also computed very recently [86, 87]. Determinations of the strong coupling constant using the newly available NNLO results [88–90] and the matched [91] NLL+NNLO [92–95] predictions led to a big improvement in the scale uncertainty and showed the need to go beyond NLL in resummation.

The resummation of large logarithmic corrections is based on a factorization of the event-shape cross section in the dijet limit into a convolution of three leading regions (soft, collinear and hard virtual). In the conventional approach [47, 59], the resummation of large logarithms is accomplished in Mellin (Laplace) space and the resummed distributions are obtained by an inverse transformation. In this approach, the NLL corrections to all standard event-shape variables were obtained [47, 48, 55], as well as NNLL results on the energy-energy correlation function [49]. By applying soft-collinear effective theory (SCET, [96]) to event-shape distributions [97, 98], the resummation can be performed directly in momentum space. SCET offers moreover a systematic framework to compute all soft, collinear and hard contributions. In this framework, the resummation for thrust [99, 101], heavy jet mass [103] and jet broadenings [105, 106] beyond NLL have been performed and applied for a precise determination of α_s. In these calculations, the hard subprocess is inferred from the three-loop quark form factor [112, 113], the collinear jet function is required to the two-loop order, which is known from earlier calculations of SCET resummation in heavy meson decays and deep inelastic scattering [114, 115], while the soft subprocess to two-loop order could be computed from the renormalization group invariance of the cross section only up to a constant term. Using the fixed-order NLO results [77], this term was determined numerically by two indepedent groups [99, 116], obtaining mutually inconsistent results. Motivated by this discrepancy, we perform an analytical calculation of the full two-loop soft subprocess for thrust from first principles in this chapter.

The major difference between conventional and SCET-based resummation is the handling of intermediate scales in the calculation. In the SCET-based resummation, these scales are fixed to their natural values directly in momentum space, on the other hand in the conventional approach they are sampled along a complex contour when peforming the Laplace inversion. Although both approaches yield identical results at NLL, owing to the presence of a Landau pole in the QCD coupling constant, power-suppressed differences between them could appear in higher order logarithmic contributions. These

power-suppressed terms are outside the scope of the logarithmic resummation, so both approaches could in principle yield different but equally correct results. To address the compatibility between the two resummations, we perform the NNLL resummation of the thrust distribution in Laplace space. The results reported in this chapter were published in [100].

4.2 Thrust distribution in perturbation theory

The thrust variable for a hadronic final state in e^+e^- annihilation is defined as [69]

$$T = \max_{\vec{n}} \left(\frac{\sum_i |\vec{p}_i \cdot \vec{n}|}{\sum_i |\vec{p}_i|} \right) , \tag{4.1}$$

where $\vec{p}_i$ denotes the three-momentum of particle i, with the sum running over all particles. The unit vector $\vec{n}$ is varied to find the thrust direction $\vec{n}_T$ which maximises the expression in parentheses on the right hand side. In the present paper we will mostly work with the quantity $\tau \equiv 1 - T$.

It can be seen that a two-particle final state has fixed $T = 1$, consequently the thrust distribution receives its first non-trivial contribution from three-particle final states, which, at order α_s, correspond to three-parton final states. Therefore, both theoretically and experimentally, the thrust distribution is closely related to three-jet production.

4.2.1 Fixed-order and resummed calculations

The differential thrust distribution in perturbation theory is known at NNLO [81, 84]. At a centre-of-mass energy Q and for a renormalization scale μ takes the form

$$\frac{1}{\sigma_0}\frac{\mathrm{d}\sigma}{\mathrm{d}\tau}(\tau, Q) = \bar{\alpha}_s(\mu)\frac{\mathrm{d}A}{\mathrm{d}\tau}(\tau) + \bar{\alpha}_s^2(\mu)\frac{\mathrm{d}B}{\mathrm{d}\tau}(\tau, x_\mu) + \bar{\alpha}_s^3(\mu)\frac{\mathrm{d}C}{\mathrm{d}\tau}(\tau, x_\mu) + \mathcal{O}(\bar{\alpha}_s^4) , \tag{4.2}$$

with

$$\bar{\alpha}_s = \frac{\alpha_s}{2\pi} , \qquad x_\mu = \frac{\mu}{Q} , \tag{4.3}$$

and where the explicit dependence on the renormalization scale is given by

$$\begin{aligned}
\frac{\mathrm{d}B}{\mathrm{d}\tau}(\tau, x_\mu) &= \frac{\mathrm{d}B}{\mathrm{d}\tau}(\tau) + 2\beta_0 \ln(x_\mu^2)\frac{\mathrm{d}A}{\mathrm{d}\tau}(\tau), \\
\frac{\mathrm{d}C}{\mathrm{d}\tau}(\tau, x_\mu) &= \frac{\mathrm{d}C}{\mathrm{d}\tau}(\tau) + 2\ln(x_\mu^2)\left(2\beta_0\frac{\mathrm{d}B}{\mathrm{d}\tau}(\tau) + 2\beta_1\frac{\mathrm{d}A}{\mathrm{d}\tau}(\tau)\right) + \left(2\beta_0\ln(x_\mu^2)\right)^2\frac{\mathrm{d}A}{\mathrm{d}\tau}(\tau).
\end{aligned} \tag{4.4}$$

For the QCD β-function we follow the convention given in Appendix A.1. In theoretical computations it is customary to normalize the distributions to the Born cross section

σ_0 since, for massless quarks, the normalization cancels all electroweak coupling factors. However, experimentally it is easier to normalize the distributions to the total hadronic cross section σ. The correction for the normalization can be done by expanding the ratio σ_0/σ in powers of $\bar{\alpha}_s$, which is nowadays known at four loops [120]. In the massless case the ratio is given by

$$\frac{\sigma}{\sigma_0} = 1 + \bar{\alpha}_s K_1 + \bar{\alpha}_s^2 \left[K_2 + 2\beta_0 \ln(x_\mu^2) K_1\right] + \mathcal{O}(\bar{\alpha}_s^3), \tag{4.5}$$

where

$$\begin{aligned} K_1 &= \frac{3}{2} C_F, \\ K_2 &= \frac{1}{4}\left[-\frac{3}{2}C_F^2 + C_F C_A\left(\frac{123}{2} - 44\zeta_3\right) + \frac{C_F n_F}{2}\left(-22 + 16\zeta_3\right)\right]. \end{aligned} \tag{4.6}$$

The dependence on the renormalization scale μ is universal and is the same in 4.4 and 4.5. Inserting the expansion of σ_0/σ we obtain the following expression:

$$\frac{1}{\sigma}\frac{\mathrm{d}\sigma}{\mathrm{d}\tau}(\tau, Q) = \bar{\alpha}_s(\mu)\frac{\mathrm{d}\bar{A}}{\mathrm{d}\tau}(\tau) + \bar{\alpha}_s^2(\mu)\frac{\mathrm{d}\bar{B}}{\mathrm{d}\tau}(\tau, x_\mu) + \bar{\alpha}_s^3(\mu)\frac{\mathrm{d}\bar{C}}{\mathrm{d}\tau}(\tau, x_\mu) + \mathcal{O}(\bar{\alpha}_s^4)\,, \tag{4.7}$$

where $\bar{A}, \bar{B}, \bar{C}$ are related to A, B, C by

$$\bar{A}(\tau) = A(\tau)\,, \tag{4.8}$$

$$\bar{B}(\tau, x_\mu) = B(\tau, x_\mu) - K_1 A(\tau)\,, \tag{4.9}$$

$$\bar{C}(\tau, x_\mu) = C(\tau, x_\mu) - K_1 B(\tau, x_\mu) + \left(K_1^2 - K_2\right) A(\tau)\,. \tag{4.10}$$

For later convenience we consider also the integrated distribution

$$R_T(\tau) \equiv \frac{1}{\sigma}\int_0^1 \frac{d\sigma\,(\tau', Q)}{d\tau'}\Theta(\tau - \tau')d\tau', \tag{4.11}$$

which has the following fixed-order expansion:

$$R_T\,(\tau) \;=\; 1 + \mathcal{A}\,(\tau)\,\bar{\alpha}_s(\mu^2) \;+\; \mathcal{B}\,\left(\tau, \mu^2\right)\bar{\alpha}_s^2(\mu^2) \;+\; \mathcal{C}\,\left(\tau, \mu^2\right)\bar{\alpha}_s^3(\mu^2). \tag{4.12}$$

The fixed-order coefficients $\mathcal{A}$, $\mathcal{B}$, $\mathcal{C}$ can be obtained by integrating the distribution 4.7 and imposing $R_T(\tau_{\max}, Q) = 1$ to all orders, where $\tau_{\max}$ is the maximal kinematically allowed value.

In the two-jet region the fixed-order thrust distribution is enhanced by large infrared logarithms which spoil the convergence of the perturbative series. The convergence can be restored by resumming the logarithms to all orders in the coupling constant. The resummed cross section can in general be written as

$$R_T(\tau) = \left(1 + \sum_{k=1}^{\infty} C_k \bar{\alpha}_s^k\right) \exp\left[L g_1(\alpha_s L) + g_2(\alpha_s L) + \frac{\alpha_s}{\pi}\beta_0 g_3(\alpha_s L) + \ldots\right], \tag{4.13}$$

where $L \equiv \ln(1/\tau)$. The function g_1 encodes all the leading logarithms, the function g_2 resums all next-to-leading logarithms and so on.

The last equation gives a better prediction of the thrust distribution in the two-jet region, but fails to describe the multijet region $\tau \to \tau_{\max}$, where non-singular pieces of the fixed-order prediction become important. To achieve a reliable description of the observable over a broader kinematical range the two expressions 4.12 and 4.13 can be matched, taking care of avoiding double counting of logarithms appearing in both expressions. To this purpose we reexpand the functions g_i in powers of $\alpha_s L$:

$$\begin{aligned} Lg_1(\alpha_s L) =& G_{12}\bar{\alpha}_s L^2 + G_{23}\bar{\alpha}_s^2 L^3 + G_{34}\bar{\alpha}_s^3 L^4 + \dots , \\ g_2(\alpha_s L) =& G_{11}\bar{\alpha}_s L + G_{22}\bar{\alpha}_s^2 L^2 + G_{33}\bar{\alpha}_s^3 L^3 + \dots , \\ \frac{\alpha_s}{\pi}\beta_0 g_3(\alpha_s L) =& G_{21}\bar{\alpha}_s^2 L + G_{32}\bar{\alpha}_s^3 L^2 + G_{43}\bar{\alpha}_s^4 L^3 + \dots . \end{aligned} \tag{4.14}$$

In a second step we reexpand the exponential function recovering the full logarithmic dependence of the fixed-order series at NNLO

$$R_{\log}^{(1)}(\tau) = C_1 + G_{11}L + G_{12}L^2 , \tag{4.15}$$

$$\begin{aligned} R_{\log}^{(2)}(\tau) =& C_2 + (G_{21} + C_1 G_{11})\, L + \left(G_{22} + \frac{1}{2}G_{11}^2 + C_1 G_{12}\right) L^2 \\ &+ (G_{23} + G_{12}G_{11})\, L^3 + \frac{1}{2}G_{12}^2 L^4 , \end{aligned} \tag{4.16}$$

$$\begin{aligned} R_{\log}^{(3)}(\tau) =& C_3 + (G_{31} + C_1 G_{21} + C_2 G_{11})\, L \\ &+ \left(G_{32} + C_1 G_{22} + \frac{1}{2}C_1 G_{11}^2 + C_2 G_{12} + G_{11}G_{21}\right) L^2 \\ &+ \left(G_{33} + G_{11}G_{22} + G_{12}G_{21} + C_1 G_{11}G_{12} + \frac{1}{6}G_{11}^3 + C_1 G_{23}\right) L^3 \\ &+ \left(G_{34} + G_{12}G_{22} + \frac{1}{2}C_1 G_{12}^2 + G_{11}G_{23} + \frac{1}{2}G_{11}^2 G_{12}\right) L^4 \\ &+ \left(G_{12}G_{23} + \frac{1}{2}G_{12}^2 G_{11}\right) L^5 + \frac{1}{6}G_{12}^3 L^6 . \end{aligned} \tag{4.17}$$

The difference between the logarithmic part and the full fixed-order series at different orders is given by

$$d_1(\tau) = \mathcal{A}(\tau) - R_{\log}^{(1)}(\tau) , \tag{4.18}$$

$$d_2(\tau) = \mathcal{B}(\tau) - R_{\log}^{(2)}(\tau) , \tag{4.19}$$

$$d_3(\tau) = \mathcal{C}(\tau) - R_{\log}^{(3)}(\tau) . \tag{4.20}$$

The functions $d_i(\tau)$ contain the non-logarithmic part of the fixed-order contribution and vanish for $\tau \to 0$. We collect them into a function $D(\tau, Q)$ defined as

$$D(\tau, Q) = \bar{\alpha}_s d_1(\tau) + \bar{\alpha}_s^2 d_2(\tau) + \bar{\alpha}_s^3 d_3(\tau) + \mathcal{O}(\bar{\alpha}_s^4). \tag{4.21}$$

4.2.2 Kinematics and factorization of thrust

The definition of thrust 4.1 splits the final-state into two hemispheres $S_{\vec{n}_T}$ and $\bar{S}_{\vec{n}_T}$ separated by the plane $P_{\vec{n}}$ orthogonal to the unit vector $\vec{n}_T$. Each final state particle with momentum $\vec{p}_i$ is assigned to either $S_{\vec{n}_T}$ or $\bar{S}_{\vec{n}_T}$ depending on whether $\vec{p}_i \cdot \vec{n}_T$ is positive or negative. As it was shown in [47], no final state momenta can lie in $P_{\vec{n}}$. We denote with p and $\bar{p}$ the total momenta in the hemispheres $S_{\vec{n}_T}$ and $\bar{S}_{\vec{n}_T}$ respectively. We can parametrize the two total momenta as

$$p^\mu = \frac{p\cdot n}{2}\bar{n}^\mu + p_\perp^\mu + \frac{p\cdot \bar{n}}{2}n^\mu, \qquad \bar{p}^\mu = \frac{\bar{p}\cdot \bar{n}}{2}n^\mu + \bar{p}_\perp^\mu + \frac{\bar{p}\cdot n}{2}\bar{n}^\mu, \tag{4.22}$$

where $n^\mu = (1, \vec{n}_T)$ and $\bar{n}^\mu = (1, -\vec{n}_T)$. A simple kinematical analysis [47] shows that in the dijet limit we can recast 4.1 as

$$\tau \equiv 1 - T = \frac{p^2}{Q^2} + \frac{\bar{p}^2}{Q^2} + \mathcal{O}((1-T)^2), \tag{4.23}$$

where we are neglecting terms of relative order $1-T$ which give rise to power-suppressed contributions to the cross section. In our analysis we need to separate soft particle contributions from collinear ones, so we have to modify 4.23 in order to single out the explicit contributions arising from each of the two kinematical configurations. Let us then consider a hard parton with momentum p^μ in the $S_{\vec{n}_T}$ hemisphere which produces a hard collinear final state parton with momentum k^μ after emitting a soft gluon with momentum q^μ (Fig. 4.1). The parent parton is moving along n^μ so its hard momentum component $p\cdot\bar{n}$ is of order $\mathcal{O}(Q)$, while the remaining components $p\cdot n$ and $|p_\perp|$ are suppressed. The soft gluon momentum components tend to zero with the same scaling ($q\cdot n \sim q\cdot\bar{n} \sim |q_\perp|$). It is then easy to see that $k^2 \simeq p^2 - Qq\cdot n$. Plugging the expression for p^2 arising from the previous equation into 4.23, we end up with the expression

$$\begin{aligned} 1 - T =& \frac{k^2}{Q^2} + \frac{\bar{k}^2}{Q^2} + \frac{q\cdot n}{Q} + \frac{\bar{q}\cdot\bar{n}}{Q} + \mathcal{O}((1-T)^2) \\ =& \frac{k^2}{Q^2} + \frac{\bar{k}^2}{Q^2} + \frac{w}{Q} + \mathcal{O}((1-T)^2), \end{aligned} \tag{4.24}$$

where k ($\bar{k}$) is the total collinear momentum in the $S_{\vec{n}_T}$ ($\bar{S}_{\vec{n}_T}$) hemisphere and q ($\bar{q}$) is the total soft momentum in the $S_{\vec{n}_T}$ ($\bar{S}_{\vec{n}_T}$) hemisphere.

An important simplification in the calculation is achieved if the recoil effects due to emissions of wide angle soft particles are neglected. Before neglecting them we have to make sure that they do not give rise to any logarithmically enhanced terms. To see it, we rewrite the thrust as

$$1 - T = \sum_i \frac{\omega_i}{Q}(1 - \cos\theta_i), \tag{4.25}$$

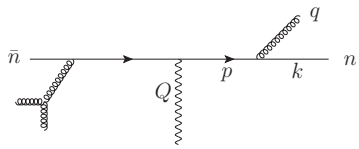

Figure 4.1: First branching kinematics.

where ω_i is the energy of the $i-$th final state particle and θ_i is the angle of its direction to the thrust axis. We now consider the wide angle soft contributions to T, but we neglect their effect on the determination of the thrust axis $\vec{n}_T$. We call this fake thrust axis $\vec{n}_{\text{fake}}$ and we define δ as the small angle of $\vec{n}_{\text{fake}}$ to the physical axis $\vec{n}_T$. In approximating $\vec{n}_T$ with $\vec{n}_{\text{fake}}$ the angles θ_i are replaced by $\theta_i' = \theta_i - \delta$.

We now consider the angle δ due to a single large angle soft emission. From simple kinematics we obtain $\delta \sim \omega_s/Q$, where ω_s is the soft particle energy. We observe that δ is of the same order as the soft emission contribution to the thrust (*i.e.*$\sim \tau$). We want to estimate the effect of neglecting the recoil δ on the thrust itself using expression 4.25. The effect of the approximation on collinear emissions ($\theta \simeq 0$, $\omega_c \sim Q$) is $\Delta\tau \sim (\omega_c/Q)\delta^2 \sim \tau^2$, while for large angle soft emissions ($\theta \gg 0$, $\omega_s \ll Q$) we find $\Delta\tau \sim (\omega_s/Q)\delta \sim \tau^2$.

We see that in both cases the effect of the recoil amounts to a contribution to T of relative order (at least) $\mathcal{O}(1-T)$, so it produces power-suppressed terms. We can then replace the thrust axis in the dijet region with the direction of the hardest (jet-initiating) parton. From now on this approximation is understood.

Factorization properties of event-shapes have been widely studied in the literature [60, 97, 121]. Referring to Fig. 4.2 we recast the cross section 4.11 as

$$\begin{aligned} R_T(\tau) = \; & H\left(\frac{Q}{\mu}, \alpha_s(\mu)\right) \int dk^2 d\bar{k}^2 \mathcal{J}(\frac{k}{\mu}, \alpha_s(\mu)) \bar{\mathcal{J}}(\frac{\bar{k}}{\mu}, \alpha_s(\mu)) \\ & \times \int dw \mathcal{S}(\frac{w}{\mu}, \alpha_s(\mu)) \Theta(Q^2\tau - \bar{k}^2 - k^2 - wQ) + \mathcal{O}(\tau). \end{aligned} \tag{4.26}$$

We use the integral representation of the Θ-function

$$\Theta(Q^2\tau - \bar{k}^2 - k^2 - wQ) = \frac{1}{2\pi i} \int_C \frac{d\nu}{\nu} \, \mathrm{e}^{\nu\tau Q^2} \mathrm{e}^{-\nu k^2} \mathrm{e}^{-\nu \bar{k}^2} \mathrm{e}^{-\nu w Q}, \tag{4.27}$$

and the Laplace transform to recast Eq. 4.26 as

$$\begin{aligned} R_T(\tau) =& H\left(\frac{Q}{\mu}, \alpha_s(\mu)\right) \frac{1}{2\pi i} \int_C \frac{dN}{N} \, \mathrm{e}^{\tau N} \tilde{J}^2 \left(\sqrt{\frac{N_0}{N}} \frac{Q}{\mu}, \alpha_s(\mu)\right) \tilde{S}\left(\frac{N_0}{N}\frac{Q}{\mu}, \alpha_s(\mu)\right) \\ =& \frac{1}{2\pi i} \int_C \frac{dN}{N} \, \mathrm{e}^{\tau N} \tilde{\sigma}_N(Q^2, \alpha_s), \end{aligned} \tag{4.28}$$

where we set $N = \nu Q^2$ and $N_0 = e^{-\gamma_E}$. For the sake of simplicity we defined $\tilde{\sigma}_N(Q^2, \alpha_s)$ as the Laplace-transformed cross section and we omitted the term $\mathcal{O}(\tau)$. The soft

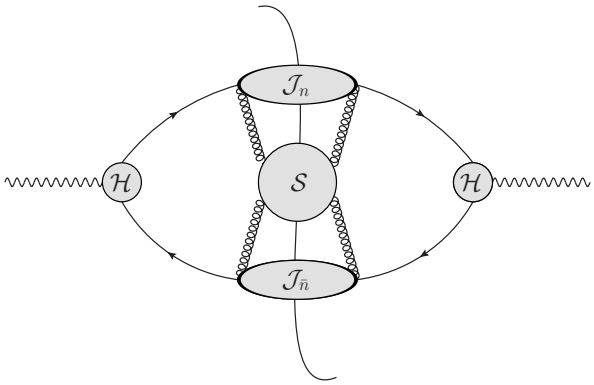

Figure 4.2: Leading regions in dijet factorization.

subprocess $\tilde{S}\left(N_0/NQ/\mu, \alpha_s(\mu)\right)$ describes the interaction between the two jets of hard collinear particles through soft gluon exchange. It can be therefore defined in a gauge invariant way as a correlator of Wilson lines

$$\tilde{S}\left(\frac{N_0}{N}\frac{Q}{\mu}, \alpha_s(\mu)\right) = \frac{Q}{N_c}\int d\tau_s \mathrm{e}^{-\tau_s N} \sum_{k_{eik}} \langle 0|W^\dagger_{\bar{n}}(0)W^\dagger_n(0)|k_{eik}\rangle \mathcal{J}_{cut}(\tau_s Q)\langle k_{eik}|W_n(0)W_{\bar{n}}(0)|0\rangle, \tag{4.29}$$

where we defined $\tau_s = w/Q$. W_n and $W_{\bar{n}}$ are Wilson lines

$$W_n(y) = \mathbf{P}\mathrm{exp}\left(ig\int_0^\infty ds\, n\cdot A(ns+y)\right), \tag{4.30}$$

describing the eikonal interaction of soft gluons with the fast moving quarks along the directions n^μ and $\bar{n}^\mu$ respectively. $A(ns+y)$ in the previous expression denotes the gluon field in QCD. The sum runs over the final states $|k_{eik}\rangle$ involving k soft particles whose phase space is constrained according to the thrust measurement function $\mathcal{J}_{cut}(\tau Q^2)$. Both soft and soft-collinear contributions are encoded into the soft subprocess. The one-loop expression of the soft subprocess is known since a long time and we compute it with two-loop accuracy in the next section.

The collinear subprocess $\mathcal{J}$ ($\bar{\mathcal{J}}$) describes the decay of the jet-initiating hard quark (antiquark) into a jet of collinear particles moving along the n^μ ($\bar{n}^\mu$) direction. It is therefore an inclusive quantity which can be found in many other relevant QCD processes such as deep inelastic scattering and heavy quarks decay [59, 114, 122]. Double-counting of soft-collinear and $\bar{n}$-collinear (n-collinear) contributions has to be avoided

when computing the n-collinear ($\bar{n}$-collinear) jet subprocess. To this end different regularization schemes can be found in the literature and they all provide the same results for the logarithmic structure of the jet subprocess. For the purposes of the present paper the explicit expression of the collinear subprocess is not required. All we need is its non-logarithmic term at two-loop order, which has been computed in [114] using dimensional regularization. In that work, all pure virtual corrections to the collinear subprocess are given by scaleless integrals and thus they vanish in dimensional regularization. As we will see in detail in Section 4.3 this property holds true also for the soft subprocess and it ensures that the whole virtual contribution is encoded into the hard subprocess defined below, which can be identified with the squared of the constant part of the quark form factor.

The short-distance hard function $H\left(Q/\mu, \alpha_s(\mu)\right) = \left|\mathcal{H}\left(Q/\mu, \alpha_s(\mu)\right)\right|^2$ takes into account the hard virtual corrections to the quark-antiquark production subprocess. It is free of large logarithms and it can be generally defined such that Eq. 4.26 reproduces the fixed-order cross section up to power suppressed terms. Since the hard function contains only constants, one can avoid it by performing a $\ln(R)$-matching to fixed-order as it will be shown in Section 4.5. We nevertheless take it into account in order to compute the full constant part of the cross section with $\mathcal{O}(\alpha_s^2)$ accuracy.

4.3 Soft gluon emission at two-loop level

Let us turn into the computation of the soft subprocess 4.29. Expanding the generating functional to the desired order we obtain the relevant set of cut Feynman diagrams. For real emissions, the integration runs over the soft gluons phase space constrained by the thrust measurement function in the dijet limit. The leading order contribution trivially reduces to $\delta(\tau_s)$. In what follows we compute $S(\tau_s, Q/\mu, \alpha_s(\mu))$ to two-loop level.

4.3.1 One-loop result

At one-loop level the evaluation of the Wilson loop is straightforward. The contributing diagrams are listed in Figure 4.3.

The virtual soft correction (Fig. 4.3(a)) to the vertex identically vanishes in dimensional regularization since the integration over the loop momentum is given by the scaleless integral

$$S_V^{(1)}\left(\tau_s, \frac{Q}{\mu}, \alpha_s(\mu)\right) = -n\cdot\bar{n} g^2 C_F \mu^{2\epsilon} \int \frac{d^d q}{(2\pi)^d} \frac{\delta(\tau_s)}{(q\cdot\bar{n}+i0^+)(q\cdot n - i0^+)(q^2+i0^+)}, \tag{4.31}$$

where the phase space constraint reduces to $\delta(\tau_s)$ since no real gluons have been emitted. The real contribution involves the emission of a soft gluon off one of the two Wilson

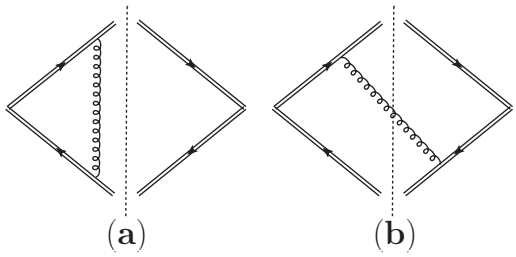

Figure 4.3: NLO contribution to the soft subprocess.

lines. The emitted gluon may go either into the $S_{\vec{n}_T}$ hemisphere or into the $\bar{S}_{\vec{n}_T}$ one. The resulting phase space measure is then

$$\frac{d^dq}{(2\pi)^d}(2\pi)\delta^{(+)}(q^2)(\delta(\tau_s Q - q\cdot n)\Theta(q\cdot\bar{n}-q\cdot n)+\delta(\tau_s Q - q\cdot\bar{n})\Theta(q\cdot n - q\cdot\bar{n})), \quad (4.32)$$

where the two Θ-functions forbid the emitted gluon from going backwards, heading towards the opposite hemisphere. The integrand is the eikonal factor corresponding to the single emission shown in Figure 4.3(b) and its mirror conjugate diagram. The sum of the two then reads

$$S^{(1)}\left(\tau_s,\frac{Q}{\mu},\alpha_s(\mu)\right) = n\cdot\bar{n}g^2C_FQ\mu^{2\epsilon}\int\frac{d^dq}{(2\pi)^d}(2\pi)\delta^{(+)}(q^2)$$
$$\times\frac{\delta(\tau_s Q - q\cdot n)\Theta(q\cdot\bar{n}-q\cdot n)+\delta(\tau_s Q - q\cdot\bar{n})\Theta(q\cdot n - q\cdot\bar{n})}{(q\cdot n+i0^+)(q\cdot\bar{n}+i0^+)}. \quad (4.33)$$

We first replace

$$d^dq = \frac{1}{2}d(q\cdot n)d(q\cdot\bar{n})d^{d-2}q_\perp\,, \quad (4.34)$$

and evaluate the integral over $q_\perp$. Since there is no explicit dependence on $q_\perp$ in the integrand function, it simply reduces to the replacement

$$d^{d-2}q_\perp\delta^{(+)}(q^2)\to\frac{\pi^{1-\epsilon}}{\Gamma(1-\epsilon)}(q\cdot n)^{-\epsilon}(q\cdot\bar{n})^{-\epsilon}\Theta(q\cdot\bar{n})\Theta(q\cdot n). \quad (4.35)$$

It is then straightforward to show that the final result reads

$$S^{(1)}\left(\tau_s,\frac{Q}{\mu},\alpha_s(\mu)\right) = C_F\frac{\alpha_s(\mu)}{\pi}\frac{e^{\epsilon\gamma_E}}{\epsilon\Gamma(1-\epsilon)}\left(\frac{Q}{\mu}\right)^{-2\epsilon}2\left(\frac{1}{\tau_s}\right)^{1+2\epsilon}, \quad (4.36)$$

where we set $n\cdot\bar{n}=2$ and we replaced the bare coupling $\alpha_s^0 = g^2/4\pi$ with the renormalized one in the $\overline{\text{MS}}$ scheme, *i.e.*

$$\alpha_s^0\mu^{2\epsilon}\to\alpha_s(\mu)\mu^{2\epsilon}\frac{e^{\epsilon\gamma_E}}{(4\pi)^\epsilon}\left(1-\frac{11C_A-2N_F}{6\epsilon}(\frac{\alpha_s(\mu)}{2\pi})+\ldots\right), \quad (4.37)$$

with $\gamma_E = 0.5772\ldots$ being the Euler-Mascheroni constant. Using the relation

$$\left(\frac{1}{\tau_s}\right)^{1+2\epsilon} = -\frac{\delta(\tau_s)}{2\epsilon} + \left[\frac{1}{\tau_s}\right]_+ - 2\epsilon\left[\frac{\ln\tau_s}{\tau_s}\right]_+ + \mathcal{O}(\epsilon^2), \tag{4.38}$$

we recast 4.36 as

$$S^{(1)}\left(\tau_s, \frac{Q}{\mu}, \alpha_s(\mu)\right) = C_F\frac{\alpha_s(\mu)}{\pi}\Bigg(-\frac{\delta(\tau_s)}{\epsilon^2} + \frac{2}{\epsilon}\left[\frac{1}{\tau_s}\right]_+ - \frac{2}{\epsilon}\ln\frac{\mu}{Q}\delta(\tau_s) + \delta(\tau_s)\left(\frac{\pi^2}{12} - 2\ln^2\frac{Q}{\mu}\right) - 4\left[\frac{\ln\frac{Q}{\mu} + \ln\tau_s}{\tau_s}\right]_+ + \mathcal{O}(\epsilon)\Bigg). \tag{4.39}$$

The above result in Laplace space reads

$$\begin{aligned}\tilde{S}^{(1)}\left(\frac{N_0 Q}{N\mu}, \alpha_s(\mu)\right) &= \int_0^\infty d\tau_s e^{-N\tau_s} S^{(1)}\left(\tau_s, \frac{Q}{\mu}, \alpha_s(\mu)\right) \\ &= C_F\frac{\alpha_s(\mu)}{\pi}\left(-\frac{1}{\epsilon^2} - \frac{2}{\epsilon}\ln\frac{N\mu}{N_0 Q} - \frac{\pi^2}{4} - 2\ln^2\frac{N\mu}{N_0 Q}\right),\end{aligned} \tag{4.40}$$

where $N_0 = e^{-\gamma_E}$.

Note the absence of single logarithms in the $\mathcal{O}(\epsilon^0)$ term meaning that the one loop soft subprocess receives logarithmic contributions only when the emitted gluon is both soft and collinear to one of the eikonal legs. Wide angle soft emissions do not contribute at this order, but they become relevant at two-loop level.

4.3.2 Two-loop result

At order $\mathcal{O}(\alpha_s^2)$ up to two real gluons are emitted. Note that diagrams with virtual dressing of eikonal lines vanish identically since the Wilson path lies on the light cone (*i.e.* $n^2 = \bar{n}^2 = 0$). Furthermore, we only need to evaluate those diagrams contributing with maximal non-abelian (*i.e.* $C_F C_A$) and fermionic (*i.e.* $C_F T_F N_F$) terms, because of the non-abelian exponentiation theorem [123, 124]. According to it we can write

$$\tilde{S}\left(\frac{N_0 Q}{N\mu}, \alpha_s(\mu)\right) = 1 + \sum_{l=1}^{\infty}\tilde{S}^{(l)}\left(\frac{N_0 Q}{N\mu}, \alpha_s(\mu)\right) = \exp\left(\sum_{l=1}^{\infty}\tilde{s}^{(l)}\left(\frac{N_0 Q}{N\mu}, \alpha_s(\mu)\right)\right), \tag{4.41}$$

where $\tilde{s}^{(2)}(N_0 Q/(N\mu), \alpha_s(\mu))$ involves $C_F C_A$ and $C_F T_F N_F$ contributions while C_F^2 terms arise from exponentiation of the $\mathcal{O}(\alpha_s)$ result $\tilde{S}^{(1)}(N_0 Q/(N\mu), \alpha_s(\mu))$. It follows that the $\mathcal{O}(\alpha_s^2)$ result is given by

$$\tilde{S}^{(2)}\left(\frac{N_0 Q}{N\mu}, \alpha_s(\mu)\right) = \frac{1}{2}\tilde{S}^{(1)}\left(\frac{N_0 Q}{N\mu}, \alpha_s(\mu)\right)^2 + \tilde{s}^{(2)}\left(\frac{N_0 Q}{N\mu}, \alpha_s(\mu)\right), \tag{4.42}$$

where $\tilde{S}^{(1)}(N_0 Q/(N\mu), \alpha_s(\mu))$ was computed in the previous section. The remaining set of (non-vanishing) diagrams contributing to $\tilde{s}^{(2)}(N_0 Q/(N\mu), \alpha_s(\mu))$ is shown in Figure 4.4, where the mirror conjugate diagrams are omitted. The vacuum polarization blob includes fermions, gluons and ghosts as depicted in Figure 4.5, since the calculation will be carried out in the Feynman gauge.

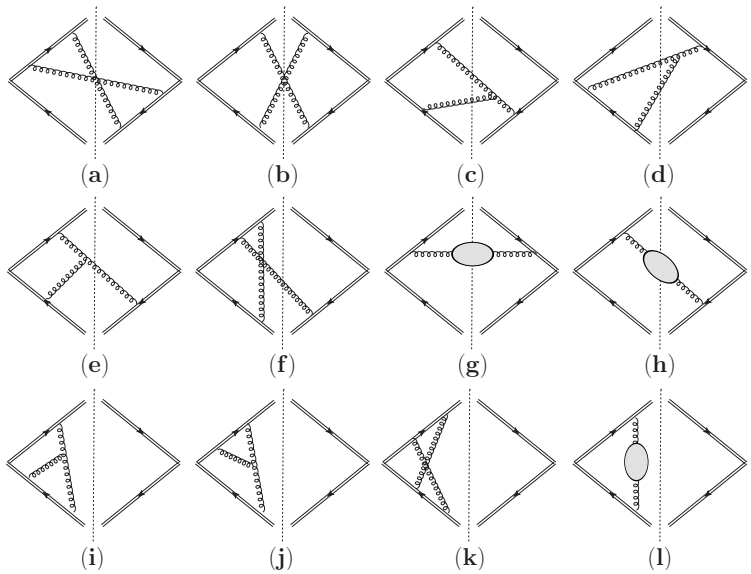

Figure 4.4: NNLO contribution to the soft subprocess. Grey blobs stand for the sum of vacuum polarization bubbles due to fermions, gluons and ghosts. To complete the set one has to take into account mirror conjugate diagrams in addition. Pure abelian diagrams (*i.e.* proportional to C_F^2) are omitted.

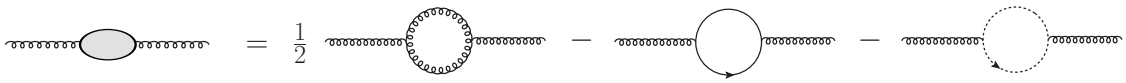

Figure 4.5: Vacuum polarization diagrams in the Feynman gauge.

The double virtual contribution (Fig. 4.4(i–l)) is made of scaleless integrals which identically vanish in dimensional regularization.
The first non-trivial contribution to consider is the one-loop virtual diagram with an extra real gluon, depicted in Fig. 4.4(e,f). The sum of such diagrams and their mirror conjugate ones is gauge invariant. Using the known expression of the soft current at one loop [125], we can write their contribution as

$$s^{(2)}_{(e),(f)}\left(\tau_s, \frac{Q}{\mu}, \alpha_s(\mu)\right) = -4\frac{g^4}{8\pi^2}(4\pi\mu^4)^\epsilon Q C_F C_A \frac{1}{\epsilon^2}\frac{\Gamma^4(1-\epsilon)\Gamma^3(1+\epsilon)}{\Gamma^2(1-2\epsilon)\Gamma(1+2\epsilon)}$$

$$\times \int \frac{d^d q}{(2\pi)^d} \frac{(2\pi)\delta^{(+)}(q^2)(\delta(\tau_s Q - q\cdot n)\Theta(q\cdot\bar{n} - q\cdot n) + \delta(\tau_s Q - q\cdot\bar{n})\Theta(q\cdot n - q\cdot\bar{n}))}{((q\cdot n)(q\cdot\bar{n}))^{1+\epsilon}}, \tag{4.43}$$

where the phase space constraint is the same as in the one loop case, since only one real soft gluon is emitted. Notice that the pole prescription $(\pm i0)$ has been omitted since the poles are never "touched" during the integration because of the Θ-functions in the numerator. From now on we write explicitly the factor $(\pm i0)$ only when relevant. Using the relation 4.34 and evaluating the straightforward integral left we obtain

$$s^{(2)}_{(e),(f)}\left(\tau_s, \frac{Q}{\mu}, \alpha_s(\mu)\right) = -\frac{\alpha_s(\mu)^2}{\pi^2}\frac{C_F C_A}{2}\frac{e^{2\gamma_E\epsilon}}{\epsilon^3}\frac{\Gamma^3(1-\epsilon)\Gamma^3(1+\epsilon)}{\Gamma^2(1-2\epsilon)\Gamma(1+2\epsilon)}\left(\frac{\mu}{Q}\right)^{4\epsilon}\left(\frac{1}{\tau_s}\right)^{1+4\epsilon}, \tag{4.44}$$

where we expressed the bare coupling according to equation 4.37.

Let us now consider the double real emission. The phase space constraint is more involved since two distinct gluons are emitted. Each of them can indeed go either into the $S_{\vec{n}_T}$ or the $\bar{S}_{\vec{n}_T}$ hemisphere, leading to the following phase space cut

$$\begin{aligned} Q(2\pi)\delta^{(+)}(q^2)(2\pi)\delta^{(+)}(k^2)\mathcal{J}_{cut}(\tau_s Q) &= Q(2\pi)\delta^{(+)}(q^2)(2\pi)\delta^{(+)}(k^2) \\ &\times(\delta(\tau_s Q - q\cdot n - k\cdot n)\Theta(q\cdot\bar{n} - q\cdot n)\Theta(k\cdot\bar{n} - k\cdot n) && (4.45)\\ &+ \delta(\tau_s Q - q\cdot\bar{n} - k\cdot\bar{n})\Theta(q\cdot n - q\cdot\bar{n})\Theta(k\cdot n - k\cdot\bar{n}) && (4.46)\\ &+ \delta(\tau_s Q - q\cdot n - k\cdot\bar{n})\Theta(q\cdot\bar{n} - q\cdot n)\Theta(k\cdot n - k\cdot\bar{n}) && (4.47)\\ &+ \delta(\tau_s Q - k\cdot n - q\cdot\bar{n})\Theta(k\cdot\bar{n} - k\cdot n)\Theta(q\cdot n - q\cdot\bar{n})). && (4.48) \end{aligned}$$

Such a constraint gives rise to non-trivial phase space integrals which are solvable using analytic techniques. We evaluate the integrals in `MATHEMATICA`, partly using the package `HypExp` [126]. An independent numerical check is also performed using the computer code `SecDec` [127], a recent implementation of sector decomposition based on the algorithms presented in [128, 129]. The numerical integration is then carried out using the Monte Carlo routines `BASES` [130] and `VEGAS` [131] included in [127] with 10^7 Monte Carlo events per coefficient. The two results agree within an uncertainty of 0.001%.

We organise the calculation considering first the class of diagrams without any internal gluons (*i.e.* gluons which are not involved in the cut) shown in Fig. 4.4(a,b) and mirror conjugate diagrams, then the class of diagrams with only one internal gluon (Fig. 4.4(c,d) and mirror conjugate diagrams) and finally vacuum polarization diagrams, containing two internal gluons (Fig. 4.4(g,h) and mirror conjugate diagrams).

4.3.2.1 Box-type diagrams

We first consider the Box-type diagrams depicted in Fig. 4.4(a,b). The second diagram (Fig. 4.4(b)) has a simple structure and can be evaluated easily. Dropping the abelian part of the colour factor we are left with

$$s_{(b)}^{(2)}\left(\tau_s,\frac{Q}{\mu},\alpha_s(\mu)\right)=-\frac{C_AC_F}{2}(n\cdot\bar{n})^2g^4\mu^{4\epsilon}$$
$$\times\int\frac{d^dq}{(2\pi)^d}\frac{d^dk}{(2\pi)^d}\frac{Q(2\pi)\delta^{(+)}(q^2)(2\pi)\delta^{(+)}(k^2)\mathcal{J}_{cut}(\tau_sQ)}{(q\cdot\bar{n})(q\cdot n)(k\cdot n)(k\cdot\bar{n})}, \tag{4.49}$$

where $\mathcal{J}_{cut}(\tau_sQ)$ is the sum of terms in round brackets defined in Eqs. 4.45–4.48. The integrand function does not depend on the transverse component of the integrated momenta, so we can use Eqs. 4.34,4.35 getting

$$s_{(b)}^{(2)}\left(\tau_s,\frac{Q}{\mu},\alpha_s(\mu)\right)=-\frac{C_AC_F}{2}Q\frac{(n\cdot\bar{n})^2}{(2\pi)^{2d-2}}g^4\mu^{4\epsilon}\frac{\pi^{2-2\epsilon}}{4\Gamma^2(1-\epsilon)}$$
$$\times\int d(q\cdot n)d(q\cdot\bar{n})d(k\cdot n)d(k\cdot\bar{n})\Bigg(\frac{\delta(\tau_sQ-q\cdot n-k\cdot n)\Theta(q\cdot\bar{n}-q\cdot n)\Theta(k\cdot\bar{n}-k\cdot n)}{(q\cdot\bar{n})^{1+\epsilon}(q\cdot n)^{1+\epsilon}(k\cdot n)^{1+\epsilon}(k\cdot\bar{n})^{1+\epsilon}}+$$
$$\frac{\delta(\tau_sQ-q\cdot\bar{n}-k\cdot\bar{n})\Theta(q\cdot n-q\cdot\bar{n})\Theta(k\cdot n-k\cdot\bar{n})}{(q\cdot\bar{n})^{1+\epsilon}(q\cdot n)^{1+\epsilon}(k\cdot n)^{1+\epsilon}(k\cdot\bar{n})^{1+\epsilon}}+$$
$$\frac{\delta(\tau_sQ-q\cdot n-k\cdot\bar{n})\Theta(q\cdot\bar{n}-q\cdot n)\Theta(k\cdot n-k\cdot\bar{n})}{(q\cdot\bar{n})^{1+\epsilon}(q\cdot n)^{1+\epsilon}(k\cdot n)^{1+\epsilon}(k\cdot\bar{n})^{1+\epsilon}}+$$
$$\frac{\delta(\tau_sQ-k\cdot n-q\cdot\bar{n})\Theta(k\cdot\bar{n}-k\cdot n)\Theta(q\cdot n-q\cdot\bar{n})}{(q\cdot\bar{n})^{1+\epsilon}(q\cdot n)^{1+\epsilon}(k\cdot n)^{1+\epsilon}(k\cdot\bar{n})^{1+\epsilon}}\Bigg). \tag{4.50}$$

We now analyse each of the integrals in Eq. 4.50. We first integrate out the $k\cdot n$ component in the first and fourth integral and the $k\cdot\bar{n}$ component in the second and third integral by using the δ-functions. We then make the following four changes of variables

$$k\cdot\bar{n}\to Q\tau_su(1-t)\qquad q\cdot\bar{n}\to Q\tau_sts\qquad q\cdot n\to Q\tau_st, \tag{4.51}$$
$$k\cdot n\to Q\tau_su(1-t)\qquad q\cdot n\to Q\tau_sts\qquad q\cdot\bar{n}\to Q\tau_st, \tag{4.52}$$
$$k\cdot n\to Q\tau_su(1-t)\qquad q\cdot\bar{n}\to Q\tau_sts\qquad q\cdot n\to Q\tau_st, \tag{4.53}$$
$$k\cdot\bar{n}\to Q\tau_su(1-t)\qquad q\cdot n\to Q\tau_sts\qquad q\cdot\bar{n}\to Q\tau_st, \tag{4.54}$$

in the first, second, third and fourth integrals of Eq. 4.50 respectively, followed by the replacements $s\to\frac{1}{s}$, $u\to\frac{1}{u}$ in each of them. We end up with four identical integrals on a three dimensional unit cube. Summing them up we obtain the following expression

$$s_{(b)}^{(2)}\left(\tau_s,\frac{Q}{\mu},\alpha_s(\mu)\right)=-\frac{C_AC_F}{2}Q\frac{(n\cdot\bar{n})^2}{(2\pi)^{2d-2}}g^4\mu^{4\epsilon}\frac{\pi^{2-2\epsilon}}{\Gamma^2(1-\epsilon)}$$

$$\times (Q\tau_s)^{-1-4\epsilon} \int_0^1 dt\, du\, ds (1-t)^{-1-2\epsilon} t^{-1-2\epsilon} u^{-1+\epsilon} s^{-1+\epsilon}, \tag{4.55}$$

that can be easily evaluated in terms of Euler beta functions yielding

$$s_{(b)}^{(2)}\left(\tau_s, \frac{Q}{\mu}, \alpha_s(\mu)\right) = -\frac{C_A C_F}{2} Q \frac{(n\cdot\bar{n})^2}{(2\pi)^{2d-2}} g^4 \mu^{4\epsilon} \frac{\pi^{2-2\epsilon}}{\Gamma^2(1-\epsilon)} (Q\tau_s)^{-1-4\epsilon} \frac{1}{\epsilon^2} B(-2\epsilon, -2\epsilon). \tag{4.56}$$

After replacing the bare coupling with the renormalized one (Eq. 4.37) and some algebra, we can recast the previous equation as follows

$$s_{(b)}^{(2)}\left(\tau_s, \frac{Q}{\mu}, \alpha_s(\mu)\right) = -\frac{C_A C_F}{2} \frac{\alpha_s(\mu)^2}{\pi^2} \left(\frac{\mu}{Q}\right)^{4\epsilon} \left(\frac{1}{\tau_s}\right)^{1+4\epsilon} \frac{e^{2\gamma_E \epsilon} B(-2\epsilon, -2\epsilon)}{\epsilon^2 \Gamma^2(1-\epsilon)}, \tag{4.57}$$

where we set $n \cdot \bar{n} = 2$.

We now consider the box diagram in Fig. 4.4(a). We note that the mirror symmetrical diagram has the same expression provided we exchange $k \leftrightarrow q$, so it can be taken into account by just including a factor of two. The full result reads

$$s_{(a)}^{(2)}\left(\tau_s, \frac{Q}{\mu}, \alpha_s(\mu)\right) = -C_A C_F (n\cdot\bar{n})^2 g^4 \mu^{4\epsilon} \times \int \frac{d^d q}{(2\pi)^d} \frac{d^d k}{(2\pi)^d} \frac{Q(2\pi)\delta^{(+)}(q^2)(2\pi)\delta^{(+)}(k^2)\mathcal{J}_{cut}(\tau_s Q)}{((q+k)\cdot\bar{n})(q\cdot n)(q\cdot\bar{n})((k+q)\cdot\bar{n})}. \tag{4.58}$$

Furthermore, exploiting the symmetry of the integrand under the transformation

$$\{k\cdot n \leftrightarrow k\cdot\bar{n}, q\cdot n \leftrightarrow q\cdot\bar{n}\},$$

we see that the integrals arising from the terms 4.45 and 4.47 equal those arising from 4.46 and 4.48 respectively. Using the parametrization shown in Eq. 4.51–4.54, we are led to the following expression

$$s_{(a)}^{(2)}\left(\tau_s, \frac{Q}{\mu}, \alpha_s(\mu)\right) = -\frac{C_A C_F}{2} \frac{\alpha_s(\mu)^2}{\pi^2} \left(\frac{\mu}{Q}\right)^{4\epsilon} \left(\frac{1}{\tau_s}\right)^{1+4\epsilon} \frac{e^{2\gamma_E\epsilon}}{\Gamma^2(1-\epsilon)} \times \left(\int_0^1 dt\, du\, ds \frac{(1-t)^{-1-2\epsilon} t^{1-2\epsilon} s^{-1+\epsilon} u^{\epsilon}}{tu + s(1-t)} + \int_0^1 dt\, du\, ds \frac{(1-t)^{-1-2\epsilon} t^{1-2\epsilon} s^{-1+\epsilon} u^{\epsilon}}{(t+s(1-t))(1-t(1-u))} \right). \tag{4.59}$$

The two integrals in Eq. 4.59 can be easily evaluated with the desired accuracy, yielding

$$\int_0^1 dt\, du\, ds \frac{(1-t)^{-1-2\epsilon} t^{1-2\epsilon} s^{-1+\epsilon} u^{\epsilon}}{tu + s(1-t)} = \frac{\pi^2}{6}\frac{1}{\epsilon} + 4\zeta_3 + \frac{\pi^4}{9}\epsilon + \mathcal{O}(\epsilon^2), \tag{4.60}$$

$$\int_0^1 dt\, du\, ds \frac{(1-t)^{-1-2\epsilon} t^{1-2\epsilon} s^{-1+\epsilon} u^{\epsilon}}{(t+s(1-t))(1-t(1-u))} = \frac{1}{2\epsilon^3} + \frac{\pi^2}{3}\frac{1}{\epsilon} + 6\zeta_3 + \frac{\pi^4}{5}\epsilon + \mathcal{O}(\epsilon^2). \tag{4.61}$$

Plugging them back into Eq. 4.59 we find

$$s^{(2)}_{(a)}\left(\tau_s,\frac{Q}{\mu},\alpha_s(\mu)\right)=-\frac{C_AC_F}{2}\frac{\alpha_s(\mu)^2}{\pi^2}\left(\frac{\mu}{Q}\right)^{4\epsilon}\left(\frac{1}{\tau_s}\right)^{1+4\epsilon}\frac{e^{2\gamma_E\epsilon}}{\Gamma^2(1-\epsilon)}\times\left(\frac{1}{2\epsilon^3}+\frac{\pi^2}{2}\frac{1}{\epsilon}+10\zeta_3+\frac{14}{45}\pi^4\epsilon+\mathcal{O}(\epsilon^2)\right). \tag{4.62}$$

This completes the evaluation of Box-type diagrams contribution to the two loop soft subprocess.

4.3.2.2 Non-abelian diagrams

The class of non-abelian diagrams (Fig. 4.4(c,d) and mirror symmetrical diagrams) is much more involved due to the presence of the three gluon vertex. The mirror conjugate diagrams in which the real gluon is connected to the opposite leg to the right of the cut are related to those depicted in Fig. 4.4(c,d) by the transformation

$$\{k\cdot n\leftrightarrow q\cdot\bar{n},k\cdot\bar{n}\leftrightarrow q\cdot n\}.$$

They can be taken into account by including a factor of two.

Thus we can write the whole non-abelian contribution as follows

$$s^{(2)}_{(c),(d)}\left(\tau_s,\frac{Q}{\mu},\alpha_s(\mu)\right)=C_FC_A\mu^{4\epsilon}g^4(n\cdot\bar{n})\int\frac{d^dq}{(2\pi)^{d-1}}\frac{d^dk}{(2\pi)^{d-1}}Q\frac{\delta^{(+)}(q^2)\delta^{(+)}(k^2)}{((q+k)^2-i0)}\times\mathcal{J}_{cut}(\tau_sQ)\Big(\frac{2k\cdot n+q\cdot n}{(k\cdot n)(q\cdot\bar{n})((q+k)\cdot n)}+\frac{q\cdot n-k\cdot n}{((k+q)\cdot n)(k\cdot n)((k+q)\cdot\bar{n})}+\{k\cdot n\leftrightarrow q\cdot\bar{n},k\cdot\bar{n}\leftrightarrow q\cdot n\}\Big). \tag{4.63}$$

Looking at the expression of the phase space constraint $\mathcal{J}_{cut}$ we see that the transformation

$$\{k\cdot n\leftrightarrow q\cdot\bar{n},k\cdot\bar{n}\leftrightarrow q\cdot n\}$$

has only the effect of exchanging the terms 4.45 and 4.47 with 4.46 and 4.48 respectively, so the contribution due to the last term in round brackets amounts to multiply once again by two. Unlike the box-type case, the integrand function depends explicitly on the transverse components through the gluon propagator. We use 4.34 and perform the integral over the transverse components as shown in Eq. A.20. Writing the result in terms of the parametrization 4.51–4.54 we end up with the following expression

$$s^{(2)}_{(c),(d)}\left(\tau_s,\frac{Q}{\mu},\alpha_s(\mu)\right)=\frac{C_FC_A}{2}g^4\frac{(n\cdot\bar{n})}{(2\pi)^{2d-2}}\left(\frac{\mu}{Q}\right)^{4\epsilon}\left(\frac{1}{\tau_s}\right)^{1+4\epsilon}\frac{\pi^{3/2-2\epsilon}}{\Gamma(1-\epsilon)}4^{-\epsilon}\frac{\Gamma(\frac{1}{2}-\epsilon)}{\Gamma(1-2\epsilon)}\times\int_0^1dt\,du\,ds\Big((1-t)^{-1-2\epsilon}t^{-1-2\epsilon}s^{-1+\epsilon}u^{-1+\epsilon}(s+u)\frac{s(t-2)(t-1)+tu(1-t)}{s(1-t)+tu}$$

$$\times\frac{{}_2F_1\left(1,\frac{1}{2}-\epsilon,1-2\epsilon,4\frac{\sqrt{su}}{(\sqrt{s}+\sqrt{u})^2}\right)}{(\sqrt{s}+\sqrt{u})^2}+(1-t)^{-1-2\epsilon}t^{-1-2\epsilon}s^{-1+\epsilon}u^{-1+\epsilon}(1+su)$$
$$\times\frac{s(1-t)(2-t(2-u))+t(1-t(1-2u))}{(s(1-t)+t)(1-t(1-u))}\frac{{}_2F_1\left(1,\frac{1}{2}-\epsilon,1-2\epsilon,4\frac{\sqrt{su}}{(1+\sqrt{su})^2}\right)}{(1+\sqrt{su})^2}\Bigg), \tag{4.64}$$

where the first integral is made of the contributions due to the terms 4.45 and 4.46, while the ones due to 4.47 and 4.48 are encoded in the second integral. Since $s\leq 1$ and $u\leq 1$ we can use Eq. A.24 to perform the following replacements

$${}_2F_1\left(1,\frac{1}{2}-\epsilon,1-2\epsilon,4\frac{\sqrt{su}}{(\sqrt{s}+\sqrt{u})^2}\right)=(\sqrt{s}+\sqrt{u})^2\Bigg(\Theta(s-u)\frac{1}{s}\,{}_2F_1\big(1,1+\epsilon,1-\epsilon,\frac{u}{s}\big)+$$
$$+\Theta(u-s)\frac{1}{u}\,{}_2F_1\big(1,1+\epsilon,1-\epsilon,\frac{s}{u}\big)\Bigg), \tag{4.65}$$
$${}_2F_1\left(1,\frac{1}{2}-\epsilon,1-2\epsilon,4\frac{\sqrt{su}}{(1+\sqrt{su})^2}\right)=(1+\sqrt{su})^2\,{}_2F_1\big(1,1+\epsilon,1-\epsilon,su\big), \tag{4.66}$$

in the first and second integral of 4.64 respectively.

Identity 4.65 splits the first integral in 4.64 into two simpler integrals. We substitute $u\to zs$ in the first of such integrals and $s\to zu$ in the second one in order to remap the integration range to the unit cube and we sum them up. After renaming the variables we finally obtain

$$s^{(2)}_{(c),(d)}\left(\tau_s,\frac{Q}{\mu},\alpha_s(\mu)\right)=\frac{C_FC_A}{8}(n\cdot\bar{n})\frac{\alpha_s^2(\mu)}{\pi^2}\frac{4^{-\epsilon}e^{2\gamma_E\epsilon}}{\sqrt{\pi}}\frac{\Gamma(\frac{1}{2}-\epsilon)}{\Gamma(1-\epsilon)\Gamma(1-2\epsilon)}\left(\frac{\mu}{Q}\right)^{4\epsilon}\left(\frac{1}{\tau_s}\right)^{1+4\epsilon}$$
$$\times\int_0^1 dt\,du\,dz\Bigg((1-t)^{-1-2\epsilon}t^{-1-2\epsilon}u^{-1+2\epsilon}z^{-1+\epsilon}(1+z)\frac{4z+t(1-t)(3-z)(1-3z)}{(1-t(1-z))(z+t(1-z))}$$
$$\times{}_2F_1(1,1+\epsilon,1-\epsilon,z)+(1-t)^{-1-2\epsilon}t^{-1-2\epsilon}u^{-1+\epsilon}z^{-1+\epsilon}(1+uz)$$
$$\times\frac{z(1-t)(2-t(2-u))+t(1-t(1-2u))}{(z(1-t)+t)(1-t(1-u))}\,{}_2F_1\big(1,1+\epsilon,1-\epsilon,zu\big)\Bigg). \tag{4.67}$$

where we used Eq. 4.37 for the coupling. The two integrals in round brackets of Eq. 4.67 are given by

$$\int_0^1 dt\,du\,dz\Bigg((1-t)^{-1-2\epsilon}t^{-1-2\epsilon}u^{-1+2\epsilon}z^{-1+\epsilon}(1+z)\frac{4z+t(1-t)(3-z)(1-3z)}{(1-t(1-z))(z+t(1-z))}$$
$$\times\,{}_2F_1(1,1+\epsilon,1-\epsilon,z)\Bigg)=\frac{1}{2\epsilon}\frac{\Gamma(1-\epsilon)}{\Gamma(1+\epsilon)\Gamma(-2\epsilon)}\Bigg(-\frac{1}{\epsilon^3}-\frac{2}{\epsilon^2}-\frac{4+\pi^2}{\epsilon}-$$
$$-\frac{4}{3}\left(6+\pi^2+6\zeta_3\right)-\frac{1}{9}\left(144+24\pi^2+\pi^4+180\zeta_3\right)\epsilon+\mathcal{O}(\epsilon^2)\Bigg), \tag{4.68}$$

$$\int_0^1 dt\,du\,dz\Bigg((1-t)^{-1-2\epsilon}t^{-1-2\epsilon}u^{-1+\epsilon}z^{-1+\epsilon}(1+uz)\frac{z(1-t)(2-t(2-u))+t(1-t(1-2u))}{(z(1-t)+t)(1-t(1-u))}$$
$$\times\,{}_2F_1\big(1,1+\epsilon,1-\epsilon,zu\big)\Bigg)=\frac{\Gamma(1-\epsilon)}{\Gamma(1+\epsilon)\Gamma(-2\epsilon)}\Bigg(-\frac{\pi^2}{3}\frac{1}{\epsilon^2}-\frac{1}{\epsilon}\left(14\zeta_3-\frac{2}{3}\pi^2\right)-$$
$$-\frac{1}{15}\left(20\pi^2+9\pi^4-420\zeta_3\right)+\mathcal{O}(\epsilon)\Bigg). \tag{4.69}$$

Plugging them into 4.67 and setting $n\cdot\bar{n}=2$ we find

$$s^{(2)}_{(c),(d)}\left(\tau_s,\frac{Q}{\mu},\alpha_s(\mu)\right)=\frac{C_FC_A}{4}\frac{\alpha_s^2(\mu)}{\pi^2}\left(\frac{\mu}{Q}\right)^{4\epsilon}\left(\frac{1}{\tau_s}\right)^{1+4\epsilon}\left(\frac{1}{\epsilon^3}+\frac{2}{\epsilon^2}+\frac{1}{\epsilon}\left(4+\frac{7}{6}\pi^2\right)+\right.$$
$$+\left(8-\pi^2+\frac{100\zeta_3}{3}\right)+$$
$$\left.+\left(16+\frac{10\pi^2}{3}+\frac{199\pi^4}{360}-\frac{124\zeta_3}{3}\right)\epsilon+\mathcal{O}(\epsilon^2)\right). \tag{4.70}$$

4.3.2.3 Vacuum polarization diagrams

The last class of diagrams we have to take into account to complete the computation of the double real radiation contribution involves diagrams of the type shown in Fig. 4.4(g,h). Summing up diagrams (g) and (h) and their mirror symmetrical ones we end up with the following expression

$$s^{(2)}_{(g),(h)}\left(\tau_s,\frac{Q}{\mu},\alpha_s(\mu)\right)=g^4\mu^{4\epsilon}\int\frac{d^dq}{(2\pi)^{d-1}}\frac{d^dk}{(2\pi)^{d-1}}Q\delta^{(+)}(q^2)\delta^{(+)}(k^2)\mathcal{J}_{cut}(Q\tau_s)$$
$$\times\left(2\frac{((q\cdot\bar{n})(k\cdot n)-(k\cdot\bar{n})(q\cdot n))^2}{((k+q)\cdot\bar{n})^2((k+q)\cdot n)^2}\frac{2(1-\epsilon)C_AC_F-4C_FT_Fn_F}{((k+q)^2+i0)((k+q)^2-i0)}+\right.$$
$$\left.+8\frac{1}{((k+q)\cdot\bar{n})((k+q)\cdot n)}\frac{C_FT_Fn_F-C_AC_F}{(k+q)^2+i0}\right), \tag{4.71}$$

where the phase space constraint $\mathcal{J}_{cut}(Q\tau_s)$ is the usual measurement function defined in 4.45-4.48. We name the two integrals appearing in 4.71 $I^{(2),(a)}_{(g),(h)}$ and $I^{(2),(b)}_{(g),(h)}$ respectively and we evaluate them below. We first use 4.34 getting

$$I^{(2),(a)}_{(g),(h)}=\frac{1}{4}\int\frac{d(q\cdot n)d(q\cdot\bar{n})}{(2\pi)^{d-1}}\frac{d(q\cdot n)d(q\cdot\bar{n})}{(2\pi)^{d-1}}Q\mathcal{J}_{cut}(Q\tau_s)\frac{((q\cdot\bar{n})(k\cdot n)-(k\cdot\bar{n})(q\cdot n))^2}{((k+q)\cdot\bar{n})^2((k+q)\cdot n)^2}$$
$$\times\int\frac{d^{d-2}q_\perp d^{d-2}q_\perp\delta^{(+)}(q^2)\delta^{(+)}(k^2)}{((k+q)^2+i0)((k+q)^2-i0)}, \tag{4.72}$$

$$I^{(2),(b)}_{(g),(h)}=\frac{1}{4}\int\frac{d(q\cdot n)d(q\cdot\bar{n})}{(2\pi)^{d-1}}\frac{d(q\cdot n)d(q\cdot\bar{n})}{(2\pi)^{d-1}}Q\mathcal{J}_{cut}(Q\tau_s)\frac{1}{((k+q)\cdot\bar{n})((k+q)\cdot n)}$$

$$\times \int \frac{d^{d-2}q_\perp d^{d-2}q_\perp \delta^{(+)}(q^2)\delta^{(+)}(k^2)}{(k+q)^2+i0}. \tag{4.73}$$

From the symmetry of the previous expressions under the transformation

$$\{k\cdot n \leftrightarrow k\cdot\bar{n}, q\cdot n \leftrightarrow q\cdot\bar{n}\},$$

we see that the terms arising from the constraints 4.46 and 4.48 are identical to those due to 4.45 and 4.47 respectively. The two internal integrals over the transverse components of the soft gluon momenta are evaluated in A.23 and A.20. Following the same technique used for the non-abelian integrals and using the following two identities (obtained from Eq. A.26)

$$\begin{aligned}{}_2F_1\left(2,\frac{1}{2}-\epsilon,1-2\epsilon,4\frac{\sqrt{su}}{(\sqrt{s}+\sqrt{u})^2}\right) &= (\sqrt{s}+\sqrt{u})^4\Bigg(\Theta(s-u)\frac{1}{s^2}\,{}_2F_1\left(2,1+\epsilon,1-\epsilon,\frac{u}{s}\right)+\\ &+\Theta(u-s)\frac{1}{u^2}\,{}_2F_1\left(2,1+\epsilon,1-\epsilon,\frac{s}{u}\right)\Bigg),\end{aligned} \tag{4.74}$$

$${}_2F_1\left(2,\frac{1}{2}-\epsilon,1-2\epsilon,4\frac{\sqrt{su}}{(1+\sqrt{su})^2}\right) = (1+\sqrt{su})^4\,{}_2F_1\left(2,1+\epsilon,1-\epsilon,su\right), \tag{4.75}$$

in addition to 4.65,4.66, after renaming some of the variables we recast $I^{(2),(a)}_{(g),(h)}$ as

$$\begin{aligned}I^{(2),(a)}_{(g),(h)} &= \frac{1}{2}\frac{\pi^{1-\epsilon}}{\Gamma(1-\epsilon)}\frac{\pi^{\frac{1}{2}-\epsilon}}{\Gamma(\frac{1}{2}-\epsilon)}\frac{4^{-\epsilon}}{(2\pi)^{2d-2}}\frac{\Gamma^2(\frac{1}{2}-\epsilon)}{\Gamma(1-2\epsilon)}\left(\frac{1}{Q}\right)^{4\epsilon}\left(\frac{1}{\tau_s}\right)^{1+4\epsilon}\\ &\times\int_0^1 dt\,du\,dz\Bigg(2(1-t)^{1-2\epsilon}t^{1-2\epsilon}u^{-1+2\epsilon}z^\epsilon\frac{(1-z)^2}{(1-t(1-z))^2}\,{}_2F_1\big(2,2+\epsilon,1-\epsilon,z\big)+\\ &+(1-t)^{1-2\epsilon}t^{1-2\epsilon}z^\epsilon u^\epsilon\frac{(1-zu)^2}{(z(1-t)+t)^2(1-t(1-u))^2}\,{}_2F_1\big(2,2+\epsilon,1-\epsilon,zu\big)\Bigg),\end{aligned} \tag{4.76}$$

and $I^{(2),(b)}_{(g),(h)}$ as

$$\begin{aligned}I^{(2),(b)}_{(g),(h)} &= \frac{1}{2}\frac{\pi^{1-\epsilon}}{\Gamma(1-\epsilon)}\frac{\pi^{\frac{1}{2}-\epsilon}}{\Gamma(\frac{1}{2}-\epsilon)}\frac{4^{-\epsilon}}{(2\pi)^{2d-2}}\frac{\Gamma^2(\frac{1}{2}-\epsilon)}{\Gamma(1-2\epsilon)}\left(\frac{1}{Q}\right)^{4\epsilon}\left(\frac{1}{\tau_s}\right)^{1+4\epsilon}\\ &\times\int_0^1 dt\,du\,dz\Bigg(2\frac{(1-t)^{-2\epsilon}t^{-2\epsilon}u^{-1+2\epsilon}z^\epsilon}{t+z(1-t)}\,{}_2F_1\big(1,1+\epsilon,1-\epsilon,z\big)+\\ &+\frac{(1-t)^{-2\epsilon}t^{-2\epsilon}u^\epsilon z^\epsilon}{(t+z(1-t))(1-t(1-u))}\,{}_2F_1\big(1,1+\epsilon,1-\epsilon,zu\big)\Bigg).\end{aligned} \tag{4.77}$$

For the four integrals appearing above we obtain

$$\int_0^1 dt\,du\,dz\frac{(1-t)^{-2\epsilon}t^{-2\epsilon}u^{-1+2\epsilon}z^\epsilon}{t+z(1-t)}\,{}_2F_1\big(1,1+\epsilon,1-\epsilon,z\big) = \frac{1}{2\epsilon}\frac{\Gamma(1-\epsilon)}{\Gamma(1+\epsilon)\Gamma(-2\epsilon)}$$

$$\times\left(\frac{1}{4\epsilon^2}+\frac{1}{2\epsilon}+\left(1+\frac{\pi^2}{6}\right)+\left(2+\frac{\pi^2}{3}+\frac{5\zeta_3}{2}\right)\epsilon+\mathcal{O}(\epsilon^2)\right), \tag{4.78}$$

$$\int_0^1 dt\,du\,dz\frac{(1-t)^{-2\epsilon}t^{-2\epsilon}u^{\epsilon}z^{\epsilon}}{(t+z(1-t))(1-t(1-u))}{}_2F_1\big(1,1+\epsilon,1-\epsilon,zu\big)=-\frac{\Gamma(1-\epsilon)}{\Gamma(1+\epsilon)\Gamma(-2\epsilon)}$$
$$\times\left(\frac{\pi^2}{6}\frac{1}{\epsilon}+7\zeta_3-\frac{\pi^2}{3}+\mathcal{O}(\epsilon)\right), \tag{4.79}$$

$$\int_0^1 dt\,du\,dz(1-t)^{1-2\epsilon}t^{1-2\epsilon}u^{-1+2\epsilon}z^{\epsilon}\frac{(1-z)^2}{(1-t(1-z))^2}{}_2F_1\big(2,2+\epsilon,1-\epsilon,z\big)=$$
$$-\frac{1}{2\epsilon}\frac{\Gamma(1-\epsilon)}{\Gamma(2+\epsilon)\Gamma(-1-2\epsilon)}\times\left(\frac{1}{12\epsilon^2}+\frac{5}{36\epsilon}+\frac{16}{27}+\frac{\pi^2}{18}+\right.$$
$$\left.+\left(\frac{59}{81}+\frac{5\pi^2}{54}+\frac{5\zeta_3}{6}\right)\epsilon+\mathcal{O}(\epsilon^2)\right), \tag{4.80}$$

$$\int_0^1 dt\,du\,dz(1-t)^{1-2\epsilon}t^{1-2\epsilon}z^{\epsilon}u^{\epsilon}\frac{(1-zu)^2}{(z(1-t)+t)^2(1-t(1-u))^2}{}_2F_1\big(2,2+\epsilon,1-\epsilon,zu\big)=$$
$$\frac{\Gamma(1-\epsilon)}{\Gamma(2+\epsilon)\Gamma(-1-2\epsilon)}\times\left(\frac{1}{\epsilon}\left(\frac{1}{6}+\frac{\pi^2}{18}\right)-\frac{7}{9}-\frac{5\pi^2}{54}+\frac{7\zeta_3}{3}+\mathcal{O}(\epsilon)\right). \tag{4.81}$$

We finally plug these expressions back into 4.71 and we obtain the following result for the vacuum polarization diagrams

$$s^{(2)}_{(g),(h)}\left(\tau_s,\frac{Q}{\mu},\alpha_s(\mu)\right)=\frac{\alpha_s(\mu)}{\pi^2}\left(\frac{\mu}{Q}\right)^{4\epsilon}\left(\frac{1}{\tau_s}\right)^{1+4\epsilon}$$
$$\times\left(-C_FT_Fn_F\left(\frac{1}{3\epsilon^2}+\frac{5}{9\epsilon}+\left(\frac{28}{27}-\frac{\pi^2}{6}\right)+\left(\frac{20}{81}+\frac{37\pi^2}{54}-\frac{62\zeta_3}{9}\right)\epsilon+\mathcal{O}(\epsilon^2)\right)+\right.$$
$$\left.+C_AC_F\left(\frac{5}{12\epsilon^2}+\frac{31}{36\epsilon}+\left(\frac{47}{27}-\frac{5\pi^2}{24}\right)+\left(\frac{211}{81}+\frac{155\pi^2}{216}-\frac{155\zeta_3}{18}\right)\epsilon+\mathcal{O}(\epsilon^2)\right)\right), \tag{4.82}$$

where we used 4.37 to replace the bare coupling with the renormalized one in the $\overline{\text{MS}}$ scheme. This completes the computation of the relevant contributions to the two-loop soft subprocess. As a further check of our calculation, we observe that summing up all the integrand functions contributing to the two-loop soft subprocess we reproduce the known double-soft current derived in [132].

4.3.3 Renormalization of the two-loop soft subprocess

Before the subtraction of the overall divergences we need to handle the subdivergences. The coupling renormalization 4.37 leads to a counter-term

$$s^{(2)}_{\text{c.t.}}\left(\tau_s,\frac{Q}{\mu},\alpha_s(\mu)\right)=\frac{\alpha_s(\mu)}{\pi}\frac{\beta_0}{\epsilon}S^{(1)}\left(\tau_s,\frac{Q}{\mu},\alpha_s(\mu)\right)=-C_F\frac{\alpha_s^2(\mu)}{\pi^2}\frac{e^{\epsilon\gamma_E}}{\epsilon^2\Gamma(1-\epsilon)}$$

$$\times \left(\frac{Q}{\mu}\right)^{-2\epsilon} \left(\frac{1}{\tau_s}\right)^{1+2\epsilon} \left(\frac{11}{6}C_A - \frac{4}{6}T_F n_F\right), \tag{4.83}$$

where $S^{(1)}(\tau_s, Q/\mu, \alpha_s(\mu))$ is the one-loop contribution 4.36.

After performing the Laplace transform of Eqs. 4.44,4.57,4.62,4.70,4.82,4.83 by means of the relation

$$\int_0^\infty d\tau_s e^{-N\tau_s} \left(\frac{Q}{\mu}\right)^{-k\epsilon} \tau_s^{-1-k\epsilon} = e^{-k\epsilon\gamma_E}\Gamma(-k\epsilon)\left(\frac{N\mu}{N_0 Q}\right)^{k\epsilon}, \tag{4.84}$$

and summing them up we obtain the following expression for the non-abelian part of the unrenormalized two loop soft subprocess $\tilde{s}^{(2)}(N_0Q/(N\mu), \alpha_s(\mu))$

$$\tilde{s}^{(2)}\left(\frac{N_0 Q}{N\mu}, \alpha_s(\mu)\right) = \frac{\alpha_s^2(\mu)}{\pi^2}\left(\tilde{s}_3^{(2)} \ln^3 \frac{N\mu}{N_0 Q} + \tilde{s}_2^{(2)} \ln^2 \frac{N\mu}{N_0 Q} + \tilde{s}_1^{(2)} \ln \frac{N\mu}{N_0 Q} + \tilde{s}_0^{(2)}\right) + \mathcal{O}(\epsilon), \tag{4.85}$$

where we find

$$\tilde{s}_3^{(2)} = -\frac{11}{9}C_A C_F + \frac{4}{9}C_F T_F n_F, \qquad \tilde{s}_2^{(2)} = -C_A C_F\left(\frac{67}{18} - \frac{\pi^2}{6}\right) + \frac{10}{9}C_F T_F n_F, \tag{4.86}$$

$$\begin{aligned}\tilde{s}_1^{(2)} = {} & -C_F T_F n_F\left(\frac{1}{3\epsilon^2} - \frac{5}{9\epsilon} - \frac{28}{27} - \frac{\pi^2}{9}\right) \\ & - C_A C_F\left(-\frac{11}{12\epsilon^2} + \frac{1}{\epsilon}\left(\frac{67}{36} - \frac{\pi^2}{12}\right) + \frac{11}{36}\pi^2 + \frac{101}{27} - \frac{7}{2}\zeta_3\right),\end{aligned} \tag{4.87}$$

$$\begin{aligned}\tilde{s}_0^{(2)} = {} & -C_F T_F n_F\left(\frac{1}{4\epsilon^3} - \frac{5}{36\epsilon^2} + \frac{1}{\epsilon}\left(-\frac{7}{27} + \frac{\pi^2}{72}\right)\right. \\ & \left. - \frac{5}{81} - \frac{77\pi^2}{216} + \frac{13\zeta_3}{18}\right) \\ & + C_A C_F\left(\frac{11}{16\epsilon^3} - \frac{1}{\epsilon^2}\left(\frac{67}{144} - \frac{\pi^2}{48}\right) - \frac{1}{\epsilon}\left(\frac{101}{108} - \frac{11}{288}\pi^2 - \frac{7}{8}\zeta_3\right)\right. \\ & \left. - \frac{535}{324} - \frac{871\pi^2}{864} + \frac{7\pi^4}{120} + \frac{143\zeta_3}{72}\right).\end{aligned} \tag{4.88}$$

Renormalization properties of Wilson loops have been studied in detail in [133–135]. The Wilson path we considered has two cusps and light-cone segments leading to additional light cone singularities. This leads us to the following evolution equation [133, 134]

$$\left(\mu\frac{\partial}{\partial\mu} + \beta(\alpha_s)\frac{\partial}{\partial\alpha_s}\right)\ln\tilde{S}\left(\frac{N_0 Q}{N\mu}, \alpha_s(\mu)\right) = -2\Gamma_{\text{cusp}}(\alpha_s(\mu))\ln\frac{N^2\mu^2}{N_0^2 Q^2} - 2\Gamma_{\text{soft}}(\alpha_s(\mu)), \tag{4.89}$$

where $\Gamma_{\text{cusp}}(g)$ is the well-known universal cusp anomalous dimension while $\Gamma_{\text{soft}}(g)$ is a path-dependent coefficient often called soft anomalous dimension. The factor 2 in front

of the cusp anomalous dimension in the evolution equation 4.89 counts the number of cusps in the integration path.

The two quantities $\Gamma_{\rm cusp}(g)$ and $\Gamma_{\rm soft}(g)$ can be evaluated through $\mathcal{O}(\alpha_s^2)$ considering the $\mathcal{O}(\alpha_s)$ and $\mathcal{O}(\alpha_s^2)$ counter-terms

$$\delta_{c.t.}^{(1)} = C_F \frac{\alpha_s(\mu)}{\pi}\left(\frac{1}{\epsilon^2}+\frac{2}{\epsilon}\ln\frac{N\mu}{N_0 Q}\right), \tag{4.90}$$

$$\begin{aligned}\delta_{c.t.}^{(2)} =& \frac{\alpha_s^2(\mu)}{\pi^2}\left(\left(C_F T_F n_F\left(\frac{1}{3\epsilon^2}-\frac{5}{9\epsilon}\right)+C_A C_F\left(-\frac{11}{12\epsilon^2}+\frac{1}{\epsilon}\left(\frac{67}{36}-\frac{\pi^2}{12}\right)\right)\right)\ln\frac{N\mu}{N_0 Q}\right.\\ &+C_F T_F n_F\left(\frac{1}{4\epsilon^3}-\frac{5}{36\epsilon^2}+\frac{1}{\epsilon}\left(-\frac{7}{27}+\frac{\pi^2}{72}\right)\right)\\ &\left.+C_A C_F\left(-\frac{11}{16\epsilon^3}+\frac{1}{\epsilon^2}\left(\frac{67}{144}-\frac{\pi^2}{48}\right)+\frac{1}{\epsilon}\left(\frac{101}{108}-\frac{11}{288}\pi^2-\frac{7}{8}\zeta_3\right)\right)\right),\end{aligned} \tag{4.91}$$

leading to the following results

$$\Gamma_{\rm cusp}(\alpha_s) = \frac{\alpha_s}{\pi}C_F+\frac{\alpha_s^2}{\pi^2}C_F\left(C_A\left(\frac{67}{36}-\frac{\pi^2}{12}\right)-\frac{5}{9}T_F n_F\right)+\mathcal{O}(\alpha_s^3), \tag{4.92}$$

$$\Gamma_{\rm soft}(\alpha_s) = -\frac{\alpha_s^2}{\pi^2}C_F\left(T_F n_F\left(\frac{14}{27}-\frac{\pi^2}{36}\right)+C_A\left(-\frac{101}{54}+\frac{11}{144}\pi^2+\frac{7}{4}\zeta_3\right)\right)+\mathcal{O}(\alpha_s^3). \tag{4.93}$$

The two-loop cusp anomalous dimension 4.92 was computed in [136], while the two-loop value of $\Gamma_{\rm soft}(g)$ was first deduced in [99] using renormalization group invariance of the cross section but it was never obtained by a direct calculation.

Exploiting the non-abelian exponentiation theorem 4.41 and 4.42, we derive a complete two-loop expression for the soft subprocess

$$\begin{aligned}\tilde{S}\left(\frac{N_0 Q}{N\mu},\alpha_s(\mu)\right) =& 1-C_F\frac{\alpha_s(\mu)}{\pi}\left(\frac{\pi^2}{4}+2\ln^2\frac{N\mu}{N_0 Q}\right)\\ &+\frac{\alpha_s^2(\mu)}{\pi^2}\left(2C_F^2\ln^4\frac{N\mu}{N_0 Q}-\left(\frac{11}{9}C_A C_F-\frac{4}{9}C_F T_F n_F\right)\ln^3\frac{N\mu}{N_0 Q}\right.\\ &+\left(\frac{\pi^2}{2}C_F^2-C_A C_F\left(\frac{67}{18}-\frac{\pi^2}{6}\right)+\frac{10}{9}C_F T_F n_F\right)\ln^2\frac{N\mu}{N_0 Q}\\ &\left.-\left(C_F T_F n_F\left(-\frac{28}{27}-\frac{\pi^2}{9}\right)+C_A C_F\left(\frac{11}{36}\pi^2+\frac{101}{27}-\frac{7}{2}\zeta_3\right)\right)\ln\frac{N\mu}{N_0 Q}\right)\\ &+\tilde{S}_0^{(2)}+\mathcal{O}(\alpha_s^3),\end{aligned} \tag{4.94}$$

where $\tilde{S}_0^{(2)}$ is the non-logarithmic piece at two-loop order for which we provide an analytic expression

$$\tilde{S}_0^{(2)} = \frac{\alpha_s^2(\mu)}{\pi^2}\left(\frac{\pi^4}{32}C_F^2+C_F T_F n_F\left(\frac{5}{81}+\frac{77\pi^2}{216}-\frac{13\zeta_3}{18}\right)\right.$$

$$+ C_A C_F \left(- \frac{535}{324} - \frac{871\pi^2}{864} + \frac{7\pi^4}{120} + \frac{143\zeta_3}{72} \right) \Bigg). \tag{4.95}$$

The constant part 4.95 has also been calculated as a specific case of the two-loop soft hemisphere function in a work done in parallel with ours [117], in full agreement with our result. Previously, it had been fitted by two different groups [99, 103, 116] using the Monte Carlo program `EVENT2` [77]. Their results are reported below

$$\tilde{S}_0^{(2),[99]} = \frac{\alpha_s^2(\mu)}{(4\pi)^2} \big((58 \pm 2) C_F^2 - (60 \pm 1) C_F C_A + (43 \pm 1) C_F T_F n_F \big), \tag{4.96}$$

$$\tilde{S}_0^{(2),[103]} = \frac{\alpha_s^2(\mu)}{(4\pi)^2} \big(48.7045 C_F^2 - (57.8) C_F C_A + (43.4) C_F T_F n_F \big), \tag{4.97}$$

$$\tilde{S}_0^{(2),[116]} = \frac{\alpha_s^2(\mu)}{(4\pi)^2} \big(48.7045 C_F^2 - (58.8 \pm 2.25) C_F C_A + (43.8 \pm 3.06) C_F T_F n_F \big), \tag{4.98}$$

while we obtain

$$\tilde{S}_0^{(2)} = \frac{\alpha_s^2(\mu)}{(4\pi)^2} \big(48.7045 C_F^2 - (56.4989) C_A C_F + (43.3905) C_F T_F n_F \big), \tag{4.99}$$

which is partly consistent with [103, 116] but not with the earlier numbers of [99], with the exception of the $C_F T_F n_F$ term. Notice that the determination of the $\tilde{S}_0^{(2)}$ constant is relevant to the matching of NNLL resummed cross section to the NNLO one since it is part of the G_{31} coefficient as it will be shown in the next section.

We now solve the evolution equation for the soft subprocess 4.89, yielding

$$\ln \frac{\tilde{S}\left(\frac{N_0 Q}{N \mu_R}, \alpha_s(\mu_R)\right)}{\tilde{S}(1, \alpha_s(\frac{N_0 Q}{N}))} = - \int_{\frac{N_0^2 Q^2}{N^2}}^{\mu_R^2} \frac{dk^2}{2k^2} \big(2\Gamma_{\text{cusp}}(\alpha_s(k^2)) \ln \frac{N^2 k^2}{N_0^2 Q^2} + 2\Gamma_{\text{soft}}(\alpha_s(k^2)) \big), \tag{4.100}$$

where μ_R is the renormalization scale of the process. We can perform the substitution

$$\ln \frac{N^2 k^2}{N_0^2 Q^2} = \int_{\frac{N_0^2 Q^2}{N^2}}^{k^2} \frac{d\mu^2}{\mu^2}, \tag{4.101}$$

and exchange the order of integration in the integral containing Γ_{cusp} getting

$$\ln \frac{\tilde{S}\left(\frac{N_0 Q}{N \mu_R}, \alpha_s(\mu_R)\right)}{\tilde{S}(1, \alpha_s(\frac{N_0 Q}{N}))} = - \int_{\frac{N_0^2 Q^2}{N^2}}^{\mu_R^2} \frac{d\mu^2}{\mu^2} \int_{\mu^2}^{\mu_R^2} \frac{dk^2}{k^2} \Gamma_{\text{cusp}}(\alpha_s(k^2)) - \int_{\frac{N_0^2 Q^2}{N^2}}^{\mu_R^2} \frac{dk^2}{k^2} \Gamma_{\text{soft}}(\alpha_s(k^2)). \tag{4.102}$$

We set $\mu_R = Q$ in order to minimize the logarithmic corrections coming from the hard function in 4.28, moreover we replace $\mu^2/Q^2 = u^2$ in the first integral of Eq. 4.102 and

$k^2/Q^2 = u^2$ in the second one and we finally obtain

$$\frac{\tilde{S}(\frac{N_0}{N}, \alpha_s(Q))}{\tilde{S}(1, \alpha_s(\frac{N_0 Q}{N}))} = \exp\Bigg(-2\int_{\frac{N_0}{N}}^{1} \frac{du}{u} \int_{u^2Q^2}^{Q^2} \frac{dk^2}{k^2} \Gamma_{\text{cusp}}(\alpha_s(k^2)) - 2\int_{\frac{N_0}{N}}^{1} \frac{du}{u} \Gamma_{\text{soft}}(\alpha_s(u^2Q^2))\Bigg). \tag{4.103}$$

The thrust observable is symmetrical under the exchange of the two hemispheres, so the factor 2 in the exponent accounts for the identical contributions due to both of them.

4.4 Resummation of large logarithms

In the present section we derive a resummed expression for the cross section 4.13 in Laplace space starting from the renormalization group (RG) evolution of each of the subprocesses. The effect of soft gluons has been taken into account in the previous section, but we still need to consider logarithmically enhanced terms due to hard gluons moving collinearly to one of the hard quark legs. Such an effect is encoded in the jet subprocess which describes the decay of a hard quark into a jet of collinear particles. The same subprocess can be found in other relevant QCD processes such as deep inelastic scattering and B-meson decay and it obeys the following evolution equation [114, 122]:

$$\left(\mu\frac{\partial}{\partial\mu} + \beta(\alpha_s)\frac{\partial}{\partial\alpha_s}\right) \ln \tilde{J}\left(\sqrt{\frac{N_0}{N}}\frac{Q}{\mu}, \alpha_s(\mu)\right) = 2\Gamma_{\text{cusp}}(\alpha_s(\mu)) \ln\frac{N\mu^2}{N_0 Q^2} - 2\Gamma_{\text{coll}}(\alpha_s(\mu)). \tag{4.104}$$

The collinear subprocess can be defined as a cut propagator of a massless quark in the axial gauge [59]. Indeed, the factorization used here is manifest in the axial gauge [59].

Equation 4.104 can be solved following the same technique used with the soft subprocess but now replacing $\mu^2/Q^2 = u$ and $k^2/Q^2 = u$ in the first and second integral in the exponent respectively. It leads to

$$\frac{\tilde{J}\left(\frac{N_0}{N}, \alpha_s(Q)\right)}{\tilde{J}\left(1, \alpha_s(\sqrt{\frac{N_0}{N}}Q)\right)} = \exp\Bigg(\int_{\frac{N_0}{N}}^{1} \frac{du}{u} \int_{uQ^2}^{Q^2} \frac{dk^2}{k^2} \Gamma_{\text{cusp}}(\alpha_s(k^2)) - \int_{\frac{N_0}{N}}^{1} \frac{du}{u} \Gamma_{\text{coll}}(\alpha_s(uQ^2))\Bigg). \tag{4.105}$$

We now combine 4.103 and 4.105 together in the expression of the cross section

$$\begin{aligned}\tilde{\sigma}_N(Q^2, \alpha_s) &= H(1, \alpha_s(\mu = Q))\tilde{J}^2\left(\frac{N_0}{N}, \alpha_s(Q)\right)\tilde{S}\left(\frac{N_0}{N}, \alpha_s(Q)\right) = \\ &= H(1, \alpha_s(Q))\tilde{J}^2\left(1, \alpha_s(\sqrt{\frac{N_0}{N}}Q)\right)\tilde{S}\left(1, \alpha_s(\frac{N_0 Q}{N})\right)\end{aligned}$$

$$\times \exp\Bigg(-2\int_{\frac{N_0}{N}}^{1}\frac{du}{u}\int_{u^2Q^2}^{uQ^2}\frac{dk^2}{k^2}\Gamma_{\rm cusp}(\alpha_s(k^2)) \\ -2\int_{\frac{N_0}{N}}^{1}\frac{du}{u}(\Gamma_{\rm soft}(\alpha_s(u^2Q^2))+\Gamma_{\rm coll}(\alpha_s(uQ^2)))\Bigg), \tag{4.106}$$

where we explicitly set the renormalization scale $\mu = Q$.

Using the relation

$$\Gamma_{\rm soft}(\alpha_s(u^2Q^2)) = \Gamma_{\rm soft}(\alpha_s(uQ^2)) - \int_{u^2Q^2}^{uQ^2}\frac{dk^2}{k^2}\beta(\alpha_s(k^2))\frac{\partial\Gamma_{\rm soft}(\alpha_s(k^2))}{\partial\alpha_s}, \tag{4.107}$$

we recast Eq. 4.106 as

$$\tilde{\sigma}_N(Q^2,\alpha_s) = H(1,\alpha_s(Q))\tilde{J}^2\left(1,\alpha_s(\sqrt{\frac{N_0}{N}}Q)\right)\tilde{S}\left(1,\alpha_s(\frac{N_0Q}{N})\right) \\ \times\exp\Bigg\{-2\int_{\frac{N_0}{N}}^{1}\frac{du}{u}\left(\int_{u^2Q^2}^{uQ^2}\frac{dk^2}{k^2}\mathcal{A}_\Gamma(\alpha_s(k^2))+\mathcal{B}_\Gamma(\alpha_s(uQ^2))\right)\Bigg\}, \tag{4.108}$$

where we defined

$$\mathcal{A}_\Gamma(\alpha_s) = \Gamma_{\rm cusp}(\alpha_s) - \beta(\alpha_s)\frac{\partial\Gamma_{\rm soft}(\alpha_s)}{\partial\alpha_s}, \\ \mathcal{B}_\Gamma(\alpha_s) = \Gamma_{\rm soft}(\alpha_s)+\Gamma_{\rm coll}(\alpha_s). \tag{4.109}$$

The two coefficients $\mathcal{A}_\Gamma(\alpha_s)$ and $\mathcal{B}_\Gamma(\alpha_s)$ can be computed in perturbative QCD. To this end we observe that the Altarelli-Parisi splitting function $P_{qq}(\alpha_s,z)$ fulfils the following limit [137] as $z\to 1$

$$P_{qq}(\alpha_s,z) = 2\frac{\Gamma_{\rm cusp}(\alpha_s)}{(1-z)_+} + 2\mathcal{B}_\Gamma(\alpha_s)\delta(1-z)+..., \tag{4.110}$$

where the dots stand for regular terms in the $z\to 1$ limit. The asymptotic expression 4.110 is valid to all orders in perturbative QCD and it can be easily proven in the context of deep inelastic scattering as shown in [115]. The Mellin transform of the structure function $F_2(Q^2,x)$ can be indeed factorized in the threshold limit $x\to 1$ as a product of a hard virtual function $H(Q/\mu,\alpha_s(\mu))$, a collinear jet function and a parton distribution function $\phi_q(N,\mu)$. Both the hard and collinear jet functions are essentially the same ones as in the thrust case (up to constants in the hard subprocess due to crossing). The collinear jet function evolution is described by Eq. 4.104, while the hard function RG equation reads

$$\left(\mu\frac{\partial}{\partial\mu}+\beta(\alpha_s)\frac{\partial}{\partial\alpha_s}\right)\ln H(\frac{Q}{\mu},\alpha_s(\mu)) = -2\Gamma_{\rm cusp}(\alpha_s(\mu))\ln\frac{\mu^2}{Q^2}$$

$$+ 2\big(\Gamma_{\rm soft}(\alpha_s(\mu)) + 2\Gamma_{\rm coll}(\alpha_s(\mu))\big), \qquad (4.111)$$

and the parton distribution function evolves according to the Altarelli-Parisi equation [138]

$$\left(\mu\frac{\partial}{\partial\mu} + \beta(\alpha_s)\frac{\partial}{\partial\alpha_s}\right)\ln\phi_q(N,\mu) = \tilde{P}_{qq}(\alpha_s,N), \qquad (4.112)$$

where

$$\tilde{P}_{qq}(\alpha_s,N) = -\int_0^1 dz\, z^{N-1}P_{qq}(\alpha_s,z) \qquad (4.113)$$

is the Mellin transform of the splitting function using the conventions of [139, 140]. We now observe that for the structure function $F_2(Q^2,x)$ to be RG invariant, we have to require that the anomalous dimensions of the hard, jet and parton distribution functions sum up to zero, proving Eq. 4.110.

As stated at the end of the previous section, since the thrust is symmetrical under the exchange of the two hemispheres, we can factorize the soft subprocess as a product of two independent "hemisphere" soft subprocesses. It follows that the resummed cross section 5.2 can be recast as a constant term multiplied by the evolution of two independent jets each of which is the product of the collinear jet and the respective "hemisphere" soft subprocess. This is in analogy to the structure obtained at NLL using the coherent branching algorithm [47]. We compare the two expressions observing that the only difference between the two exponents is the term $\beta(\alpha_s)\partial\Gamma_{\rm soft}(\alpha_s)/\partial\alpha_s$ which gives a non-vanishing contribution only beyond NLL. It essentially accounts for large angle soft emissions whose effects do not contribute at NLL (it is easy to see that the first non-trivial term arises at $\mathcal{O}(\alpha_s^3)$). A second interesting feature which shows up beyond the NLL approximation is the interplay between constant terms and logarithms due to the factor $\tilde{J}^2(1,\alpha_s(\sqrt{(N_0/N)}Q))\tilde{S}(1,\alpha_s(N_0Q/N))$ that will be analyzed below.

The resummed cross section in the dijet limit 5.2 takes the following form

$$\begin{aligned}
\tilde{\sigma}_N(Q^2,\alpha_s) &= \left(1+\sum_{k=1}^{\infty}\tilde{C}_k\left(\frac{\alpha_s}{2\pi}\right)^k\right)\Sigma_N(Q^2,\alpha_s),\\
\Sigma_N(Q^2,\alpha_s) &= \exp\Bigg\{Lf_1\left(\frac{\alpha_s}{\pi}\beta_0L\right) + f_2\left(\frac{\alpha_s}{\pi}\beta_0L\right) + \frac{\alpha_s}{\pi}\beta_0 f_3\left(\frac{\alpha_s}{\pi}\beta_0L\right) + \tilde{G}_{31}\left(\frac{\alpha_s}{2\pi}\right)^3 L\\
&\quad + \mathcal{O}(\alpha_s^4L^2)\Bigg\},
\end{aligned} \qquad (4.114)$$

where here $L=\ln N$. The function $f_1((\alpha_s/\pi)\beta_0L)$ resums all the leading logarithmic contributions $\alpha_s^nL^{n+1}$, $f_2((\alpha_s/\pi)\beta_0L)$ resums the next to leading terms $\alpha_s^nL^n$ and so

on. We furthermore require that $f_i(0) = 0$ so that at $\mathrm{N}^n\mathrm{LL}$ we can write

$$f_1\left(\frac{\alpha_s}{\pi}\beta_0 L\right) = \sum_{k\geq 1} \tilde{G}_{k,k+1}\left(\frac{\alpha_s}{2\pi}\right)^k L^{k+1}, \qquad n = 0; \tag{4.115}$$

$$f_{n+1}\left(\frac{\alpha_s}{\pi}\beta_0 L\right) = \sum_{k\geq n} \tilde{G}_{k,k+1-n}\left(\frac{\alpha_s}{2\pi}\right)^k L^{k+1-n}, \qquad n \geq 1. \tag{4.116}$$

With this notation we see that the term $\tilde{G}_{31}\alpha_s^3 L$ is a $\mathrm{N}^3\mathrm{LL}$ contribution due to the Taylor expansion of $f_4(\frac{\alpha_s}{\pi}\beta_0 L)$. Nevertheless, such a term is relevant for the R-matching of the NNLL resummed cross section to the $\mathcal{O}(\alpha_s^3)$ fixed-order result, which will be discussed below. After expanding the functions $\mathcal{A}_\Gamma(\alpha_s)$ and $\mathcal{B}_\Gamma(\alpha_s)$ as

$$\mathcal{A}_\Gamma(\alpha_s) = \sum_{k\geq 1} A^{(k)}\left(\frac{\alpha_s}{\pi}\right)^k, \qquad \mathcal{B}_\Gamma(\alpha_s) = \sum_{k\geq 1} B^{(k)}\left(\frac{\alpha_s}{\pi}\right)^k, \tag{4.117}$$

in Eq. 5.2, we observe that $A^{(k)}$ gives rise to terms of order $\alpha_s^n L^{n+2-k}$ while $B^{(k)}$ contributes with terms of order $\alpha_s^n L^{n+1-k}$ with $n \geq k$.

The previous property ensures that the knowledge of $B^{(3)}$ is sufficient to compute $\tilde{G}_{31}$ and we do not need to know $A^{(4)}$ which has not been computed yet (Γ_{soft} is known at three loops [99], but the four loop value of Γ_{cusp} is still unknown).

The coefficient $H(1,\alpha_s(Q))\tilde{J}^2(1,\alpha_s(\sqrt{(N_0/N)}Q))\tilde{S}(1,\alpha_s(N_0Q/N))$ in Eq. 5.2 contains all the constant terms and it can be expanded in perturbation theory. The function $H(1,\alpha_s(Q))$ is known at three loop order [112, 113] (this result has subsequently to be normalized to the total hadronic cross section σ) and the two-loop non-logarithmic value of the collinear subprocess was computed in [114]. The constant part of the two-loop soft subprocess was evaluated in the previous section. We see that the coupling is evaluated at different scales in each of the three functions. We use the expression for the running coupling A.3 to express them in terms of $\alpha_s(Q)$ evaluated at the renormalization scale $\mu_R = Q$. The resulting expression has additional resummed logarithms sitting outside the exponent of Eq. 5.2 due to the running of α_s and giving a well defined and finite contribution at large N. Such terms contribute from NNLL on and do not exponentiate naturally. Nevertheless, in order to bring the cross section to the form 4.114, we raise them to the exponent and we expand them to the desired order.

One finds that the one-loop constants of the collinear and soft subprocesses contribute to $f_3((\alpha_s/\pi)\beta_0 L)$ while the two-loop ones contribute to $\tilde{G}_{31}$.
To evaluate the integrals in Eq. 5.2 we use the renormalization group equation A.1 to change the integration variable to α_s. After imposing the normalization condition $f_i(0) = 0$ we find

$$f_1(\lambda) = -\frac{A^{(1)}}{\beta_0\lambda}[(1-2\lambda)\ln(1-2\lambda) - 2(1-\lambda)\ln(1-\lambda)], \tag{4.118}$$

$$
\begin{aligned}
f_2(\lambda) = &-\frac{A^{(2)}}{\beta_0^2}[2\ln(1-\lambda)-\ln(1-2\lambda)] + 2\frac{B^{(1)}}{\beta_0}\ln(1-\lambda) \\
&-\frac{A^{(1)}\beta_1}{\beta_0^3}[\ln(1-2\lambda)+\frac{1}{2}\ln^2(1-2\lambda)-\ln(1-\lambda)(2+\ln(1-\lambda)] \\
&-2\frac{A^{(1)}\gamma_E}{\beta_0}\ln\frac{1-\lambda}{1-2\lambda},
\end{aligned}
\tag{4.119}
$$

$$
\begin{aligned}
f_3(\lambda) = &\frac{2c_s^{(1)}}{\beta_0}\frac{\lambda}{1-2\lambda} + \frac{2c_j^{(1)}}{\beta_0}\frac{\lambda}{1-\lambda} - \frac{2B^{(2)}}{\beta_0^2}\frac{\lambda}{1-\lambda} - \frac{A^{(3)}}{\beta_0^3}\frac{\lambda^2}{(1-\lambda)(1-2\lambda)} \\
&-\frac{2A^{(2)}\gamma_E}{\beta_0^2}\frac{\lambda}{(1-\lambda)(1-2\lambda)} + \frac{A^{(2)}\beta_1}{\beta_0^4}\frac{3\lambda^2+(1-\lambda)\ln(1-2\lambda)-2(1-2\lambda)\ln(1-\lambda)}{(1-\lambda)(1-2\lambda)} \\
&-2\frac{B^{(1)}}{\beta_0}\gamma_E\frac{\lambda}{1-\lambda} + \frac{2B^{(1)}\beta_1}{\beta_0^3}\frac{\lambda+\ln(1-\lambda)}{1-\lambda} \\
&+\frac{A^{(1)}}{\beta_0}\frac{1}{(1-\lambda)(1-2\lambda)}\Big[-\gamma_E^2\lambda(3-2\lambda)+\frac{2\gamma_E\beta_1}{\beta_0^2}[\lambda+(1-\lambda)\ln(1-2\lambda) \\
&-(1-2\lambda)\ln(1-\lambda)]+\frac{\beta_2}{\beta_0^3}[-\lambda^2+(1-3\lambda+2\lambda^2)(2\ln(1-\lambda)-\ln(1-2\lambda))]\Big] \\
&-\frac{A^{(1)}\beta_1^2}{\beta_0^5}\Bigg[\frac{1-\lambda}{2(1-\lambda)(1-2\lambda)}\ln(1-2\lambda)[4\lambda+\ln(1-2\lambda)] \\
&-\frac{2}{2(1-\lambda)(1-2\lambda)}[\lambda^2-(1-2\lambda)\ln(1-\lambda)(2\lambda+\ln(1-\lambda))]\Bigg],
\end{aligned}
\tag{4.120}
$$

where $\lambda = \frac{\alpha_s(Q)}{\pi}\beta_0 \ln N$.

At NLL the previous functions reproduce the result obtained in [47]. The constants $c_j^{(1)}$ and $c_s^{(1)}$ are the one-loop non-logarithmic terms of the collinear and the soft subprocesses respectively. They arise from the term $\tilde{J}^2(1,\alpha_s(\sqrt{(N_0/N)}Q))\tilde{S}(1,\alpha_s(N_0Q/N))$, as discussed above. The coefficients $A^{(i)}$ and $B^{(i)}$ can be determined as shown in Eq. 4.109 using the two-loop value of $\Gamma_{\rm soft}$ computed above and the three-loop splitting functions [139, 140]. They are reported in Appendix A.

We observe that the normalization condition $f_i(0) = 0$ is automatically fulfilled by both $f_1(\lambda)$ and $f_2(\lambda)$ while it has to be imposed to obtain $f_3(\lambda)$ 4.120. This could be considered as a signal of the breakdown of natural exponentiation beyond NLL. Forcing such a constraint gives rise to a residual constant value which has to be taken out of the exponent and that contributes to the constants $\tilde{C}_i$. We will determine the value of such constants directly in thrust space in section 4.4.1.

4.4.1 Inversion of the integral transform

In the present section we perform the inverse Laplace transform of the resummed cross section. We recall the definition of the normalized cross section

$$R_T(\tau) = \frac{1}{2\pi i}\int_C \frac{dN}{N} e^{N\tau}\tilde{\sigma}_N(Q^2,\alpha_s) + \mathcal{O}(\tau), \tag{4.121}$$

where $\tilde{\sigma}_N(Q^2,\alpha_s)$ is defined in Eq. 4.114. The contour C runs parallel to the imaginary axis to the right of all the singularities of the integrand function. A method to invert 4.121 was proposed in [47]. Keeping their notation we rewrite $\Sigma_N(Q^2,\alpha_s)$ in 4.114 as

$$\Sigma_N(Q^2,\alpha_s) = e^{\tilde{\mathcal{F}}(\alpha_s(Q^2),\ln N)}, \tag{4.122}$$

where

$$\begin{aligned}\tilde{\mathcal{F}}(\alpha_s(Q^2),L) =& Lf_1\left(\frac{\alpha_s}{\pi}\beta_0 L\right) + f_2\left(\frac{\alpha_s}{\pi}\beta_0 L\right) + \frac{\alpha_s}{\pi}\beta_0 f_3\left(\frac{\alpha_s}{\pi}\beta_0 L\right) + \tilde{G}_{31}\left(\frac{\alpha_s}{2\pi}\right)^3 L \\ &+ \mathcal{O}(\alpha_s^4 L^2).\end{aligned} \tag{4.123}$$

With this notation $\tilde{\sigma}_N(Q^2,\alpha_s)$ reads

$$\tilde{\sigma}_N(Q^2,\alpha_s) = \left(1 + \sum_{k=1}^{\infty}\tilde{C}_k\left(\frac{\alpha_s}{2\pi}\right)^k\right) e^{\tilde{\mathcal{F}}(\alpha_s(Q^2),\ln N)}. \tag{4.124}$$

We now Taylor expand the exponent $\tilde{\mathcal{F}}$ with respect to $\ln N$ around $\ln N = \ln(1/\tau)$ up to the desired order and we end up with the following expression for $R_T(\tau)$

$$\begin{aligned}R_T(\tau) =& \left(1 + \sum_{k=1}^{3}\tilde{C}_k\left(\frac{\alpha_s}{2\pi}\right)^k\right) e^{\tilde{\mathcal{F}}(\alpha_s(Q^2),\ln\frac{1}{\tau})}\frac{1}{2\pi i}\int_C \frac{d\nu}{\nu}\exp\Bigg[\nu + \tilde{\mathcal{F}}^{(1)}(\alpha_s(Q^2),\ln\frac{1}{\tau})\ln\nu \\ &+ \frac{1}{2}\tilde{\mathcal{F}}^{(2)}(\alpha_s(Q^2),\ln\frac{1}{\tau})\ln^2\nu + \mathcal{O}(\alpha_s^n\ln^{n-2}(1/\tau))\Bigg],\end{aligned} \tag{4.125}$$

where $\nu = N\tau$ and

$$\tilde{\mathcal{F}}^{(n)}\left(\alpha_s(Q^2),\ln\frac{1}{\tau}\right) = \frac{\partial^n}{\partial\ln^n\frac{1}{\tau}}\tilde{\mathcal{F}}(\alpha_s(Q^2),\ln(1/\tau)). \tag{4.126}$$

More precisely, we have

$$\tilde{\mathcal{F}}^{(1)}(\alpha_s(Q^2),\ln(1/\tau)) = f_1(\lambda) + \lambda f_1'(\lambda) + \frac{\alpha_s}{\pi}\beta_0 f_2'(\lambda) + \mathcal{O}(\alpha_s^n\ln^{n-2}(1/\tau)), \tag{4.127}$$

$$\tilde{\mathcal{F}}^{(2)}\left(\alpha_s(Q^2),\ln(1/\tau)\right) = 2\frac{\alpha_s}{\pi}\beta_0 f_1'(\lambda) + \frac{\alpha_s}{\pi}\beta_0\lambda f_1''(\lambda) + \mathcal{O}(\alpha_s^n\ln^{n-2}(1/\tau)), \tag{4.128}$$

where, from now on, $\lambda = (\alpha_s/\pi)\beta_0\ln(1/\tau)$. Without loss of generality we expand the factor

$$\exp\left[\frac{1}{2}\tilde{\mathcal{F}}^{(2)}(\alpha_s(Q^2),\ln(1/\tau))\ln^2\nu\right] \tag{4.129}$$

in a Taylor series in $\tilde{\mathcal{F}}^{(2)}$ itself and we see that the series of terms $(\tilde{\mathcal{F}}^{(2)})^k$ with $k \geq 2$ gives at most rise to terms of order $\mathcal{O}(\alpha_s^k(\alpha_s \ln(1/\tau))^n)$, so we drop them. Using the result [47]

$$\frac{1}{2\pi i}\int_C \frac{d\nu}{\nu}\ln^k\nu \exp\left[\nu + \tilde{\mathcal{F}}^{(1)}\ln\nu\right] = \frac{d^k}{d(\tilde{\mathcal{F}}^{(1)})^k}\frac{1}{\Gamma(1-\tilde{\mathcal{F}}^{(1)})}, \tag{4.130}$$

we obtain

$$\begin{aligned} R_T(\tau) =& \left(1+\sum_{k=1}^{3}\tilde{C}_k\left(\frac{\alpha_s}{2\pi}\right)^k\right)e^{\tilde{\mathcal{F}}(\alpha_s(Q^2),\ln\frac{1}{\tau})}\left[\frac{1}{\Gamma(1-\gamma(\lambda))}+\frac{\alpha_s}{\pi}\beta_0 f_2'(\lambda)\frac{\psi^{(0)}(1-\gamma(\lambda))}{\Gamma(1-\gamma(\lambda))}\right.\\ &\left.+\frac{1}{2}\tilde{\mathcal{F}}^{(2)}\frac{d^2}{d\gamma^2(\lambda)}\frac{1}{\Gamma(1-\gamma(\lambda))}+\mathcal{O}(\alpha_s^2(\alpha_s\ln(1/\tau))^n)\right], \end{aligned} \tag{4.131}$$

where we neglected subleading terms and we defined $\gamma(\lambda) = f_1(\lambda) + \lambda f_1'(\lambda)$. $\psi^{(m)}$ is the $(m+1)$-th derivative of the logarithm of the Euler Γ-function.

After replacing the coefficients $\tilde{C}_k$ and $\tilde{G}_{31}$ in the previous expression with C_k and G_{31} computed as explained in Appendix A.2, we can recast $R_T(\tau)$ as

$$\begin{aligned} R_T(\tau) =& \left(1+\sum_{k=1}^{3}C_k\left(\frac{\alpha_s}{2\pi}\right)^k\right)e^{\mathcal{F}(\alpha_s(Q^2),\ln\frac{1}{\tau})}\frac{1}{\Gamma(1-\gamma(\lambda))}\left[1+\frac{\alpha_s}{\pi}\beta_0 f_2'(\lambda)\psi^{(0)}(1-\gamma(\lambda))\right.\\ &\left.+\frac{1}{2}\frac{\alpha_s}{\pi}\beta_0\gamma'(\lambda)\Gamma(1-\gamma(\lambda))\frac{d^2}{d\gamma^2(\lambda)}\frac{1}{\Gamma(1-\gamma(\lambda))}+\frac{\alpha_s}{\pi}C_F\left(\gamma_E\left(\frac{3}{2}-\gamma_E\right)-\frac{\pi^2}{6}\right)\right], \end{aligned} \tag{4.132}$$

where now

$$\begin{aligned} \mathcal{F}(\alpha_s(Q^2),L) =& Lf_1\left(\frac{\alpha_s}{\pi}\beta_0 L\right)+f_2\left(\frac{\alpha_s}{\pi}\beta_0 L\right)+\frac{\alpha_s}{\pi}\beta_0 f_3\left(\frac{\alpha_s}{\pi}\beta_0 L\right)+G_{31}\left(\frac{\alpha_s}{2\pi}\right)^3 L\\ &+\mathcal{O}(\alpha_s^4 L^2). \end{aligned} \tag{4.133}$$

The expression 4.132 for $R_T(\tau)$ resums all large logarithms through NNLL and it holds up to terms of order $\mathcal{O}(\alpha_s^4\ln^2(1/\tau))$.

The constant term $\alpha_s/\pi C_F\,(\gamma_E(3/2-\gamma_E)-\pi^2/6)$ is defined such that the term in square brackets is normalized to one as $\lambda \to 0$ and ensures that all the constant terms are included in the C_k coefficients which read

$$C_1 = C_F\left(-\frac{5}{2}+\frac{\pi^2}{3}\right), \tag{4.134}$$

$$\begin{aligned} C_2 =& C_F^2\left(\frac{41}{8}-\frac{7}{8}\pi^2+\frac{5}{36}\pi^4-6\zeta_3\right)+C_A C_F\left(-\frac{491}{24}-\frac{53\pi^2}{108}+\frac{11\pi^4}{360}+\frac{104\zeta_3}{3}\right)\\ &+C_F T_F n_F\left(\frac{35}{6}+\frac{7\pi^2}{27}-\frac{28\zeta_3}{3}\right). \end{aligned} \tag{4.135}$$

The coefficient G_{31} is found to be

$$\begin{aligned} G_{31} = \; & C_F^2 n_F \left(-\frac{77}{8} - \frac{19\pi^2}{36} + \frac{8\pi^4}{45} - \frac{104\zeta_3}{9} \right) + C_A C_F n_F \left(-\frac{1118}{27} + \frac{644\pi^2}{81} - \frac{17\pi^4}{135} - \frac{292\zeta_3}{9} \right) \\ & + C_F n_F^2 \left(\frac{191}{54} - \frac{61\pi^2}{81} + \frac{32\zeta_3}{9} \right) + C_A^2 C_F \left(\frac{5951}{54} - \frac{6625\pi^2}{324} + \frac{383\pi^4}{540} + \frac{404\zeta_3}{9} + 10\zeta_5 \right) \\ & + C_A C_F^2 \left(\frac{23}{2} + \frac{161\pi^2}{72} - \frac{53\pi^4}{45} + \frac{452\zeta_3}{9} + 2\pi^2\zeta_3 + 30\zeta_5 \right) \\ & + C_F^3 \left(\frac{29}{8} + \frac{5\pi^2}{4} - \frac{8\pi^4}{15} + 53\zeta_3 - \frac{44}{3}\pi^2\zeta_3 + 132\zeta_5 \right). \end{aligned} \tag{4.136}$$

The value of the $\mathcal{O}(\alpha_s^3)$ constant C_3 is unknown and we fit it using the Monte Carlo program `EERAD3` [80]. Details about the fitting procedure are explained in the next section. Following the conventions of [47] the final resummed expression $R_T(\tau)$ 4.132 can be written as

$$R_T(\tau) = \left(1 + \sum_{k=1}^{3} C_k \left(\frac{\alpha_s}{2\pi} \right)^k \right) \exp \left[\ln \frac{1}{\tau} g_1(\lambda) + g_2(\lambda) + \frac{\alpha_s}{\pi} \beta_0 g_3(\lambda) + \left(\frac{\alpha_s}{2\pi} \right)^3 G_{31} \ln \frac{1}{\tau} \right], \tag{4.137}$$

where

$$\begin{aligned} g_1(\lambda) = \; & f_1(\lambda), \\ g_2(\lambda) = \; & f_2(\lambda) - \ln \Gamma(1 - f_1(\lambda) - \lambda f_1'(\lambda)), \\ g_3(\lambda) = \; & f_3(\lambda) + \left(f_1' + \frac{1}{2}\lambda f_1''(\lambda) \right) \left(\psi^{(0)}(1-\gamma(\lambda))^2 - \psi^{(1)}(1-\gamma(\lambda)) \right) + f_2'(\lambda)\psi^{(0)}(1-\gamma(\lambda)) \\ & + \frac{C_F}{\beta_0} \left(\gamma_E \left(\frac{3}{2} - \gamma_E \right) - \frac{\pi^2}{6} \right), \end{aligned} \tag{4.138}$$

notice that the functions $g_i(\lambda)$ do not generate any constants (*i.e.* $g_i(0) = 0$).

The resummed expression at different logarithmic orders evaluated around the peak region is shown in Figure 4.6.

We observe that an exact inversion of Eq. 4.121 requires to choose the integration contour C to the right of the Landau singularities present in the resummed functions $f_i(\lambda)$. Following the prescription of [47] for the inversion, we avoid such singularities by expanding around $\ln N = \ln \frac{1}{\tau}$ and then integrating by means of the residue theorem closing the contour in the left half-plane using Eq. 4.130. In doing so, we are neglecting the contribution due to the residue at the Landau pole, which gives rise to power suppressed terms [141]. The Landau singularity is then mapped onto the thrust space without contributing to the Laplace inversion. By expressing the SCET result of [99] in the form 4.137 [142], we obtain full analytic agreement on $g_3(\lambda)$. This is a non-trivial result, since in [99] the scales in the resummation kernels are fixed at the

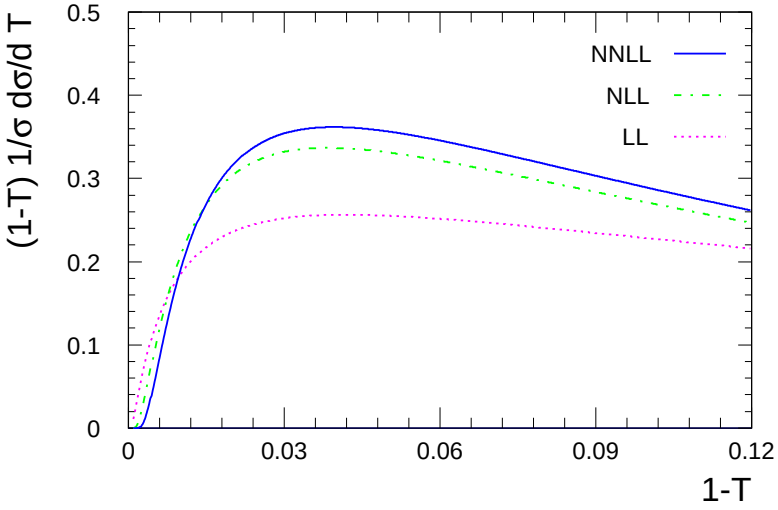

Figure 4.6: Comparison of the resummed result at different logarithmic orders around the peak region.

outset of the calculation, while in our analysis, they are integrated over in the Laplace inversion. This difference results in a different treatment of the Landau singularity in the resummed expressions, which could produce a power-suppressed difference between the cross sections obtained in both approaches. The exact agreement of our $g_3(\lambda)$ with [99] demonstrates that there is no Landau-pole ambiguity between the two approaches. However, in [99] subleading terms arising from the scale fixing in T-space and part of the constants are kept in the exponent resulting in a numerical difference when compared to our result.

4.4.2 Determination of the $\mathcal{O}(\alpha_s^3)$ constant C_3

In order to match the resummed result to the NNLO cross section the $\mathcal{O}(\alpha_s^3)$ constant C_3 must be extracted from fixed-order data. We do it by subtracting the logarithms from the fixed-order $\mathcal{C}(\tau)$ coefficient obtained from `EERAD3`. The logarithmic part $R^{(3)}_{\log}(\tau)$ of the NNLO coefficient is decomposed into its different color contributions according to

$$R^{(3)}_{\log}(\tau) = R^{(3)}_{\log}\Big|_{N^2} + R^{(3)}_{\log}\Big|_{N^0} + R^{(3)}_{\log}\Big|_{1/N^2} + R^{(3)}_{\log}\Big|_{n_F N} + R^{(3)}_{\log}\Big|_{n_F/N} + R^{(3)}_{\log}\Big|_{n_F^2} . \tag{4.139}$$

`EERAD3` is run with a technical cutoff $y_0 = 10^{-5}$ which affects the thrust distribution below $\tau_0 \sim \sqrt{y_0}$. This forbids us from probing the far infrared region and we perform the fit for values of τ larger than τ_0. Numerical fixed order results are obtained with 6×10^7 points for the leading colour contribution and 10^7 points for the subleading colour structures. Because of the presence of large fluctuations in the Monte Carlo results,

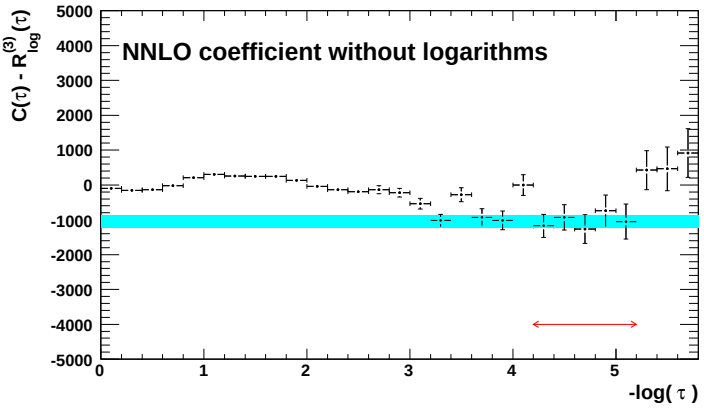

Figure 4.7: Fit of the $\mathcal{O}(\alpha_s^3)$ coefficient C_3. The blue band shows the statistical error of C_3 and the red arrow indicates the fitting interval.

each color contribution is fitted separately over an interval where the distribution is stable and the different results are combined to find the numerical value of C_3. The results of the fits and the different fit intervals are given in Table 4.1. As an alternative

Color	$(-\ln\tau)_{\min}$	$(-\ln\tau)_{\max}$	Fit result
N^2	4.2	5.2	3541 ± 51
N^0	4.2	5.4	-265 ± 8
$1/N^2$	3.8	5.2	-71 ± 3
Nn_F	4.6	5.6	-5078 ± 145
n_F/N	4.6	5.8	236 ± 7
n_F^2	4.2	5.2	95 ± 120
Sum of all colors			-1543 ± 147
All colors	4.2	5.2	-1051 ± 178

Table 4.1: Intervals and results of the fits for C_3 for the different color contributions.

approach we first sum all the color contributions to the $\mathcal{C}(\tau)$ coefficient, then we subtract Eq. 4.17 and finally fit C_3. The result of the second approach is shown in Figure 4.7. We consider the difference between the two approaches as a systematic error and as final result we obtain

$$C_3 = -1050 \pm 180(\text{stat.}) \pm 500(\text{syst.})\,. \tag{4.140}$$

Considering that there is no statistical correlation between different bin errors, as a different possible estimate of the systematic uncertainty due to the sizeable fluctuation, we varied the fit range observing that it does not alter the result in any significant way outside the quoted systematic error margins. It is worth stressing that the numerical

impact of C_3 on the distributions is negligible, as it will be shown in Section 4.6, such that the large relative error range is tolerable for all practical purposes. With the determination of the $\mathcal{O}(\alpha_s^3)$ constant we now have all the needed ingredients to perform the matching of the NNLL resummed result to the fixed NNLO.

4.5 Matching of resummation to fixed-order calculations

There are different matching schemes proposed in the literature, however mainly two are used: the R-matching scheme and the $\ln(R)$-matching scheme [47, 78]. The new results presented in the previous sections allow us to compare for the first time the predictions of the two schemes at NNLL+NNLO accuracy. In the R-matching scheme the two expressions 4.11 and 4.13 are matched and logarithms appearing twice are subtracted. The explicit expression for the matched integrated cross section $R(\tau, Q)$ depends on both the logarithmic and fixed-order accuracy considered in the matching. At NNLL+NNLO the following formula holds (for the sake of clarity we drop any dependence on the renormalization scale, which will be analyzed separately and write only $\alpha_s L$ as arguments of the g_i functions):

$$\begin{aligned} R(\tau,Q) = &\left(1 + C_1\bar{\alpha}_s + C_2\bar{\alpha}_s^2 + C_3\bar{\alpha}_s^3\right) e^{\left(L\, g_1(\alpha_s L)+g_2(\alpha_s L)+\frac{\alpha_s}{\pi}\beta_0\, g_3(\alpha_s L)+\bar{\alpha}_s^3 L\, G_{31}\right)} \\ &+ \bar{\alpha}_s\left(\mathcal{A}(\tau) - R^{(1)}_{\log}(\tau)\right) + \bar{\alpha}_s^2\left(\mathcal{B}(\tau) - R^{(2)}_{\log}(\tau)\right) + \bar{\alpha}_s^3\left(\mathcal{C}(\tau) - R^{(3)}_{\log}(\tau)\right). \end{aligned} \tag{4.141}$$

The terms in the second line correspond to the remainder functions $d_i(\tau)$ defined above. It is however preferable to write it as difference between the full fixed-order coefficient and its logarithmic part since these are the functions which are known in practice.

The $\ln(R)$-matching scheme [47] is believed to be theoretically the most stable one and for this reason it is generally preferred [78]. In this case the matching procedure is given by

$$\begin{aligned} \ln\left(R(\tau,\alpha_s)\right) =& L\, g_1(\alpha_s L) + g_2(\alpha_s L) + \bar{\alpha}_s g_3(\alpha_s L) \\ &+ \bar{\alpha}_s\left(\mathcal{A}(\tau) - G_{11}L - G_{12}L^2\right) + \\ &+ \bar{\alpha}_s^2\left(\mathcal{B}(\tau) - \frac{1}{2}\mathcal{A}_1^2(\tau) - G_{21}L - G_{22}L^2 - G_{23}L^3\right) \\ &+ \bar{\alpha}_s^3\left(\mathcal{C}(\tau) - \mathcal{A}(\tau)\mathcal{B}(\tau) + \frac{1}{3}\mathcal{A}^3(\tau) - G_{32}L^2 - G_{33}L^3 - G_{34}L^4\right). \end{aligned} \tag{4.142}$$

It is worth noting that the dependence on the $\mathcal{O}(\alpha_s^3)$ coefficients C_3 and G_{31} disappears in this scheme. The matching procedures presented above are valid over the

whole phase space. However, unlike to the fixed-order prediction 4.11, in which every coefficient vanishes in the kinematical limit such that $R(\tau_{\max}) = 1$, in the limit $\tau \to \tau_{\max}$ the two predictions 4.141 and 4.142 give a wrong (*i.e.* non-vanishing) result. A fixed-order calculation takes into account only a finite (in fact very few) number of final state particles so the differential cross section $\mathrm{d}\sigma/\mathrm{d}\tau$ obviously has to vanish at the kinematical limit $\tau = \tau_{\max}$.

For the NNLO fixed-order prediction, the maximum number of final state jets is five. Therefore the cross section should vanish at the kinematical limit for six partons. The limited predictive ability of the two matching schemes in the multijet region can be solved by modifying them slightly. This is done by imposing a kinematical constraint, which assures the right prediction for $\tau \to \tau_{\max}$.

The constraints for the so-called modified $\ln(R)$-matching scheme are [78]

$$\ln\left(R(\tau_{\max}, \alpha_s)\right) \;=\; 0 \qquad , \qquad \frac{1}{\sigma}\,\frac{\mathrm{d}\sigma(\tau)}{\mathrm{d}\tau}\bigg|_{\tau=\tau_{\max}} \;=\; \frac{\mathrm{d}R(\tau)}{\mathrm{d}\tau}\bigg|_{\tau=\tau_{\max}} \;=\; 0. \tag{4.143}$$

In order to fulfil these two constraints, we follow the prescription proposed in [78] and redefine L as follows:

$$L \;\longrightarrow\; L' \;=\; \frac{1}{p}\ln\left(\left(\frac{1}{\tau}\right)^p - \left(\frac{1}{\tau_{\max}}\right)^p + 1\right). \tag{4.144}$$

The power p is called "degree of modification". We choose $p = 1$, as usual in literature. It determines how fast the integrated cross section is damped at the kinematical limit. The value of $\tau_{\max}$ is given by symmetry arguments and at LO and NLO can be computed exactly giving respectively $\tau_{\max,\mathrm{LO}} = 1/3$ and $\tau_{\max,\mathrm{NLO}} = 1 - 1/\sqrt{3}$. At NNLO we can fix it using the result given by `EERAD3` at $\tau_{\max} = 0.4275$.

For the $\ln(R)$-matching scheme, the substitution 4.144 is sufficient to fulfil the constraints 4.143. In the R-matching scheme one further modification is needed

$$G_{i1} \to G_{i1}(\tau) \;=\; G_{i1}\left[1 - \left(\frac{\tau}{\tau_{\max}}\right)^p\right], \quad i = 1, 2, 3\,, \tag{4.145}$$

leading to the following expression for the R-matching at NNLL+NNLO:

$$\begin{aligned}
R\left(\tau\right) = {} & \left(1 + C_1\bar{\alpha}_s + C_2\bar{\alpha}_s^2 + C_3\bar{\alpha}_s^3\right) \\
& \times \exp\left[L'\,g_1(\alpha_s L') + g_2(\alpha_s L') + \frac{\alpha_s}{\pi}\beta_0 g_3(\alpha_s L') + \bar{\alpha}_s^3 L'\,G_{31}(\tau) - \left(\frac{\tau}{\tau_{\max}}\right)^p (G_{11} + G_{21})\right] \\
& + \bar{\alpha}_s\left(\mathcal{A}(\tau) - R^{(1)}_{\log}\left(\tau\right)|_{L\to L', G_{11}\to G_{11}(\tau)}\right) \\
& + \bar{\alpha}_s^2\left(\mathcal{B}(\tau) - R^{(2)}_{\log}\left(\tau\right)|_{L\to L', G_{11}\to G_{11}(\tau), G_{21}\to G_{21}(\tau)}\right) \\
& + \bar{\alpha}_s^3\left(\mathcal{C}(\tau) - R^{(3)}_{\log}\left(\tau\right)|_{L\to L', G_{11}\to G_{11}(\tau), G_{21}\to G_{21}(\tau), G_{31}\to G_{31}(\tau)}\right).
\end{aligned} \tag{4.146}$$

The dependence on the renormalization scale was so far not considered. Every term beyond the leading order acquires an explicit μ-dependence, which for the fixed-order coefficients is given in 4.4. For the resummation functions $g_i\left(\alpha_s L\right)$ the renormalization scale dependence is given by

$$g_2(\alpha_s L) \to \bar{g}_2\left(\alpha_s L, \mu^2\right) = g_2(\alpha_s L) + \frac{\beta_0}{\pi}(\alpha_s L)^2 g_1'(\alpha_s L)\ln(x_\mu^2) \tag{4.147}$$

$$\begin{aligned} g_3(\alpha_s L) \to \bar{g}_3\left(\alpha_s L, \mu^2\right) =& g_3(\alpha_s L) + \left[(\alpha_s L) g_2'(\alpha_s L) + \frac{\beta_1}{\pi\beta_0}(\alpha_s L)^2 g_1'(\alpha_s L)\right]\ln(x_\mu^2) \\ &+ \left[\frac{\beta_0}{\pi}(\alpha_s L)^2 g_1'(\alpha_s L) + \frac{\beta_0}{2\pi}(\alpha_s L)^3 g_1''(\alpha_s L)\right]\ln(x_\mu^2)^2, \end{aligned} \tag{4.148}$$

where $g_i'(\alpha_s L)$ stands for the derivative of $g_i(\alpha_s L)$ with respect to $\alpha_s L$. Correspondingly the coefficients G_{ij} and C_i change as follows:

$$\begin{aligned} G_{21} \to \bar{G}_{21}\left(\mu^2\right) &= G_{21} + 2\beta_0 G_{11}\ln(x_\mu^2) \\ G_{22} \to \bar{G}_{22}\left(\mu^2\right) &= G_{22} + 2\beta_0 G_{12}\ln(x_\mu^2) \\ G_{33} \to \bar{G}_{33}\left(\mu^2\right) &= G_{33} + 2\beta_0 2G_{23}\ln(x_\mu^2) \\ G_{31} \to \bar{G}_{31}\left(\mu^2\right) &= G_{31} + \left(2\beta_0\ln(x_\mu^2)\right)^2 G_{11} + 2\ln(x_\mu^2)\left(2\beta_0 G_{21} + 2\beta_1 G_{11}\right) \\ G_{32} \to \bar{G}_{32}\left(\mu^2\right) &= G_{32} + \left(2\beta_0\ln(x_\mu^2)\right)^2 G_{12} + 2\ln(x_\mu^2)\left(2\beta_0 G_{22} + 2\beta_1 G_{12}\right) \\ C_2 \to \bar{C}_2\left(\mu^2\right) &= C_2 + 2\beta_0 C_1\ln(x_\mu^2) \\ C_3 \to \bar{C}_3\left(\mu^2\right) &= C_3 + 2\left(2\beta_0 C_2 + 2\beta_1 C_1\right)\ln(x_\mu^2) + \left(2\beta_0\ln(x_\mu^2)\right)^2 C_1. \end{aligned} \tag{4.149}$$

One further source of arbitrariness is the choice of the logarithm to be resummed. In fact, it is not clear whether powers of $\alpha_s\ln(1/\tau)$ or powers of $\alpha_s\ln(2/\tau)$ have to be resummed. The origin of this arbitrariness has to do with how much of the non-logarithmic part of the fixed-order prediction is exponentiated together with the logarithms. We can express this arbitrariness by introducing a new constant x_L, which rescales the logarithm to be resummed [78]:

$$L \to \hat{L} = \frac{1}{p}\ln\left[\left(\frac{1}{x_L\tau}\right)^p - \left(\frac{1}{x_L\tau_{\max}}\right)^p + 1\right]. \tag{4.150}$$

This rescaling modifies once more the resummed formulae and their expansion coefficients. By requiring $\hat{R}(\tau) \stackrel{!}{=} R(\tau)$, where $\hat{R}(\tau)$ denotes the rescaled integrated cross section according to 4.150, we find the following replacements:

$$\hat{C}_1(\tau) = C_1 + G_{11}\ln(x_L) + G_{12}\ln(x_L)^2, \tag{4.151}$$

$$\hat{C}_2(\tau) = C_2 + (G_{21} + C_1 G_{11})\ln(x_L) + \left(G_{22} + \frac{1}{2}G_{11}^2 + C_1 G_{12}\right)\ln(x_L)^2$$

$$+ (G_{23} + G_{12}G_{11}) \ln(x_L)^3 + \frac{1}{2} G_{12}^2 \ln(x_L)^4 \,, \tag{4.152}$$

$$\begin{aligned}
\hat{C}_3(\tau) \;=\; & C_3 + (G_{31} + C_1 G_{21} + C_2 G_{11}) \ln(x_L) \\
& + \left(G_{32} + C_1 G_{22} + \frac{1}{2} C_1 G_{11}^2 + C_2 G_{12} + G_{11} G_{21} \right) \ln(x_L)^2 \\
& + \left(G_{33} + G_{11} G_{22} + G_{12} G_{21} + C_1 G_{11} G_{12} + \frac{1}{6} G_{11}^3 + C_1 G_{23} \right) \ln(x_L)^3 \\
& + \left(G_{34} + G_{12} G_{22} + \frac{1}{2} C_1 G_{12}^2 + G_{11} G_{23} + \frac{1}{2} G_{11}^2 G_{12} \right) \ln(x_L)^4 \\
& + \left(G_{12} G_{23} + \frac{1}{2} G_{12}^2 G_{11} \right) \ln(x_L)^5 \;+\; \frac{1}{6} G_{12}^3 \ln(x_L)^6 \,,
\end{aligned} \tag{4.153}$$

$$\begin{aligned}
G_{12} \to \hat{G}_{12} &= G_{12} \,, \qquad \hat{G}_{23} = G_{23} \,, \qquad \hat{G}_{34} = G_{34} \,, \\
G_{11} \to \hat{G}_{11} &= G_{11} + 2 G_{12} \ln(x_L) \,, \\
G_{22} \to \hat{G}_{22} &= G_{22} + 3 G_{23} \ln(x_L) \,, \\
G_{33} \to \hat{G}_{33} &= G_{33} + 4 G_{34} \ln(x_L) \,, \\
G_{21} \to \hat{G}_{21} &= G_{21} + 2 G_{22} \ln(x_L) + 3 G_{23} \ln(x_L)^2 \,, \\
G_{32} \to \hat{G}_{32} &= G_{32} + 3 G_{33} \ln(x_L) + 6 G_{34} \ln(x_L)^2 \,, \\
G_{31} \to \hat{G}_{31} &= G_{31} + 2 G_{32} \ln(x_L) + 3 G_{33} \ln(x_L)^2 + 4 G_{34} \ln(x_L)^3 \,.
\end{aligned} \tag{4.154}$$

The corresponding changes of the g_i functions are

$$\begin{aligned}
g_1(\alpha_s L) \to\; & \hat{g}_1(\alpha_s \hat{L}) = g_1(\alpha_s \hat{L}) \,, \\
g_2(\alpha_s L) \to\; & \hat{g}_2(\alpha_s \hat{L}) = g_2(\alpha_s \hat{L}) + \Big(g_1(\alpha_s \hat{L}) + (\alpha_s \hat{L}) g_1'(\alpha_s \hat{L}) \Big) \ln(x_L) \,, \\
g_3(\alpha_s L) \to\; & \hat{g}_3(\alpha_s \hat{L}) = g_3(\alpha_s \hat{L}) + \frac{\pi}{\beta_0} g_2'(\alpha_s \hat{L}) \ln(x_L) \\
& \qquad + \frac{\pi}{\beta_0} \left(g_1'(\alpha_s \hat{L}) + \frac{1}{2} (\alpha_s \hat{L}) g_1''(\alpha_s \hat{L}) \right) \ln(x_L)^2 \,.
\end{aligned} \tag{4.155}$$

The transformations due to a variation of x_μ and x_L are completely general and hold for all possible event-shape observables which can be described with this matching formalism. Furthermore the order in which they are carried out is not important since they commute.

4.6 Results

Having set up the matching formalism in a way to access the theoretical uncertainties, we can apply it to the case of thrust derived in Section 4.4 using the fixed order result from `EERAD3` [81, 82].

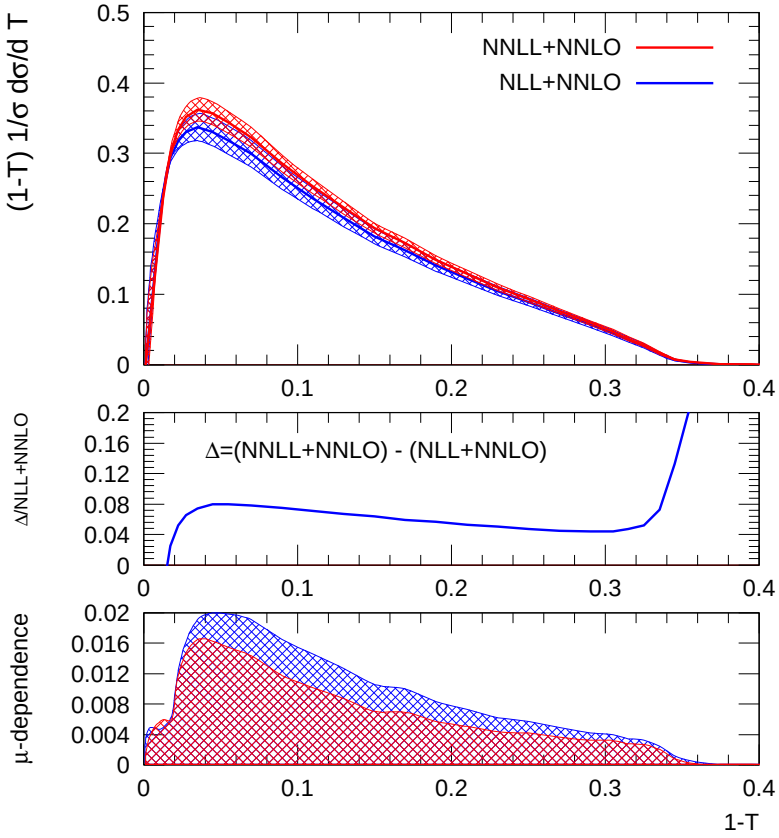

Figure 4.8: Comparison of the weighted cross section in the $\ln(R)$-matching using NNLL+NNLO and NLL+NNLO. The plot on the top shows the two distributions, with the uncertainty band due to scale dependence. The curve in the middle shows the difference between NNLL+NNLO and NLL+NNLO normalized to the NLL+NNLO curve. The impact of the resummation at NNLL is an increase in the distribution of order 5-8%. The lowest plot shows the absolute scale dependence of the two curves.

In Figure 4.8 we compare the weighted cross section of the new matched NNLL+NNLO results with the old NLL+NNLO derived in [91]. The modification due to the resummation is sizable, leading to a 8% increase of the distribution around the peak region. The effect of the additional resummed subleading logarithms becomes progressively less important towards the multijet region, where the increase is nevertheless of about 5%. It is interesting to note that the matching of NNLO with NNLL resummation shifts the pure NNLO result also in the multijet region (Figure 4.9). This was not the case for NLL+NNLO, for which the impact of resummation in the region of large τ was negligible. This is another sign of the importance of the NNLL contribution.

The renormalization scale dependence, which was observed to increase from pure NNLO to NLL+NNLO [91, 94] because of a mismatch in the cancellation of renormalization scale logarithms, is obtained by varying $0.5 < x_\mu < 2$. It decreases at

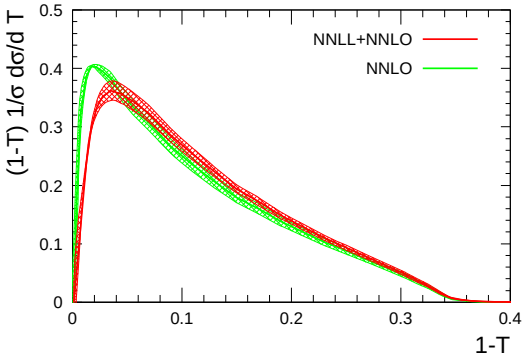

Figure 4.9: Comparison of the weighted cross section at NNLO with the matched NNLL+NNLO predictions. The contribution of NNLL resummation is sizable over the full thrust range.

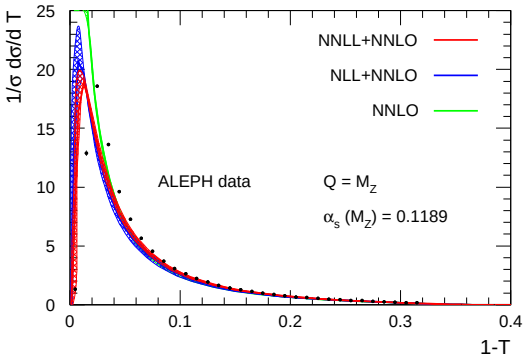

Figure 4.10: Comparison of the parton level fixed-order prediction at NNLO to NLL+NNLO and NNLL+NNLO distributions. Experimental data are taken from the ALEPH collaboration [62].

NNLL+NNLO by 20% in the peak region compared to NLL+NNLO. The magnitude of the scale uncertainty varies between 4% in the 3-jet region and 5% around the peak.

In Figure 4.10 we compare the unweighted parton-level cross section at NNLO with the matched NLL+NNLO and NNLL+NNLO cross sections and with experimental hadron-level data from the ALEPH experiment [62]. We note that there is a visible shift of the theoretical prediction towards the experimental data, which are best described by the newly computed NNLL+NNLO distribution. Around the peak region, where non-perturbative hadronisation corrections are large, the parton level prediction fails to describe the data. Hadronisation effects can account for this discrepancy. We will address this issue in a future publication.

The computation of the two-loop constant C_2 presented in Section 4.3 and the fit of the $\mathcal{O}(\alpha_s^3)$ constant C_3 of Section 4.4.2 allow us to perform for the first time the matching in the R-scheme using NNLL accuracy and fixed NNLO results. On the left plot in Figure 4.11 we compare the R-matching and the $\ln(R)$-matching scheme predictions at NNLL+NNLO. The difference between the two matching prescriptions is very small and lies well below the scale uncertainty. This implies a very good stability of the theoretical predictions under variation of the matching scheme. Because of the big uncertainty in the value of the constant C_3, we vary it within its error to investigate the phenomenological impact on the cross section. The results are shown in the right plot of Figure 4.11. The upper plot shows the different distributions obtained by setting $C_3 = -500, -1000, -1500$ respectively. The three curves are almost indistinguishable and the tiny fluctuations in the distributions are due to the fluctuations of the NNLO result. In the lower plot we take the distribution with $C_3 = -1000$ as reference and plot the difference between the reference cross section and those obtained with $C_3 = -500$

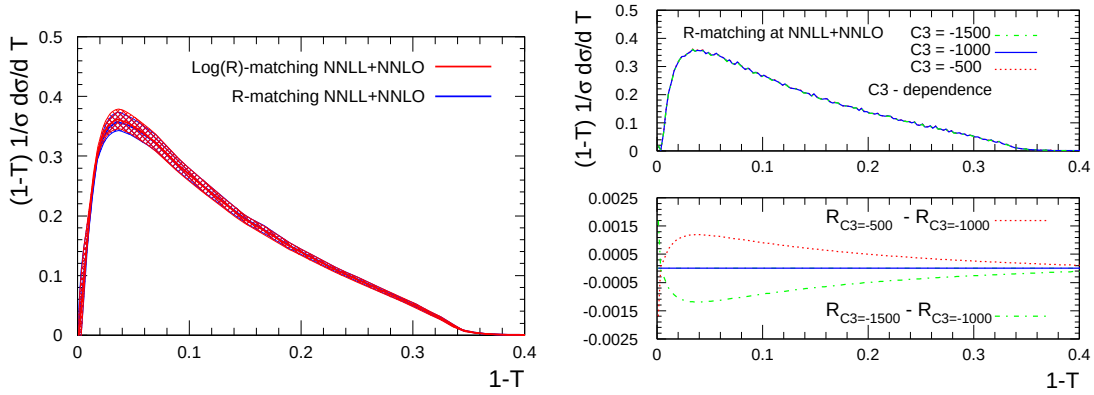

Figure 4.11: The left plot shows the comparison of the R-matching scheme and the $\ln(R)$-matching scheme results. The width of the curve shows the uncertainty related to the scale variation. The two matching schemes agree very well over the full thrust range. The right plot shows the impact of the variation of the $\mathcal{O}(\alpha_s^3)$ constant C_3 on the distribution in the R-matching scheme. The difference is at the per mille level.

and $C_3 = -1500$ respectively. The difference is less than 1.5‰ and it is therefore completely negligible compared the other theoretical uncertainties.

As discussed in the previous section, another source of theoretical uncertainty is the choice of the logarithms to be resummed. We can estimate this uncertainty by varying the parameter x_L. In Ref. [78] several prescriptions are given on how to set the correct variation range for x_L for different observables. For the sake of simplicity and since we are not performing a fit of the strong coupling constant, we choose to vary x_L within the canonical interval $0.5 < x_L < 2$, similarly to what is chosen to quantify the renormalization scale uncertainty. This choice is also close to the nominal range of variation proposed in [78]. The impact of this variation is shown in Figure 4.12. The left plots show a comparison of the x_L-dependence between NLL+NNLO and NNLL+NNLO predictions. The lower plot allows to quantify the reduction of the uncertainty due to a variation x_L. Apart from the far infrared region, it is observed to decrease by 50% in the peak region. The scale-dependence reduction is smaller towards the multijet region, where the contribution of the logarithmic part becomes less important. The resummation uncertainty at NNLL+NNLO varies between 2% and 3%. In the right plots the same comparison is made at NNLL+NNLO using the R-matching and $\ln(R)$-matching schemes. We observe a similar x_L-dependence in both schemes.

A comparison with experimental data has to include hadronisation effects, which are most pronounced in the two-jet region. In the past, these were often obtained using leading-logarithmic parton shower Monte Carlo programs, which turn out to be clearly insufficient [94] in view of the precision now attained by the perturbative description.

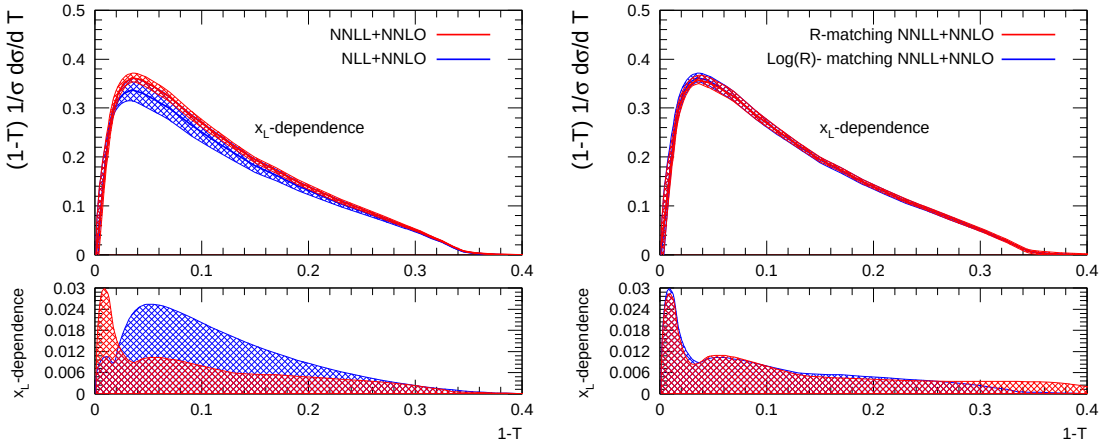

Figure 4.12: Dependence on the resummed logarithms, determined by varying the parameter x_L. The left plot shows the change in the x_L dependence between NLL+NNLO and NNLL+NNLO. The upper plot shows the distributions with the corresponding uncertainty band, in the lower plot we compare only the uncertainties. In the right plots the x_L dependence using the two different matching schemes is shown.

Systematic approaches to hadronisation within the dispersive model [90, 146] or by using the shape function formalism [101] are offering a more reliable description.

5

An application: fit of α_s from thrust in electron-positron annihilation

In this chapter we make use of the theoretical predictions obtained in Section 4 to perform a fit of the strong coupling constant using experimental data over a broad range of energies of the order of a few hundred GeV. At such energies the perturbative prediction does not provide an accurate description of data since power-suppressed corrections ($\sim 1/Q^p$) to the factorisation theorem (*cf.* Section 2.3.1 can be numerically sizeable. In case of e^+e^- annihilation, such corrections are mainly due to non-perturbative effects related to the hadronisation process where the final state (*massless*) partons are converted into (*massive*) hadrons of different species. Moreover, there exist additional perturbative contributions which scale in the same fashion with the centre-of-mass energy. Such terms are not accounted for in the factorisation theorem and they are related to the infrared behaviour of the theory (*renormalons*). The inclusion of such terms recasts the convergence of the otherwise asymptotic perturbative expansion. In the present chapter we will refer to both type of corrections as *power corrections*. This kind of corrections are described using phenomenological models based on different theoretical principles, and so far a detailed and satisfactory field-theoretical description of power corrections is still missing.

The literature contains several fits of the strong coupling constant obtained by using different observables and experimental data sets. Values obtained using data from different processes are often incompatible with each other, and for this reason further studies on the subject are required. Regarding event-shape observables, fits based on the NNLO perturbative predition [80, 83] can be found in [88, 90, 143]. The same fixed-order predictions were matched to resummed calculations to fit α_s in [91–95, 99, 101, 102]. Further fits based on the analysis of jet-rates were performed in [89, 144, 145].

5. AN APPLICATION: FIT OF α_S FROM THRUST IN ELECTRON-POSITRON ANNIHILATION

In what follows we perform a fit if α_s based on theoretical NNLL predictions matched to NNLO for the thrust distribution, reporting the results of [79]. To describe hadronisation effects, we extend the dispersive model [146, 147] to match NNLL+NNLO accuracy and perform a subtraction of the leading renormalon at NNLO. Bottom-quark mass effects are considered to NLO. The theoretical parton level results are reviewed below for completeness. In Section 5.1 we describe the inclusion of bottom-quark mass corrections, whereas the non-perturbative corrections and the extension of the dispersive model to match the perturbative NNLL+NNLO is described in Section 5.2. Section 5.3 is dedicated to the determination of α_s, the fit procedure and the results.

We recall the form of the NNLL-resummed cross section (Eq. 4.106)

$$R_T(\tau) \;=\; \frac{1}{2\pi i}\int_C \frac{dN}{N} e^{\tau N}\tilde{\sigma}_N(Q^2,\alpha_s) + \mathcal{O}(\tau), \tag{5.1}$$

where ($N_0 = e^{-\gamma_E}$)

$$\tilde{\sigma}_N(Q^2,\alpha_s) \;=\; H(1,\alpha_s(Q))\tilde{J}^2\left(1,\alpha_s(\sqrt{\frac{N_0}{N}}Q)\right)\tilde{S}\left(1,\alpha_s(\frac{N_0 Q}{N})\right)e^{-R\left(\frac{N_0}{N}\right)}. \tag{5.2}$$

The radiator $R(N_0/N)$ encodes the probability to emit a dressed gluon (*i.e.* with radiative corrections) with momentum

$$k = up + v\bar{p} + k_\perp, \tag{5.3}$$

where p and $\bar{p}$ are the momenta of the back-to-back quark and antiquark, respectively. Its expression reads

$$R\left(\frac{N_0}{N}\right) = 2\int_{\frac{N_0}{N}}^1 \frac{du}{u}\int_{u^2Q^2}^{uQ^2}\frac{dk_\perp^2}{k_\perp^2}\mathcal{A}_\Gamma(\alpha_s(k_\perp^2)) + 2\int_{\frac{N_0}{N}}^1\frac{du}{u}\mathcal{B}_\Gamma(\alpha_s(uQ^2))\,. \tag{5.4}$$

In Section 4 it was shown that the function $\mathcal{A}_\Gamma(\alpha_s)$ has a soft origin, while $\mathcal{B}_\Gamma(\alpha_s)$ accounts for the hard collinear contributions. They both admit a perturbative expansion in α_s

$$\mathcal{A}_\Gamma(\alpha_s) = \sum_i \frac{\alpha_s^i}{\pi^i}A^{(i)}, \qquad \mathcal{B}_\Gamma(\alpha_s) = \sum_i \frac{\alpha_s^i}{\pi^i}B^{(i)}, \tag{5.5}$$

and their expressions are reported in Appendix A.1. From Eq. 5.4 we see that the integral over u in the exponent is regularised by the lower bound $\frac{N_0}{N}$. Such a bound acts as an infrared regulator which prevents the strong coupling constant from being evaluated at non-perturbative scales ($\leq \Lambda_{QCD}$). This can be seen from Eq. 5.1 where the contour should be set away from all the singularities (in particular from the Landau

pole). Nevertheless, for resummation purposes we can set the contour to the left of the Landau singularity since it would contribute with a non-logarithmic effect suppressed by some negative power of the centre-of-mass energy scale. Such contributions, together with hadronisation corrections, are numerically sizeable at low energies and they are relevant to fit the strong coupling.
Several phenomenological hadronisation models can be found in the literature: analytical [147–150], empirical [151–153] and statistical [154]. Each of them is based on different theoretical assumptions. In our analysis we restrict ourselves to the analytical dispersive model developed in [146, 147].

5.1 Finite bottom-quark mass corrections

An additional effect to be considered concerns the assumption of vanishing quark masses we made in computing the cross section. Such an assumption is not fully justified for low energy data samples (*e.g.* LEP1, PETRA energies) for which finite bottom quark mass effects are relevant at the percent level [155, 156]. We include bottom mass corrections directly at the level of the matched distribution by subtracting the fraction of massless b-quark events ($r_b(Q)$) and adding back the corresponding massive contributions. This results in

$$\frac{1}{\sigma}\frac{\mathrm{d}\sigma}{\mathrm{d}\tau}(\tau,Q) = \frac{1}{\sigma}\left((1-r_b(Q))\frac{\mathrm{d}\sigma}{\mathrm{d}\tau}(\tau,Q)|_{\text{massless}} + +r_b(Q)\frac{\mathrm{d}\sigma}{\mathrm{d}\tau}(\tau,Q)|_{\text{massive}}\right). \tag{5.6}$$

Here $\frac{\mathrm{d}\sigma}{\mathrm{d}\tau}(\tau,Q)|_{\text{massless}}$ is the NNLL+NNLO matched distribution and $\frac{\mathrm{d}\sigma}{\mathrm{d}\tau}(\tau,Q)|_{\text{massive}}$ is the NLO massive distribution obtained with the parton level Monte Carlo `Zbb4` [156]. Since the NNLO correction to the massive distribution is currently unknown, we replace it with the corresponding massless result

$$\frac{\mathrm{d}C}{\mathrm{d}\tau}(\tau)|_{\text{massive}} = \frac{\mathrm{d}C}{\mathrm{d}\tau}(\tau)|_{\text{massless}}. \tag{5.7}$$

The b-quark mass corrections are generated for the considered energies. Futhermore, we perform a bin-by-bin interpolation of the energy dependence in order to compute them for any value of Q included in the considered energy range.

5.2 Non-perturbative corrections

In the dispersive model [146, 147] non-perturbative corrections are accounted for by means of an effective coupling $\alpha_{\text{eff}}(k^2)$ which is supposed to be finite in the infrared region down to $k^2 \to 0$. To introduce the non-perturbative correction, we use the parametrisation 5.3 for the momentum of a soft gluon, or an object with gluon quantum numbers (*i.e.* the offspring of a gluon decay). The two *Sudakov* parameters u and v

are related by $v = (k_\perp^2 + m^2)/u$, where m^2 is the invariant mass of the parent gluon. The strong coupling is defined in a physical scheme as the anomalous dimension Γ controlling the evolution of the *inclusive* soft gluon emission probability

$$dw = \frac{2C_F}{\pi}\frac{du}{u}\frac{dk_\perp^2}{k_\perp^2}\Gamma(\alpha_s). \tag{5.8}$$

The expression for the physical coupling then becomes

$$\tilde{\alpha}_s(k_\perp^2) \equiv \Gamma(\alpha_s) = \tilde{\alpha}_s(0) + \int_0^\infty dm^2 \frac{k_\perp^2}{k_\perp^2 + m^2}\frac{d\alpha_{\text{eff}}(m^2)}{dm^2}, \tag{5.9}$$

where the *effective* coupling α_{eff} is defined as the logarithmic derivative of the spectral density for the dispersive relation 5.9. Integrating 5.9 by parts (notice that $\tilde{\alpha}_s(0) = \alpha_{\text{eff}}(0)$) we obtain a dispersive relation for the physical coupling $\tilde{\alpha}_s$

$$\tilde{\alpha}_s(k_\perp^2) = \int_0^\infty dm^2 \frac{k_\perp^2}{(m^2 + k_\perp^2)^2}\alpha_{\text{eff}}(m^2). \tag{5.10}$$

This relation ensures that the strong coupling constant $\tilde{\alpha}_s(k_\perp^2)$ remains finite at very low momenta, where the perturbative picture fails. It can be recast symbolically as the sum of a perturbative and a non-perturbative components

$$\tilde{\alpha}_s(k_\perp^2) = \alpha_s^{\text{PT}}(k_\perp^2) + \alpha_s^{\text{NP}}(k_\perp^2). \tag{5.11}$$

None of the two terms in the r.h.s. of 5.11 is separately well defined in the infrared region, but their sum is finite down to $k_\perp^2 = 0$.

The perturbative component in Eq. 5.11 of the physical coupling is defined as the perturbative contribution to the physical scheme [45] (CMW scheme) used above to define the strong coupling $\tilde{\alpha}_s$. The inclusive-probability picture used in this scheme requires that we integrate *inclusively* over the invariant mass m^2 of the parent gluon. Such an approximation is accurate up to NLL and to this accuracy the relation between the physical and the $\overline{\text{MS}}$ coupling can be extracted from the soft contribution to the Sudakov radiator 5.4 and reads [45]

$$\alpha_s^{\text{PT}} = \alpha_s\left(1 + \frac{\alpha_s}{\pi}\frac{A^{(2)}}{A^{(1)}} + \dots\right). \tag{5.12}$$

At NNLL, the non-inclusiveness of the thrust plays an important role, and it must be taken into account. We need to account for it both at the perturbative as well as at the non-perturbative level. At the perturbative level we can extend Eq. 5.12 by including the NNLL soft contribution in Laplace space (where the thrust factorises) $A^{(3)}$, which correctly contains non-inclusive effects

$$\alpha_s^{\text{PT}} = \alpha_s\left(1 + \frac{\alpha_s}{\pi}\frac{A^{(2)}}{A^{(1)}} + \frac{\alpha_s^2}{\pi^2}\frac{A^{(3)}}{A^{(1)}} + \dots\right). \tag{5.13}$$

It should be noted that the NNLL perturbative coefficient $A^{(3)}$ might be different for different observables. This would lead to a breakdown of the universality of the physical scheme for hadronisation corrections at this order.
According to Eq. 5.11, the effective coupling α_{eff} can be split into a perturbative term $\alpha_{\text{eff}}^{\text{PT}}$ and a non-perturbative contribution $\alpha_{\text{eff}}^{\text{NP}}$ which is supposed to be a rapidly falling function in the ultra-violet region, where the running of the physical coupling 5.10 matches the solution of the renormalisation group equation for the perturbative component α_s^{PT}. The former is responsible for the perturbative strong coupling α_s^{PT} in Eq. 5.11, while the latter gives rise to the non-perturbative component α_s^{NP}. Imposing that for large momenta α_s^{NP} does not produce any power correction leads to the relation [146, 157]

$$\int_0^\infty \frac{dm^2}{m^2} m^{2n} \alpha_{\text{eff}}^{\text{NP}}(m^2) = 0, \qquad n = 1, 2, ... \tag{5.14}$$

By means of Eq. 5.10 we can find the following useful relations between the perturbative and non-perturbative components of α_{eff} and the respective couplings

$$\int_0^\infty \frac{dk_\perp^2}{k_\perp^2} \alpha_s^{\text{PT}}(k_\perp^2) = \int_0^\infty \frac{dm^2}{m^2} \alpha_{\text{eff}}^{\text{PT}}(m^2), \tag{5.15}$$

$$\int_0^{\mu_I} dk_\perp \alpha_s^{\text{NP}}(k_\perp^2) = \frac{\pi}{4} \int_0^\infty \frac{dm^2}{m^2} m\, \alpha_{\text{eff}}^{\text{NP}}(m^2). \tag{5.16}$$

To obtain Eq. 5.16 we integrated over $k_\perp^2$ and expanded the result in a power series of m^2. This is motivated by the fact that $\alpha_{\text{eff}}^{\text{NP}}(m^2)$ is concentrated at small scales. Using Eq. 5.14 it is straightforward to see that only the first term of the series survives yielding Eq. 5.16.
In order to match the non-perturbative and the perturbative couplings we introduce an infrared matching scale $\mu_I \geq \Lambda_{\text{QCD}}$ such that $\alpha_s^{\text{NP}}(k^2)$ is negligible for $k^2 \geq \mu_I^2$, and the coupling is well approximated by the perturbative part α_s^{PT}. Since we are only interested in the leading power correction ($\sim 1/Q$), we limit our analysis to the region where $\tau \gg \mu_I/Q$ and we assume that the effective coupling is small enough to neglect terms of order $\mathcal{O}(\alpha_{\text{eff}}^2)$. It is straightforward to see that all the terms but $R(N_0/N)$ in Eq. 5.2 are evaluated at perturbative scales (*i.e.* the scales at which the strong coupling is evaluated are always larger than the matching scale μ_I). This implies that the only contribution to the leading power correction arises from the radiator $R(N_0/N)$. In Eq. 5.4 the latter is expressed in terms of the perturbative coupling in the $\overline{\text{MS}}$ scheme and we need to redefine it using the full physical coupling 5.10. We first rewrite Eq. 5.4 using the identity [54]

$$e^{-Nu} - 1 = -\Theta\left(u - \frac{N_0}{N}\right) + \Gamma_2(\partial_{\ln N})\partial_{\ln N}^2 \Theta\left(u - \frac{N_0}{N}\right) + \mathcal{O}\left(\frac{N_0}{N}\right), \tag{5.17}$$

where

$$\Gamma_2(\epsilon) = \frac{1}{\epsilon^2}(1 - e^{-\gamma_E \epsilon}\Gamma(1-\epsilon)) = -\frac{\zeta_2}{2} - \frac{\zeta_3}{3}\epsilon + \mathcal{O}(\epsilon^2), \tag{5.18}$$

and the derivative is meant to act on the whole integral whose boundaries are set by the $\Theta(u - N_0/N)$ function. Eq. 5.4 then becomes

$$\begin{aligned} R\left(\frac{N_0}{N}\right) = &-2\int_0^1 \frac{du}{u}(e^{-N\,u} - 1)\int_{u^2Q^2}^{uQ^2} \frac{dk_\perp^2}{k_\perp^2}\mathcal{A}_\Gamma(\alpha_s(k_\perp^2)) \\ &- 2\int_0^1 \frac{du}{u}(e^{-N\,u} - 1)\mathcal{B}_\Gamma(\alpha_s(uQ^2)) \\ &- \zeta_2\Bigg(2\mathcal{A}_\Gamma\left(\alpha_s\left(\frac{N_0^2}{N^2}Q^2\right)\right) - \mathcal{A}_\Gamma\left(\alpha_s\left(\frac{N_0}{N}Q^2\right)\right) \\ &+ \partial_{\ln N}\mathcal{B}_\Gamma(\alpha_s(\frac{N_0}{N}Q^2))\Bigg) + \mathcal{O}\left(\alpha_s^n \ln^{n-2} N\right), \end{aligned} \tag{5.19}$$

where we used the Leibniz's rule to perform the derivatives of the integrals. It is straightforward to check that the term proportional to ζ_2 contributes to NNLL accuracy. However, we see that it is always evaluated at perturbative scales, so it does not contribute to the leading power correction. We now observe that the integral involving the collinear $\mathcal{B}_\Gamma(\alpha_s(uQ^2))$ function in Eq. 5.19 gives rise to a subleading power-suppressed term which scales as $1/Q^2$, so we can neglect it in the non-perturbative analysis. The only contribution to the leading power correction stems from the double integral in Eq. 5.19, involving the soft contribution $\mathcal{A}_\Gamma(\alpha_s(k_\perp^2))$. Making use of Eq. 5.13 we can recast this contribution using the physical coupling $\alpha_s^{\rm PT}$ (to NNLL accuracy) as

$$\begin{aligned} R\left(\frac{N_0}{N}, \alpha_s\right) = &-\frac{2C_F}{\pi}\int_0^1 \frac{du}{u}(e^{-N\,u} - 1)\int \frac{dk_\perp^2}{k_\perp^2}\alpha_s^{\rm PT}(k_\perp^2) \\ &\times \Theta(k_\perp^2 - u^2Q^2)\Theta(uQ^2 - k_\perp^2) + \ldots, \end{aligned} \tag{5.20}$$

where the ellipsis stand for the remaining perturbative terms in the radiator. Eq. 5.20 is nothing but the single soft emission contribution to the cross section, with the coupling being defined in the physical scheme.

To correctly account for non-perturbative corrections, we replace $\alpha_s^{\rm PT}$ in Eq. 5.20 with the full coupling 5.10. Moreover, since the physical definition of the coupling deals with *massive* gluons, the massless phase space in Eq. 5.20 is modified to take into account the gluon mass. This amounts to performing the replacement $k_\perp^2 \to k_\perp^2 + m^2$ in the two Θ-functions in Eq. 5.20, obtaining

$$R\left(\frac{N_0}{N}, \alpha_s\right) = -\frac{2C_F}{\pi}\int_0^1 \frac{du}{u}(e^{-N\,u} - 1)$$

$$\times \int \frac{dk_\perp^2}{k_\perp^2}\left(\tilde{\alpha}_s(0)+\int_0^\infty dm^2 \frac{k_\perp^2}{k_\perp^2+m^2}\frac{d\alpha_{\rm eff}(m^2)}{dm^2}\right)$$
$$\times \Theta(k_\perp^2+m^2-u^2Q^2)\Theta(uQ^2-k_\perp^2-m^2)+\dots \tag{5.21}$$

We integrate by parts over m^2 in Eq. 5.21 getting rid of the boundary term $\tilde{\alpha}_s(0)$, and we integrate over $k_\perp^2$:

$$R\left(\frac{N_0}{N},\alpha_s\right) = -\frac{2C_F}{\pi}\int_0^1 \frac{du}{u}(e^{-N\,u}-1)$$
$$\int_0^\infty \frac{dm^2}{m^2}\alpha_{\rm eff}(m^2)\Theta(m^2-u^2Q^2)\Theta(uQ^2-m^2)+\dots \tag{5.22}$$

We now split the effective coupling into its perturbative ($\alpha_{\rm eff}^{\rm PT}$) and non-perturbative ($\alpha_{\rm eff}^{\rm NP}$) components.

For the perturbative term we use Eq. 5.15 to reproduce the perturbative soft piece of the radiator 5.20. Replacing the perturbative coupling $\alpha_s^{\rm PT}$ with its expression 5.13 we reproduce Eq. 5.19. We then can write the radiator as

$$R\left(\frac{N_0}{N},\alpha_s\right) = R^{\rm PT}\left(\frac{N_0}{N},\alpha_s\right)+R^{\rm NP}\left(\frac{N_0}{N},\alpha_s\right). \tag{5.23}$$

$R^{\rm PT}(\frac{N_0}{N},\alpha_s)$ is the full perturbative radiator 5.19 that we recast as

$$R^{\rm PT}\left(\frac{N_0}{N},\alpha_s\right) = -\ln N h_1(\alpha_s\ln N)-h_2(\alpha_s\ln N)$$
$$-\frac{\alpha_s}{\pi}\beta_0 h_3(\alpha_s\ln N)+\mathcal{O}(\alpha_s^n\ln^{n-2}N), \tag{5.24}$$

where the functions $h_i(\alpha_s\ln N)$ can be straightforwardly obtained from Eqs. 4.118, 4.119 and 4.120 by subtracting the terms proportional to the constants $c_s^{(1)}$ and $c_j^{(1)}$. For the sake of clarity we report them in Appendix A.1.

The second term in the r.h.s. of Eq. 5.23 $R^{\rm NP}(\frac{N_0}{N},\alpha_s)$ is the non-perturbative component, given by

$$R^{\rm NP}\left(\frac{N_0}{N},\alpha_s\right) = -\frac{2C_F}{\pi}\int_0^1 \frac{du}{u}(e^{-N\,u}-1)$$
$$\times\int_0^\infty \frac{dm^2}{m^2}\alpha_{\rm eff}^{\rm NP}(m^2)\Theta(m^2-u^2Q^2)\Theta(uQ^2-m^2). \tag{5.25}$$

The non-perturbative term requires some more attention. We first recall that we are working in the approximation $\mu_I/Q \ll \tau$, which allows one to expand the exponential function as $e^{-N\,u}\simeq 1-Nu+...$, neglecting subleading terms since they give rise to $\mathcal{O}(1/Q^2)$ corrections. It is then straightforward to perform the integral over u, obtaining

$$R^{\rm NP}\left(\frac{N_0}{N},\alpha_s\right) = N\frac{2C_F}{\pi}\int_0^\infty \frac{dm^2}{m^2}\alpha_{\rm eff}^{\rm NP}(m^2)\left(\frac{m}{Q}-\frac{m^2}{Q^2}\right). \tag{5.26}$$

The term proportional to m^2 in the round brackets leads to a vanishing contribution because of Eq. 5.14. Making use of Eq. 5.16 we end up with

$$R^{\rm NP}\left(\frac{N_0}{N},\alpha_s\right)=\frac{N}{Q}\frac{8C_F}{\pi^2}\int_0^{\mu_I}dk_\perp\alpha_s^{\rm NP}(k_\perp^2). \tag{5.27}$$

To evaluate Eq. 5.27 we replace $\alpha_s^{\rm NP}=\tilde{\alpha}_s-\alpha_s^{\rm PT}$. Introducing the mean value of the physical coupling below μ_I

$$\alpha_0(\mu_I)=\frac{1}{\mu_I}\int_0^{\mu_I}dk_\perp\tilde{\alpha}_s(k_\perp^2), \tag{5.28}$$

and expanding perturbatively $\alpha_s^{\rm PT}$ to perform the integral, we obtain

$$R^{\rm NP}\left(\frac{N_0}{N},\alpha_s\right)=N\Delta\tau. \tag{5.29}$$

Using the expression 5.13 for $\alpha_s^{\rm PT}$, the quantity $\Delta\tau$ amounts to

$$\begin{aligned}\Delta\tau=&\frac{\mu_I}{Q}\frac{8C_F}{\pi^2}\left[\alpha_0(\mu_I^2)-\alpha_s(\mu_R^2)-\alpha_s^2(\mu_R^2)\frac{\beta_0}{\pi}\left(2\ln\frac{\mu_R}{\mu_I}+\frac{A^{(2)}}{A^{(1)}\beta_0}+2\right)\right.\\&\left.-\alpha_s^3(\mu_R^2)\frac{\beta_0^2}{\pi^2}\left(4\ln^2\frac{\mu_R}{\mu_I}+4\left(\ln\frac{\mu_R}{\mu_I}+1\right)\left(2+\frac{\beta_1}{2\beta_0^2}+\frac{A^{(2)}}{A^{(1)}\beta_0}\right)+\frac{A^{(3)}}{A^{(1)}\beta_0^2}\right)\right].\end{aligned} \tag{5.30}$$

Note that the NNLO contribution $A^{(3)}$ in Eq. 5.30 is found to be different from what obtained in [90] and [92], where two different assumptions for this new term were made. The final expression for $A^{(3)}$ (*cf.* Section 4) is reported in Appendix A.1 and it consists of the sum of two contributions: the observable-independent three-loop cusp anomalous dimension computed in [139] and an observable-dependent term proportional to the two-loop soft anomalous dimension obtained from the $\mathcal{O}(\alpha_s^2)$ soft contribution to the thrust cross section [99, 100, 158, 159]. The latter turns out to give the leading numerical contribution to $A^{(3)}$.

Using Eq. 5.30 in Eq. 5.1 results in a shift of the cross section by an amount $\Delta\tau$. This shift encodes the leading non-perturbative correction to the thrust cross section.

The result in Eq. 5.30 is not yet complete. So far we have considered the dispersive model in its inclusive form. The non-perturbative effect of the thrust's non-inclusiveness can be accounted for using perturbation theory by computing the correction to the form reported in Eq. 5.27. Since the physical coupling is defined as the soft emission probability, one can compute the corrections due to incomplete cancellations between real and virtual contributions as well as to scenarios in which the progeny of the massive

gluon goes into opposite hemispheres. These corrections were computed up to $\mathcal{O}(\alpha_s^2)$ in [160] where it was shown that they amount to a multiplicative (*Milan*) factor $\mathcal{M}$

$$\mathcal{M} = 1 + \frac{1}{4\beta_0}(1.575\, C_A - 0.104\, n_F) = 1.490, \quad n_F = 3, \tag{5.31}$$

where we set the number of active flavours to 3 since it is only sensitive to low energy soft radiation. In particular, the n_F factor in 5.31 is due to a soft gluon splitting into a $q\bar{q}$ pair of light quarks. It is difficult to estimate the uncertainty on $\mathcal{M}$. It can not be excluded that higher order $\mathcal{O}(\alpha_s^3)$ corrections to the Milan factor could be as large as 20% [161]. We use this value as uncertainty on $\mathcal{M}$ in our analysis. Since the matched distribution is given in terms of a binned histogram, the shift 5.30 cannot be straightforwardly performed since in general $\Delta\tau$ is not a multiple of the bin width. We then interpolate between different bins with a cubic spline with the "not-a-knot" condition in order to evaluate the distribution at intermediate values of τ. The shift 5.30 is then performed directly on the resulting interpolating spline.

5.2.1 Hadron masses and decay effects

In deriving the dispersive contribution to the leading power correction ($\sim 1/Q$), all offspring particles produced in the *massive* gluon decay were assumed to be massless. Taking their finite masses into account would change the expression of the thrust in the soft region, leading to an additional kind of power corrections [162] whose leading scaling is $\ln^A Q/Q$, where A is a constant. Such corrections are present in experimental data, where massive hadrons contribute to the thrust. Moreover, a similar power-suppressed term arises from the final state momenta reshuffle due to unstable hadron decays into lighter particles. Unlike the dispersive contribution, these power correction cannot be expressed as the product of a universal non-perturbative quantity (*e.g.* α_0) and an observable dependent factor, thus they break universality. A direct consequence is that they have a completely different impact on different event shape observables. An initial detailed assessment of hadron mass effects on event shapes has been presented in [162], where the constant A was evaluated under the hypothesis of local parton-hadron duality, and assuming massless partons in the perturbative calculation, finding $A = 4C_A/\beta_0$. Bottom quark mass effects in the perturbative contribution could potentially modify this value. A more recent systematic analysis of hadron mass effects on power corrections has been performed in Ref. [163]. In Refs. [162, 163] it is shown that the universality of mass-dependent power corrections to two-jet event-shape cross sections can be *rescued* by properly redefining the measurement scheme. This allows one to study systematically the impact of non-perturbative mass corrections for different event-shape observables. In particular, they were found to lead to sizeable corrections for jet-masses and related quantities, while their impact on the thrust is

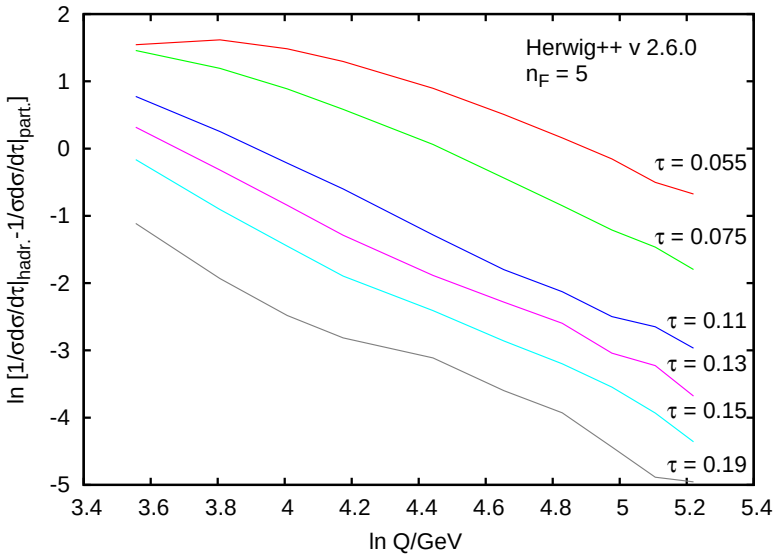

Figure 5.1: Hadronisation corrections for different values of $\tau = 1 - T$ as a function of the centre-of-mass enrgy.

very much limited [162, 163]. Consequently, we do not include hadron-mass effects in our study here.

We qualitatively check the behaviour of hadronisation corrections using the Monte Carlo generator `Herwig++` (Fig. 5.1). We observe that non-perturbative corrections can be well approximated by straight lines with a negative slope, consistently with terms of the form $1/Q^n$. We exclude the possibility of performing a three-parameter fit to determine this additional correction since the result would be extremely degenerate and unstable.

5.3 Determination of α_s and α_0

In order to measure the strong coupling constant α_s and the non-perturbative parameter α_0 we fit the QCD predictions to experimental data reported in Table 5.1, in the centre-of-mass energy range $14\,\text{GeV} \leq Q \leq 206\,\text{GeV}$. For consistency we consider data sets which have been corrected for QED radiation effects. The other data sets would require the inclusion of electroweak corrections [86] into the theoretical description. Therefore we limit our analysis to data measured by the ALEPH [62], the L3 [64] and the TASSO [68] collaborations.

The theory distributions are computed in form of binned histograms. We rebin the theory results in order to match the data binning, which is different for each experiment. We set the upper limit of the fit range to $\tau \leq 1/3$ (the leading order kinematical upper limit) excluding the multi-particle region where the theoretical prediction fails

Exp.	Q (GeV)	Fit range	N. Pts.	Ref.
TASSO	14.0	$0.200 < \tau < 0.32$	3	[68]
TASSO	22.0	$0.120 < \tau < 0.32$	5	[68]
TASSO	35.0	$0.080 < \tau < 0.32$	7	[68]
TASSO	44.0	$0.080 < \tau < 0.32$	7	[68]
ALEPH	91.2	$0.050 < \tau < 0.33$	28	[62]
ALEPH	133.0	$0.040 < \tau < 0.30$	7	[62]
ALEPH	161.0	$0.040 < \tau < 0.30$	7	[62]
ALEPH	172.0	$0.040 < \tau < 0.30$	7	[62]
ALEPH	183.0	$0.040 < \tau < 0.30$	7	[62]
ALEPH	189.0	$0.040 < \tau < 0.30$	7	[62]
ALEPH	200.0	$0.040 < \tau < 0.30$	7	[62]
ALEPH	206.0	$0.040 < \tau < 0.30$	7	[62]
L3	41.4	$0.065 < \tau < 0.33$	8	[64]
L3	55.5	$0.065 < \tau < 0.33$	8	[64]
L3	65.4	$0.065 < \tau < 0.33$	8	[64]
L3	75.7	$0.045 < \tau < 0.33$	9	[64]
L3	82.3	$0.045 < \tau < 0.33$	9	[64]
L3	85.1	$0.045 < \tau < 0.33$	9	[64]
L3	130.0	$0.050 < \tau < 0.30$	10	[64]
L3	136.0	$0.050 < \tau < 0.30$	10	[64]
L3	161.0	$0.050 < \tau < 0.30$	10	[64]
L3	172.0	$0.050 < \tau < 0.30$	10	[64]
L3	183.0	$0.050 < \tau < 0.30$	10	[64]
L3	189.0	$0.050 < \tau < 0.30$	10	[64]
L3	194.0	$0.050 < \tau < 0.30$	10	[64]
L3	200.0	$0.050 < \tau < 0.30$	10	[64]
L3	206.0	$0.050 < \tau < 0.30$	10	[64]

Table 5.1: Data set considered for the simultaneous χ^2 fit of α_s and α_0.

because of the small number of final-state partons considered. The lower limit is set two bins away from $\tau = \mu_I/Q$ excluding the peak region where our treatment of power corrections is not accurate. Fig. 5.2 shows results for different fits of the strong coupling, obtained by shifting the lower bin around the default configuration (labeled by 0). For values of the lower bin shift below -2 the peak region is included in the fit range, which leads to larger values of α_s. This region is excluded since the assumption $\tau \gg \mu_I/Q$ made in computing the leading power correction breaks down and subleading contributions become numerically important. The fit is performed by minimising the χ^2 function defined as

$$\chi^2 = \sum_{i,j} \left(\frac{1}{\sigma}\frac{d\sigma}{d\tau}(\tau_i)\Big|^{\text{exp}} - \frac{1}{\sigma}\frac{d\sigma}{d\tau}(\tau_i)\Big|^{\text{th}} \right) V_{ij}^{-1} \times \left(\frac{1}{\sigma}\frac{d\sigma}{d\tau}(\tau_j)\Big|^{\text{exp}} - \frac{1}{\sigma}\frac{d\sigma}{d\tau}(\tau_j)\Big|^{\text{th}} \right) , \tag{5.32}$$

where V_{ij} are the covariances of the distribution between the bins τ_i and τ_j. The general form of the covariance matrix is $V_{ij} = S_{ij} + E_{ij}$, where $S_{ij} = \sigma^2_{\text{stat},i}\delta_{ij}$ is the diagonal matrix of the (uncorrelated) statistical errors, while E_{ij} contains the experimental systematic convariances. The diagonal entries of $E_{ii} = \sigma^2_{\text{syst},i}$ are given by the systematic uncertainty on the i-th bin, while we need to make a plausible assumption on the form of the off-diagonal elements. We consider the minimal-overlap model, which defines E_{ij} as

$$E_{ij} = \min\left(\sigma^2_{\text{syst},i}, \sigma^2_{\text{syst},j}\right) . \tag{5.33}$$

The χ^2 minimization is carried out with the `TMinuit` routine distributed with `ROOT` and the whole analysis was implemented in a `C++` code.

To estimate the fit uncertainties, different approaches have been proposed in the literature [78, 92]. We decide to perform a scan of the theoretical parameters involved in the calculation as follows:

- the renormalisation scale fraction x_μ (default value $x_\mu = 1$) is randomly varied between 1/2 and 2,
- the resummation scale fraction x_L (default value $x_L = 1$) is randomly varied between 2/3 and 3/2,
- the Milan factor $\mathcal{M}$ is randomly varied within its theoretical uncertainty (20 %),
- the default value of the modified-logarithm parameter $p = 1$ is replaced by $p = 2$,
- the default b-quark mass ($m_b = 4.5$ GeV) is replaced by $m_b = 4.0$ GeV and $m_b = 5.0$ GeV.

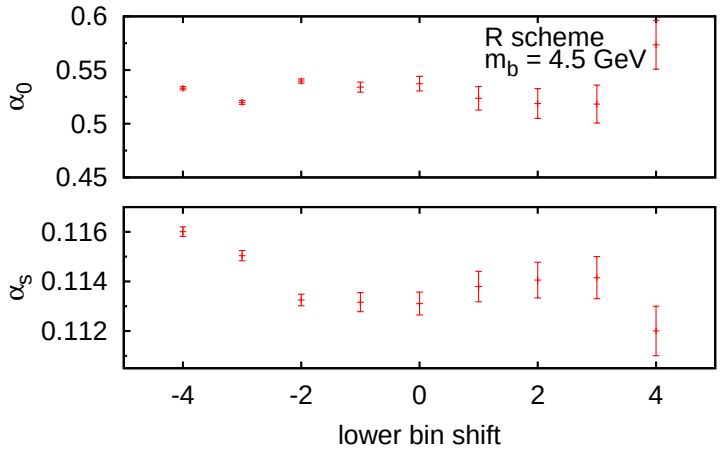

Figure 5.2: Check of the fit stability, when the lower bound of the fit range is shifted. The quoted error bars represent the statistical uncertainty on the single fit. The plots show that the chosen default range is in the middle of a stable plateau. Shifting the lower bound of the fit to include more bins in the far infrared region leads to large deviations from the stable value of α_s.

The random scans for x_μ, x_L and $\mathcal{M}$ are performed with high statistics for each combination of m_b and p (3×10^4 fits in total). The final error on α_s and α_0 is obtained as the envelope of such variations. Moreover, we consider two different matching schemes (R and log-R) and take the difference between the two central values as systematic uncertainty. The quoted central values correspond to the fit results with the default parameter setting.

The scatter plots are shown in Fig. 5.3. Using the R scheme leads to a lower central value and a smaller uncertainty on α_s than in the log-R scheme. We report the results separately for the R and log-R matching schemes:

scheme	$\alpha_s(M_Z)$	$\alpha_0(2\text{ GeV})$	χ^2/d.o.f.
R	$0.1131^{+0.0028}_{-0.0022}$	$0.538^{+0.102}_{-0.047}$	1.54
log-R	$0.1137^{+0.0034}_{-0.0027}$	$0.524^{+0.096}_{-0.044}$	1.60

The difference between the central values is contained into the scan error bands, so it does not affect the final uncertainty. The final uncertainties on α_s and α_0 can be considered to a good approximation as uncorrelated. This feature is visible from the scatter plot in Fig. 5.3. To check the dependence of the α_s fit upon the infrared matching scale μ_I we perform a fit replacing the default value $\mu_I = 2$ GeV by $\mu_I = 3$ GeV. The

corresponding results for the mean effective coupling and for the perturbative strong coupling are:

scheme	$\alpha_s(M_Z)$	$\alpha_0(3\text{ GeV})$	χ^2/d.o.f.
R	$0.1130^{+0.0028}_{-0.0021}$	$0.430^{+0.068}_{-0.032}$	1.56
log-R	$0.1136^{+0.0034}_{-0.0027}$	$0.422^{+0.060}_{-0.029}$	1.62

The α_s value is not affected by the infrared matching scale, whilst α_0 decreases for larger values of μ_I. We also observe that the relative uncertainty on the non-perturbative parameter α_0 is smaller for $\mu_I = 3$ GeV. This can be explained by observing that the uncertainty on α_0 is mostly controlled by the variation of the Milan factor $\mathcal{M}$. Given the multiplicative relationship between the two quantities, a symmetric variation of $\mathcal{M}$ does not correspond to a symmetric uncertainty on α_0. Moreover, it implies that for smaller central values of α_0, the size of the resulting uncertainty decreases. We have assumed that above $\mu_I = 2$ GeV the physical running coupling is well approximated by its perturbative component, this allows us to perform a consistency check on the running of α_0. Since α_0 is a mean value, we consider the integral of the physical $\tilde{\alpha}_s$ from 2 GeV to 3 GeV

$$\int_{2\,\mathrm{GeV}}^{3\,\mathrm{GeV}} dk\, \tilde{\alpha}_s(k^2) = 3\alpha_0(3\,\mathrm{GeV}) - 2\alpha_0(2\,\mathrm{GeV}) = 0.214, \tag{5.34}$$

and we compare it to the perturbative result with four active flavours

$$\int_{2\,\mathrm{GeV}}^{3\,\mathrm{GeV}} dk\, \alpha_s^{\mathrm{PT}}(k^2) = 0.218^{+0.013}_{-0.009}, \tag{5.35}$$

where the values for α_0 and $\alpha_s(M_Z)$ refer to the findings in the R matching scheme. We observe that the two quantities are in very good agreement within the fit uncertainty. This observation indicates that the non-perturbative effects on the running of α_s can be considered negligible above $\mu_I = 2\,\mathrm{GeV}$, thereby justifying this choice for the non-perturbative matching scale.

To estimate the impact on α_s of the finite bottom-quark mass corrections we performed a further scan without including this correction (setting $m_b = 0$), using therefore only pure massless QCD results. With this setting we obtain the following values

scheme	$\alpha_s(M_Z)$	$\alpha_0(2\text{ GeV})$	χ^2/d.o.f.
R	$0.1115^{+0.0022}_{-0.0017}$	$0.539^{+0.122}_{-0.048}$	1.56
log-R	$0.1123^{+0.0031}_{-0.0021}$	$0.522^{+0.113}_{-0.047}$	1.63

The values for α_0 remain almost unchanged while, with respect to the nominal scan, the values of α_s in both matching schemes decrease. This can be explained by observing that the mass corrections tend to lower the thrust distribution in the fit range leading to a higher value for α_s. The errors on α_s are slightly smaller since now we are not accounting for the uncertainty on m_b.

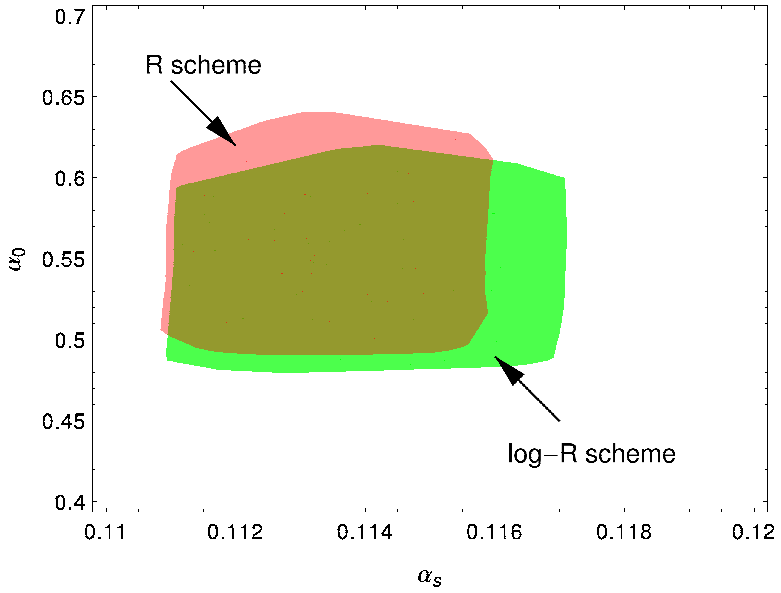

Figure 5.3: Scatter plot for the simultaneous fit of α_s and α_0 using two different matching schemes.

5.4 Comparison with other α_s determinations

We compare our results to other recent determinations of the strong coupling based on thrust. The comparison is shown in Fig. 5.4. The central value is consistent with the findings of [101]. On the other hand our theory uncertainty is larger. The reduced uncertainty of [101] can be explained to some extent by including the subleading approximated N^{3}LL terms, which rely on a Padé approximation for the four loop cusp anomalous dimension. Such terms carry a scale dependence which leads to a reduction of the final error. In our case, we do not include the full approximated N^{3}LL tower, but only consider the necessary term for the R matching scheme, *i.e.* $G_{31}\alpha_s^3 L$, for which an exact analytic expression is available [100]. Moreover, a different non-perturbative model based on a shape function approach was used in [101], and a different technique to perform the renormalon subtraction was implemented. The latter turned out to have an important impact on the fit uncertainty.

In the context of the dispersive model, a global fit was performed in [92] to NLL+NNLO accuracy in the log-R matching scheme, using a larger data set. The quoted values for the perturbative coupling and the non-perturbative parameter were updated in [165] and are $\alpha_s(M_Z) = 0.1164^{+0.0034}_{-0.0032}$ and $\alpha_0(2\text{ GeV}) = 0.62 \pm 0.02$, respectively. In the log-R matching scheme, we note that our resulting fit uncertainty is comparable to what was obtained in [165], despite the higher logarithmic accuracy of the resummation in our

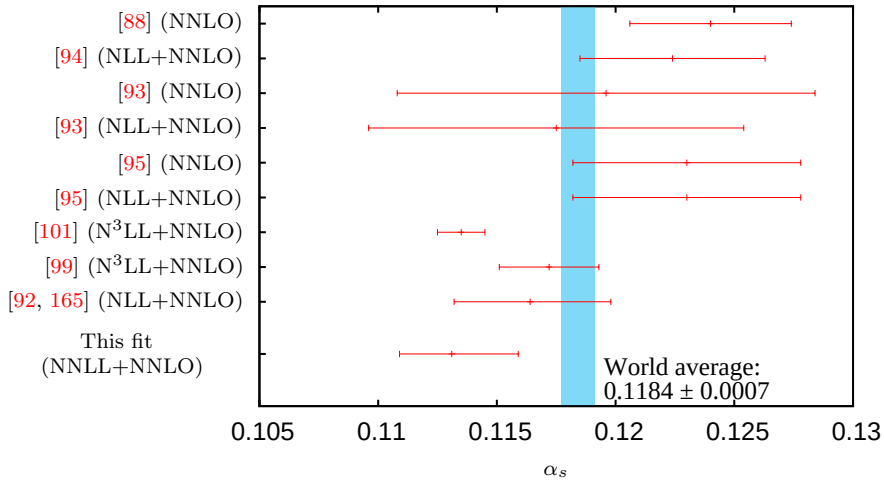

Figure 5.4: Comparison with other determinations of the strong coupling based on data for thrust distribution. The band shows the global world average [164].

analysis. This is because we consider the simultaneous variation of different parameters to assess the theory error, leading to a more conservative estimate. The uncertainty in the α_0 value quoted above does not account for the 20% variation of the Milan factor. Considering such a systematic uncertainty leads to a similar theoretical error on α_0 (*cf.* erratum to [92]). For completeness, we report our fit result obtained with NLL+NNLO perturbative accuracy in the log-R scheme:

scheme	$\alpha_s(M_Z)$	$\alpha_0(2\text{ GeV})$	χ^2/d.o.f.
log-R	$0.1160^{+0.0050}_{-0.0051}$	$0.565^{+0.109}_{-0.085}$	1.44

whose central value is consistent with [92, 165] but the uncertainties are larger as expected.

Compared to previous determinations of the strong coupling, where Monte Carlo hadronisation corrections were used, the present determination leads to smaller values for α_s. This can be mainly explained by observing that Monte Carlo models are currently tuned on experimental data using a showered (to leading logarithmic accuracy) leading order perturbative prediction. The effect of the NNLL resummation on the determination of α_s has been discussed in Section 5.4, and it shows that higher order logarithmic terms have a sizeable impact on its final value. This suggests that Monte Carlo hadronisation should not be used together with higher order resummed predictions since this would misestimate the real hadronisation corrections. This issue has been already discussed in [90, 94]. Our final value for α_s is also smaller than the current world average [164], whose determination involves many results from both lattice computations and τ-decay,

which lead to larger values of α_s. In view of recent developments in extending the resummation beyond NLL accuracy for event-shape variables other than thrust, it would be interesting to repeat a similar analysis for a wider set of event-shape observables to obtain a more robust fit of the strong coupling constant.

5. AN APPLICATION: FIT OF α_S FROM THRUST IN ELECTRON-POSITRON ANNIHILATION

6

Coherent algorithm: resummation for jet veto

In Chapter 4 we performed the Sudakov resummation for the thrust distribution using a factorisation theorem and solving RGE evolution equations. As we mentioned in the introduction (*cf.* Section 3), different possible approaches can be used to resum the Sudakov logarithms. In this chapter we present a second example of resummation carried out using an extension of the `CAESAR` algorithm briefly discussed in Section 3. The results presented in this section are mainly borrowed from two recent publications in this matter [57, 58].

In measuring the Higgs-boson properties at the LHC, one of the channels with a good sensitivity is the production via gluon-fusion process and subsequent decay into a W^+W^- pair, one of which may be off-shell [166, 167]. In this channel, a severe background comes from $t\bar{t}$ production, whose decay products also include a W^+W^- pair. However, this background can be separated from the signal because its W^+W^- pair usually comes together with hard jets, since in each top decay the W is accompanied by an energetic (b) quark.

Relative to classifications based on objects such as leptons (used e.g. to identify the W decays), one of the difficulties of hadronic jets is that they may originate not just from the decay of a heavy particle, but also as quantum chromodynamic radiation. This is the case in our example, where the incoming gluons that fuse to produce the Higgs boson quite often radiate additional partons. Consequently, while vetoing the presence of jets eliminates much of the $t\bar{t}$ background, it also removes some fraction of signal events. To fully interpret the search results, including measuring Higgs couplings, it is crucial to be able to predict the fraction of the signal that survives the jet veto, which depends, for example, on the transverse momentum threshold $p_{\mathrm{t,veto}}$ used to identify vetoed jets.

One way to evaluate jet veto efficiencies is to use a fixed-order perturbative expansion in the strong coupling α_s, notably to next-next-to-leading order (NNLO), as in the Higgs-boson production calculations of Refs. [168–170]. Such calculations, however, become unreliable for $p_{\mathrm{t,veto}} \ll M$, with M the boson mass, since large terms $\alpha_s^n L^{2n}$ appear ($L = \ln(M/p_{\mathrm{t,veto}})$) in the cross section to all orders in the coupling constant. These enhanced classes of terms can, however, be resummed to all orders in the coupling, often involving a functional form $\exp(Lg_1(\alpha_s L) + g_2(\alpha_s L) + \alpha_s g_3(\alpha_s L)/\pi + \ldots)$.

There exist next-to-next-to-leading logarithmic (NNLL) resummations, involving the $g_n(\alpha_s L)$ functions up to and including g_3, for a number of quantities that are more inclusive than a jet veto: e.g., a Higgs or vector-boson transverse momentum [52, 53, 110, 171], the beam thrust [172], and related observables [173, 174]. To obtain estimates for jet vetoes, some of these calculations have been compared to or used to reweight [172, 175–178] parton-shower predictions [179, 180] matched to NLO results [181, 182]. However, with reweighting, neither the NNLO nor NNLL accuracy of the original calculation carries through to the jet veto prediction.
In the following sections we will examine the resummation, matching to fixed-order and phenomenology for the jet veto observable in the case if Higgs- and Z-boson (Drell-Yan process) production at hadron colliders.

6.1 The jet veto efficiency

We consider the production of either a Higgs- or a Z-boson accompanied by N extra QCD partons $p_1, \ldots p_N$,

$$pp \to H + p_1 + \ldots p_N\,, \quad \text{and} \quad pp \to Z + p_1 + \ldots p_N\,. \tag{6.1}$$

A jet veto condition is imposed by clustering the events into jets using a suitable hadron-collider jet-definition (JD) and requiring that the event has no jets with transverse momentum above a certain threshold, typically in the range of $25 - 30$ GeV. To define the jets, the LHC experiments usually use the anti-k_t algorithm [188], which repeatedly merges the pair of particles with smallest distance measure $d_{ij} = \min(p_{ti}^{-2}, p_{tj}^{-2})\Delta R_{ij}^2/R^2$, unless there exists a particle with a $d_{iB} = p_{ti}^{-2}$ value that is smaller, in which case i becomes a jet and is removed from the list of particles. Here $\Delta R_{ij}^2 = (y_i - y_j)^2 + (\phi_i - \phi_j)^2$, where y_i and ϕ_i are respectively the rapidity and azimuth of particle i. The parameter R sets the typical angular reach of the jet definition and is often referred to as the jet radius. After the clustering, one may choose to consider all jets, or alternatively only those within some limited rapidity range, in reflection of actual experimental acceptances.

The cross section with a jet veto is defined as

$$\Sigma(p_{\mathrm{t,veto}}) = \sum_N \int d\Phi_N \frac{d\sigma_N}{d\Phi_N} \Theta(p_{\mathrm{t,veto}} - p_{\mathrm{t,j1}}^{(\mathrm{JD})}(p_1, \ldots, p_N)) \,, \tag{6.2}$$

where $p_{\mathrm{t,j1}}$ is the transverse momentum of the hardest (highest p_t) of the jets found in the event, $d\sigma_N$ denotes the partonic cross-section to produce a Higgs- or a Z- boson accompanied by N extra partons and $d\Phi_N$ is the corresponding phase space.

It is also useful to consider the jet veto efficiency defined as

$$\epsilon(p_{\mathrm{t,veto}}) \equiv \frac{\Sigma(p_{\mathrm{t,veto}})}{\sigma} \,, \tag{6.3}$$

where σ is the total cross-section. The veto efficiency is of interest because it essentially encodes just the information about the Sudakov suppression associated with forbidding radiation of jets. In contrast, the vetoed cross section mixes in also the physics that determines the total cross section. Thus, in the absence of a veto, $p_{\mathrm{t,veto}} = \infty$, the efficiency is exactly 1 and one can reliably discuss small departures from $\epsilon = 1$ as $p_{\mathrm{t,veto}}$ is reduced. In the vetoed cross section, $\Sigma(p_{\mathrm{t,veto}})$, it is harder to disentangle those effects from uncertainties on the total cross section. Later, we will argue that even for ϵ substantially below 1, it makes sense to treat the efficiency and total cross section as independent quantities, and that the uncertainties that govern them are relatively uncorrelated.

Each of $\Sigma(p_{\mathrm{t,veto}})$, σ and $\epsilon(p_{\mathrm{t,veto}})$ has a fixed-order perturbative expansion, which we write as

$$\Sigma(p_{\mathrm{t,veto}}) = \Sigma_0(p_{\mathrm{t,veto}}) + \Sigma_1(p_{\mathrm{t,veto}}) + \Sigma_2(p_{\mathrm{t,veto}}) + \ldots \,, \tag{6.4a}$$

$$\epsilon(p_{\mathrm{t,veto}}) = \epsilon_0(p_{\mathrm{t,veto}}) + \epsilon_1(p_{\mathrm{t,veto}}) + \epsilon_2(p_{\mathrm{t,veto}}) + \ldots \,, \tag{6.4b}$$

$$\sigma = \sigma_0 + \sigma_1 + \sigma_2 + \ldots \,, \tag{6.4c}$$

where the index i signifies that the contribution is proportional to α_s^i relative to the Born term. The properties $\Sigma_0(p_{\mathrm{t,veto}}) \equiv \sigma_0$ and $\epsilon_0 = 1$ follow from the fact that no jets are present at Born level. There is little ambiguity in the definition of the fixed order results for the total and jet-vetoed cross-sections, with the only freedom being, as usual, in the choice of renormalisation and factorisation scales. However, given the expressions of Σ and σ at a given perturbative order, there is some additional freedom in the way one computes the jet veto efficiency. It turns out that at N^{n}LO one can define $n+1$ different schemes that differ by subleading terms and in this sense they can be considered as equivalent. The spread between different matching schemes is a new source of systematic uncertainty that will be used later to obtain a reliable estimate of

the theory uncertainty. Up to N^{3}LO, we can introduce the following schemes

$$\epsilon^{(a)}(p_{\mathrm{t,veto}}) = 1 + \frac{1}{\sigma_{\mathrm{tot}}}\sum_{i=1}^{n}\bar{\Sigma}_i(p_{\mathrm{t,veto}}), \qquad \sigma_{\mathrm{tot}} = \sum_{i=0}^{n}\sigma_i \tag{6.5a}$$

$$\epsilon^{(b)}(p_{\mathrm{t,veto}}) = 1 + \frac{1}{\sigma_{\mathrm{tot}}}\sum_{i=1}^{n}\bar{\Sigma}_i(p_{\mathrm{t,veto}}), \qquad \sigma_{\mathrm{tot}} = \sum_{i=0}^{n-1}\sigma_i \tag{6.5b}$$

$$\epsilon^{(c)}(p_{\mathrm{t,veto}}) = 1 + \frac{1}{\sigma_{\mathrm{tot}}}\sum_{i=1}^{n}\bar{\Sigma}_i(p_{\mathrm{t,veto}}) - \frac{\sigma_{n-1}}{\sigma_{\mathrm{tot}}^2}\bar{\Sigma}_1(p_{\mathrm{t,veto}}), \qquad \sigma_{\mathrm{tot}} = \sum_{i=0}^{n-2}\sigma_i \tag{6.5c}$$

$$\epsilon^{(d)}(p_{\mathrm{t,veto}}) = 1 + \frac{1}{\sigma_{\mathrm{tot}}}\sum_{i=1}^{n}\bar{\Sigma}_i(p_{\mathrm{t,veto}}) - \frac{\sigma_{n-2}}{\sigma_{\mathrm{tot}}^2}(\bar{\Sigma}_1(p_{\mathrm{t,veto}}) + \bar{\Sigma}_2(p_{\mathrm{t,veto}})) + \frac{\sigma_1\sigma_{n-2} - \sigma_0\sigma_{n-1}}{\sigma_{\mathrm{tot}}^3}\bar{\Sigma}_1(p_{\mathrm{t,veto}}), \qquad \sigma_{\mathrm{tot}} = \sum_{i=0}^{n-3}\sigma_i \tag{6.5d}$$

The scheme (c) makes sense at NNLO and beyond, while the scheme (d) can be defined from N^{3}LO on. In all cases

$$\Sigma_i(p_{\mathrm{t,veto}}) = \sigma_i + \bar{\Sigma}_i(p_{\mathrm{t,veto}}) \tag{6.6}$$

being the $\mathcal{O}(\alpha_s^i)-$th correction relative to the Born cross section where

$$\bar{\Sigma}_i(p_{\mathrm{t,veto}}) = -\int_{p_{\mathrm{t,veto}}}^{\infty} dp_{\mathrm{t}}\frac{d\Sigma_i(p_{\mathrm{t}})}{dp_{\mathrm{t}}}, \tag{6.7}$$

can be determined from MCFM, while σ_i is the i^{th} order contribution to the total cross section (cf. [199–204]). The above three prescriptions differ by terms $\mathcal{O}(\alpha_s^3)$, which are beyond the control of current fixed-order calculations.

6.2 Resummation of large Sudakov logarithms

We derive all the ingredients needed to achieve the full NNLL accuracy for the jet veto cross section and efficiency.

6.2.1 Sudakov radiator

As already mentioned in Chapter 3, the Sudakov radiator is given by virtual corrections and unresolved real emissions. It must encode all virtual contributions at scales larger

than $p_{\mathrm{t,veto}}$, at which the first emission takes place. To correctly account for running coupling effects, it can be computed as the single dressed gluon emission probability, that is the probability to emit a single gluon with the coupling evaluated at the $k_\perp$ of the emission and in the physical (CMW) scheme, as shown in Chapter 5. As discussed in Chapter 5, the $\mathcal{O}(\alpha_s^3)$ extension of the CMW scheme could be observable dependent, and some work is currently ongoing to understand whether a universal pattern can be found. Instead of computing it explicitly for the jet veto case, we can obtain it in a different and more clever way by looking at its logarithmic structure. The radiator contains *all* the double (leading) logarithms by definition and it is not accurate at the single-logarithmic level (NLL). Corrections at and beyond NLL are encoded in the multiple emission function that we are going to study in the next section. This implies that, in order to compute the radiator, we can use a simpler (*test*) observable which has the same double logarithmic structure as the jet veto has. Different test observables can be defined, and for some of them the Sudakov radiator is already available in the literature. One possible choice is the transverse momentum of the colour singlet (Higgs or Z) produced in the reaction in association with jets. This observable is simpler and well known and it has been resummed to NNLL accuracy in [52, 110]. To relate the two observables we observe that the boson transverse momentum (p_t^B) is obtained by summing inclusively over all jets' transverse momenta. Non inclusive corrections to this approximation contribute to NNLL and they will be accounted for in the multiple emission function $\mathcal{F}(R')$.
The core of boson transverse-momentum (p_t^B) resummations lies in the fact that soft, collinear emissions at disparate rapidities are effectively emitted independently. Summing over all independent emissions, one obtains the differential boson p_t cross section

$$\frac{d\Sigma^{(B)}}{d^2\vec{p}_t^{\,B}} = \sigma_0 \int \frac{d^2\vec{b}}{4\pi^2} e^{-i\vec{b}.\vec{p}_t^{\,B}} \sum_n \frac{1}{n!} \prod_{i=1}^{n} \int [dk_i] |M(k_i)|^2 (e^{i\vec{b}.\vec{k}_{ti}} - 1), \tag{6.8}$$

where σ_0 is the leading-order total cross section, $[dk_i]|M(k_i)|^2$ is the phase space and matrix element for emitting a soft, collinear gluon of momentum k_i, while the exponential factors and b integral encode in a factorised form the constraint relating the boson p_t and those of individual emissions $\delta^2(\vec{p}_t^{\,B} - \sum_{i=1}^n \vec{k}_{ti})$ [183]. The -1 term in the round brackets arises because, by unitarity, virtual corrections come with a weight opposite to that of real emissions, but do not contribute to the p_t^B sum.

To relate Eq. 6.8 to a cross section with a jet veto, let us first make two simplifying assumptions: that the independent-emission picture is exact and that a jet algorithm clusters each emission into a separate jet. The resummation for the cross section for the highest jet p_t to be below some threshold $p_{\mathrm{t,veto}}$, considering jets at all rapidities,

is then equivalent to requiring all emissions to be below that threshold:

$$\Sigma^{(J)}(p_{\mathrm{t,veto}}) = \sigma_0 \sum_{n=0}^{\infty} \frac{1}{n!} \prod_{i=1}^{n} \int [dk_i] |M(k_i)|^2 (\Theta(p_{\mathrm{t,veto}} - k_{ti}) - 1)$$
$$= \sigma_0 \exp\left[- \int [dk_i] |M(k_i)|^2 \Theta(k_{ti} - p_{\mathrm{t,veto}}) \right] , \tag{6.9}$$

with the same universal matrix element $M(k_i)$ entering Eqs. 6.8 and 6.9. Equation 6.9 is clearly an oversimplification. Corrections to this picture are next-to-next-leading-logarithmic and they will be included later. We see that the two quantities are similar, with the main difference being that Eq. 6.8 involves a Fourier transformation, whereas in Eq. 6.9 we need related integrals but with a theta-function instead of the $(\exp(ib.k_t)-1)$ factor.

To relate the two quantities, we start from the expression for the resummed p_t distribution in Eq. 6.8 and concentrate on the part of the matrix-element in the right-hand integral that is responsible for the leading logarithms. Integrating over azimuthal angles we obtain:

$$\frac{d\Sigma^{(B)}(p_t)}{p_t dp_t} = \sigma_0 \int b db J_0(bp_t) \exp[-\mathcal{R}(b)] , \qquad \mathcal{R}(b) = \int [dk] |M(k)|^2 (1 - J_0(bk_t)) . \tag{6.10}$$

We wish to show that we can safely perform the replacement

$$(1 - J_0(bk_t)) \to \Theta(k_t - b_0/b) , \quad b_0 = 2e^{-\gamma_E} , \tag{6.11}$$

up to and including NNLL accuracy. Integrating over rapidity $\mathcal{R}(b)$ has the form

$$\mathcal{R}(b) = \int_0^M \frac{dk_t}{k_t} F\left(\alpha_s \ln \frac{M}{k_t}\right) (1 - J_0(bk_t)) , \quad F\left(\alpha_s \ln \frac{M}{k_t}\right) = 4C \frac{\alpha_s}{\pi} \ln \frac{M}{k_t} \frac{1}{1 - 2\alpha_s \beta_0 \ln \frac{M}{k_t}} . \tag{6.12}$$

To evaluate separately real and virtual contributions in Eq. 6.12, we introduce a dimensional regulator and write

$$\mathcal{R}(b) = F\left(\alpha_s \partial_\epsilon\right) \int_0^M \frac{dk_t}{k_t} \left(\frac{k_t}{M}\right)^{-\epsilon} (1 - J_0(bk_t)) \Big|_{\epsilon=0} , \tag{6.13}$$

which yields

$$\mathcal{R}(b) = R_{\mathrm{LL}}(b_0/b) + \delta\mathcal{R}(b) , \tag{6.14}$$

where, neglecting terms suppressed by powers of $1/(bM)$,

$$R_{\mathrm{LL}}(b_0/b) = \int_0^M \frac{dk_t}{k_t} F\left(\alpha_s \ln \frac{M}{k_t}\right) \Theta(k_t - b_0/b) , \tag{6.15}$$

and

$$\delta\mathcal{R}(b) = F\left(\alpha_s\partial_\epsilon\right)\frac{(b/b_0)^\epsilon}{\epsilon}\left[-1+e^{-\gamma_E\epsilon}\frac{\Gamma(1-\frac{\epsilon}{2})}{\Gamma(1+\frac{\epsilon}{2})}\right]\Bigg|_{\epsilon=0} \tag{6.16a}$$

$$= F\left(\alpha_s\partial_\epsilon\right)\left(\frac{b}{b_0}\right)^\epsilon\left[\frac{\zeta_3}{12}\epsilon^2+\mathcal{O}(\epsilon^4)\right]\Bigg|_{\epsilon=0}. \tag{6.16b}$$

$\delta\mathcal{R}(b)$ gives at most a term of order $\alpha_s^n\ln^{n-2}(Mb/b_0)$, *i.e.* a N^{3}LL term. A similar argument can be applied to contributions to $\mathcal{R}(b)$ arising from less singular regions, giving also rise to terms that are beyond NNLL. Consequently, this ensures that up to NNLL (but not beyond) the two observables have the same double logarithms and thus the same Sudakov radiator. In the next section we address the computation of corrections to this picture and achieve a full NNLL accuracy.

6.2.2 Multiple emission function $\mathcal{F}(R')$

The multiple emission function $\mathcal{F}(R')$ encodes the single-logarithmic effect due to any number of soft and/or collinear emissions. Its NLL expression was defined in Eq. 3.29. In this section we extend Eq. 3.29 to include the NNLL corrections for the jet veto case. For a generic observable, the NNLL corrections can be more involved and require some additional contributions which are not present in the $p_{\mathrm{t,veto}}$ case. The generalisation of the NNLL algorithm to a generic rIRC safe observable is ongoing and we will briefly discuss it in Chapter 7. At NLL accuracy the jet veto cross section is surprisingly simple. Looking at Eq. 3.29 we see that in the independent emission picture all emissions are widely separated in rapidity and get clustered into separate jets by the jet algorithm. So only the emission with highest transverse momentum actually contributes to the observable. This statement is implemented by the replacement

$$\Theta(v-v(k_1,...,k_n))\to\Theta(p_{\mathrm{t,veto}}-\max(k_{t1},...,k_{tn}))=\prod_{i=1}^{n}\Theta(p_{\mathrm{t,veto}}-k_{ti}). \tag{6.17}$$

As a consequence, the sum in Eq. 3.29 exponentiates and cancels against the factor $\exp\left(-R'\ln 1/\epsilon\right)$ leading to the trivial result $\mathcal{F}(R')=1$ at NLL accuracy [57]. The NLL resummed cross section simply amounts to a Sudakov radiator involving the functions $g_1(\alpha_s L)$ and $g_2(\alpha_s L)$ reported in Appendix B.
To go beyond NLL, we need to relax some of the approximations we made previously and compute the corresponding corrections.

There are two sources of corrections, related to the fact that the emission of two soft-collinear gluons can be separated into two parts: an independent-emission term

and a correlated emission term, the latter being non-zero only when the two gluons are close in rapidity:

$$|M_{gg}(k_1,k_2)|^2 = |M_g(k_1)|^2\,|M_g(k_2)|^2 + |\widetilde{M}_{gg}(k_1,k_2)|^2\,, \tag{6.18}$$

where $|M_g(k)|^2$ is the factorised matrix element for the emission of a single gluon and $|\widetilde{M}_{gg}(k_1,k_2)|^2$ is the correlated-emission part of two-gluon emission matrix element in the limit where both are soft and collinear with respect to the beam direction. There is also a corresponding correlated-emission component for the production of a quark-antiquark pair, $|\widetilde{M}_{q\bar{q}}|^2$. We will use $|\widetilde{M}|^2$ to denote $|\widetilde{M}_{gg}|^2 + 2|\widetilde{M}_{q\bar{q}}|^2$. For double soft (and collinear) emission off a quark line, the non-trivial correlated part of the matrix element was given as early as Refs. [189, 190] and was rederived for more general event structures in Refs. [132, 191]. Apart from colour factors (C_F^2, $C_F C_A$, $C_F T_R n_f$ respectively for independent and correlated gluon and quark-pair emission from a quark line; C_A^2, C_A^2 and $C_A T_R n_f$ for emission from a gluon line), the matrix elements are the same regardless of whether the gluon pair or $q\bar{q}$ pair are emitted from a quark line or a gluon line, as can be seen clearly in the formulae of Ref. [132]. The following results hold for the generalized-k_t jet-algorithm family [184–188], with a jet radius parameter R, with clustering condition given by $J(k_1,k_2) = \Theta(R^2 - (y_1-y_2)^2 - (\phi_1-\phi_2)^2)$.

6.2.2.1 Correlated emission

We start with the correlated-emission component, and in particular from the contribution associated with the presence of any number of independent emissions and one correlated pair:

$$\begin{aligned}\mathcal{F}^{\text{correl}} = \exp\left(-\int_{\epsilon v}^{v}[dk]|M_{g,rc}(k)|^2\right)\times\\ \times\sum_{n=0}\frac{1}{n!}\left(\prod_{i=1}^{n}\int_{\epsilon v}[dk_i]|M_{g,rc}(k_i)|^2\right)\frac{1}{2!}\int[dk_a][dk_b]|\widetilde{M}_{gg,rc}(k_a,k_b)|^2\times\\ \times\left[\Theta(v - V(k_1,\ldots,k_n,k_a,k_b)) - \Theta(v - V(k_1,\ldots,k_n,k_a+k_b))\right]\,.\end{aligned} \tag{6.19}$$

This formula can be understood as the correction that arises when an observable is sensitive to the kinematics of the individual a and b partons rather than just their sum. For the resummation of a sufficiently inclusive quantity, notably the boson p_t distribution, it is explicitly zero. We work in a limit where $\alpha_s \ll 1$, $\ln 1/v \gg 1$ and $\alpha_s \ln 1/v$ is finite. The parameter ϵ, which serves as a regularisation cutoff, is to be taken $\epsilon \ll 1$, but also such that $\alpha_s \ln 1/\epsilon \ll 1$. In this limit the phase space integrals $[dk_i]$ essentially extend up to a rapidity $|y_i| \lesssim \ln 1/v$ and the dependence of the precise upper rapidity limit on a given parton's transverse momentum will turn out to be irrelevant at our accuracy. Additionally, to within a factor $\mathcal{O}(\epsilon)$, all emissions have a

$p_t \sim vM \equiv p_{\mathrm{t,veto}}$ ($v = p_{\mathrm{t,veto}}/M$ and M, we recall, is the boson mass). The matrix elements include a subscript "rc" to indicate that the strong coupling is to be evaluated at a scale of order vM.

A NNLL contribution arises only when all emissions $i = 1 \dots n$ are well separated from each other and from a and b. For the case of the hardest jet's p_t, we then have

$$\Theta(v - V(k_1, \dots, k_n, k_a, k_b)) = \left[\prod_{i=1}^{n} \Theta(v - V(k_i))\right] \Theta(v - V(k_a, k_b)), \tag{6.20a}$$

$$\Theta(v - V(k_1, \dots, k_n, k_a + k_b)) = \left[\prod_{i=1}^{n} \Theta(v - V(k_i))\right] \Theta(v - V(k_a + k_b)) \,. \tag{6.20b}$$

Making use of the fact that

$$\sum_{n=0} \frac{1}{n!} \left(\prod_{i=1}^{n} \int_{\epsilon v} [dk_i] |M_{g,rc}(k_i)|^2 \Theta(v - V(k_i))\right) = \exp\left(\int_{\epsilon v}^{v} [dk] |M_{g,rc}(k)|^2\right) \,, \tag{6.21}$$

we can then rewrite Eq. 6.19 simply as

$$\mathcal{F}^{\mathrm{correl}} = \frac{1}{2!} \int [dk_a][dk_b] |\widetilde{M}_{gg,rc}(k_a, k_b)|^2 \left[\Theta(v - V(k_a, k_b)) - \Theta(v - V(k_a + k_b))\right] \,, \tag{6.22}$$

i.e. it reduces to a pure two-gluon result (with a running-coupling).

It is simplest to first evaluate the leading R-dependence of this formula in the limit of a small jet radius R. When the angle between the two partons a and b is small, $\Delta_{ab}^2 = (y_a - y_b)^2 + (\phi_a - \phi_b)^2 \ll 1$, we can write the phase-space and matrix element as

$$\begin{aligned}[dk_a][dk_b] |\widetilde{M}_{gg,rc}(k_a, k_b)|^2 = \frac{2C\alpha_s(k_{t,ab})}{\pi} \frac{dk_{t,ab}}{k_{t,ab}} \frac{d\phi_{ab}}{2\pi} dy_{ab} \times \\ \times \frac{\alpha_s(k_{t,ab}\Delta_{ab})}{\pi} \frac{d\Delta_{ab}}{\Delta_{ab}} dz \left(P_{gg}(z) + 2n_f P_{qg}(z)\right) \,,\end{aligned} \tag{6.23}$$

where $C = C_F$ or C_A depending on the nature of the beam partons, $k_{ab} \equiv k_a + k_b$ and the P_{gg} and P_{qg} are the real parts of the usual leading order splitting functions:

$$P_{gg}(z) = 2C_A \left(\frac{z}{1-z} + \frac{1-z}{z} + z(1-z)\right) \,, \tag{6.24a}$$

$$P_{qg}(z) = T_R \left(z^2 + (1-z)^2\right) \,. \tag{6.24b}$$

With these variables, for $\Delta_{ab} \ll 1$, the difference of Θ functions in Eq. 6.22 reduces to

$$\begin{aligned}[\Theta(v - V(k_a, k_b)) - \Theta(v - V(k_a + k_b))] = \\ \Theta(\Delta_{ab} - R) \left[\Theta(vM - \max(z, 1-z) k_{t,ab}) - \Theta(vM - k_{t,ab})\right] \,,\end{aligned} \tag{6.25}$$

as long as one restricts one's attention to jet algorithms from the generalised-k_t family. We can now rewrite Eq. 6.22 as

$$\mathcal{F}^{\text{correl}} = \frac{1}{2!}\int\left(\frac{2C\alpha_s(k_{t,ab})}{\pi}\frac{d\phi_{ab}}{2\pi}dy_{ab}\right)\left(\frac{d\Delta_{ab}}{\Delta_{ab}}\Theta(\Delta_{ab}-R)\right)\times \\ \times\frac{\alpha_s(k_{t,ab}\Delta_{ab})}{\pi}dz\,(P_{gg}(z)+2n_fP_{qg}(z))\times \\ \times\left(\frac{dk_{t,ab}}{k_{t,ab}}\left[\Theta(vM-\max(z,1-z)k_{t,ab})-\Theta(vM-k_{t,ab})\right]\right). \quad (6.26)$$

A first point is that $k_{t,ab}$ will be limited to be of order $vM = p_{\text{t,veto}}$. Secondly, while we take $R < \Delta_{ab} \ll 1$, we will still assume that $\alpha_s \ln R$ is negligible. Accordingly we can replace each of the running couplings with $\alpha_s(p_{\text{t,veto}})$. This puts us in a position to carry out the integrations in each of the three lines of Eq. 6.26 independently. The contents of the first round brackets on the first line give $R' = 4C\alpha_s(p_{\text{t,veto}})/\pi \ln 1/v$; the second set of round brackets on that line gives $-\ln R$ (for now we neglect the $\mathcal{O}(1)$ contribution from the ill-defined upper limit in Δ_{ab}); the last line gives $\ln(1/\max(z,1-z))$. We are therefore left with

$$\mathcal{F}^{\text{correl}} = R'\left(\ln\frac{1}{R}+\mathcal{O}(1)\right)\frac{\alpha_s(p_{\text{t,veto}})}{\pi}\int_0^1 dz\frac{1}{2!}\left(P_{gg}(z)+2n_fP_{qg}(z)\right)\ln\frac{1}{\max(z,1-z)}. \quad (6.27)$$

This is straightforward to evaluate and gives [57]

$$\mathcal{F}^{\text{correl}} = R'\frac{\alpha_s(p_{\text{t,veto}})}{\pi}\left(C_A\frac{12\pi^2+132\ln 2-131}{72}+n_fT_R\frac{23-24\ln 2}{36}\right)\left(\ln\frac{1}{R}+\mathcal{O}(1)\right), \quad (6.28a)$$

$$\simeq R'\frac{\alpha_s(p_{\text{t,veto}})}{\pi}(1.09626C_A+0.176791n_fT_R)\left(\ln\frac{1}{R}+\mathcal{O}(1)\right). \quad (6.28b)$$

For a complete evaluation of the $\mathcal{F}^{\text{correl}}$, we start again from Eq. 6.22. We multiply and divide $|\widetilde{M}_{gg,rc}(k_a,k_b)|^2$ by a factor $|M_{g,rc}(k_a)|^2|M_{g,rc}(k_b)|^2$, and make use of

$$[dk]|M_{g,rc}(k)|^2 = \frac{2\alpha_s(k_t)C}{\pi}\frac{dk_t}{k_t}\frac{d\phi}{2\pi}dy\,. \quad (6.29)$$

We then replace the integration measure $dk_{t,b}/k_{t,b}d\phi_b dy_b$ with $d\zeta/\zeta d\Delta\phi d\Delta y$ where $\zeta = k_{t,b}/k_{t,a}$, $\Delta\phi = \phi_b - \phi_a$, $\Delta y = y_b - y_a$. This gives us

$$\mathcal{F}^{\text{correl}} = \frac{1}{2!}\int\left(\frac{2\alpha_sC}{\pi}\frac{d\phi_a}{2\pi}dy_a\right)\frac{2\alpha_sC}{\pi}\int_0^\infty\frac{d\zeta}{\zeta}\int_{-\pi}^{\pi}\frac{d\Delta\phi}{2\pi}\int_{-\infty}^{\infty}d\Delta y\times \\ \times\frac{|\widetilde{M}_{gg}(k_a,k_b)|^2}{|M_g(k_a)|^2|M_g(k_b)|^2}\frac{dk_{t,a}}{k_{t,a}}\left[\Theta(v-V(k_a,k_b))-\Theta(v-V(k_a+k_b))\right]. \quad (6.30)$$

As before, the first factor in round brackets on the first line will integrate to give R'. The difference of Θ functions on the second line will be non-zero only when the two partons are separated by $\Delta\phi^2+\Delta y^2 > R^2$ (this statement holds only for a recombination scheme such as the E-scheme, which directly sums 4-vectors). In the ratio of matrix elements we drop the "rc" subscript, since at our accuracy running coupling effects are entirely accounted for in the scale choice that we will make, $\alpha_s(p_{\mathrm{t,veto}})$, for the explicit factors of α_s (cf. the discussion in the small-R limit). Observing that $k_{t,ab}^2/k_{t,a}^2$ is independent of $k_{t,a}^2$ and equal to $(1+\zeta^2+2\zeta\cos\Delta\phi)$, we can then perform the $k_{t,a}$ integration together with the Θ-function constraints in the square brackets to yield a factor

$$\frac{1}{2}\ln\left[\frac{1+\zeta^2+2\zeta\cos\Delta\phi}{\max\{\zeta^2,1\}}\right]. \tag{6.31}$$

Our result for $\mathcal{F}^{\mathrm{correl}}$ is then

$$\begin{aligned}\mathcal{F}^{\mathrm{correl}} = R'\,\frac{2\alpha_s(p_{\mathrm{t,veto}})C}{\pi}\int_0^\infty\frac{d\zeta}{\zeta}\int_{-\pi}^{\pi}\frac{d\Delta\phi}{2\pi}\int_{-\infty}^{\infty}d\Delta y\;\Theta(\Delta\phi^2+\Delta y^2-R^2)\times\\ \times\,\frac{1}{2!}\frac{|\widetilde{M}_{gg}(k_a,k_b)|^2}{|M_g(k_a)|^2|M_g(k_b)|^2}\frac{1}{2}\ln\left[\frac{1+\zeta^2+2\zeta\cos\Delta\phi}{\max\{\zeta^2,1\}}\right].\end{aligned} \tag{6.32}$$

In both R' and the explicit factor of α_s, the coupling is evaluated at scale $p_{\mathrm{t,veto}}$, as before. The derivative with respect to R of Eq. 6.32 can be straightforwardly evaluated as an expansion in powers of R. Integrating that expansion gives us a result for $\mathcal{F}^{\mathrm{correl}}$ that is missing a constant of integration. This constant can easily be determined through a numerical integration of Eq. 6.32, which also allows for a check of the range of validity of the power series in R. The result that we obtain is [57]

$$\begin{aligned}\mathcal{F}^{\mathrm{correl}} = R'\,\frac{\alpha_s(p_{\mathrm{t,veto}})}{\pi}\Bigg[&\frac{\left(-131+12\pi^2+132\ln 2\right)C_A}{72}\ln\frac{1.74}{R}+\frac{(23-24\ln 2)n_f}{72}\ln\frac{0.84}{R}\\ &+\frac{\left(1429+3600\pi^2+12480\ln 2\right)C_A+(3071-1680\ln 2)n_f}{172800}R^2\\ &+\frac{\left(-9383279-117600\pi^2+1972320\ln 2\right)C_A+2(178080\ln 2-168401)n_f}{406425600}R^4\\ &+\frac{(74801417-33384960\ln 2)C_A+(7001023-5322240\ln 2)n_f}{97542144000}R^6+O\left(R^8\right)\Bigg].\end{aligned} \tag{6.33}$$

This result is compared to the full numerical determination in Fig. 6.1 [57].

6.2.2.2 Independent emission

In the case of the jet observables that we have been discussing, the starting point for the independent-emission correction is

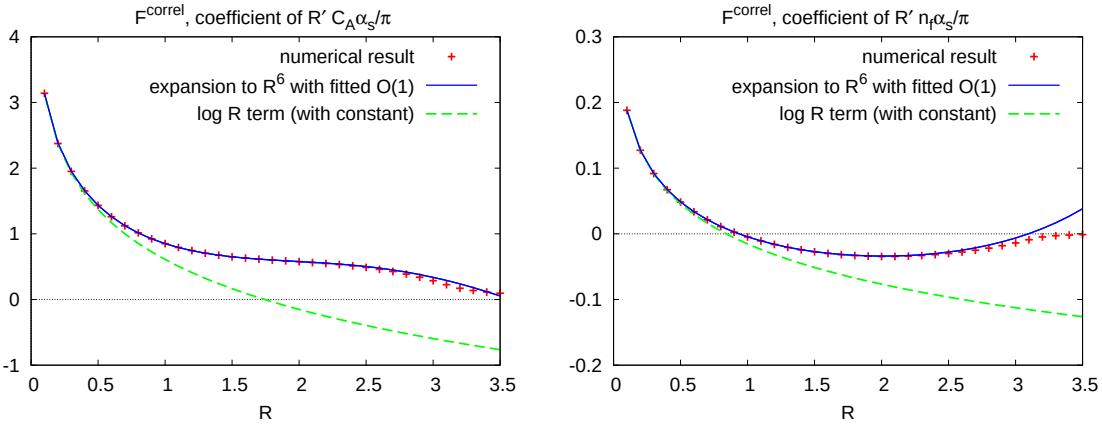

Figure 6.1: Comparison of the numerical and small-R analytical determinations of the C_A and C_F pieces of $\mathcal{F}^{\text{correl}}$.

$$\mathcal{F}^{\text{clust}} = \exp\left(-\int_{\epsilon v}^{v}[dk]|M_{g,rc}(k)|^2\right)\times$$
$$\times\sum_{n=0}\frac{1}{n!}\left(\prod_{i=1}^{n}\int_{\epsilon v}[dk_i]|M_{g,rc}(k_i)|^2\Theta(v-V(k_i))\right)\frac{1}{2!}\int[dk_a][dk_b]|M_{g,rc}(k_a)|^2|M_{g,rc}(k_b)|^2\times$$
$$\times\left[\Theta(v-V(k_a,k_b))-\Theta(v-V(k_a))\Theta(v-V(k_b))\right]. \quad (6.34)$$

The second term in square brackets on the last line corresponds to the approximation made in obtaining $\mathcal{F}(R')=1$ at NLL; the first term corresponds to the actual value of the observable. The evaluation of this formula largely follows the working given above in the correlated emission case, with the main difference that now the only region that contributes is that where the two gluons have $\Delta_{ab}<R$. The result for $R<\pi$ is [57] [1]

$$\mathcal{F}^{\text{clust}} = -R'\frac{\alpha_s(p_{\text{t,veto}})C}{\pi}\int_0^R\Delta_{ab}d\Delta_{ab}\int_0^{2\pi}\frac{d\psi}{2\pi}\int_0^\infty\frac{d\zeta}{\zeta}\ln\left[\frac{1+\zeta^2+2\zeta\cos(\Delta_{ab}\cos\psi)}{\max\{\zeta^2,1\}}\right]$$
$$= R'\frac{\alpha_s(p_{\text{t,veto}})C}{\pi}\left(-\frac{\pi^2R^2}{12}+\frac{R^4}{16}\right). \quad (6.35)$$

For more than two emissions, two situations are possible: (1) three or more emissions are close in rapidity, giving extra powers of α_s without extra log enhancements (N^{3}LL and beyond); (2) any number of extra emissions are far in rapidity, each giving a factor $\alpha_s L$, i.e. also NNLL. The latter contribution is simple because, independently of whether the two nearby emissions clustered, those that are far away must still have $p_{ti}<p_{\text{t,veto}}$. Thus the full "clustering" correction to the independent-emission picture is a multiplicative factor $(1+\mathcal{F}^{\text{clust}})$.

[1] This result is sufficient for phenomenological applications. A more general result valid for any R is reported in Appendix B.

All remaining contributions to a NNLL resummation, such as the 3-loop cusp anomalous dimension or a multiplicative $C_1\alpha_s$ term are either purely virtual, so independent of the precise observable, or involve at most a single real emission, so can be taken from the boson p_t resummations [52, 53, 110, 171] as already stated above. [1]

6.2.3 NNLL resummation and numerical checks

From the previous sections it is straightforward to deduce the form of the NNLL resummed cross section for the jet veto which reads

$$\begin{aligned}\Sigma^{(J)}_{\rm NNLL}(p_{\rm t,veto}) = \sum_{i,j}\int dx_1 dx_2\,|\mathcal{M}_B|^2\delta(x_1x_2s-M^2)\\ \times\left[f_i\big(x_1,e^{-L}\mu_F\big)\,f_j\big(x_2,e^{-L}\mu_F\big)\left(1+\frac{\alpha_s}{2\pi}\mathcal{H}^{(1)}\right)++\frac{\alpha_s}{2\pi}\frac{1}{1-2\alpha_s\beta_0 L}\right.\\ \left.\times\sum_k\int_{x_1}^1\frac{dz}{z}\left(C^{(1)}_{ki}(z)f_i\Big(\frac{x_1}{z},e^{-L}\mu_F\Big)\times f_j\big(x_2,e^{-L}\mu_F\big)+\{(x_1,i)\leftrightarrow(x_2,j)\}\right)\right]\\ \times(1+\mathcal{F}^{\rm clust}+\mathcal{F}^{\rm correl})e^{Lg_1(\alpha_sL)+g_2(\alpha_sL)+\frac{\alpha_s}{\pi}g_3(\alpha_sL)}\,,\end{aligned}\tag{6.36}$$

where the coefficient functions $\mathcal{H}^{(1)}$ and $C^{(1)}_{ki}$, and resummation functions g_1, g_2 and g_3 are as derived for the boson p_t^B resummation [52, 53, 110] and reported for completeness in Appendix B. The results are expressed in terms of $L=\ln(Q/p_{\rm t,veto})$, $\alpha_s\equiv\alpha_s(\mu_R)$; the resummation, renormalisation and factorisation scales Q,μ_R and μ_F are to be chosen of order of M.

A form similar to Eq. 6.36 was derived independently in Ref. [109] for Higgs production, also using ingredients from Ref. [57]. Reference [109] had used a NNLL analysis of the $R\to\infty$ limit to relate jet and boson-p_t resummations. A subtlety of this limit is that one must then account for a N^{3}LL α_s^2R term, which for $R\gtrsim\ln M/p_t$ is promoted to an additional NNLL $\alpha_s^2\ln M/p_t$ contribution (*cf.* Appendix B). One check of Eq. 6.36 is to expand it in powers of α_s, $\Sigma^{(J)}_{\rm NNLL}(p_t)=\alpha_s^2\sum_{n=0}^\infty\Sigma^{(J)}_{{\rm NNLL},n}(p_t)$, and compare $d\Sigma^{(J)}_{{\rm NNLL},2}(p_t)/d\ln p_t$ to the NLO Higgs+1 jet prediction [193–195] from the NLO program MCFM [196], $d\Sigma^{(J)}_2(p_t)/d\ln p_t$. NNLL resummation implies control of terms $\alpha_s^2L^3\ldots\alpha_s^2$ (constant terms) in this quantity and so the difference between MCFM and the second order expansion of the resummation should vanish for large L. This is what we find within reasonable precision. The precision of the test can be increased if one considers the $\mathcal{O}\left(\alpha_s^2\right)$ difference between the jet and boson-p_t resummations, which has fewer logarithms and so is numerically easier to determine in MCFM. It is predicted to be (we write $\mathcal{F}^{\rm clust/correl}=4\alpha_s^2(p_{\rm t,veto})/\pi^2Cf^{\rm clust/correl}(R)$)

[1] For generic processes, subtleties can arise with spin-correlation effects [192]. These are simpler for jet vetoes, which do not correlate distinct collinear regions.

$$\frac{d\Sigma^{(J)}_{\mathrm{NNLL},2}(p_t)}{d\ln p_t} - \frac{d\Sigma^{(B)}_{\mathrm{NNLL},2}(p_t)}{d\ln p_t} = -\frac{4C\alpha_s^2\sigma_0}{\pi^2}\left(f^{\mathrm{clust}}(R) + f^{\mathrm{correl}}(R) + \zeta_3\, C\right) . \quad (6.37)$$

This is compared to MCFM's LO H+2-jet result in the upper panel of Fig. 6.2. There is excellent agreement at small p_t, for each of three R values.

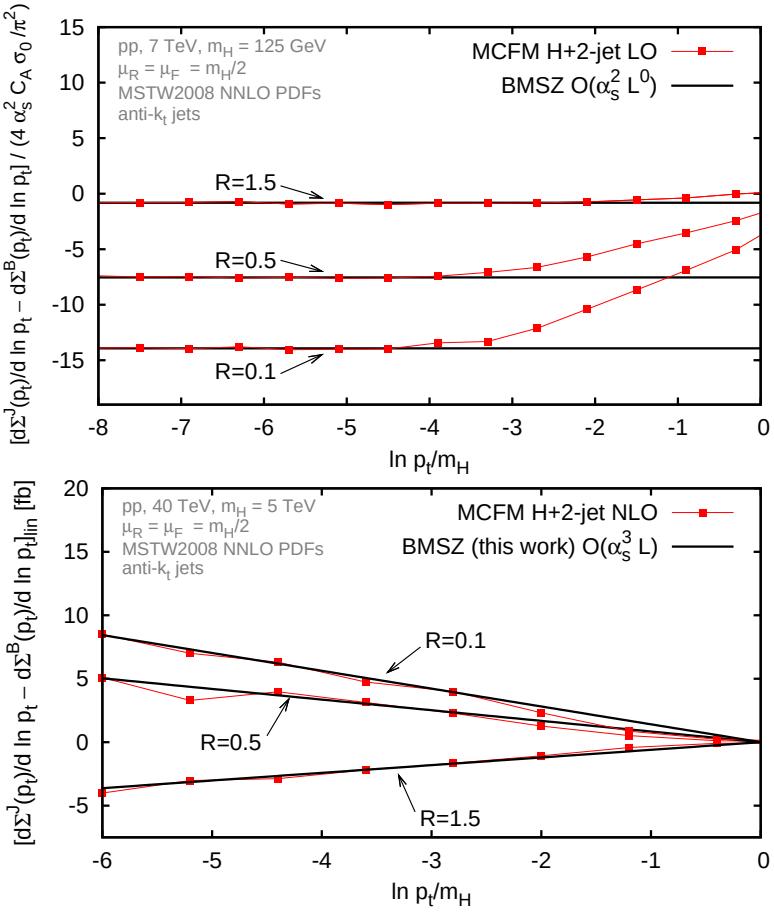

Figure 6.2: Upper panel: second order difference between jet and Higgs-boson $\ln p_t$ differential distributions, showing the coefficient of $4\alpha_s^2 C_A \sigma_0/\pi^2$ as determined with MCFM and predicted in Eq. 6.37, for three R values. Lower panel: differences at $\mathcal{O}\left(\alpha_s^3\sigma_0\right)$ between jet and boson $\ln p_t$ differential distributions, with the expected $\alpha_s^3\sigma_0 L^2$ term subtracted (denoted by a subscript $_{\mathrm{lin}}$), showing the MCFM H+2-jet NLO result compared to our NNLL prediction for the $\alpha_s^3\sigma_0 L$ term.

The above test can be extended one order further by examining the order $\alpha_s^3\sigma_0$ difference between the jet and boson p_t differential distributions. The comparison between our predictions and MCFM H+2-jet NLO results [197, 198] is given in Fig. 6.2 (lower panel), for each of three R values (we use here a different center-of-mass energy and Higgs mass compared to the LO calculation to improve the convergence of MCFM).

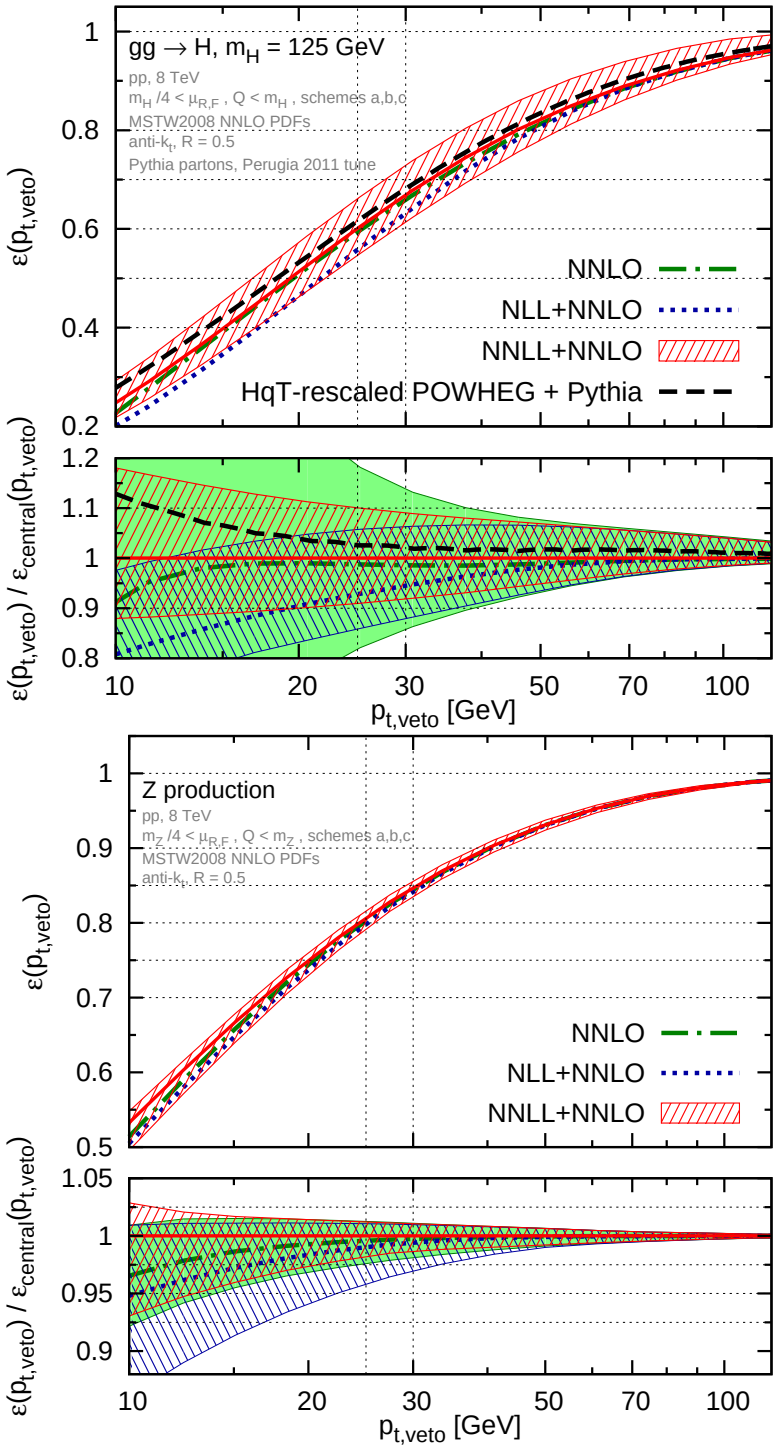

Figure 6.3: Comparison of NNLO (dot-dashed line, solid band), NLL+NNLO (dotted line, downards-right oblique band) and NNLL+NNLO (solid line, upwards-right oblique band) results for jet veto efficiencies for Higgs (left) and Z-boson (right) production at the 8 TeV LHC. The Higgs plot includes the result from a POWHEG (revision 1683) [182, 212] plus Pythia (6.426) [179, 213] simulation (dashed line) in which the Higgs-boson p_t distribution was reweighted to match the NNLL+NNLO prediction from HqT 2.0 [53] as in [57]. The lower panels show results normalized to the central NNLL+NNLO efficiencies.

To facilitate visual interpretation of the results, the expected $\alpha_s^3\sigma_0 L^2$ term has been subtracted. The residual $\alpha_s^3\sigma_0 L$ term is clearly visible in the MCFM results and, within the fluctuations, coincides well with our predictions, providing a good degree of corroborating evidence for the correctness of our results beyond order $\alpha_s^2\sigma_0$.

6.3 Matching to fixed-order

In the context of resummation, as done in Chapter 4, we need to match the resummed efficiency to the fixed-order one in order to obtain a reliable prediction which holds for any value of the jet veto. The jet veto matched efficiency should tend to one and the differential distribution should vanish at the maximum allowed transverse momentum $p_{\mathrm{t,veto}}^{\mathrm{max}}$

$$\epsilon(p_{\mathrm{t,veto}}^{\mathrm{max}}) = 1, \qquad \frac{d\epsilon}{dp_{\mathrm{t,veto}}}(p_{\mathrm{t,veto}}^{\mathrm{max}}) = 0. \tag{6.38}$$

To fulfil such requirements, we modify the resummed logarithms as follows

$$L \to \tilde{L} = \left(1 - \frac{p_{\mathrm{t,veto}}}{p_{\mathrm{t,veto}}^{\mathrm{max}}}\right)\frac{1}{p}\ln\left(\left(\frac{Q}{p_{\mathrm{t,veto}}}\right)^p - \left(\frac{Q}{p_{\mathrm{t,veto}}^{\mathrm{max}}}\right)^p + 1\right), \tag{6.39}$$

where p is some integer power. By default we choose $p = 5$ [57]. The factor $\left(1 - \frac{p_{\mathrm{t,veto}}}{p_{\mathrm{t,veto}}^{\mathrm{max}}}\right)$ is necessary to fulfil Eq. 6.38 but it is largely irrelevant in practice since $p_{\mathrm{t,veto}}^{\mathrm{max}}$ is much larger than the typical values of the jet transverse momentum veto (in practice, we set $p_{\mathrm{t,max}} = \infty$). We introduce three multiplicative matching schemes [221], each of them corresponding to one of the three efficiency definitions 6.5a, 6.5b, 6.5c. To simplify the notation, we split the luminosity factor in the square brackets of Eq. 6.36 into two terms $\mathcal{L}^{(0)}(\tilde{L})$ and $\mathcal{L}^{(1)}(\tilde{L})$, which start at order α_s^0 and α_s^1 respectively,

$$\mathcal{L}^{(0)}(\tilde{L}) = \sum_{i,j}\int dx_1 dx_2 \delta(x_1x_2s - M^2) f_i\left(x_1, e^{-\tilde{L}}\mu_F\right) f_j\left(x_2, e^{-\tilde{L}}\mu_F\right), \tag{6.40}$$

$$\begin{aligned}\mathcal{L}^{(1)}(\tilde{L}) = \frac{\alpha_s}{2\pi}\sum_{i,j}\int dx_1 dx_2 \delta(x_1x_2s - M^2)\Bigg[&f_i\left(x_1, e^{-\tilde{L}}\mu_F\right) f_j\left(x_2, e^{-\tilde{L}}\mu_F\right)\mathcal{H}^{(1)} \\ &+ \frac{1}{1 - 2\alpha_s\beta_0\tilde{L}}\sum_k\left(\int_{x_1}^1 \frac{dz}{z}C_{ki}^{(1)}(z) f_i\left(\frac{x_1}{z}, e^{-\tilde{L}}\mu_F\right) f_j\left(x_2, e^{-\tilde{L}}\mu_F\right)\right. \\ &\left.+ \{(x_1, i) \leftrightarrow (x_2, j)\}\right)\Bigg],\end{aligned} \tag{6.41}$$

where all the constants entering the previous expressions are defined in Appendix B.

6.3.1 Matching to NLO

At NLO, the previous prescription gives two matching schemes. The first of the two reads

$$\Sigma^{(a)}_{\text{matched}}(p_{\text{t,veto}}) = \frac{1}{\sigma_0}\frac{\Sigma_{\text{NNLL}}(p_{\text{t,veto}})}{1+\mathcal{L}^{(1)}(\tilde{L})/\mathcal{L}^{(0)}(\tilde{L})}\left[\sigma_0\left(1+\frac{\mathcal{L}^{(1)}(\tilde{L})}{\mathcal{L}^{(0)}(\tilde{L})}\right)+\Sigma^{(1)}(p_{\text{t,veto}})-\Sigma^{(1)}_{\text{NNLL}}(p_{\text{t,veto}})\right], \tag{6.42}$$

and the corresponding jet veto efficiency is

$$\epsilon^{(a)}_{\text{matched}}(p_{\text{t,veto}}) = \frac{\Sigma^{(a)}_{\text{matched}}(p_{\text{t,veto}})}{\Sigma^{(a)}_{\text{matched}}(p^{\text{max}}_{\text{t,veto}})}\,. \tag{6.43}$$

while the second is

$$\epsilon^{(b)}_{\text{matched}}(p_{\text{t,veto}}) = \frac{1}{\sigma_0^2}\frac{\Sigma_{\text{NNLL}}(p_{\text{t,veto}})}{1+\mathcal{L}^{(1)}(\tilde{L})/\mathcal{L}^{(0)}(\tilde{L})}\left[\sigma_0\left(1+\frac{\mathcal{L}^{(1)}(\tilde{L})}{\mathcal{L}^{(0)}(\tilde{L})}\right)+\bar{\Sigma}^{(1)}(p_{\text{t,veto}})-\Sigma^{(1)}_{\text{NNLL}}(p_{\text{t,veto}})\right]. \tag{6.44}$$

6.3.2 Matching to NNLO

The first of the three NNLO matching schemes reads

$$\begin{aligned}\Sigma^{(a)}_{\text{matched}}(p_{\text{t,veto}}) = \frac{1}{\sigma_0}\frac{\Sigma_{\text{NNLL}}(p_{\text{t,veto}})}{1+\mathcal{L}^{(1)}(\tilde{L})/\mathcal{L}^{(0)}(\tilde{L})}\Bigg[&\sigma_0\left(1+\frac{\mathcal{L}^{(1)}(\tilde{L})}{\mathcal{L}^{(0)}(\tilde{L})}\right)+\Sigma^{(1)}(p_{\text{t,veto}})-\Sigma^{(1)}_{\text{NNLL}}(p_{\text{t,veto}})\\ &+\Sigma^{(2)}(p_{\text{t,veto}})-\Sigma^{(2)}_{\text{NNLL}}(p_{\text{t,veto}})+\left(\frac{\mathcal{L}^{(1)}(0)}{\mathcal{L}^{(0)}(0)}-\frac{\Sigma^{(1)}_{\text{NNLL}}(p_{\text{t,veto}})}{\sigma_0}\right)\left(\Sigma^{(1)}(p_{\text{t,veto}})-\Sigma^{(1)}_{\text{NNLL}}(p_{\text{t,veto}})\right)\Bigg],\end{aligned} \tag{6.45}$$

and the corresponding jet veto efficiency is

$$\epsilon^{(a)}_{\text{matched}}(p_{\text{t,veto}}) = \frac{\Sigma^{(a)}_{\text{matched}}(p_{\text{t,veto}})}{\Sigma^{(a)}_{\text{matched}}(p^{\text{max}}_{\text{t,veto}})}\,. \tag{6.46}$$

The second scheme can be derived from the previous one by replacing $\Sigma^{(2)}(p_{\text{t,veto}})$ with $\bar{\Sigma}^{(2)}(p_{\text{t,veto}})$. For the vetoed cross section we get

$$\begin{aligned}\Sigma^{(b)}_{\text{matched}}(p_{\text{t,veto}}) = \frac{1}{\sigma_0}\frac{\Sigma_{\text{NNLL}}(p_{\text{t,veto}})}{1+\mathcal{L}^{(1)}(\tilde{L})/\mathcal{L}^{(0)}(\tilde{L})}\Bigg[&\sigma_0\left(1+\frac{\mathcal{L}^{(1)}(\tilde{L})}{\mathcal{L}^{(0)}(\tilde{L})}\right)+\Sigma^{(1)}(p_{\text{t,veto}})-\Sigma^{(1)}_{\text{NNLL}}(p_{\text{t,veto}})\\ &+\bar{\Sigma}^{(2)}(p_{\text{t,veto}})-\Sigma^{(2)}_{\text{NNLL}}(p_{\text{t,veto}})+\left(\frac{\mathcal{L}^{(1)}(0)}{\mathcal{L}^{(0)}(0)}-\frac{\Sigma^{(1)}_{\text{NNLL}}(p_{\text{t,veto}})}{\sigma_0}\right)\left(\Sigma^{(1)}(p_{\text{t,veto}})-\Sigma^{(1)}_{\text{NNLL}}(p_{\text{t,veto}})\right)\Bigg],\end{aligned} \tag{6.47}$$

while for its efficiency

$$\epsilon^{(b)}_{\text{matched}}(p_{\text{t,veto}}) = \frac{\Sigma^{(b)}_{\text{matched}}(p_{\text{t,veto}})}{\Sigma^{(b)}_{\text{matched}}(p^{\text{max}}_{\text{t,veto}})}\,. \tag{6.48}$$

Finally, the third matching scheme is directly formulated for the efficiency resulting in

$$\begin{aligned}\epsilon^{(c)}_{\text{matched}}(p_{\text{t,veto}}) = \frac{1}{\sigma_0^2}\frac{\Sigma_{\text{NNLL}}(p_{\text{t,veto}})}{1+\mathcal{L}^{(1)}(\tilde{L})/\mathcal{L}^{(0)}(\tilde{L})}\Bigg[\sigma_0\left(1+\frac{\mathcal{L}^{(1)}(\tilde{L})}{\mathcal{L}^{(0)}(\tilde{L})}\right)+\bar{\Sigma}^{(1)}(p_{\text{t,veto}})-\Sigma^{(1)}_{\text{NNLL}}(p_{\text{t,veto}})\\ +\bar{\Sigma}^{(2)}(p_{\text{t,veto}})-\frac{\sigma_1}{\sigma_0}\bar{\Sigma}^{(1)}(p_{\text{t,veto}})-\Sigma^{(2)}_{\text{NNLL}}(p_{\text{t,veto}})\\ +\left(\frac{\mathcal{L}^{(1)}(0)}{\mathcal{L}^{(0)}(0)}-\frac{\Sigma^{(1)}_{\text{NNLL}}(p_{\text{t,veto}})}{\sigma_0}\right)\left(\bar{\Sigma}^{(1)}(p_{\text{t,veto}})-\Sigma^{(1)}_{\text{NNLL}}(p_{\text{t,veto}})\right)\Bigg].\end{aligned} \tag{6.49}$$

The four matching schemes which can be defined at N^{3}LO can be derived in a straightforward way, but we do not report them here since they are not needed for the present analysis.

6.4 Numerical results and phenomenology

To illustrate the phenomenological implications of our work, we examine the jet veto efficiency $\epsilon(p_t) \equiv \Sigma^{(J)}(p_t)/\sigma_{\text{tot}}$, where σ_{tot} is the total cross section, known up to NNLO [199–204]. We combine ("match") the resummation with fixed-order predictions, available from fully differential NNLO boson-production calculations [169, 170, 205, 206] or NLO boson+jet calculations [193, 207] implemented in MCFM [208]. We use the three matching schemes, denoted a, b, and c, defined in the previous section.

Our central predictions have $\mu_R = \mu_F = Q = M/2$ and use scheme a matching, with MSTW2008NNLO PDFs [209]. We use the anti-k_t [188] jet-algorithm with $R = 0.5$, as implemented in FastJet [210]. For the Higgs case we use the large m_{top} approximation and ignore $b\bar{b}$ fusion and b's in the $gg \to H$ loops (corrections beyond this approximation have a relevant impact [178, 211]). To determine uncertainties we vary μ_R and μ_F by a factor of 2 in either direction, requiring $1/2 \leq \mu_R/\mu_F \leq 2$. Maintaining central $\mu_{R,F}$ values, we also vary Q by a factor of 2 and change to matching schemes b and c. Our final uncertainty band is the envelope of these variations (cf. Ref. [57]). In the fixed-order results, the band is just the envelope of $\mu_{R,F}$ variations.

The results for the jet veto efficiency in Higgs and Z-boson production are shown in Fig. 6.3 for 8 TeV LHC collisions. Compared to pure NNLO results, the central value is slightly higher and for Higgs production, the uncertainties reduced, especially for lower $p_{\text{t,veto}}$ values. Compared to NNLO+NLL results [57], the central values are higher, sometimes close to the edge of the NNLO+NLL bands; since the NNLO+NLL

results used the same approach for estimating the uncertainties, this suggests that the approach is not unduly conservative. In the Higgs case, the NNLO+NNLL uncertainty band is not particularly smaller than the NNLO+NLL one. This should not be a surprise, since Ref. [57] highlighted the existence of possible substantial corrections beyond NNLL and beyond NNLO accuracy. For the Higgs case, we also show a prediction from POWHEG [182, 212] interfaced to Pythia 6.4 [179] at parton level (Perugia 2011 shower tune [213]), reweighted to describe the NNLL+NNLO Higgs-boson p_t distribution from HqT (v2.0) [53], as used by the LHC experiments. Though reweighting fails to provide NNLO or NNLL accuracy for the jet veto, for $p_{\mathrm{t,veto}}$ scales of practical relevance, the result agrees well with our central prediction. It is, however, harder to reliably estimate uncertainties in reweighting approaches than in direct calculations.

Figure 6.4 shows the the jet veto efficiency as a function of $p_{\mathrm{t,veto}}$ for several different jet-radius (R) values. Increasing the jet radius, more radiation is captured and therefore a jet is more likely to pass the $p_{\mathrm{t,veto}}$ threshold and so be vetoed. As a consequence the jet veto efficiency is expected to be lower for larger R values. This is precisely as observed in Fig. 6.4.

Quantitatively, the differences between the $R = 0.4$ and $R = 0.5$ results (the values used respectively by ATLAS and CMS) are small compared to the uncertainties on the predictions. In contrast, for $R = 1$ the differences compared to the smaller-R results are not negligible. One interesting feature is that for the Higgs-boson case, the uncertainties are somewhat smaller for $R = 1$ than for $R = 0.4$ and $R = 0.5$, especially the upper part of the uncertainty band. This can be understood with the help of the observation that the upper edge of the uncertainty band for the small R values is set by the $Q = M_H$ variant of the resummation (recall that our default Q is $M_H/2$). Using $Q = M_H$ increases the size of L. Since the $f(R) = f^{\mathrm{correl}}(R) + f^{\mathrm{clust}}(R)$ function grows for small R and multiplies $\alpha_s^2 L$, a smaller R value magnifies the impact of an increase in Q.

If, experimentally, one were to consider using larger R values for performing jet vetoes in order to reduce the theoretical uncertainties, one concern might be the greater contamination of the jet's p_t from the underlying event and pileup. To some extent this could be mitigated by methods such as subtraction [222], filtering [223] or trimming [224]. Note that with subtraction and filtering (when the latter uses two filtering subjets, or more) our jet veto predictions remain unchanged at NNLO and at NNLL accuracy.

Finally, we provide central results and uncertainties for the jet veto efficiencies and 0-jet cross sections (in pb) with cuts (in GeV) like those used by ATLAS and CMS, and also for a larger R value:

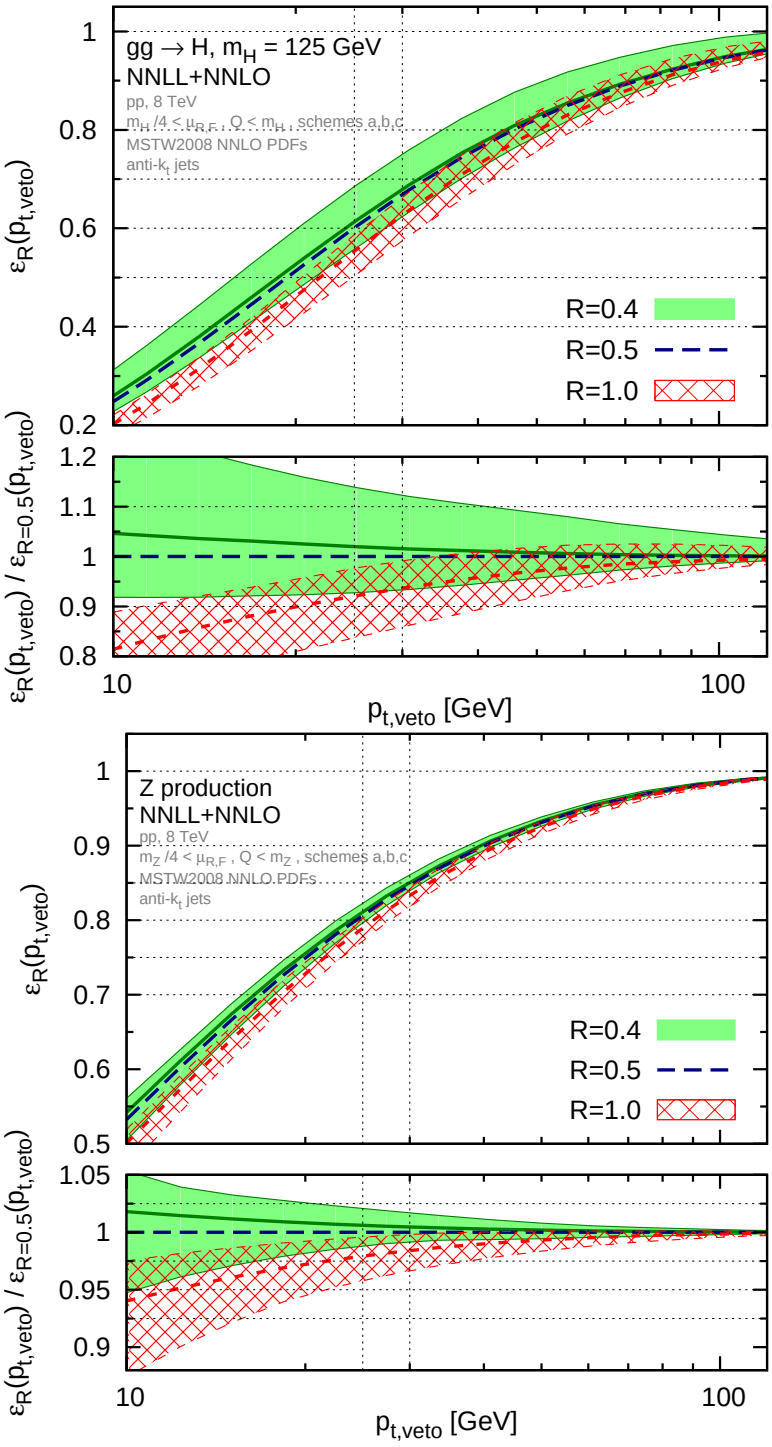

Figure 6.4: Jet veto efficiency at NNLL+NNLO as a function of $p_{\mathrm{t,veto}}$, comparing several jet-radius values; shown for pp collisions at a centre-of-mass energy of 8 TeV, for gluon-fusion Higgs production with $M_H = 125$ GeV (large m_{top} limit) and for Z-boson production. Uncertainty bands are shown only for $R = 0.4$ and $R = 1.0$ in order to enhance the clarity of the figure. The $R = 0.5$ uncertainty band is to be found in Fig. 6.3. The lower panels show the predictions normalised to the central $R = 0.5$ results.

R	$p_{\mathrm{t,veto}}$	$\epsilon^{(7\ \mathrm{TeV})}$	$\sigma_{0\text{-jet}}^{(7\ \mathrm{TeV})}$	$\epsilon^{(8\ \mathrm{TeV})}$	$\sigma_{0\text{-jet}}^{(8\ \mathrm{TeV})}$
0.4	25	$0.63^{+0.07}_{-0.05}$	$9.6^{+1.3}_{-1.1}$	$0.61^{+0.07}_{-0.06}$	$12.0^{+1.6}_{-1.4}$
0.5	30	$0.68^{+0.06}_{-0.05}$	$10.4^{+1.2}_{-1.1}$	$0.67^{+0.06}_{-0.05}$	$13.0^{+1.5}_{-1.5}$
1.0	30	$0.64^{+0.03}_{-0.05}$	$9.8^{+0.8}_{-1.1}$	$0.63^{+0.04}_{-0.05}$	$12.2^{+1.1}_{-1.4}$

Interestingly, the $R = 1$ results have reduced upper uncertainties, due to the smaller value of the NNLL $f(R)$ correction (as shown above a large $f(R)$ introduces significant Q-scale dependence). The above results are without a rapidity cut on the jets; the rapidity cuts used by ATLAS and CMS lead only to small, $< 1\%$, differences [57].

For the 0-jet cross sections above, we used total cross sections at 7 and 8 TeV of $15.3^{+1.1}_{-1.2}$ and $19.5^{+1.4}_{-1.5}$ pb respectively [214, 215] (based on results including Refs. [200–204]) and took their scale uncertainties to be uncorrelated with those of the efficiencies. Symmetrizing uncertainties, we find correlation coefficients between the 0-jet and ≥ 1-jet cross sections of -0.43 (-0.50) for $R = 0.4$ ($R = 0.5$), using the covariance matrix in Appendix B. [1]

[1] The computer programme to perform resummation and matching is publicly available at the URL [216].

7

Conclusions and Outlook

In the present thesis we studied the infrared and collinear structure of Quantum Chromodynamics beyond fixed-order perturbation theory. In Chapters 4, 6 we discussed two different approaches to the resummation of Sudakov logarithms where the enhanced terms are resummed to all orders in the strong coupling constant either via RGE evolution of each kinematical subprocess entering the factorisation theorem or simulating the effect of any number of singular emissions through a particular implementation of the coherent-branching algorithm. In Chapter 5 we performed a fit of the strong coupling at M_Z using experimental data from electron-positron annihilation. In the same chapter we extended the dispersive model for the low energy coupling constant to describe non-perturbative corrections to the thrust distribution, matching the NNLO+NNLL perturbative prediction. Using these tools, we carried out a simultaneous fit of both α_s and the mean effective coupling α_0.

The resummation method presented in Chapter 6 for the resummation of the leading jet transverse momentum in the context of the production of any colour singlet at hadron colliders can be extended to treat a variety of observables in different processes. We are currently working on a generalisation of the algorithm to perform the resummation to NNLL accuracy for any rIRC safe observable. Since the work and some results are highly preliminary, we do not discuss them here. However, it can be useful to list and discuss briefly all the corrections (some of which were previously discussed in [42]) which are needed to achieve a full NNLL accuracy. Theoretical details of the results discussed here and corresponding numerical implementation will be discussed in a forthcoming publication.

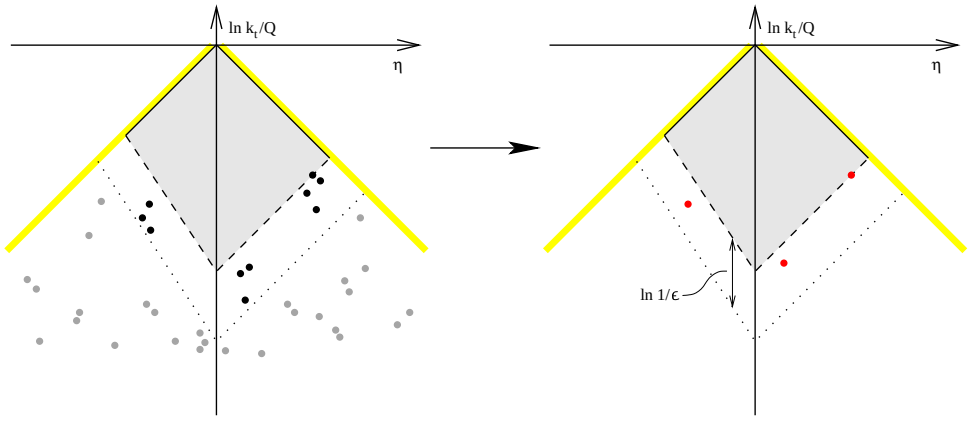

Figure 7.1: Single emission phase space.

7.1 Comments on higher order corrections to the CAESAR algorithm

In Chapter 3 we made use of the properties of coherent emissions jointly with the scaling properties of the observable (rIRC safety) to carry out the resummation to NLL accuracy. In doing so, we assumed that we could neglect emissions whose contribution to the observable is smaller than a quantity ϵv where ϵ is chosen independently of v. This requirement was formulated in the context of the recursive Infrared and Collinear safety condition which simply amounts to require that in the presence of any number of soft and/or collinear emissions of similar hardness the observable scales as it would do in presence of only one of such emissions. To understand the implications of these two properties more in detail, we consider the phase space for a single emission in presence of two hard emitters (*i.e.* e^+e^- collisions, Drell-Yan). We limit ourselves to this case for the only sake of simplicity and because the processes analysed in this thesis are of this type. The results can be extended to configurations with more than two hard legs, to which the same qualitative conclusions apply.
The phase space of a single (singular) emission can be parametrised using the observable's dependence on rapidity η and transverse momentum k_t as shown in Fig. 7.1 [42].

The shadowed region encodes the virtual corrections accounted for in the Sudakov radiator and real emissions are vetoed in this area, which is defined by the condition $\Theta(v(k)-v)$. The two yellow edges parametrise the hard collinear regions (each of them corresponding to one of the two hard legs) and the lower vertex of the rhombus at $\eta = 0$ corresponds to the wide-angle soft region. The spots in the left plot represent possible real emissions. The rIRC safe property ensures that we can introduce a parameter ϵ independent of the observable's value, such that we can safely neglect emissions for which $v(k) < \epsilon v$. This allows us to forget about the grey spots without altering the

observable significantly. Moreover, colour coherence ensures that at NLL accuracy, all real emissions can be considered as uncorrelated and widely separated in rapidity. This means that we can formally replace the black spots in the left plot of Fig. 7.1 with a new set of emissions obtained by replacing clusters of emissions close in rapidity with a single emission obtained by integrating inclusively over the momenta of the cluster partons, while keeping the total cluster momentum fixed. This reproduces the all-order strong running coupling in the physical scheme and the resulting red spot can be expressed as a single emission with the coupling constant evaluated at k_t in the CMW scheme at the desired logarithmic accuracy (*i.e.* the CMW coupling must be truncated at $\mathcal{O}(\alpha_s^2)$ at NLL). This can be done easily by decomposing the m-emission matrix element $|M(k_1,...,k_m)|^2$ as a sum of products of cluster matrix elements $|\widetilde{M}(k_1,...,k_k)|^2$ with up to $m-1$ correlated emissions ($k \leq m-1$) plus a remainder with m correlated emissions $|\widetilde{M}(k_1,...,k_m)|^2$. The first few steps of this iterative definition read

$$|\widetilde{M}(k_1)|^2 = |M(k_1)|^2 \tag{7.1}$$

$$|\widetilde{M}(k_1,k_2)|^2 = |M(k_1,k_2)|^2 - |\widetilde{M}(k_1)|^2|\widetilde{M}(k_2)|^2 \tag{7.2}$$

$$\begin{aligned}|\widetilde{M}(k_1,k_2,k_3)|^2 = {} & |M(k_1,k_2,k_3)|^2 - |\widetilde{M}(k_1)|^2|\widetilde{M}(k_2)|^2|\widetilde{M}(k_3)|^2 \\ & - \Big(|\widetilde{M}(k_1,k_2)|^2|\widetilde{M}(k_3)|^2 + \text{ permutations}\Big)\,.\end{aligned} \tag{7.3}$$

As discussed in Chapter 3, to reproduce the running coupling effects to NLL accuracy it is enough to consider the inclusive contribution to the cluster due to $|\widetilde{M}(k_1,k_2)|^2$, plus an arbitrary number of single emissions $|\widetilde{M}(k_1)|^2$. As a result, we can simulate the all-order effect of QCD radiation by simulating an ensamble of rapidity-separated uncorrelated emissions [1]. The latter effect is encoded in the multiple emission function $\mathcal{F}(R')$.

To go beyond NLL, we need to consider a number of corrections to the approximations we have made so far. In the following we discuss qualitatively such corrections, leaving the technical details for future work.

7.1.1 Radiator and running effects

The first correction to NLL formula 3.28 is at the level of the Sudakov radiator $R(v)$. To obtain the radiator to NNLL accuracy, we need to correctly extend the CMW physical scheme for the running coupling to $\mathcal{O}(\alpha_s^3)$ accounting for the strength of the soft radiation. The result amounts to considering the three-loop cusp anomalous dimension and a process-dependent soft anomalous dimension (*cf.* Chapters 4 and 6). The CMW

[1] In practice, for the Monte Carlo implementation, the emissions need to be actually separated in rapidity only in case of observables defined by means of jet algorithms. For other observables, such as event-shapes, it is enough to generate soft and/or collinear emissions located everywhere in the physical phase space.

scheme fails in describing the hard-collinear region, so we need to account for the correct collinear anomalous dimension which can be obtained by including the full Altarelli-Parisi kernels. Once we include the correct radiator, we can express the resulting cross section (note that it is not yet NNLL accurate) as

$$\Sigma(v) = e^{-R(v)-R'\ln\frac{1}{\epsilon}-\frac{1}{2}R''\ln^2\frac{1}{\epsilon}\dots}\sum_{n=1}^{\infty}\frac{1}{n!}\prod_{i=1}^{n}\int_{\epsilon v}[dk_i]|M(k_i)|^2\Theta(v-v(k_1,...,k_n)). \quad (7.4)$$

We can recast the integrand function in the real emission factor as [1]

$$\int[dk_i]|M(k_i)|^2 = \int\frac{dv_i}{v_i}\int[dk_i]|M(k_i)|^2\delta(v(k_i)-v_i) = \int\frac{dv_i}{v_i}\frac{d\phi}{2\pi}R'(v_i). \quad (7.5)$$

At NLL we can replace the value of the observable corresponding to the i-th emission v_i with the total value v and take $R'(v)$ out of the integral. At NNLL we need to keep one more term in the expansion writing

$$R'(v_i) = R'(v) + R''(v)\ln\frac{v}{v_i} + \dots. \quad (7.6)$$

To neglect subleading logarithmic effects in the multiple emission function, we only need to correct one single emission according to Eq. 7.6. We now expand the exponential factor in Eq. 7.4 neglecting subleading terms

$$e^{-R(v)-R'\ln\frac{1}{\epsilon}-\frac{1}{2}R''\ln^2\frac{1}{\epsilon}\dots} = e^{-R(v)-R'\ln\frac{1}{\epsilon}}\left(1-\frac{1}{2}R''\ln^2\frac{1}{\epsilon}\dots\right). \quad (7.7)$$

It is then straightforward to show that the first term in the r.h.s. of Eq. 7.6 combines with the factor $e^{-R'\ln\frac{1}{\epsilon}}$ to give the NLL multiple emission function 3.29, that can be recast as

$$\mathcal{F} = e^{-R'\ln\frac{1}{\epsilon}}\sum_{n=1}^{\infty}\frac{1}{n!}\prod_{i=1}^{n}\int_{\epsilon v}\frac{dv_i}{v_i}\frac{d\phi}{2\pi}R'(v)\Theta(v-v(k_1,...,k_n)). \quad (7.8)$$

The remaining term proportional to R'' in Eq. 7.6 gives rise to a new contribution whose divergences are cancelled by the corrections stemming from the factor $\frac{1}{2}R''\ln^2\frac{1}{\epsilon}$ in Eq. 7.7. The resulting correction to the multiple emission formula reads

$$\mathcal{F}^{\text{running}} = e^{-R'\ln\frac{1}{\epsilon}} \times\int_{\epsilon v}\frac{dv_k}{v_k}R''(v)\ln\frac{v}{v_k}\sum_{n=1}^{\infty}\frac{1}{n!}\prod_{i=1,i\neq k}^{n}\int_{\epsilon v}\frac{dv_i}{v_i}\frac{d\phi}{2\pi}R'(v)$$

[1] In this change of variables we assume that the observable does not depend on the rapidity fraction (ratio of the emission's rapidity to the maximum possible rapidity) for small v_i. This property is fulfilled by all event-shape-like observables treated in the present thesis. For observables which explicitly depend on the rapidity fraction, Eq. 7.5 can be easily modified accordingly [42].

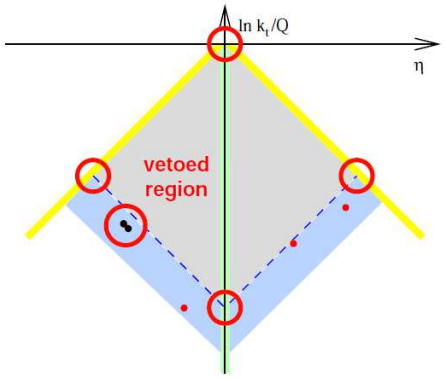

Figure 7.2: Corrections to the independent emission picture.

$$\times \Theta(v - v(k_1, ..., k_k, ..., k_n)) - \frac{1}{2} R''(v) \ln^2 \frac{1}{\epsilon} \mathcal{F}(R'), \tag{7.9}$$

and it can be computed by Monte Carlo methods.

Note that in general R' will contain NNLL terms (due to the physical CMW scheme for the running coupling as well as to hard-collinear contributions) that cannot be neglected as done for the NLL result. We can decompose R' as a sum of a NLL and a NNLL ($\delta R'(v)$) term

$$R'(v) \to R'(v) + \delta R'(v). \tag{7.10}$$

In order to avoid subleading effects, these terms can be treated explicitly by expanding the factor $e^{-\delta R' \ln \frac{1}{\epsilon}}$ to first order and combining it with the corresponding contribution arising from the decomposition 7.6.

7.1.2 Corrections to the independent emission picture

A second class of corrections comes from real configurations which have been ignored when deriving the multiple emission formula at NLL accuracy. We can discuss them with the help of Fig. 7.2 [42]. In this section we discuss corrections due to configurations in which *two* emissions are actually close in rapidity and azimuth angle, as depicted on the left of Fig. 7.2. The first of such corrections consists of a final state with any number of independent emissions, one of which splits into a correlated gg or $q\bar{q}$ pair ($k_k \to k_a + k_b$) with amplitude squared $|\widetilde{M}(k_a, k_b)|^2$. This configuration was ignored in the independent emission picture, but part of it was already included in the Sudakov radiator through the definition of the running coupling in the CMW scheme. The latter accounts for the contribution due to the inclusive correlated splitting mentioned above.

Thus, for a generic rIRC safe observable, the difference between the full observable and its inclusive treatment amounts to a NNLL contribution which reads

$$\mathcal{F}^{\text{correl}} = e^{-R' \ln \frac{1}{\epsilon}} \sum_{n=0} \frac{1}{n!} \left(\prod_{i=1}^{n} \int_{\epsilon v} [dk_i] |M(k_i)|^2 \right) \frac{1}{2!} \int [dk_a][dk_b] |\widetilde{M}_{rc}(k_a, k_b)|^2 \times \left[\Theta(v - v(k_1, \ldots, k_n, k_a, k_b)) - \Theta(v - v(k_1, \ldots, k_n, k_a + k_b)) \right] , \quad (7.11)$$

where the rc subscript means that the coupling in the correlated emission is evaluated at a scale of order v.

The second type of correction is due to two independent emissions which happen to be close in rapidity. This configuration violates the independent emission picture where the emissions are required to be widely separated from each other. In practice it is not straightforward to generate emissions with a buffer in rapidity and, normally, this is not an issue since to neglect subleding effects it is enough to approximate the m-emission matrix element with its uncorrelated part $|\widetilde{M}(k_1)|^2 |\widetilde{M}(k_2)|^2 ... |\widetilde{M}(k_m)|^2$. However, it becomes a problem when the observable is defined through a jet algorithm since the clustering routine will combine emissions which are close in rapidity, often giving rise to (large) subleading terms. In this cases we need to examine the infrared and collinear structure of the observable and replace it with an approximated one (v_{indep}), in which the configurations leading to subleading effects have been neglected (*cf.* the jet veto case). For this kind of observables we have an additional correction term which reads

$$\mathcal{F}^{\text{clust}} = e^{-R' \ln \frac{1}{\epsilon}} \sum_{n=0} \frac{1}{n!} \left(\prod_{i=1}^{n} \int_{\epsilon v} [dk_i] |M(k_i)|^2 \right) \frac{1}{2!} \int [dk_a][dk_b] |M(k_a)|^2 |M(k_b)|^2 \times \left[\Theta(v - v(k_1, ..., k_n, k_a, k_b)) - \Theta(v - v_{\text{indep}}(k_1, ..., k_n, k_a, k_b)) \right] . \quad (7.12)$$

7.1.3 Corrections at the corner of the phase space

The last type of NNLL corrections come from emissions that take place at the corners of the phase space, depicted with red circles in Fig. 7.2. As we showed already in Chapter 3, the logarithms originate from the η and k_t singularities of the emission's matrix element and phase space. Looking at Fig. 7.2 is clear that to have a double logarithm, one needs to integrate over a two-dimensional phase space slice. This is what is obtained by integrating over the grey vetoed region which yields all the double logarithms encoded in the Sudakov radiator. Single logarithmic contributions due to the hard collinear and soft large angle one-dimensional lines are also present in the radiator. The remaining single logarithms are obtained by integrating over the soft and collinear emissions in the thin blue stripe defined by the parameter ϵ. These contributions are single logarithmic despite the matrix-element being soft and collinear since the k_t is

bounded both from above and from below in this phase space region. The corners of the single emission phase space, give rise to constant contributions that are beyond the scope of the NLL resummation. At NNLL one has to include such corrections that will contribute to the global logarithmic structure through the running of the coupling. So we can distinguish three different contributions, some of which can vanish depending on the observable. The first constant term arises from a single emission at the upper corner of the rhombus where $k_t \sim Q$. This constant amounts to the hard virtual (one-loop) contribution to the process (*e.g.* form factor). The corresponding running coupling constant is to be evaluated at the k_t of the emission, so in this case $\alpha_s(Q)$. The second constant contribution is due to an emission at the left (right) corner of the phase space and it corresponds to the constant part obtained in the hard-collinear approximation. The last contribution arises from the lower corner and it is due to a soft emission with large angle ($\eta \sim 0$). The scale at which the running coupling is evaluated in the latter two cases is set according to the way the observable scales with the k_t of the emission in these kinematic regions. Since this scale will depend on the observable v, the constant terms will give rise to NNLL logarithmic terms, where the logarithms originate from the running of the coupling.
The corrections discussed above will ensure a full NNLL accuracy of the cross section in case of two hard emitters. For multijet processes, additional soft large angle contributions will be present, and they can be introduced as additional corrections to the Sudakov radiator according to the non-abelian soft exponentiation theorem [123, 124].

7.1.4 Thrust resummation revisited

In the general case all the previous corrections to the multiple emission picture will be non-trivial, but in some fortunate cases some of them will vanish. Let us consider as an example the case of the thrust studied in Chapter 4. Using the method discussed above we can carry out the resummation to NNLL in thrust space, without using the Laplace space formalism [1]. All the ingredients we need have been obtained in Chapter 4. The thrust is an additive observable, *i.e.* the contribution of any number of soft and/or collinear emissions can be expressed as the sum of individual contributions. Its expression in the soft and collinear limit was obtained in [42, 47] and reads

$$\tau(k_1, ..., k_n) = \sum_{i=1}^{n} \zeta_i, \tag{7.13}$$

with $\zeta_i = \tau_i/\tau$, where τ_i is the contribution of the i-th emission. This approximation is not accurate in the hard collinear limit, so we cannot use it to obtain the Sudakov

[1] Work done in collaboration with A. Banfi.

radiator. In Chapter 4, we showed a possible way to take into account the hard-collinear contribution in the radiator. We can use the same anomalous dimensions reported there, but the integration boundaries are to be replaced with the physical soft and collinear bounds in thrust space. After evaluating the relevant integrals we end up with the following radiator

$$R(\tau) = -\ln\frac{1}{\tau}t_1(\lambda) - t_2(\lambda) - \frac{\alpha_s}{\pi}\beta_0 t_3(\lambda), \tag{7.14}$$

where now $\lambda = \alpha_s/\pi\beta_0 \ln 1/\tau$ and the functions $t_i(\lambda)$ read

$$t_1(\lambda) = -\frac{A^{(1)}}{\beta_0\lambda}\left[(1-2\lambda)\ln(1-2\lambda) - 2(1-\lambda)\ln(1-\lambda)\right], \tag{7.15}$$

$$\begin{aligned} t_2(\lambda) = &-\frac{A^{(2)}}{\beta_0^2}\left[2\ln(1-\lambda) - \ln(1-2\lambda)\right] + 2\frac{B^{(1)}}{\beta_0}\ln(1-\lambda) - \frac{A^{(1)}\beta_1}{\beta_0^3}\left[\ln(1-2\lambda)\right. \\ &\left. + \frac{1}{2}\ln^2(1-2\lambda) - \ln(1-\lambda)(2+\ln(1-\lambda)\right], \end{aligned} \tag{7.16}$$

$$\begin{aligned} t_3(\lambda) = &-\frac{2B^{(2)}}{\beta_0^2}\frac{\lambda}{1-\lambda} - \frac{A^{(3)}}{\beta_0^3}\frac{\lambda^2}{(1-\lambda)(1-2\lambda)} \\ &+ \frac{A^{(2)}\beta_1}{\beta_0^4}\left[\frac{3\lambda^2}{(1-\lambda)(1-2\lambda)} + \frac{\ln(1-2\lambda)}{1-2\lambda} - 2\frac{\ln(1-\lambda)}{1-\lambda}\right] + \frac{2B^{(1)}\beta_1}{\beta_0^3}\frac{\lambda+\ln(1-\lambda)}{1-\lambda} \\ &+ \frac{A^{(1)}}{\beta_0}\frac{1}{(1-\lambda)(1-2\lambda)}\left[+\frac{\beta_2}{\beta_0^3}\left[-\lambda^2 + (1-\lambda)(1-2\lambda)\ln\frac{(1-\lambda)^2}{1-2\lambda}\right]\right] \\ &- \frac{A^{(1)}\beta_1^2}{\beta_0^5}\left[\frac{1}{2(1-2\lambda)}\ln(1-2\lambda)\left[4\lambda+\ln(1-2\lambda)\right] - \frac{1}{(1-\lambda)(1-2\lambda)}\right. \\ &\left.\times\left[\lambda^2 - (1-2\lambda)\ln(1-\lambda)(2\lambda+\ln(1-\lambda))\right]\right]. \end{aligned} \tag{7.17}$$

The corrections due to emissions at the corners of the phase space give rise to NNLL logarithmic terms, whose coefficients are entirely given by the single emission constant contributions. Rather than recomputing such contributions in the `CAESAR` formalism [1], we can exploit the results reported in Chapter 4 and in Appendix A.1 where the constant terms were computed in Laplace space. Our approach directly works in momentum

[1] In this framework what is referred to as the *soft* constant term vanishes identically since it would arise from the integration over the purely logarithmic soft *and* collinear region. The corresponding contribution is then reabsorbed into the hard part of the constant term. As a consequence, the anomalous dimension coefficients $A^{(3)}$ and $B^{(2)}$ change accordingly. We will not discuss this effect here, and we use the conventions reported in Chapter 4 for the constant terms.

space, so we need to use the corresponding expressions for the single emission constant terms which read

$$c_h^{(1)} = C_F \left(-\frac{19}{4} + \frac{7\pi^2}{12} \right), \tag{7.18}$$

$$c_s^{(1)} = C_F \frac{\pi^2}{12}, \tag{7.19}$$

$$c_j^{(1)} = C_F \left(\frac{7}{4} - \frac{\pi^2}{4} \right). \tag{7.20}$$

Using these values, we obtain the following multiplicative NNLL correction

$$C(\alpha_s, \tau) = 1 + \frac{\alpha_s}{\pi} \left(c_h^{(1)} + c_s^{(1)} \frac{1}{1-2\lambda} + 2c_j^{(1)} \frac{1}{1-\lambda} \right) + \mathcal{O}(\alpha_s^2). \tag{7.21}$$

Let us now discuss the structure of the multiple emission function $\mathcal{F}(R')$. Its NLL expression in the context of the CAESAR algorithm was obtained in [42], in agreement with the results of [47]

$$\mathcal{F}(R') = e^{-R' \ln \frac{1}{\epsilon}} \sum_{n=1}^{\infty} \frac{1}{n!} \prod_{i=1}^{n} \int_{\epsilon}^{1} \frac{d\zeta_i}{\zeta_i} R' \Theta(1 - \sum_{i=1}^{n} \zeta_i) = \frac{e^{-\gamma_E R'}}{\Gamma(1+R')}. \tag{7.22}$$

The NNLL corrections to this formula can be computed using the results presented above and, given the simple structure of the thrust in the soft limit, they can be expressed analytically. The correction $\mathcal{F}^{\text{clust}}$ 7.12 to the independent emission picture identically vanishes since the thrust does not involve any clustering of the final state partons. The non-inclusive correction $\mathcal{F}^{\text{correl}}$ 7.11 is non-trivial but it amounts to a subleading N^{3}LL term. To show this we recall that such a correction arises from configurations with a correlated *soft* pair plus any number of soft and collinear independent emissions. The phase space trigger function is given by the difference between the thrust and its inclusive approximation where the soft correlated pair is replaced by the parent gluon. The expression for the thrust in the soft limit was obtained in Chapter 4, where it was used to compute the double soft contribution. We clearly see that the difference

$$\Theta(\tau - \tau(k_1, \ldots, k_n, k_a, k_b)) - \Theta(\tau - \tau(k_1, \ldots, k_n, k_a + k_b)), \tag{7.23}$$

is non-vanishing only when the two correlated partons move into opposite hemispheres. This situation requires the parent gluon to be emitted at large angle off the Born dipole system, restricting its phase space to a small region around the $\eta = 0$ vertex. This region is not large enough to generate any logarithms and the integration leads to a $\mathcal{O}(\alpha_s^2)$ constant term, multiplied by the contribution of any number of independent emissions. This contribution is N^{3}L logarithmic, and thus it can be neglected. To perform a quantitative check, we consider the leading order contribution to the $\mathcal{F}^{\text{correl}}$

function, where only a soft correlated pair is actually emitted. The matrix elements are given in Chapter 4 while the phase space trigger function is replaced by

$$Q(2\pi)\delta^{(+)}(k_b^2)(2\pi)\delta^{(+)}(k_a^2)\left(\mathcal{J}_{cut}(\tau_s Q)-\mathcal{J}^{\text{incl}}_{cut}(\tau_s Q)\right), \tag{7.24}$$

where $\mathcal{J}_{cut}(\tau_s Q)$ is obtained from Eqs. 4.45, 4.46, 4.47, 4.48 by replacing the δ-functions with Θ-functions, and $\mathcal{J}^{\text{incl}}_{cut}(\tau_s Q)$ is a modified trigger function, inclusive in the correlated pair. The difference between the two reads

$$\begin{aligned}
&\mathcal{J}_{cut}(\tau_s Q)-\mathcal{J}^{\text{incl}}_{cut}(\tau_s Q)\\
&=Q(2\pi)\delta^{(+)}(k_a^2)(2\pi)\delta^{(+)}(k_b^2)\\
&\times\left(\Theta(\tau_s Q-k_a\cdot n-k_b\cdot n)\Theta(k_a\cdot\bar n-k_a\cdot n)\Theta(k_b\cdot\bar n-k_b\cdot n)\right.\\
&+\Theta(\tau_s Q-k_a\cdot\bar n-k_b\cdot\bar n)\Theta(k_a\cdot n-k_a\cdot\bar n)\Theta(k_b\cdot n-k_b\cdot\bar n)\\
&+\Theta(\tau_s Q-k_a\cdot n-k_b\cdot\bar n)\Theta(k_a\cdot\bar n-k_a\cdot n)\Theta(k_b\cdot n-k_b\cdot\bar n)\\
&+\Theta(\tau_s Q-k_b\cdot n-k_a\cdot\bar n)\Theta(k_b\cdot\bar n-k_b\cdot n)\Theta(k_a\cdot n-k_a\cdot\bar n))\\
&-\Theta(\tau_s Q-k_b\cdot n-k_a\cdot n)\Theta(k_b\cdot\bar n+k_a\cdot\bar n-k_b\cdot n-k_a\cdot n)\\
&\left.-\Theta(\tau_s Q-k_b\cdot\bar n-k_a\cdot\bar n)\Theta(k_b\cdot n+k_a\cdot n-k_b\cdot\bar n-k_a\cdot\bar n)\right)
\end{aligned} \tag{7.25}$$

which is non-zero only if the two partons move towards opposite hemispheres. We computed the phase space integrals numerically using the sector decomposition code `SecDec`, and we found that the result amounts to a $\mathcal{O}(\alpha_s^2)$ constant term, confirming the above claim. The only non-trivial corrections to the Sudakov radiator come from emissions taking place at the phase space corners and from the running corrections $\mathcal{F}^{\text{running}}$ 7.9. The $\mathcal{O}(\alpha_s)$ constants are reported in Eqs. 7.20, while the $\mathcal{F}^{\text{running}}$ function can be easily computed as follows

$$\begin{aligned}
\mathcal{F}^{\text{running}}=&\,e^{-R'\ln\frac{1}{\epsilon}}\int_\epsilon^1\frac{d\zeta_k}{\zeta_k}R''\ln\frac{1}{\zeta_k}\sum_{n=1}^{\infty}\frac{1}{n!}\prod_{i=1,i\neq k}^{n}\int_\epsilon^1\frac{d\zeta_i}{\zeta_i}R'\Theta(1-\sum_{i=1}^{n}\zeta_i)\\
&-\frac{1}{2}R''\ln^2\frac{1}{\epsilon}\mathcal{F}(R'),
\end{aligned} \tag{7.26}$$

where we integrated inclusively Eq. 7.9 over the azimuth angle, since the observable 7.13 only depends on the individual values ζ_i. Moreover, we performed a change of variable $v_i\to v\zeta_i$ and used the expression of the observable 7.13. To evaluate the above integral, we can write the factor $-\frac{1}{2}R''\ln^2\frac{1}{\epsilon}$ in the virtual corrections as $-\int_\epsilon^1 d\zeta_k/\zeta_k\ln 1/\zeta_k$ so as to express it as a dummy real emission that will not contribute to the observable. To evaluate the real corrections

$$-e^{-R'\ln\frac{1}{\epsilon}}\int_\epsilon^1\frac{d\zeta_k}{\zeta_k}R''\ln\zeta_k\sum_{n=1}^{\infty}\frac{1}{n!}\prod_{i=1,i\neq k}^{n}\int_\epsilon^1\frac{d\zeta_i}{\zeta_i}R'\Theta(1-\sum_{i=1}^{n}\zeta_i) \tag{7.27}$$

we decompose the virtual factor for the independent emissions $e^{-R' \ln \frac{1}{\epsilon}}$ as

$$e^{-R' \ln \frac{1}{\epsilon}} = e^{R' \ln(1-\zeta_k)} e^{-R' \ln \frac{1-\zeta_k}{\epsilon}}, \tag{7.28}$$

and perform the change of variables $\zeta_i \to \zeta_i(1-\zeta_k)$, for $i \neq k$ getting

$$\begin{aligned}
&- e^{-R' \ln \frac{1}{\epsilon}} \int_\epsilon^1 \frac{d\zeta_k}{\zeta_k} R'' \ln \zeta_k \sum_{n=1}^{\infty} \frac{1}{n!} \prod_{i=1, i\neq k}^{n} \int_\epsilon^1 \frac{d\zeta_i}{\zeta_i} R' \Theta(1 - \sum_{i=1}^{n} \zeta_i) \\
&= - \int_\epsilon^1 \frac{d\zeta_k}{\zeta_k} R'' \ln \zeta_k e^{R' \ln(1-\zeta_k)} \\
&\times \left(e^{-R' \ln \frac{1-\zeta_k}{\epsilon}} \sum_{n=1}^{\infty} \frac{1}{n!} \prod_{i=1, i\neq k}^{n} \int_{\frac{\epsilon}{1-\zeta_k}}^1 \frac{d\zeta_i}{\zeta_i} R' \Theta(1 - \sum_{i=1, i\neq k}^{n} \frac{\zeta_i}{1-\zeta_k}) \right) \\
&= - \int_\epsilon^1 \frac{d\zeta_k}{\zeta_k} R'' \ln \zeta_k e^{R' \ln(1-\zeta_k)} \mathcal{F}(R'),
\end{aligned} \tag{7.29}$$

where we identified the expression in round brackets with the multiple emission function at NLL accuracy 7.22. It is now straightforward to combine it with the virtual term getting (we can safely take the limit $\epsilon \to 0$ since the result is finite)

$$\begin{aligned}
\mathcal{F}^{\text{running}} &= - \int_0^1 \frac{d\zeta_k}{\zeta_k} R'' \ln \zeta_k \left((1-\zeta_k)^{R'} - 1 \right) \mathcal{F}(R') \\
&= - R'' \left(\frac{\pi^2}{12} + \frac{1}{2} \partial_{R'}^2 \right) \mathcal{F}(R'),
\end{aligned} \tag{7.30}$$

where $R'' = -\alpha_s / \pi \beta_0 \left(2h_1'(\lambda) + \lambda h_1''(\lambda) \right)$.

As mentioned above, at this accuracy, another NNLL correction arises from the fact that R' contains a NNLL term. It is convenient to single out such a contribution by writing R' as

$$R' \to R' + \delta R', \tag{7.31}$$

where $R' = -h_1(\lambda) - \lambda h_1'(\lambda)$ and $\delta R' = -\alpha_s / \pi \beta_0 h_2'(\lambda)$ is the NNLL piece. We can thus further expand the NLL result $\mathcal{F}(R')$ to first order in $\delta R'$ neglecting subleading terms as

$$\frac{e^{-\gamma_E R'}}{\Gamma(1+R')} \to (1 + \delta R' \partial_{R'}) \frac{e^{-\gamma_E R'}}{\Gamma(1+R')}. \tag{7.32}$$

Merging all the contributions leads to the final result

$$R_T(\tau) = C(\alpha_s, \tau) e^{-R(\tau)} \left(1 + \delta R' \partial_{R'} - R'' \frac{\pi^2}{12} - R'' \frac{1}{2} \partial_{R'}^2 \right) \frac{e^{-\gamma_E R'}}{\Gamma(1+R')}. \tag{7.33}$$

It is then straightforward to show that Eq. 7.33 is equivalent to Eq. 4.132 up to $\mathrm{N^3LL}$ corrections. The $\mathrm{N^3LL}$ terms G_{31} and the constant C_2 can be included as done in Chapter 4 to perform the R-matching to the fixed-order result.

Unlike the thrust, in the jet veto case studied in Chapter 6, the $\mathcal{F}^{\text{running}}$ corrections are identically zero, while the correlated correction $\mathcal{F}^{\text{correl}}$ (Eq. 6.33) and the clutering correction $\mathcal{F}^{\text{clust}}$ (Eq. 6.35) are non-trivial.
In the present thesis we limited our analysis to the so called *global* logarithms. Many collider observables of phenomenological interest require an exclusive number of jets and this leads to the appearance of a *non-global* logarithmic structure [43]. Such logarithms can be resummed using Monte Carlo methods [43, 44] in the large N_c limit to NLL accuracy and their treatment can be included in the algorithm discussed above. Further studies on the resummation properties of non-global logarithms beyond NLL are currently being carried out by several research groups.

Appendix A

Resummation coefficients and useful formulae for thrust

A.1 Constants and anomalous dimensions for thrust resummation

The renormalization group equation for the QCD coupling constant reads

$$\frac{\partial\alpha_s(\mu)}{\partial\ln\mu^2} = -\alpha_s(\mu)\left(\frac{\alpha_s(\mu)}{\pi}\beta_0 + \frac{\alpha_s^2(\mu)}{\pi^2}\beta_1 + \left(\frac{\alpha_s^2(\mu)}{\pi^2}\right)^2\beta_2 + \left(\frac{\alpha_s^2(\mu)}{\pi^2}\right)^3\beta_3 + \dots\right), \quad \text{(A.1)}$$

where the coefficients of the $\beta(\alpha_s)$ functions are

$$\begin{aligned}
\beta_0 =& \frac{11}{12}C_A - \frac{1}{3}T_F n_F,\\
\beta_1 =& \frac{17}{24}C_A^2 - \frac{5}{12}C_A T_F n_F - \frac{1}{4}C_F T_F n_F,\\
\beta_2 =& \frac{325}{3456}n_F^2 - \frac{5033}{1152}n_F + \frac{2857}{128},\\
\beta_3 =& \frac{1093}{186624}n_F^3 + \left(\frac{50065}{41472} + \frac{809}{2592}\zeta_3\right)n_F^2 - \left(\frac{1078361}{41472} + \frac{1627}{1728}\zeta_3\right)n_F + \frac{891}{64}\zeta_3 + \frac{149753}{256}.
\end{aligned} \quad \text{(A.2)}$$

Equation A.1 can be solved in perturbation theory and it gives the following resummed expression for the strong coupling

$$\begin{aligned}
\alpha_s(\mu) = \frac{\alpha_s(\mu_R)}{1+2\lambda}\Bigg(1 &- \frac{\alpha_s(\mu_R)}{\pi(1+2\lambda)}\frac{\beta_1}{\beta_0}\ln(1+2\lambda)\\
&+ \frac{\alpha_s^2(\mu_R)}{\pi^2(1+2\lambda)^2}\left(\frac{\beta_1^2}{\beta_0^2}\big(\ln(1+2\lambda)(\ln(1+2\lambda)-1)+2\lambda\big) - \frac{\beta_2}{\beta_0}2\lambda\right)\\
&+ \frac{\alpha_s^3(\mu_R)}{\pi^3(1+2\lambda)^3}\left(\frac{\beta_1^3}{\beta_0^3}\big(-4\lambda\ln(1+2\lambda) + \frac{5}{2}\ln^2(1+2\lambda) - \ln^3(1+2\lambda) - 2\lambda^2\big)\right.
\end{aligned}$$

$$
\left. - \frac{\beta_3}{\beta_0} 2\lambda(1+\lambda) + \frac{\beta_1\beta_2}{\beta_0^2}\big(2(1+2\lambda)\ln(1+2\lambda) - 3\ln(1+2\lambda) + 2\lambda(1+2\lambda)\big)\right)\Bigg)
$$
$$
+ \ldots, \tag{A.3}
$$

where here $\lambda = (\alpha_s(\mu_R)/\pi)\beta_0 \ln(\mu/\mu_R)$. The coefficients $A^{(i)}$ and $B^{(i)}$ used in the resummed cross section 5.2 can be computed using Γ_{soft} at two-loop order and the three-loop Altarelli-Parisi splitting functions computed in [**?** **?**]. Using the notation 4.117 we find

$$
\begin{aligned}
A^{(1)} &= C_F, \\
A^{(2)} &= C_F\left(C_A\left(\frac{67}{36} - \frac{\pi^2}{12}\right) - \frac{5}{9}T_F n_F\right), \\
A^{(3)} &= C_F n_F^2\left(\frac{25}{324} - \frac{\pi^2}{216}\right) + C_A C_F n_F\left(-\frac{2051}{1296} + \frac{7\pi^2}{72}\right) + C_F^2 n_F\left(-\frac{55}{96} + \frac{\zeta_3}{2}\right) \\
&\quad + C_A^2 C_F\left(\frac{15503}{2592} - \frac{389\pi^2}{864} + \frac{11\pi^4}{720} - \frac{11\zeta_3}{4}\right), \\
B^{(1)} &= -\frac{3}{4}C_F, \\
B^{(2)} &= C_F n_F\left(\frac{1}{48} + \frac{\pi^2}{36}\right) + C_F^2\left(-\frac{3}{32} + \frac{\pi^2}{8} - \frac{3\zeta_3}{2}\right) + C_A C_F\left(-\frac{17}{96} - \frac{11\pi^2}{72} + \frac{3\zeta_3}{4}\right),
\end{aligned} \tag{A.4}
$$

$$
\begin{aligned}
B^{(3)} =& C_A C_F n_F\left(-\frac{5}{16} + \frac{167\pi^2}{1296} - \frac{\pi^4}{2880} - \frac{25\zeta_3}{72}\right) + C_F n_F^2\left(\frac{17}{576} - \frac{5\pi^2}{648} + \frac{\zeta_3}{36}\right) \\
&+ C_F^2 n_F\left(\frac{23}{64} - \frac{5\pi^2}{288} - \frac{29\pi^4}{4320} + \frac{17\zeta_3}{24}\right) + C_A C_F^2\left(-\frac{151}{256} + \frac{205\pi^2}{576} + \frac{247\pi^4}{8640} - \frac{211\zeta_3}{48}\right. \\
&\left. - \frac{1}{24}\pi^2\zeta_3 - \frac{15\zeta_5}{8}\right) + C_A^2 C_F\left(\frac{1657}{2304} - \frac{281\pi^2}{648} + \frac{\pi^4}{1152} + \frac{97\zeta_3}{36} - \frac{5\zeta_5}{8}\right) \\
&+ C_F^3\left(-\frac{29}{128} - \frac{3\pi^2}{64} - \frac{\pi^4}{40} - \frac{17\zeta_3}{16} + \frac{1}{12}\pi^2\zeta_3 + \frac{15\zeta_5}{4}\right).
\end{aligned} \tag{A.5}
$$

The functions $H(1,\alpha_s(Q))$, $\tilde{J}(1,\alpha_s(\sqrt{(N_0/N)}Q))$ and $\tilde{S}(1,\alpha_s(N_0Q/N))$ can be expanded in a power series in the coupling as

$$
H(1,\alpha_s(Q)) = 1 + \sum_{i\geq 1} c_h^{(i)} \frac{\alpha_s^i(Q)}{\pi^i}, \qquad \tilde{J}\left(1,\alpha_s(\sqrt{(N_0/N)}Q)\right) = 1 + \sum_{i\geq 1} c_j^{(i)} \frac{\alpha_s^i(\sqrt{(N_0/N)}Q)}{\pi^i},
$$
$$
\tilde{S}(1,\alpha_s(N_0Q/N)) = 1 + \sum_{i\geq 1} c_s^{(i)} \frac{\alpha_s^i(N_0Q/N)}{\pi^i}. \tag{A.6}
$$

The coefficients $c_h^{(i)}$ can be evaluated using the on-shell quark form factor [112, 113], normalized to the total hadronic cross section

$$\begin{aligned} c_h^{(1)} &= C_F\left(-\frac{19}{4}+\frac{7\pi^2}{12}\right), \\ c_h^{(2)} &= C_F^2\left(\frac{745}{64}-\frac{13\pi^2}{6}+\frac{67\pi^4}{480}-\frac{15\zeta_3}{4}\right)+C_F n_F T_F\left(\frac{5867}{1296}-\frac{91\pi^2}{216}-\frac{17\zeta_3}{18}\right) \\ &\quad + C_A C_F\left(-\frac{71083}{5184}+\frac{1061\pi^2}{864}-\frac{\pi^4}{90}+\frac{511\zeta_3}{72}\right). \end{aligned} \tag{A.7}$$

The two loop non-logarithmic term of the collinear subprocess was computed in [114], resulting in

$$\begin{aligned} c_j^{(1)} &= C_F\left(\frac{7}{4}-\frac{\pi^2}{6}\right), \\ c_j^{(2)} &= C_F T_F n_F\left(-\frac{4057}{2592}+\frac{13\pi^2}{144}\right)+C_F C_A\left(\frac{53129}{10368}-\frac{155\pi^2}{576}-\frac{37\pi^4}{2880}-\frac{9\zeta_3}{8}\right) \\ &\quad + C_F^2\left(\frac{205}{128}-\frac{97\pi^2}{192}+\frac{61\pi^4}{1440}-\frac{3\zeta_3}{8}\right), \end{aligned} \tag{A.8}$$

and the non-logarithmic part of the two loop soft subprocess was computed in section 2 4.94, 4.95

$$\begin{aligned} c_s^{(1)} &= -C_F\frac{\pi^2}{4}, \\ c_s^{(2)} &= \frac{\pi^4}{32}C_F^2+C_F T_F n_F\left(\frac{5}{81}+\frac{77\pi^2}{216}-\frac{13\zeta_3}{18}\right)+C_A C_F\left(-\frac{535}{324}-\frac{871\pi^2}{864}+\frac{7\pi^4}{120}+\frac{143\zeta_3}{72}\right). \end{aligned} \tag{A.9}$$

The resummation functions used in Chapter 5 are reported as a function of $\lambda = \frac{\alpha_s(\mu)}{\pi}\beta_0 \ln N$

$$h_1(\lambda) = -\frac{A^{(1)}}{\beta_0\lambda}[(1-2\lambda)\ln(1-2\lambda)-2(1-\lambda)\ln(1-\lambda)], \tag{A.10}$$

$$\begin{aligned} h_2(\lambda) &= -\frac{A^{(2)}}{\beta_0^2}[2\ln(1-\lambda)-\ln(1-2\lambda)]+2\frac{B^{(1)}}{\beta_0}\ln(1-\lambda)-\frac{A^{(1)}\beta_1}{\beta_0^3}[\ln(1-2\lambda) \\ &\quad +\frac{1}{2}\ln^2(1-2\lambda)-\ln(1-\lambda)(2+\ln(1-\lambda)]-2\frac{A^{(1)}\gamma_E}{\beta_0}\ln\frac{1-\lambda}{1-2\lambda}, \end{aligned} \tag{A.11}$$

$$h_3(\lambda) = -\frac{2B^{(2)}}{\beta_0^2}\frac{\lambda}{1-\lambda}-\frac{A^{(3)}}{\beta_0^3}\frac{\lambda^2}{(1-\lambda)(1-2\lambda)}-\frac{2A^{(2)}\gamma_E}{\beta_0^2}\frac{\lambda}{(1-\lambda)(1-2\lambda)}$$

$$
\begin{aligned}
&+\frac{A^{(2)}\beta_1}{\beta_0^4}\left[\frac{3\lambda^2}{(1-\lambda)(1-2\lambda)}+\frac{\ln(1-2\lambda)}{1-2\lambda}-2\frac{\ln(1-\lambda)}{1-\lambda}\right]-2\frac{B^{(1)}}{\beta_0}\gamma_E\frac{\lambda}{1-\lambda}\\
&+\frac{2B^{(1)}\beta_1}{\beta_0^3}\frac{\lambda+\ln(1-\lambda)}{1-\lambda}+\frac{A^{(1)}}{\beta_0}\frac{1}{(1-\lambda)(1-2\lambda)}\left[\frac{2\gamma_E\beta_1}{\beta_0^2}\big[\lambda+(1-\lambda)\ln(1-2\lambda)\right.\\
&\left.-(1-2\lambda)\ln(1-\lambda)\big]-\gamma_E^2\lambda(3-2\lambda)+\frac{\beta_2}{\beta_0^3}\big[-\lambda^2+(1-\lambda)(1-2\lambda)\ln\frac{(1-\lambda)^2}{1-2\lambda}\big]\right]\\
&-\frac{A^{(1)}\beta_1^2}{\beta_0^5}\left[\frac{1-\lambda}{2(1-\lambda)(1-2\lambda)}\ln(1-2\lambda)\big[4\lambda+\ln(1-2\lambda)\big]-\frac{1}{(1-\lambda)(1-2\lambda)}\right.\\
&\left.\times\big[\lambda^2-(1-2\lambda)\ln(1-\lambda)(2\lambda+\ln(1-\lambda))\big]\right]. \qquad \text{(A.12)}
\end{aligned}
$$

A.2 Computation of the G_{31} coefficient and of the constant terms

The starting point to obtain Eq. 4.132 is the cross section in Laplace space 5.2 in which we include the coefficients $A^{(i)}$ and $B^{(i)}$ with $i \leq 3$. In Section 4.4 we show that this is sufficient to compute the N^{2}LL function $f_3(\lambda)$ and the N^{3}LL coefficient $\tilde{G}_{31}$. The latter combines with terms arising from the inverse Laplace transform to produce G_{31}. With the normalization chosen for the functions $f_i(\lambda)$ (Eqs. 4.118–4.120) the constant terms in Eq. 4.114 are defined as

$$
H(\frac{Q}{\mu},\alpha_s(\mu))\exp\left(\frac{\alpha_s}{2\pi}\tilde{G}_{10}+\frac{\alpha_s^2}{(2\pi)^2}\tilde{G}_{20}+\mathcal{O}(\alpha_s^3)\right)=1+\frac{\alpha_s}{2\pi}\tilde{C}_1+\left(\frac{\alpha_s}{2\pi}\right)^2\tilde{C}_2+\mathcal{O}(\alpha_s^3), \qquad \text{(A.13)}
$$

where $\tilde{G}_{10}$ and $\tilde{G}_{20}$ are the constant terms left in the exponent after computing $f_3(\lambda)$ and $\tilde{G}_{31}$.

In the Laplace inversion we have to add the N^{3}LL term $\frac{1}{6}\tilde{\mathcal{F}}^{(3)}(\alpha_s(Q^2),\ln\frac{1}{\tau})\ln^3\nu$ in square brackets of Eq. 4.125 and include the next subleading term in the definition of $\tilde{\mathcal{F}}^{(1)}$ and $\tilde{\mathcal{F}}^{(2)}$ getting

$$
\begin{aligned}
\mathcal{F}^{(1)}(\alpha_s(Q^2),\ln\frac{1}{\tau}) &= f_1(\lambda)+\lambda f_1'(\lambda)+\frac{\alpha_s}{\pi}\beta_0 f_2'(\lambda)+\left(\frac{\alpha_s}{\pi}\beta_0\right)^2 f_3'(\lambda)+\mathcal{O}(\alpha_s^n\ln^{n-3}\frac{1}{\tau}),\\
\mathcal{F}^{(2)}(\alpha_s(Q^2),\ln\frac{1}{\tau}) &= 2\frac{\alpha_s}{\pi}\beta_0 f_1'(\lambda)+\frac{\alpha_s}{\pi}\beta_0\lambda f_1''(\lambda)+\left(\frac{\alpha_s}{\pi}\beta_0\right)^2 f_2''(\lambda)+\mathcal{O}(\alpha_s^n\ln^{n-3}\frac{1}{\tau}),\\
\mathcal{F}^{(3)}(\alpha_s(Q^2),\ln\frac{1}{\tau}) &= 3\left(\frac{\alpha_s}{\pi}\beta_0\right)^2 f_1''(\lambda)+\left(\frac{\alpha_s}{\pi}\beta_0\right)^2\lambda f_1'''(\lambda)+\mathcal{O}(\alpha_s^n\ln^{n-3}\frac{1}{\tau}). \qquad \text{(A.14)}
\end{aligned}
$$

It is important to notice that the terms $f_2''(\lambda)$, $f_3'(\lambda)$ and the whole $\mathcal{F}^{(3)}(\alpha_s(Q^2),\ln\frac{1}{\tau})$ contribute at most with logarithmic order $\mathcal{O}(\alpha_s^n\ln^{n-2}\frac{1}{\tau})$ (*i.e.* N^{3}LL) and we do not need them for a N^{2}LL order resummation. Nevertheless, they are relevant for the computation of the coefficient G_{31}, so we keep them. We now solve the integrals as shown

in Section 4.4.1 neglecting subleading (N^4LL) terms and we expand the final result through order $\mathcal{O}(\alpha_s^3 \ln \frac{1}{\tau})$ obtaining C_1, C_2 explicitly as reported in Eq. 4.134,4.135. To determine G_{31} we observe that the coefficient of $\alpha_s^3 \ln \frac{1}{\tau}$ in the previous expansion is $G_{31} + C_1 G_{21} + C_2 G_{11}$, where G_{21} and G_{11} are known. The result is reported in Eq. 4.136.

A.3 Evaluation of the integrals over soft gluons transverse momentum

In the present section we show how to evaluate the integrals over the transverse component of soft gluon momenta used in the text. Let us consider the integral

$$\int d^{d-2}q_\perp d^{d-2}k_\perp \frac{\delta^{(+)}(q^2)\delta^{(+)}(k^2)}{(q+k)^2 - i0}. \tag{A.15}$$

Using the relations

$$k^2 = (k\cdot n)(k\cdot \bar{n}) - k_\perp^2, \qquad d^{d-2}k_\perp = \frac{\pi^{1-\epsilon}}{\Gamma(1-\epsilon)}(k_\perp^2)^{-\epsilon} dk_\perp^2, \tag{A.16}$$

$$q^2 = (q\cdot n)(q\cdot \bar{n}) - q_\perp^2, \qquad d^{d-2}q_\perp = \frac{\pi^{\frac{1}{2}-\epsilon}}{\Gamma(\frac{1}{2}-\epsilon)}(q_\perp^2)^{-\epsilon} dq_\perp^2 \sin^{-2\epsilon}(\theta) d\theta, \tag{A.17}$$

where θ is the angle between the $d-2$-dimensional euclidean vectors $q_\perp$ and $k_\perp$, we can recast A.15 as follows

$$\frac{\pi^{1-\epsilon}}{\Gamma(1-\epsilon)}\frac{\pi^{\frac{1}{2}-\epsilon}}{\Gamma(\frac{1}{2}-\epsilon)} \int dk_\perp^2 dq_\perp^2 (k_\perp^2)^{-\epsilon}(q_\perp^2)^{-\epsilon} \frac{\delta^{(+)}((k\cdot n)(k\cdot\bar{n}) - k_\perp^2)\delta^{(+)}((q\cdot n)(q\cdot\bar{n}) - q_\perp^2)}{-2|k_\perp||q_\perp|} \times \frac{(\sin^2(\theta))^{-\epsilon} d\theta}{\cos(\theta) - \frac{(k\cdot n)(q\cdot\bar{n}) + (q\cdot n)(k\cdot\bar{n})}{2|k_\perp||q_\perp|} + i0}. \tag{A.18}$$

The integrals over $q_\perp^2$ and $k_\perp^2$ can be easily evaluated using the two δ functions while the angular integral needs some attention. We set $\frac{(k\cdot n)(q\cdot\bar{n}) + (q\cdot n)(k\cdot\bar{n})}{2|k_\perp||q_\perp|} = \mathcal{K}$ and we consider the angular part of Eq. A.18

$$\int_0^\pi \frac{(\sin^2(\theta))^{-\epsilon}}{\cos(\theta) - \mathcal{K} + i0} d\theta,$$

where it is straightforward to show that $\mathcal{K} \geq 1$. The previous integral can be evaluated by setting $\cos(\theta) \to 2t - 1$ and using the integral representation of the Hypergeometric function

$$\int_0^\pi \frac{(\sin^2(\theta))^{-\epsilon}}{\cos(\theta) - \mathcal{K} + i0} d\theta = -4^{-\epsilon} \frac{1}{1 + \mathcal{K} - i0} \int_0^1 dt \frac{(1-t)^{-\frac{1}{2}-\epsilon} t^{-\frac{1}{2}-\epsilon}}{1 - \frac{2}{1+\mathcal{K}-i0} t} =$$

$$= -4^{-\epsilon}\frac{\Gamma^2(\frac{1}{2}-\epsilon)}{\Gamma(1-2\epsilon)}\frac{{}_2F_1(1,\frac{1}{2}-\epsilon,1-2\epsilon,\frac{2}{1+\mathcal{K}-i0})}{1+\mathcal{K}-i0}. \tag{A.19}$$

This leads to the solution of A.18

$$\int d^{d-2}q_\perp d^{d-2}k_\perp \frac{\delta^{(+)}(q^2)\delta^{(+)}(k^2)}{(q+k)^2-i0} = \frac{\pi^{1-\epsilon}}{\Gamma(1-\epsilon)}\frac{\pi^{\frac{1}{2}-\epsilon}}{\Gamma(\frac{1}{2}-\epsilon)}4^{-\epsilon}\frac{\Gamma^2(\frac{1}{2}-\epsilon)}{\Gamma(1-2\epsilon)}$$
$$\times(q\cdot n)^{-\epsilon}(q\cdot\bar{n})^{-\epsilon}(k\cdot n)^{-\epsilon}(k\cdot\bar{n})^{-\epsilon}\frac{{}_2F_1\left(1,\frac{1}{2}-\epsilon,1-2\epsilon,4\frac{\sqrt{(q\cdot n)(q\cdot\bar{n})(k\cdot n)(k\cdot\bar{n})}}{\left(\sqrt{(q\cdot n)(k\cdot\bar{n})}+\sqrt{(q\cdot\bar{n})(k\cdot n)}\right)^2}\right)}{\left(\sqrt{(q\cdot n)(k\cdot\bar{n})}+\sqrt{(q\cdot\bar{n})(k\cdot n)}\right)^2}, \tag{A.20}$$

used in the text. The second relevant integral is

$$\int d^{d-2}q_\perp d^{d-2}k_\perp \frac{\delta^{(+)}(q^2)\delta^{(+)}(k^2)}{((q+k)^2+i0)((q+k)^2-i0)}, \tag{A.21}$$

appearing in the computation of the vacuum polarization diagrams. Such an integral can be evaluated easily using the previous reult A.20. We can indeed write it as

$$-\frac{1}{2}\frac{1}{i0}\left(\int d^{d-2}q_\perp d^{d-2}k_\perp \frac{\delta^{(+)}(q^2)\delta^{(+)}(k^2)}{(q+k)^2+i0} - \int d^{d-2}q_\perp d^{d-2}k_\perp \frac{\delta^{(+)}(q^2)\delta^{(+)}(k^2)}{(q+k)^2-i0}\right), \tag{A.22}$$

so it amounts to use A.20 with two different pole prescriptions. It is then straightforward to show that

$$\int d^{d-2}q_\perp d^{d-2}k_\perp \frac{\delta^{(+)}(q^2)\delta^{(+)}(k^2)}{((q+k)^2+i0)((q+k)^2-i0)} = \frac{\pi^{1-\epsilon}}{\Gamma(1-\epsilon)}\frac{\pi^{\frac{1}{2}-\epsilon}}{\Gamma(\frac{1}{2}-\epsilon)}4^{-\epsilon}\frac{\Gamma^2(\frac{1}{2}-\epsilon)}{\Gamma(1-2\epsilon)}$$
$$\times(q\cdot n)^{-\epsilon}(q\cdot\bar{n})^{-\epsilon}(k\cdot n)^{-\epsilon}(k\cdot\bar{n})^{-\epsilon}\frac{{}_2F_1\left(2,\frac{1}{2}-\epsilon,1-2\epsilon,4\frac{\sqrt{(q\cdot n)(q\cdot\bar{n})(k\cdot n)(k\cdot\bar{n})}}{\left(\sqrt{(q\cdot n)(k\cdot\bar{n})}+\sqrt{(q\cdot\bar{n})(k\cdot n)}\right)^2}\right)}{\left(\sqrt{(q\cdot n)(k\cdot\bar{n})}+\sqrt{(q\cdot\bar{n})(k\cdot n)}\right)^4}. \tag{A.23}$$

In the last part of the present section we report some identities for the hypergeometric functions appearing in the calculation:

$${}_2F_1\big(1,\frac{1}{2}-\epsilon,1-2\epsilon,4\frac{z}{(1+z)^2}\big) = (1+z)^2{}_2F_1\big(1,1+\epsilon,1-\epsilon,z^2\big), \quad |z|\leq 1; \tag{A.24}$$

$${}_2F_1(1,1+\epsilon,1-\epsilon,z) = \frac{\Gamma(1-\epsilon)}{\Gamma(1+\epsilon)\Gamma(-2\epsilon)}\int_0^1 dy\,\frac{y^\epsilon(1-y)^{-1-2\epsilon}}{1-yz}, \quad \epsilon<0; \tag{A.25}$$

$$ {}_2F_1\left(2,\frac{1}{2}-\epsilon,1-2\epsilon,4\frac{z}{(1+z)^2}\right)=(1+z)^4{}_2F_1\big(2,2+\epsilon,1-\epsilon,z^2\big),\quad |z|\leq 1; \tag{A.26} $$

$$ {}_2F_1(2,2+\epsilon,1-\epsilon,z)=\frac{\Gamma(1-\epsilon)}{\Gamma(1+\epsilon)\Gamma(-2\epsilon)}\frac{1}{1-z}\int_0^1 dy\, y^{\epsilon}(1-y)^{-1-2\epsilon}\frac{1+zy}{(1-yz)^2},\qquad \epsilon<0. \tag{A.27} $$

To prove A.27 we consider the following relation

$$ {}_2F_1\left(2,2+\epsilon,1-\epsilon,z\right)=\frac{1}{1-z}\left({}_2F_1(2,1+\epsilon,1-\epsilon,z)+z\frac{1+\epsilon}{1-\epsilon}{}_2F_1(2,2+\epsilon,2-\epsilon,z)\right), \tag{A.28} $$

and then we use the integral reppresentation of the hypergeometric functions in the right hand side of the previous equation getting

$$ \begin{aligned} {}_2F_1(2,2+\epsilon,1-\epsilon,z)=\frac{1}{1-z}\Bigg(&\frac{\Gamma(1-\epsilon)}{\Gamma(1+\epsilon)\Gamma(-2\epsilon)}\int_0^1 dy\,\frac{y^{\epsilon}(1-y)^{-1-2\epsilon}}{(1-yz)^2}+\\ &\frac{1+\epsilon}{1-\epsilon}\frac{\Gamma(2-\epsilon)}{\Gamma(2+\epsilon)\Gamma(-2\epsilon)}z\int_0^1 dy\,\frac{y^{1+\epsilon}(1-y)^{-1-2\epsilon}}{(1-yz)^2}\Bigg). \end{aligned} \tag{A.29} $$

Using the relation

$$ \frac{1+\epsilon}{1-\epsilon}\frac{\Gamma(2-\epsilon)}{\Gamma(2+\epsilon)\Gamma(-2\epsilon)}=\frac{\Gamma(1-\epsilon)}{\Gamma(1+\epsilon)\Gamma(-2\epsilon)}, \tag{A.30} $$

we prove A.27.

A. RESUMMATION COEFFICIENTS AND USEFUL FORMULAE FOR THRUST

Appendix B

Resummation coefficients and useful formulae for jet-veto

B.1 Explicit resummation formulae

In the present section we report the explicit expressions for the resummation functions g_1, g_2 and g_3 computed in [52, 53], as functions of $\lambda = \alpha_s\beta_0 L$, with $L = \ln(Q/p_t)$. α_s denotes $\alpha_s(\mu_R)$ unless otherwise stated, and Q is the resummation scale (see main text)

$$g_1(\lambda) = \frac{A^{(1)}}{\pi\beta_0}\frac{2\lambda+\ln(1-2\lambda)}{2\lambda}, \tag{B.1a}$$

$$\begin{aligned} g_2(\lambda) = {} & \frac{1}{2\pi\beta_0}\ln(1-2\lambda)\left(A^{(1)}\ln\frac{M^2}{Q^2}+B^{(1)}\right) - \frac{A^{(2)}}{4\pi^2\beta_0^2}\frac{2\lambda+(1-2\lambda)\ln(1-2\lambda)}{1-2\lambda} \\ & + A^{(1)}\left(-\frac{\beta_1}{4\pi\beta_0^3}\frac{\ln(1-2\lambda)((2\lambda-1)\ln(1-2\lambda)-2)-4\lambda}{1-2\lambda}\right. \\ & \left. - \frac{1}{2\pi\beta_0}\frac{(2\lambda(1-\ln(1-2\lambda))+\ln(1-2\lambda))}{1-2\lambda}\ln\frac{\mu_R^2}{Q^2}\right), \end{aligned} \tag{B.1b}$$

$$\begin{aligned} g_3(\lambda) = {} & \left(A^{(1)}\ln\frac{M^2}{Q^2}+B^{(1)}\right)\left(-\frac{\lambda}{1-2\lambda}\ln\frac{\mu_R^2}{Q^2}+\frac{\beta_1}{2\beta_0^2}\frac{2\lambda+\ln(1-2\lambda)}{1-2\lambda}\right) \\ & - \frac{1}{2\pi\beta_0}\frac{\lambda}{1-2\lambda}\left(A^{(2)}\ln\frac{M^2}{Q^2}+B^{(2)}\right) - \frac{A^{(3)}}{4\pi^2\beta_0^2}\frac{\lambda^2}{(1-2\lambda)^2} \\ & + A^{(2)}\left(\frac{\beta_1}{4\pi\beta_0^3}\frac{2\lambda(3\lambda-1)+(4\lambda-1)\ln(1-2\lambda)}{(1-2\lambda)^2} - \frac{1}{\pi\beta_0}\frac{\lambda^2}{(1-2\lambda)^2}\ln\frac{\mu_R^2}{Q^2}\right) \\ & + A^{(1)}\left(\frac{\lambda\left(\beta_0\beta_2(1-3\lambda)+\beta_1^2\lambda\right)}{\beta_0^4(1-2\lambda)^2} + \frac{(1-2\lambda)\ln(1-2\lambda)\left(\beta_0\beta_2(1-2\lambda)+2\beta_1^2\lambda\right)}{2\beta_0^4(1-2\lambda)^2}\right. \\ & \left. + \frac{\beta_1^2}{4\beta_0^4}\frac{(1-4\lambda)\ln^2(1-2\lambda)}{(1-2\lambda)^2} - \frac{\lambda^2}{(1-2\lambda)^2}\ln^2\frac{\mu_R^2}{Q^2}\right. \end{aligned}$$

$$- \frac{\beta_1}{2\beta_0^2} \frac{(2\lambda(1-2\lambda) + (1-4\lambda)\ln(1-2\lambda))}{(1-2\lambda)^2} \ln \frac{\mu_R^2}{Q^2}\Big), \tag{B.1c}$$

where, for Higgs, $A^{(1)} = 2C_A$ and $B^{(1)} = -4\pi\beta_0$, while for Drell-Yan, $A^{(1)} = 2C_F$ and $B^{(1)} = -3C_F$. The remaining coefficients can be expressed in a unique way as [110, 140, 218]:

$$A^{(2)} = A^{(1)} K^{(1)}_{\rm CMW}, \quad A^{(3)} = A^{(1)} K^{(2)}_{\rm CMW} + \pi\beta_0 C d^{(2)}, \quad B^{(2)} = -2\gamma^{(2)} + 2\pi\beta_0 C\zeta_2\,, \tag{B.2}$$

$$\beta_0 = \frac{11C_A - 2n_f}{12\pi}\,, \quad \beta_1 = \frac{17C_A^2 - 5C_A n_f - 3C_F n_f}{24\pi^2}\,, \tag{B.3}$$

$$\beta_2 = \frac{2857C_A^3 + (54C_F^2 - 615C_F C_A - 1415C_A^2)n_f + (66C_F + 79C_A)n_f^2}{3456\pi^3}\,, \tag{B.4}$$

in terms of the Casimir $C = C_A$ for Higgs and $C = C_F$ for Drell-Yan, and of the well known constants

$$K^{(1)}_{CMW} = C_A\left(\frac{67}{18} - \frac{\pi^2}{6}\right) - \frac{5}{9}n_f\,, \qquad d^{(2)} = C_A\left(\frac{808}{27} - 28\zeta_3\right) - \frac{224}{54}n_f, \tag{B.5a}$$

$$K^{(2)}_{CMW} = C_A^2\left(\frac{245}{24} - \frac{67}{9}\zeta_2 + \frac{11}{6}\zeta_3 + \frac{11}{5}\zeta_2^2\right) + C_F n_f\left(-\frac{55}{24} + 2\zeta_3\right) + C_A n_f\left(-\frac{209}{108} + \frac{10}{9}\zeta_2 - \frac{7}{3}\zeta_3\right) - \frac{1}{27}n_f^2\,. \tag{B.5b}$$

Here $\gamma^{(2)}$ [219, 220] are the coefficients of the $\delta(1-z)$ term in the NLO splitting functions $P^{(1)}$. For Higgs production we have

$$\gamma^{(2)} = C_A^2\left(\frac{8}{3} + 3\zeta_3\right) - \frac{1}{2}C_F n_f - \frac{2}{3}C_A n_f\,, \tag{B.6}$$

whilst for the Drell-Yan process

$$\gamma^{(2)} = C_F^2\left(\frac{3}{8} - \frac{\pi^2}{2} + 6\zeta_3\right) + C_F C_A\left(\frac{17}{24} + \frac{11}{18}\pi^2 - 3\zeta_3\right) - C_F n_f\left(\frac{1}{12} + \frac{\pi^2}{9}\right). \tag{B.7}$$

We finally report the expressions for the collinear coefficient function $C_{ij}^{(1)}(z)$ and the hard virtual term $\mathcal{H}^{(1)}$ in Eq. 6.36 [1]

$$C_{ij}^{(1)}(z) = -P_{ij}^{(0),\epsilon}(z) - \delta_{ij}\delta(1-z)C\frac{\pi^2}{12} + P_{ij}^{(0)}(z)\ln\frac{Q^2}{\mu_F^2}, \tag{B.8a}$$

[1] Often in the literature, the hard coefficient $H^{(1)}$ is considered as part of the $\delta(1-z)$ term in the coefficient function $C_{ij}^{(1)}(z)$, so it comes with a factor $1/(1-\alpha_s\beta_0 L)$ in Eq. 6.36. This results in a different convention for the resummation coefficient $B^{(2)}$ which will differ by an amount $2\pi\beta_0 H^{(1)}$ from what reported here.

$$\mathcal{H}^{(1)} = H^{(1)} - \left(B^{(1)} + \frac{A^{(1)}}{2} \ln \frac{M^2}{Q^2} \right) \ln \frac{M^2}{Q^2} + \mathrm{q}\, 2\pi\beta_0 \ln \frac{\mu_R^2}{M^2}\,, \tag{B.8b}$$

where q is the α_s power of the LO cross section ($\mathrm{q} = 2$ for Higgs production and $\mathrm{q} = 0$ for Drell-Yan). The coefficient $H^{(1)}$ encodes the pure hard virtual correction to the leading order process, it is given by

$$\mathrm{Higgs}: \qquad H^{(1)} = C_A \left(5 + \frac{7}{6}\pi^2 \right) - 3C_F\,, \tag{B.9a}$$

$$\mathrm{Drell-Yan}: \qquad H^{(1)} = C_F \left(-8 + \frac{7}{6}\pi^2 \right)\,. \tag{B.9b}$$

Finally, $P_{ij}^{(0),\epsilon}(z)$ is the $\mathcal{O}(\epsilon)$ term of the LO splitting function $P_{ij}^{(0)}(z)$:

$$P_{qq}^{(0),\epsilon}(z) = -C_F(1-z)\,, \tag{B.10a}$$

$$P_{gq}^{(0),\epsilon}(z) = -C_F z\,, \tag{B.10b}$$

$$P_{qg}^{(0),\epsilon}(z) = -z(1-z)\,, \tag{B.10c}$$

$$P_{gg}^{(0),\epsilon}(z) = 0. \tag{B.10d}$$

B.2 Evaluation of the boson-p_t integrated cross section

To facilitate comparisons between the jet and boson p_t resummations at fixed order, it is convenient to have an expression for the boson p_t resummation whose fixed-order expansion can be straightforwardly obtained. The full expression for the cumulative p_t cross section can be found in [52, 53, 110] and reads

$$\Sigma^{(B)}(p_t) = \int_0^\infty dy J_1(y)\, |M(k)|^2 e^{-R(b_0/b)} \left(\mathcal{L}^{(0)}(\ln(Qb/b_0)) + \mathcal{L}^{(1)}(\ln(Qb/b_0)) \right)\,, \tag{B.11}$$

where

$$-R(b_0/b) = \ln(Qb/b_0) g_1(\alpha_s \ln(Qb/b_0)) + g_2(\alpha_s \ln(Qb/b_0)) + \frac{\alpha_s}{\pi} g_3(\alpha_s \ln(Qb/b_0)) \tag{B.12}$$

is the full NNLL radiator. As discussed above, the resummation functions g_1, g_2 and g_3 are those used for the jet veto case. To perform the inverse Fourier transform we expand $R(b_0/b)$ and the full luminosity factor around $b = b_0/p_t$ and neglect subleading logarithmic terms getting, at NNLL accuracy,

$$\Sigma^{(B)}(p_t) = \int_0^\infty dy J_1(y)\, |M(k)|^2 \Big[\mathcal{L}^{(0)}(\ln(Q/p_t)) + \mathcal{L}^{(1)}(\ln(Q/p_t))$$

$$+\partial_{\ln p_t}\mathcal{L}^{(0)}(\ln(Q/p_t))\ln(y/b_0)\Big]\left(\frac{y}{b_0}\right)^{-R'} e^{-R(p_t)}\left(1-\frac{1}{2}R''\ln^2(y/b_0)\right), \tag{B.13}$$

where we have performed the change of variable $y = bp_t$, and we have made use of R' and R'', the first and second derivatives of R with respect to $\ln(Q/p_t)$. To order $\alpha_s L$, $R' = 4\alpha_s C\ln(Q/p_t)/\pi$. Moreover, from Eq. 6.40, we see that the variation of $\mathcal{L}^{(0)}(L)$ reads

$$\partial_{\ln p_t}\mathcal{L}^{(0)}(L) = \frac{\alpha_s}{\pi}\sum_{i,j,k}\int dx_1 dx_2\delta(x_1x_2s-M^2)\Big[\left(P^{(0)}_{ki}\otimes f_i\right)(x_1,e^{-L}\mu_F)\, f_j\big(x_2,e^{-L}\mu_F\big) + \{(x_1,i)\leftrightarrow(x_2,j)\}\Big]. \tag{B.14}$$

It is straightforward to show that Eq. B.13 evaluates to

$$\Sigma^{(B)}(p_t) = |M(k)|^2 e^{-R(p_t)}\Big[\mathcal{L}^{(0)}(\ln(Q/p_t))\left(1-\frac{1}{2}R''\partial^2_{R'}\right) + \mathcal{L}^{(1)}(\ln(Q/p_t)) - \partial_{\ln p_t}\mathcal{L}^{(0)}(\ln(Q/p_t))\partial_{R'}\Big]e^{-\gamma_E R'}\frac{\Gamma(1-\frac{R'}{2})}{\Gamma(1+\frac{R'}{2})}. \tag{B.15}$$

In this notation, the result for the jet-veto cross section is simply $|M(k)|^2e^{-R(p_t)}(\mathcal{L}^{(0)}+\mathcal{L}^{(1)})(1+\mathcal{F}^{\text{clust}}+\mathcal{F}^{\text{correl}})$. It is therefore immediate to evaluate the differences between the two formulae at any given fixed order and in particular to derive Eq. 6.37: making use of the fact that $e^{-\gamma_E R'}\Gamma(1-\frac{R'}{2})/\Gamma(1+\frac{R'}{2})$ has an expansion of the form $1+\frac{\zeta_3}{12}R'^3+\mathcal{O}\left(R'^5\right)$, one sees that the only terms in the difference that survive at order $\alpha_s^2 L$ are the $\mathcal{F}^{\text{clust}}$ and $\mathcal{F}^{\text{correl}}$ contributions and the $R''\partial^2_{R'}$ term of Eq. B.15, with the latter giving

$$-\sigma_0\frac{1}{2}R''\partial^2_{R'}e^{-\gamma_E R'}\frac{\Gamma(1-\frac{R'}{2})}{\Gamma(1+\frac{R'}{2})} = \sigma_0\left(-4\frac{\alpha_s^2}{\pi^2}\zeta_3 C^2\ln\frac{Q}{p_t}+\mathcal{O}\left(\alpha_s^2L^0\right)+\mathcal{O}\left(\alpha_s^3L^2\right)\right), \tag{B.16}$$

which is the source of the ζ_3 in Eq. 6.37.[1]

[1] One point to note in evaluating the difference between the jet and boson p_t resummations at order $\alpha_s^3L^2$ is that it is necessary to account also for the difference between C_2 terms for the two resummations. One of the properties of this difference of C_2 terms is that is has Q dependence that ensures that the final prediction for the difference of $\alpha_s^3L^2$ terms is Q-independent. To produce figure 6.2 the difference of C_2 terms was taken from a numerical determination based on the MCFM leading-order $H+2$-jet calculation.

B.3 Use of the large-R limit to relate boson and jet-p_t resummations

One natural way of relating jet and boson-p_t resummations is to make the observation that for an infinite jet radius, all partons will be clustered into a single jet, which will have a transverse momentum that balances exactly that of the boson. This approach was taken in Ref. [109] and here we examine it in detail.

First, let us consider the properties of $\mathcal{F}^{\text{clust}}$ and $\mathcal{F}^{\text{correl}}$ for large R. It is straightforward to see that $\mathcal{F}^{\text{correl}}$ vanishes for large R, since the two partons will always clustered together, giving $1 - J(k_1, k_2) = 0$. For $\mathcal{F}^{\text{clust}}$, the NNLL component for $R > \pi$ can be evaluated in closed form and is given by

$$\mathcal{F}^{\text{clust}} = -4\frac{\alpha_s^2(p_{\text{t,veto}})C^2}{\pi^2}\ln(Q/p_t)\left(\left(\frac{\pi}{6}R^2 - \frac{R^4}{8\pi}\right)\arctan\frac{\pi}{\sqrt{R^2-\pi^2}} + \left(\frac{R^2}{8} - \frac{\pi^2}{12}\right)\sqrt{R^2-\pi^2}\right). \tag{B.17}$$

This has the property that it vanishes as $1/R$ for large R. Thus it would appear that at order $\alpha_s^2 L$ the difference between jet and boson-p_t resummations should be given by [109]

$$\frac{d\Sigma^{(J)}_{\text{NNLL},2}(p_t)}{d\ln p_t} - \frac{d\Sigma^{(B)}_{\text{NNLL},2}(p_t)}{d\ln p_t} = (f(R) - f(\infty))\,\alpha_s^2\sigma_0 = f(R)\,\alpha_s^2\sigma_0\,, \tag{B.18}$$

which differs from the result in Eq. 6.37 (here $f(R) = f^{\text{correl}}(R) + f^{\text{clust}}(R)$).

To understand the origin of this difference, it is helpful to examine the structures that lead to $\mathcal{F}^{\text{clust}}$ vanishing for large R. A first observation is that for large R, $J(k_1, k_2)$ can be written as

$$J(k_1,k_2) = \Theta\left(R - |\Delta y| + \frac{\Delta\phi^2}{2R} + \mathcal{O}\left(\frac{1}{R^3}\right)\right), \qquad \Delta y \equiv y_1 - y_2\,, \quad \Delta\phi = \phi_1 - \phi_2\,. \tag{B.19}$$

Neglecting the term of order $1/R$ will allow us to simplify our discussion and so we will instead examine a "rapidity-only" jet algorithm with the clustering function

$$J_{\text{rap}}(k_1,k_2) = \Theta(R - |\Delta y|)\,. \tag{B.20}$$

Let us now evaluate $\mathcal{F}^{\text{clust}}$ with J_{rap}. We break the problem into rapidity, transverse momentum and azimuthal integrals. Each emission i is limited to a rapidity $|y_i| < \ln(M/k_{ti})$. Assuming that we can neglect terms $\ln(k_{t1}/k_{t2})$ from the rapidity integration, we can write the latter as

$$\int dy_1 dy_2 \Theta\left(|y_1| - \ln\frac{M}{k_{t1}}\right)\Theta\left(|y_2| - \ln\frac{M}{k_{t2}}\right)\Theta(R - |y_1 - y_2|) = 4R\ln\frac{M}{k_{t1}} - R^2 + \mathcal{O}\left(R\ln\zeta\right), \tag{B.21}$$

where $\zeta = k_{t2}/k_{t1}$ and we have included the constraint that $J_{\text{rap}}(k_1, k_2)$ be non-zero. We can then write $\mathcal{F}^{\text{clust}}$ as

$$\mathcal{F}^{\text{clust}} = 4\frac{\alpha_s^2 C^2}{\pi^2}\int_0^1 \frac{d\zeta}{\zeta}\int_{-\pi}^{\pi}\frac{d\phi}{2\pi}\int_{p_t}^{\frac{p_t}{\sqrt{1+\zeta^2+2\zeta\cos\phi}}}\frac{dk_{t,1}}{k_{t,1}}\left(4R\ln\frac{M}{k_{t1}} - R^2\right), \tag{B.22}$$

where we have dropped the $\mathcal{O}(R\ln\zeta)$ term of Eq. B.21. Performing the k_{t1} integration gives

$$\begin{aligned}\mathcal{F}^{\text{clust}} = 4\frac{\alpha_s^2 C^2}{\pi^2}\int_0^1 \frac{d\zeta}{\zeta}\int_{-\pi}^{\pi}\frac{d\phi}{2\pi}\Bigg[&\left(-2R\ln\frac{M}{p_t} + \frac{R^2}{2}\right)\ln(1+\zeta^2+2\zeta\cos\phi)\\ &- \frac{R}{2}\ln^2(1+\zeta^2+2\zeta\cos\phi)\Bigg].\end{aligned} \tag{B.23}$$

Because $\int_0^{2\pi} d\phi \ln(1+\zeta^2+2\zeta\cos\phi) = 0$, the first term in square brackets vanishes. This was the only term that had a NNLL $\alpha_s^2 \ln M/p_t$ factor and so at NNLL accuracy $\mathcal{F}^{\text{clust}}$ is zero at large R, modulo $1/R$ corrections associated with the $1/R$ term in Eq. B.19. The only element that survives the azimuthal integration in Eq. B.23 is the second term in square brackets, resulting in

$$\mathcal{F}^{\text{clust}} = -2\frac{\alpha_s^2 C^2}{\pi^2} R\,\zeta_3\,. \tag{B.24}$$

This is N^{3}LL, so beyond our accuracy. Note, however, that it is enhanced by a factor of R. In the large R limit, the separation between partons is limited to be at most $2\ln M/p_t$ and thus the R factor is effectively replaced with a coefficient of order $\ln M/p_t$. Consequently the apparently N^{3}LL term of Eq. B.24 is "promoted" and becomes a NNLL $\alpha_s^2 \ln M/p_t$ contribution. This is not accounted for in the purely NNLL R-dependent analysis that led to Eq. B.18.

The exact infinite R result can be obtained at order $\alpha_s^2 L$ by evaluating $\mathcal{F}^{\text{clust}}$ with $J(k_1, k_2) = 1$, giving

$$\begin{aligned}\mathcal{F}^{\text{clust}} &= 16\frac{\alpha_s^2 C^2}{\pi^2}\int_0^1 \frac{d\zeta}{\zeta}\int_{-\pi}^{\pi}\frac{d\phi}{2\pi}\int_{p_t}^{\frac{p_t}{\sqrt{1+\zeta^2+2\zeta\cos\phi}}}\frac{dk_{t,1}}{k_{t,1}}\left(\ln\frac{M}{k_{t,1}} - \ln\zeta\right)\ln\frac{M}{k_{t,1}}\\ &= -4\frac{\alpha_s^2}{\pi^2}\zeta_3 C^2\ln\frac{M}{p_t} + \mathcal{O}(\alpha_s^2\ln^0\frac{M}{p_t}).\end{aligned} \tag{B.25}$$

Note the agreement of the ζ_3 term here with that derived in Eq. B.16. It is this contribution that corresponds to the ζ_3 term in Eq. 6.37.

B.4 Correlation matrix between 0-jet and inclusive 1-jet cross sections

As discussed in [57], the prescription that we propose for determining the uncertainties on the 0-jet cross section is to treat the uncertainties on the jet-veto efficiency and on

the total cross section as uncorrelated. This gives the following covariance matrix for the uncertainties of the 0-jet ($\sigma_{0\text{-jet}}$) and inclusive 1-jet ($\sigma_{\geq 1\text{-jet}}$) cross sections:

$$\begin{pmatrix} \epsilon^2\delta_\sigma^2 + \sigma^2\delta_\epsilon^2 & \epsilon(1-\epsilon)\delta_\sigma^2 - \sigma^2\delta_\epsilon^2 \\ \epsilon(1-\epsilon)\delta_\sigma^2 - \sigma^2\delta_\epsilon^2 & (1-\epsilon)^2\delta_\sigma^2 + \sigma^2\delta_\epsilon^2 \end{pmatrix} \tag{B.26}$$

B. RESUMMATION COEFFICIENTS AND USEFUL FORMULAE FOR JET-VETO

References

[1] P. W. Higgs, *Broken symmetries, massless particles and gauge fields*, *Phys. Lett.* **12** (1964) 132–133.

[2] P. W. Higgs, *Broken symmetries and the masses of gauge bosons*, *Phys. Rev. Lett.* **13** (1964) 508–509.

[3] P. W. Higgs, *Spontaneous Symmetry Breakdown without Massless Bosons*, *Phys. Rev.* **145** (1966) 1156–1163.

[4] F. Englert and R. Brout, *Broken symmetries and the mass of gauge vector bosons*, *Phys. Rev. Lett.* **13** (1964) 321–322.

[5] G. S. Guralnik, C. R. Hagen and T. W. B. Kibble, *Global conservation laws and massless particles*, *Phys. Rev. Lett.* **13** (1964) 585–587.

[6] S. Chatrchyan *et al.* [CMS Collaboration], Phys. Lett. B **716** (2012) 30 [arXiv:1207.7235 [hep-ex]].

[7] G. Aad *et al.* [ATLAS Collaboration], Phys. Lett. B **716** (2012) 1 [arXiv:1207.7214 [hep-ex]].

[8] F. Halzen and A. D. Martin, *Quarks and leptons: an introductory course in modern particle physics*. New York, Usa: Wiley (1984) 396 p.

[9] T. P. Cheng and L. F. Li, *Gauge theory of elementary particle physics*. Oxford, Uk: Clarendon (1984) 536 p. (Oxford Science Publications).

[10] M. Bohm, A. Denner and H. Joos, *Gauge theories of the strong and electroweak interaction*. Stuttgart, Germany: Teubner (2001) 784 p.

[11] G. Dissertori, I. G. Knowles and M. Schmelling, *High energy experiments and theory*. Oxford, UK: Clarendon (2003) 538 p.

[12] R. K. Ellis, W. J. Stirling and B. R. Webber, *QCD and collider physics*, vol. 8. 1996.

[13] T. Muta, *Foundations of quantum chromodynamics. Second edition*, vol. 57. 1998.

[14] Y. Dothan, M. Gell-Mann and Y. Ne'eman, *Series of hadron energy levels as representations of noncompact groups*, *Phys. Lett.* **17** (1965) 148–151.

[15] H. Fritzsch, M. Gell-Mann and H. Leutwyler, *Advantages of the Color Octet Gluon Picture*, *Phys. Lett.* **B47** (1973) 365–368.

[16] C. N. Yang and R. L. Mills, *Conservation of isotopic spin and isotopic gauge invariance*, *Phys. Rev.* **96** (Oct, 1954) 191–195.

[17] C. Becchi, A. Rouet and R. Stora, *Renormalization of Gauge Theories*, *Annals Phys.* **98** (1976) 287–321.

[18] G. 't Hooft and M. J. G. Veltman, *Regularization and Renormalization of Gauge Fields*, *Nucl. Phys.* **B44** (1972) 189–213.

[19] M. E. Peskin and D. V. Schroeder, *An Introduction to quantum field theory.* Reading, USA: Addison-Wesley (1995) 842 p.

[20] G. Leibbrandt, *Introduction to the technique of dimensional regularization*, *Rew. Mod. Phys.* **47** (1975) 849.

[21] G. Giavarini and G. Marchesini, *IR finite S matrix in the QCD coherent state basis*, *Nucl. Phys.* **B296** (1988) 546.

[22] F. Bloch and A. Nordsieck, *Note on the radiation field of the electron*, *Phys. Rev.* **52** (1937) 54.

[23] T. Kinoshita, *Mass singularities of Feynman amplitudes*, *J. Math. Phys.* **3** (1962) 650.

[24] T. Lee and M. Nauenberg, *Degenerate systems and mass singularities*, *Phys. Rev.* **B133** (1964) 1549.

[25] Z. Kunszt and D.E. Soper, Phys. Rev. D **46** (1992) 192;
S. Frixione, Z. Kunszt and A. Signer, Nucl. Phys. B **467**, 399 (1996) [hep-ph/9512328].

[26] S. Catani and M.H. Seymour, Nucl. Phys. B **485** (1997) 291; **510** (1997) 503(E) [hep-ph/9605323].

[27] D.A. Kosower, Phys. Rev. D **57** (1998) 5410 [hep-ph/9710213]; Phys. Rev. D **71** (2005) 045016 [hep-ph/0311272].

[28] G. Somogyi, JHEP **0905** (2009) 016 [arXiv:0903.1218].

[29] D. A. Kosower, Phys. Rev. D **67** (2003) 116003 [hep-ph/0212097].

[30] S. Weinzierl, JHEP **0303** (2003) 062 [hep-ph/0302180].

[31] W.B. Kilgore, Phys. Rev. D **70** (2004) 031501 [hep-ph/0403128].

[32] M. Grazzini and S. Frixione, JHEP **0506** (2005) 010 [hep-ph/0411399].

[33] G. Somogyi, Z. Trocsanyi and V. Del Duca, JHEP **0506** (2005) 024 [hep-ph/0502226]; JHEP **0701** (2007) 070 [hep-ph/0609042];
G. Somogyi and Z. Trocsanyi, JHEP **0701** (2007) 052 [hep-ph/0609043]; JHEP **0808** (2008) 042 [arXiv:0807.0509];
U. Aglietti, V. Del Duca, C. Duhr, G. Somogyi and Z. Trocsanyi, JHEP **0809** (2008) 107 [arXiv:0807.0514];
P. Bolzoni, S. Moch, G. Somogyi and Z. Trocsanyi, JHEP **0908** (2009) 079 [arXiv:0905.4390];
P. Bolzoni, G. Somogyi and Z. Trocsanyi, JHEP **1101** (2011) 059 [arXiv:1011.1909].

[34] S. Catani and M. Grazzini, Phys. Rev. Lett. **98** (2007) 222002 [hep-ph/0703012].

[35] M. Czakon, Phys. Lett. B **693** (2010) 259 [arXiv:1005.0274]; Nucl. Phys. B **849** (2011) 250 [arXiv:1101.0642].

[36] C. Anastasiou, F. Herzog and A. Lazopoulos, JHEP **1103** (2011) 038 [arXiv:1011.4867].

[37] A. Gehrmann-De Ridder, T. Gehrmann and E.W.N. Glover, JHEP **0509** (2005) 056 [hep-ph/0505111].

[38] G. Altarelli and G. Parisi, *Asymptotic Freedom in Parton Language*, *Nucl. Phys.* **B126** (1977) 298.

[39] G. F. Sterman and S. Weinberg, Phys. Rev. Lett. **39** (1977) 1436.

[40] J. E. Huth *et. al.*, *Toward a standardization of jet definitions*, . Presented at Summer Study on High Energy Physics, Reaearch Directions for the Decade, Snowmass, CO, Jun 25 - Jul 13, 1990.

[41] G. P. Salam, Eur. Phys. J. C **67** (2010) 637 [arXiv:0906.1833 [hep-ph]].

[42] A. Banfi, G. P. Salam, G. Zanderighi, JHEP **0503** (2005) 073. [arXiv:hep-ph/0407286 [hep-ph]].

[43] M. Dasgupta and G. P. Salam, Phys. Lett. B **512** (2001) 323 [hep-ph/0104277].

[44] A. Banfi, G. Marchesini and G. Smye, JHEP **0208** (2002) 006 [hep-ph/0206076].

[45] S. Catani, B. R. Webber and G. Marchesini, Nucl. Phys. B **349** (1991) 635.

[46] S. Catani and B. R. Webber, Phys. Lett. B **427** (1998) 377 [hep-ph/9801350].

[47] S. Catani, L. Trentadue, G. Turnock, B. R. Webber, Nucl. Phys. **B407** (1993) 3.

[48] Y.L. Dokshitzer, A. Lucenti, G. Marchesini and G.P. Salam, JHEP **9801** (1998) 011 [hep-ph/9801324].

[49] D. de Florian and M. Grazzini, Nucl. Phys. B **704** (2005) 387 [hep-ph/0407241].

[50] S. Catani, B. R. Webber, Y. L. Dokshitzer and F. Fiorani, Nucl. Phys. B **383** (1992) 419.

[51] S. Catani, Y. L. Dokshitzer, F. Fiorani and B. R. Webber, Nucl. Phys. B **377** (1992) 445.

[52] G. Bozzi, S. Catani, D. de Florian and M. Grazzini, Phys. Lett. B **564** (2003) 65 [hep-ph/0302104].

[53] G. Bozzi, S. Catani, D. de Florian and M. Grazzini, Nucl. Phys. B **737** (2006) 73 [hep-ph/0508068].

[54] S. Catani, D. de Florian, M. Grazzini and P. Nason, JHEP **0307** (2003) 028 [hep-ph/0306211].

[55] A. Banfi, G.P. Salam and G. Zanderighi, JHEP **0201** (2002) 018 [hep-ph/0112156].

[56] A. Banfi, G. P. Salam and G. Zanderighi, JHEP **0408** (2004) 062 [hep-ph/0407287].

[57] A. Banfi, G. P. Salam and G. Zanderighi, JHEP **1206** (2012) 159 [arXiv:1203.5773 [hep-ph]].

[58] A. Banfi, P. F. Monni, G. P. Salam and G. Zanderighi, Phys. Rev. Lett. **109** (2012) 202001 [arXiv:1206.4998 [hep-ph]].

[59] G. F. Sterman, Nucl. Phys. B **281** (1987) 310.

[60] J.C Collins, D.E. Soper, G. Sterman, in *Perturbative Quantum Chromodynamics*, ed. A.H. Mueller (World Scientific Singapore, 1989).

[61] G. F. Sterman, In *Boulder 1995, QCD and beyond* 327-406 [hep-ph/9606312].

[62] D. Buskulic *et al.* [ALEPH Collaboration], Z. Phys. C **73** (1997) 409; A. Heister *et al.* [ALEPH Collaboration], Eur. Phys. J. C **35** (2004) 457.

[63] P.D. Acton *et al.* [OPAL Collaboration], Z. Phys. C **59** (1993) 1; G. Alexander *et al.* [OPAL Collaboration], Z. Phys. C **72** (1996) 191; K. Ackerstaff *et al.* [OPAL Collaboration], Z. Phys. C **75** (1997) 193; G. Abbiendi *et al.* [OPAL Collaboration], Eur. Phys. J. C **16** (2000) 185 [hep-ex/0002012]; G. Abbiendi *et al.* [OPAL Collaboration], Eur. Phys. J. C **40** (2005) 287 [hep-ex/0503051]. G. Abbiendi *et al.* [OPAL Collaboration], Eur. Phys. J. C **53** (2008) 21.

[64] M. Acciarri *et al.* [L3 Collaboration], Phys. Lett. B **371** (1996) 137; M. Acciarri *et al.* [L3 Collaboration], Phys. Lett. B **404** (1997) 390; M. Acciarri *et al.* [L3 Collaboration], Phys. Lett. B **444** (1998) 569; P. Achard *et al.* [L3 Collaboration], Phys. Lett. B **536** (2002) 217 [hep-ex/0206052]; P. Achard *et al.* [L3 Collaboration], Phys. Rept. **399** (2004) 71 [hep-ex/0406049].

[65] P. Abreu *et al.* [DELPHI Collaboration], Phys. Lett. B **456** (1999) 322; J. AbdaLLh *et al.* [DELPHI Collaboration], Eur. Phys. J. C **29** (2003) 285 [hep-ex/0307048]; J. AbdaLLh *et al.* [DELPHI Collaboration], Eur. Phys. J. C **37** (2004) 1 [hep-ex/0406011].

[66] K. Abe *et al.* [SLD Collaboration], Phys. Rev. D **51** (1995) 962 [hep-ex/9501003].

[67] P. Pfeifenschneider *et al.* [JADE collaboration], Eur. Phys. J. C **17** (2000) 19 [hep-ex/0001055].

[68] W. Braunschweig *et al.* [TASSO Collaboration], Z. Phys. C **47** (1990) 187.

[69] S. Brandt, C. Peyrou, R. Sosnowski and A. Wroblewski, Phys. Lett. **12** (1964) 57;
E. Farhi, Phys. Rev. Lett. **39** (1977) 1587.

[70] R. K. Ellis, D. A. Ross and A. E. Terrano, Nucl. Phys. B **178** (1981) 421.

[71] R. K. Ellis, D. A. Ross and A. E. Terrano, Phys. Rev. Lett. **45** (1980) 1226.

[72] Z. Kunszt, Phys. Lett. B **99** (1981) 429.

[73] J. A. M. Vermaseren, K. J. F. Gaemers and S. J. Oldham, Nucl. Phys. B **187** (1981) 301.

[74] K. Fabricius, I. Schmitt, G. Kramer and G. Schierholz, Z. Phys. C **11** (1981) 315.

[75] Z. Kunszt and P. Nason, *QCD at LEP*, CERN Yellow Report 89-08 (1989), p.373.

[76] W. T. Giele and E. W. N. Glover, Phys. Rev. D **46** (1992) 1980.

[77] S. Catani, M. H. Seymour, Phys. Lett. **B378** (1996) 287. [hep-ph/9602277].

[78] R. W. L. Jones, M. Ford, G. P. Salam, H. Stenzel, D. Wicke, JHEP **0312** (2003) 007. [hep-ph/0312016].

[79] T. Gehrmann, G. Luisoni and P. F. Monni, Eur. Phys. J. C **73** (2013) 2265 [arXiv:1210.6945 [hep-ph]].

[80] A. Gehrmann-De Ridder, T. Gehrmann, E. W. N. Glover, G. Heinrich, JHEP **0711** (2007) 058 [arXiv:0710.0346].

[81] A. Gehrmann-De Ridder, T. Gehrmann, E. W. N. Glover, G. Heinrich, JHEP **0712** (2007) 094 [arXiv:0711.4711].

[82] A. Gehrmann-De Ridder, T. Gehrmann, E. W. N. Glover, G. Heinrich, Phys. Rev. Lett. **99** (2007) 132002 [arXiv:0707.1285].

[83] S. Weinzierl, JHEP **0907** (2009) 009 [arXiv:0904.1145].

[84] S. Weinzierl, JHEP **0906** (2009) 041 [arXiv:0904.1077].

[85] S. Weinzierl, Eur. Phys. J. C **71** (2011) 1565 [arXiv:1011.6247].

[86] A. Denner, S. Dittmaier, T. Gehrmann, C. Kurz, Phys. Lett. **B679** (2009) 219 [arXiv:0906.0372].

[87] A. Denner, S. Dittmaier, T. Gehrmann, C. Kurz, Nucl. Phys. **B836** (2010) 37 [arXiv:1003.0986].

[88] G. Dissertori, A. Gehrmann-De Ridder, T. Gehrmann, E. W. N. Glover, G. Heinrich, H. Stenzel, JHEP **0802** (2008) 040. [arXiv:0712.0327].

[89] G. Dissertori, *et al.*, Phys. Rev. Lett. **104** (2010) 072002 [arXiv:0910.4283].

[90] T. Gehrmann, M. Jaquier and G. Luisoni, Eur. Phys. J. C **67** (2010) 57 [arXiv:0911.2422].

[91] T. Gehrmann, G. Luisoni, H. Stenzel, Phys. Lett. **B664** (2008) 265 [arXiv:0803.0695].

[92] R. A. Davison and B. R. Webber, Eur. Phys. J. C **59** (2009) 13 [arXiv:0809.3326].

[93] S. Bethke, S. Kluth, C. Pahl and J. Schieck [JADE Collaboration], Eur. Phys. J. C **64** (2009) 351 [arXiv:0810.1389].

[94] G. Dissertori, A. Gehrmann-De Ridder, T. Gehrmann, E. W. N. Glover, G. Heinrich, G. Luisoni, H. Stenzel, JHEP **0908** (2009) 036. [arXiv:0906.3436].

[95] G. Abbiendi *et al.* [OPAL Collaboration], [arXiv:1101.1470].

[96] C.W. Bauer, D. Pirjol and I.W. Stewart, Phys. Rev. D **65** (2002) 054022 [hep-ph/0109045];
C.W. Bauer, S. Fleming, D. Pirjol, I.Z. Rothstein and I.W. Stewart, Phys. Rev. D **66** (2002) 014017 [hep-ph/0202088];
M. Beneke, A. P. Chapovsky, M. Diehl and T. Feldmann, Nucl. Phys. B **643** (2002) 431 [hep-ph/0206152].

[97] M. D. Schwartz, Phys. Rev. D **77** (2008) 014026 [arXiv:0709.2709].

[98] S. Fleming, A. H. Hoang, S. Mantry and I. W. Stewart, Phys. Rev. D **77** (2008) 074010 [hep-ph/0703207]; Phys. Rev. D **77** (2008) 114003 [arXiv:0711.2079].

[99] T. Becher, M.D. Schwartz, JHEP **0807** (2008) 034 [arXiv:0803.0342].

[100] P. F. Monni, T. Gehrmann and G. Luisoni, JHEP **1108** (2011) 010 [arXiv:1105.4560].

[101] R. Abbate, M. Fickinger, A. H. Hoang, V. Mateu, I. W. Stewart, Phys. Rev. **D83** (2011) 074021, [arXiv:1006.3080].

[102] R. Abbate, M. Fickinger, A. H. Hoang, V. Mateu and I. W. Stewart, Phys. Rev. D **86** (2012) 094002 [arXiv:1204.5746].

[103] Y.T. Chien, M.D. Schwartz, JHEP **1008** (2010) 058 [arXiv:1005.1644].

[104] J. -y. Chiu, A. Jain, D. Neill, I. Z. Rothstein, [arXiv:1104.0881].

[105] T. Becher, G. Bell, M. Neubert, [arXiv:1104.4108].

[106] T. Becher and G. Bell, JHEP **1211** (2012) 126 [arXiv:1210.0580 [hep-ph]].

[107] I. W. Stewart, F. J. Tackmann and W. J. Waalewijn, Phys. Rev. Lett. **106** (2011) 032001 [arXiv:1005.4060 [hep-ph]].

[108] I. W. Stewart, F. J. Tackmann and W. J. Waalewijn, Phys. Rev. Lett. **105** (2010) 092002 [arXiv:1004.2489 [hep-ph]].

[109] T. Becher and M. Neubert, JHEP **1207** (2012) 108 [arXiv:1205.3806 [hep-ph]].

[110] T. Becher and M. Neubert, Eur. Phys. J. C **71** (2011) 1665 [arXiv:1007.4005 [hep-ph]].

[111] T. Becher and M. Neubert, Phys. Rev. Lett. **97** (2006) 082001 [hep-ph/0605050].

[112] S. Moch, J. A. M. Vermaseren and A. Vogt, JHEP **0508** (2005) 049 [hep-ph/0507039].

[113] P. A. Baikov, K. G. Chetyrkin, A. V. Smirnov, V. A. Smirnov and M. Steinhauser, Phys. Rev. Lett. **102** (2009) 212002 [arXiv:0902.3519]; R. N. Lee, A. V. Smirnov and V. A. Smirnov, JHEP **1004** (2010) 020 [arXiv:1001.2887]; T. Gehrmann, E. W. N. Glover, T. Huber, N. Ikizlerli and C. Studerus, JHEP **1006** (2010) 094 [arXiv:1004.3653].

[114] T. Becher and M. Neubert, Phys. Lett. B **637** (2006) 251 [hep-ph/0603140].

[115] T. Becher, M. Neubert and B. D. Pecjak, JHEP **0701** (2007) 076 [hep-ph/0607228].

[116] A. H. Hoang and S. Kluth, [arXiv:0806.3852].

[117] R. Kelley, R. M. Schabinger, M. D. Schwartz and H. X. Zhu, [arXiv:1105.3676].

[118] A. Hornig, C. Lee, I. W. Stewart, J. R. Walsh and S. Zuberi, [arXiv:1105.4628].

[119] Y. Li, S. Mantry and F. Petriello, [arXiv:1105.5171].

[120] P.A. Baikov, K.G. Chetyrkin and J.H. Kühn, Phys. Rev. Lett. **101** (2008) 012002 [arXiv:0801.1821].

[121] C. F. Berger, T. Kucs, G. F. Sterman, Phys. Rev. **D68** (2003) 014012. [hep-ph/0303051]; Int. J. Mod. Phys. **A18** (2003) 4159. [hep-ph/0212343].

[122] G. P. Korchemsky and G. F. Sterman, Phys. Lett. B **340** (1994) 96 [hep-ph/9407344].

[123] J. Frenkel and J. C. Taylor, Nucl. Phys. B **246** (1984) 231.

[124] J. G. M. Gatheral, Phys. Lett. B **133** (1983) 90.

[125] S. Catani and M. Grazzini, Nucl. Phys. B **591** (2000) 435 [hep-ph/0007142].

[126] T. Huber and D. Maître, Comput. Phys. Commun. **175** (2006) 122 [hep-ph/0507094]; Comput. Phys. Commun. **178** (2008) 755. [arXiv:0708.2443].

[127] J. Carter and G. Heinrich, Comput. Phys. Commun. **182** (2011) 1566 [arXiv:1011.5493].

[128] G. Heinrich, Int. J. Mod. Phys. A **23** (2008) 1457 [arXiv:0803.4177].

[129] T. Binoth and G. Heinrich, Nucl. Phys. B **585** (2000) 741 [hep-ph/0004013].

[130] S. Kawabata, Comput. Phys. Commun. **88** (1995) 309.

[131] G. P. Lepage, J. Comput. Phys. **27** (1978) 192;
T. Hahn, Comput. Phys. Commun. **168** (2005) 78 [hep-ph/0404043].

[132] S. Catani and M. Grazzini, Nucl. Phys. B **570** (2000) 287 [hep-ph/9908523].

[133] G. P. Korchemsky and G. Marchesini, Phys. Lett. B **313** (1993) 433.

[134] G. P. Korchemsky and G. Marchesini, Nucl. Phys. B **406** (1993) 225 [hep-ph/9210281].

[135] I. A. Korchemskaya and G. P. Korchemsky, Phys. Lett. B **287** (1992) 169.

[136] G. P. Korchemsky and A. V. Radyushkin, Nucl. Phys. B **283** (1987) 342.

[137] G. P. Korchemsky, Mod. Phys. Lett. A **4** (1989) 1257.

[138] G. Altarelli and G. Parisi, Nucl. Phys. B **126** (1977) 298.

[139] A. Vogt, S. Moch and J. A. M. Vermaseren, Nucl. Phys. B **691** (2004) 129 [hep-ph/0404111].

[140] S. Moch, J. A. M. Vermaseren and A. Vogt, Nucl. Phys. B **688** (2004) 101 [hep-ph/0403192].

[141] S. Catani, M. L. Mangano, P. Nason, L. Trentadue, Nucl. Phys. **B478** (1996) 273 [hep-ph/9604351].

[142] T. Becher, *private communication.*

[143] C. J. Maxwell and K. E. Morgan, Nucl. Phys. B **858** (2012) 405 [arXiv:1108.6204].

[144] J. Schieck, S. Bethke, S. Kluth, C. Pahl and Z. Trocsanyi, arXiv:1205.3714 [hep-ex].

[145] R. Frederix, S. Frixione, K. Melnikov and G. Zanderighi, JHEP **1011** (2010) 050 [arXiv:1008.5313].

[146] Y. L. Dokshitzer, G. Marchesini and B. R. Webber, Nucl. Phys. B **469** (1996) 93 [hep-ph/9512336].

[147] Y. L. Dokshitzer and B. R. Webber, Phys. Lett. B **404** (1997) 321 [hep-ph/9704298].

[148] G. P. Korchemsky and G. F. Sterman, Nucl. Phys. B **555** (1999) 335 [hep-ph/9902341]. G. P. Korchemsky and S. Tafat, JHEP **0010** (2000) 010 [hep-ph/0007005].

[149] E. Gardi and G. Grunberg, JHEP **9911** (1999) 016 [hep-ph/9908458]. E. Gardi, JHEP **0004** (2000) 030 [hep-ph/0003179]. E. Gardi and J. Rathsman, Nucl. Phys. B **609** (2001) 123 [hep-ph/0103217].

[150] A. H. Hoang and I. W. Stewart, Phys. Lett. B **660** (2008) 483 [arXiv:0709.3519].

[151] T. Sjostrand, L. Lonnblad, S. Mrenna and P. Z. Skands, hep-ph/0308153. T. Sjostrand, S. Mrenna and P. Z. Skands, Comput. Phys. Commun. **178** (2008) 852 [arXiv:0710.3820].

[152] G. Corcella, I.G. Knowles, G. Marchesini, S. Moretti, K. Odagiri, P. Richardson, M.H. Seymour and B.R. Webber, JHEP **0101** (2001) 010 [hep-ph/0011363; hep-ph/0210213]. M. Bahr, S. Gieseke, M. A. Gigg, D. Grellscheid, K. Hamilton, O. Latunde-Dada, S. Platzer and P. Richardson *et al.*, Eur. Phys. J. C **58** (2008) 639 [arXiv:0803.0883].

[153] T. Gleisberg, S. .Hoeche, F. Krauss, M. Schonherr, S. Schumann, F. Siegert and J. Winter, JHEP **0902** (2009) 007 [arXiv:0811.4622].

[154] C. Bignamini, F. Becattini and F. Piccinini, Eur. Phys. J. C **72** (2012) 2176 [arXiv:1204.2300].

[155] W. Bernreuther, A. Brandenburg and P. Uwer, Phys. Rev. Lett. **79** (1997) 189 [hep-ph/9703305];
A. Brandenburg and P. Uwer, Nucl. Phys. B **515** (1998) 279 [hep-ph/9708350];
G. Rodrigo, A. Santamaria and M.S. Bilenky, Phys. Rev. Lett. **79** (1997) 193 [hep-ph/9703358].

[156] P. Nason and C. Oleari, Nucl. Phys. B **521** (1998) 237 [hep-ph/9709360].

[157] M. A. Shifman, A. I. Vainshtein and V. I. Zakharov, Nucl. Phys. B **147** (1979) 448. Nucl. Phys. B **147** (1979) 385. Nucl. Phys. B **147** (1979) 519.

[158] R. Kelley, M. D. Schwartz, R. M. Schabinger and H. X. Zhu, Phys. Rev. D **84** (2011) 045022 [arXiv:1105.3676].

[159] A. Hornig, C. Lee, I. W. Stewart, J. R. Walsh and S. Zuberi, JHEP **1108** (2011) 054 [arXiv:1105.4628].

[160] Y. L. Dokshitzer, A. Lucenti, G. Marchesini and G. P. Salam, Nucl. Phys. B **511** (1998) 396 [Erratum-ibid. B **593** (2001) 729] [hep-ph/9707532].

[161] Y. L. Dokshitzer, In *Vancouver 1998, High energy physics, vol. 1* 305-324 [hep-ph/9812252].

[162] G. P. Salam and D. Wicke, JHEP **0105** (2001) 061 [hep-ph/0102343].

[163] V. Mateu, I. W. Stewart and J. Thaler, [arXiv:1209.3781].

[164] S. Bethke, Nucl. Phys. Proc. Suppl. **222-224** (2012) 94.

[165] B. Webber in "Workshop on Precision Measurements of α_s" 44-45, [arXiv:1110.0016].

[166] S. Chatrchyan *et al.* [CMS Collaboration], Phys. Lett. B **710** (2012) 91 [arXiv:1202.1489 [hep-ex]].

[167] G. Aad *et al.* [ATLAS Collaboration], Phys. Lett. B **716** (2012) 62 [arXiv:1206.0756 [hep-ex]].

[168] S. Catani, D. de Florian and M. Grazzini, JHEP **0201** (2002) 015 [hep-ph/0111164].

[169] C. Anastasiou, K. Melnikov, F. Petriello, Nucl. Phys. **B724** (2005) 197-246. [hep-ph/0501130].

[170] M. Grazzini, JHEP **0802** (2008) 043. [arXiv:0801.3232 [hep-ph]].

[171] G. Bozzi, S. Catani, G. Ferrera, D. de Florian and M. Grazzini, Phys. Lett. B **696** (2011) 207 [arXiv:1007.2351 [hep-ph]].

[172] C. F. Berger, C. Marcantonini, I. W. Stewart, F. J. Tackmann and W. J. Waalewijn, JHEP **1104** (2011) 092 [arXiv:1012.4480 [hep-ph]].

[173] A. Banfi, M. Dasgupta and S. Marzani, Phys. Lett. B **701** (2011) 75 [arXiv:1102.3594 [hep-ph]].

[174] A. Banfi, M. Dasgupta, S. Marzani and L. Tomlinson, Phys. Lett. **715** (2012) 152 [arXiv:1205.4760 [hep-ph]].

[175] G. Davatz, F. Stockli, C. Anastasiou, G. Dissertori, M. Dittmar, K. Melnikov and F. Petriello, JHEP **0607** (2006) 037 [hep-ph/0604077].

[176] C. Anastasiou, G. Dissertori, F. Stockli and B. R. Webber, JHEP **0803** (2008) 017 [arXiv:0801.2682 [hep-ph]].

[177] C. Anastasiou, G. Dissertori, M. Grazzini, F. Stockli and B. R. Webber, JHEP **0908** (2009) 099 [arXiv:0905.3529 [hep-ph]].

[178] S. Dittmaier, C. Mariotti, G. Passarino, R. Tanaka, S. Alekhin, J. Alwall and E. A. Bagnaschi *et al.*, arXiv:1201.3084 [hep-ph].

[179] T. Sjostrand, S. Mrenna and P. Skands, JHEP **0605** (2006) 026 [arXiv:hep-ph/0603175].

[180] G. Corcella *et al.*, arXiv:hep-ph/0210213.

[181] S. Frixione and B. R. Webber, JHEP **0206** (2002) 029 [hep-ph/0204244].

[182] P. Nason, JHEP **0411** (2004) 040 [hep-ph/0409146].

[183] G. Parisi and R. Petronzio, Nucl. Phys. B **154** (1979) 427.

[184] S. Catani, Y. L. Dokshitzer, M. H. Seymour and B. R. Webber, Nucl. Phys. B **406** (1993) 187.

[185] S. D. Ellis and D. E. Soper, Phys. Rev. D **48**, 3160 (1993) [hep-ph/9305266].

[186] Y. L. Dokshitzer, G. D. Leder, S. Moretti and B. R. Webber, JHEP **9708**, 001 (1997) [hep-ph/9707323];

[187] M. Wobisch and T. Wengler, arXiv:hep-ph/9907280; M. Wobisch, DESY-THESIS-2000-049.

[188] M. Cacciari, G. P. Salam, G. Soyez, JHEP **0804** (2008) 063 [arXiv:0802.1189 [hep-ph]].

[189] F. A. Berends and W. T. Giele, Nucl. Phys. B **313** (1989) 595.

[190] Y. L. Dokshitzer, G. Marchesini and G. Oriani, Nucl. Phys. B **387** (1992) 675.

[191] J. M. Campbell and E. W. N. Glover, Nucl. Phys. B **527** (1998) 264 [hep-ph/9710255].

[192] S. Catani and M. Grazzini, Nucl. Phys. B **845** (2011) 297 [arXiv:1011.3918 [hep-ph]].

[193] D. de Florian, M. Grazzini and Z. Kunszt, Phys. Rev. Lett. **82** (1999) 5209 [hep-ph/9902483].

[194] V. Ravindran, J. Smith and W. L. Van Neerven, Nucl. Phys. B **634** (2002) 247 [hep-ph/0201114].

[195] C. J. Glosser and C. R. Schmidt, JHEP **0212** (2002) 016 [hep-ph/0209248].

[196] J. M. Campbell and R. K. Ellis, Phys. Rev. D **65** (2002) 113007 [hep-ph/0202176].

[197] J. M. Campbell, R. K. Ellis and G. Zanderighi, JHEP **0610** (2006) 028 [hep-ph/0608194].

[198] J. M. Campbell, R. K. Ellis and C. Williams, Phys. Rev. D **81** (2010) 074023 [arXiv:1001.4495 [hep-ph]].

[199] R. Hamberg, W. L. van Neerven and T. Matsuura, Nucl. Phys. B **359** (1991) 343 [Erratum-ibid. B **644** (2002) 403].

[200] S. Dawson, Nucl. Phys. B **359** (1991) 283.

[201] A. Djouadi, M. Spira and P. M. Zerwas, Phys. Lett. B **264** (1991) 440.

[202] R. V. Harlander and W. B. Kilgore, Phys. Rev. Lett. **88** (2002) 201801 [hep-ph/0201206].

[203] C. Anastasiou and K. Melnikov, Nucl. Phys. B **646** (2002) 220 [hep-ph/0207004].

[204] V. Ravindran, J. Smith and W. L. van Neerven, Nucl. Phys. B **665** (2003) 325 [hep-ph/0302135].

[205] K. Melnikov and F. Petriello, Phys. Rev. Lett. **96** (2006) 231803 [hep-ph/0603182].

[206] S. Catani, L. Cieri, G. Ferrera, D. de Florian, M. Grazzini, Phys. Rev. Lett. **103** (2009) 082001. [arXiv:0903.2120 [hep-ph]].

[207] W. T. Giele, E. W. N. Glover and D. A. Kosower, Nucl. Phys. B **403** (1993) 633 [hep-ph/9302225].

[208] J. M. Campbell and R. K. Ellis, Phys. Rev. D **60** (1999) 113006 [hep-ph/9905386].

[209] A. D. Martin, W. J. Stirling, R. S. Thorne, G. Watt, Eur. Phys. J. **C63** (2009) 189 [arXiv:0901.0002 [hep-ph]].

[210] M. Cacciari and G. P. Salam, Phys. Lett. B **641** (2006) 57 [arXiv:hep-ph/0512210];
M. Cacciari, G. P. Salam and G. Soyez, arXiv:1111.6097 [hep-ph].

[211] E. Bagnaschi, G. Degrassi, P. Slavich and A. Vicini, JHEP **1202** (2012) 088 [arXiv:1111.2854 [hep-ph]].

[212] S. Alioli, P. Nason, C. Oleari and E. Re, JHEP **0904** (2009) 002 [arXiv:0812.0578 [hep-ph]].

[213] P. Z. Skands, Phys. Rev. D **82** (2010) 074018 [arXiv:1005.3457 [hep-ph]].

[214] S. Dittmaier *et al.* [LHC Higgs Cross Section Working Group Collaboration], arXiv:1101.0593 [hep-ph].

[215] D. de Florian and M. Grazzini, arXiv:1206.4133 [hep-ph].

[216] http://jetvheto.hepforge.org/

[217] F. J. Tackmann, J. R. Walsh and S. Zuberi, arXiv:1206.4312 [hep-ph].

[218] D. de Florian and M. Grazzini, Nucl. Phys. B **616** (2001) 247 [hep-ph/0108273].

[219] W. Furmanski and R. Petronzio, Phys. Lett. B **97** (1980) 437.

[220] G. Curci, W. Furmanski and R. Petronzio, Nucl. Phys. B **175** (1980) 27.

[221] M. Dasgupta and G. P. Salam, JHEP **0208** (2002) 032 [arXiv:hep-ph/0208073].

[222] M. Cacciari and G. P. Salam, Phys. Lett. B **659** (2008) 119 [arXiv:0707.1378 [hep-ph]].

[223] J. M. Butterworth, A. R. Davison, M. Rubin and G. P. Salam, Phys. Rev. Lett. **100** (2008) 242001 [arXiv:0802.2470 [hep-ph]].

[224] D. Krohn, J. Thaler and L. -T. Wang, JHEP **1002** (2010) 084 [arXiv:0912.1342 [hep-ph]].